Delft University of Technology
Faculty of Electrical Engineering, Mathematics and Computer Science
Delft Institute of Applied Mathematics

Numerical treatment of stochastic control problems by Fourier-cosine series expansions

The dike height problem

A thesis submitted to the
Delft Institute of Applied Mathematics
in partial fulfillment of the requirements

for the degree

MASTER OF SCIENCE
in
APPLIED MATHEMATICS

by

Marjon Ruijter
Delft, the Netherlands
September 2010

TU Delft

MSc THESIS APPLIED MATHEMATICS

"Numerical treatment of stochastic control problems by Fourier-cosine series expansions, the dike height problem"

M.J. Ruijter

Delft University of Technology

Daily supervisor

Prof.dr.ir. C.W. Oosterlee

Responsible professor

Prof.dr.ir. C.W. Oosterlee

Other thesis committee members

Dr. J.A.M. van der Weide

Dr.ir. F.J. Vermolen

September 2010

Delft, the Netherlands

Preface

This report is part of my Master Thesis for the degree of Master of Science in Applied Mathematics at Delft University of Technology, the Netherlands. This thesis was completed at the faculty of Electrical Engineering, Mathematics and Computer Science at the chair of Numerical Analysis and the National Research Institute for Mathematics and Computer Science (CWI), located in Amsterdam.

I would like to acknowledge the advice and guidance of my supervisor Prof.dr.ir. C.W. Oosterlee. I also thank the members of my graduate committee and the members of the department at the CWI. Special thanks go to Bowen Zhang and Fang Fang, for helping me with the Matlab code and understanding their methodology. Finally I wish to express my gratitude to my family and friends who supported me through the duration of my study.

Marjon Ruijter
Delft, 2010

Contents

List of Figures

List of Tables

1 Introduction

In financial markets traders deal in stocks and options, such as the well-known call and put options. An option is a contract between a buyer and a seller that gives the buyer the right to buy or sell a particular stock under prescribed conditions. In this turbulent trading world, questions about a 'fair' option price and the hedging of risks arise. In the recent decades financial mathematics has developed fast to contribute to this theory and to improve the pricing methods.

In economical, but also in personal or societal contexts, one may face options in the sense of real 'choices'. For example, should one build a new factory now or later. These options are called real options and can be related to the financial options. An introduction to real options is given in Section 1.2. Also the contingent claims approach and the dynamic programming approach are introduced there.

A (real) option problem can often be formulated as a stochastic optimisation problem. We start with a general model for these problems in Section 2. This section is mainly based on the literature report ([34]), which is also a part of the Master Thesis. Concepts, such as control, the dynamic programming principle, the Hamilton-Jacobi-Bellman equation and impulse control problems are introduced. At the end of the section three examples of stochastic optimisation problems are discussed. The first two examples are financial problems, the optimal utility of wealth and put option prices are derived. The other example does not originate from the financial world but is a real option problem where optimal choices are made about when to harvest a forest.

Section 3 presents the dike height problem, where one has to choose when to increase the dike level and by which amount. The model includes a deterministic average water level and a stochastic economic value of endangered goods. This problem is the application of interest in this work. The relation and the differences between the harvesting and dike height problems are discussed in Section 3.2. After this, improved models for the dike height problem are proposed in Section 3.3.

Subsequently, a numerical method to solve the dike height problem is developed in Section 4. First the COS method, which is based on Fourier-cosine series expansions, is presented. This option pricing method has been used for pricing European, Bermudan, barrier and swing options. We adapt the method to the impulse control problem in order to estimate the costs of flooding and dike reinforcements. Then the resulting algorithm, the dike-COS method, comes up in Section 4.2 and an extensive error analysis is given in Section 5.

Numerical experiments to investigate the error of the COS method are performed in Section 6. The tests are based on the COS formula for pricing European options and they give insight into possible difficulties we may face using the more involved dike-COS method. We show how errors at the boundaries of the computational domain arise and how roundoff errors may spoil the error convergence.

The dike-COS method is applied to a model of an island in Section 7. We obtain a control law, which describes when it is optimal to increase the dikes and by which amount, depending on the economic value of endangered goods and the current dike level. Various model parameters are varied to investigate their influence.

Then in Section 8 we introduce an extended model for the dike height problem. The water level is stochastic in this model in order to be prepared for an uncertain rise in the future water level. The dike-COS method is extended using a quadrature rule for the additional dimension and the corresponding algorithm is developed thereafter. The error analysis can be found in Section 8.5. At the end we apply the method to a model of an island with stochastic water level. The results are presented in Section 8.6.

Finally, a summary is made and the main results are presented in Section 9.

Some notations are used two times through the different sections of this report. For example, ϵ denotes an arbitrary positive constant in Theorem 2.2, whereas it represents an error in sections thereafter. We suppose that the meaning of all notations becomes clear by its context.

In some experiments the results are shown with many decimal digits, because we investigate the performance of numerical solution methods and their convergence. For engineering purposes a lower accuracy is often sufficient.

1.1 Research questions

In this Master Thesis we focus on the numerical treatment of stochastic impulse control problems, in particular to determine the optimal height and reinforcement times for dikes. We adapt a financial option pricing method, based on Fourier-cosine series expansions, to pricing real options. The main research questions we work on are:

- Can we adapt the COS pricing method for Bermudan or swing options to solve the dike height impulse control problem?
- How can we efficiently calculate the optimal dike increase level?
- What can we tell about the error convergence of the numerical method and the errors close to the boundaries of the computational domain?
- Is it possible to extend the pricing method to using it with more than one stochastic process, such as both stochastic water level and stochastic economic value?
- How do the real option prices change when it is possible to hedge the risks of, for example, floods?

1.2 Real options approach

In this section we explain the idea of real options. A detailed introduction to real options theory can be found in [38] and [8].

In the financial world many different options exist, the most well-known are the European call and put options. More involved options are path-dependent and exotic options, such as barrier options, Asian options, swing options and rainbow options. In recent times the financial options theory for pricing options has been well developed. We refer to [14] for an introduction to financial option valuation and to [36] for a financial mathematical background.

A *real option* is not a financial derivative, but an actual option in the sense of a 'choice' that, for instance, a company or government may have by undertaking investments. For example, by investing in a particular project (e.g., a new factory), a company may have the real option of delaying, expanding, deferring or abandoning the project in the future. Such real options have a certain value which can greatly affect the valuation of investments and may not be neglected. Most investment decisions share three important characteristics: (partially or completely) irreversibility, uncertainty over the future rewards of the investment and some leeway regarding the timing of the investment.

The opportunity to invest can be modelled by means of a financial option. The company has the option, but not the obligation, to spend investment costs and to receive a project. Frequently the investment opportunity remains only for a certain time interval. The expiration time can be the time from a patent's right or the anticipated entry time of a competitor. The investment opportunity can be seen as a call

option, the investment costs represent the exercise price and the project is modelled as the stock received by exercising the option. The value of the implanted project, after investment, fluctuates stochastically like the value of stocks. There is a value of waiting before investment in order to gain more information, and the option is only exercised if the project is sufficiently profitable.

In classical valuation methods one often uses the net-present value (NPV) of a project to determine the profitability, which does not include the benefits of real options. In these methods one invests when the present value of the expected stream of profits is larger than the costs required, i.e., when the NPV is greater than zero. However, this ignores the opportunity of delaying an investment. Delaying can create costs, but it may also give rise to large benefits as uncertainty is resolved. If an option is exercised the opportunity costs of the lost option must be included as part of the total cost.

The real options theory can be applied when we have irreversibility, ongoing uncertainty and some leeway in timing. Some techniques developed for valuing financial options appear to be useful in the real option context. A clarifying example of two valuation methods is given in [8], page 27-33. The valuation approach of constructing a risk-free portfolio, consisting of the investment option and hedge instruments, is called the *contingent claims approach*. With this approach it is assumed that markets are complete in order to hedge the risk of an investment. The assumption of the absence of arbitrage opportunities allows the derivation of the fair value using the risk-free discount rate. For example, the well-known Black-Scholes equation can be derived using this approach.

The limitations attached to the use of financial option pricing techniques for real option values are due to the differences between real options and the financial options. Two important differences that can arise are:

- The underlying asset is not tradeable (e.g., the factory cannot easily be sold).
- The real option itself is not tradeable (e.g., the option to built the factory cannot usually be sold to another investor).

If there are no assets to trade or other assets that cover the price risk we can employ the *dynamic programming* or expected value approach. Here we calculate the NPV for each investment strategy, invest now or wait, under a risk adjusted discount rate, which is usually higher than the risk-free rate. The risk adjusted discount rate reflects the return the investor would require for holding the risky option. We choose the strategy that yields the highest NPV. This approach has the disadvantage that it is necessary to choose a future discount rate for the risky investment. The basic principle behind this approach is Bellman's Principle of Optimality ([3]):

"Principle of Optimality. An optimal policy has the property that whatever the initial state and initial decision are, the remaining decisions must constitute an optimal policy with regard to the state resulting from the first decision."

In the next sections we will deal with the dynamic programming approach, and later on with the contingent claims approach, for continuous time models.

2 Basics of stochastic optimisation

This section provides the mathematical background of stochastic optimisation problems. In these problems we can apply a certain control to optimise an objective function which is subject to stochastic processes. In Section 2.1 we introduce the notation for stochastic optimisation problems. Then the dynamic programming principle in Section 2.2 helps in deriving the Hamilton-Jacobi-Bellman equation in Section 2.3. Finally, three concrete examples of stochastic optimisation problems are discussed. A comprehensive introduction to stochastic control and optimisation can be found in [31] and [30], from which we employ the notation system and moreover most theorems.

2.1 Stochastic optimisation problems

We can subdivide the problem class into finite and infinite horizon problems, where we optimise the objective either over a given finite or over an infinite domain. We start with the notation of both types of control problems.

Let $(\Omega, \mathcal{F}, P)$ be a probability space, $\mathbb{F} = (\mathcal{F}_t)_{t\geq 0}$ a filtration satisfying the usual conditions and W a d-dimensional Brownian motion on the filtered probability space $(\Omega, \mathcal{F}, \mathbb{F}, P)$. The controlled state process X_t is valued in $\mathbb{R}^n$ and satisfies the stochastic differential equation

$$dX_s = b(X_s, \alpha_s)ds + \sigma(X_s, \alpha_s)dW_s, \tag{2.1}$$

or componentwise

$$dX_s^{(i)} = b_i(X_s, \alpha_s)ds + \sum_{j=1}^{d} \sigma_{ij}(X_s, \alpha_s)dW_s^{(j)}, \qquad 1 \leq i \leq n. \tag{2.2}$$

The control process $\alpha = (\alpha_s)$ is progressively measurable with respect to $\mathbb{F}$ and is valued in the control set A, a subset of $\mathbb{R}^m$. The state process is typically influenced by this control process α whose value is determined at any time t based on the available information.

The measurable functions $b : \mathbb{R}^n \times A \to \mathbb{R}^n$ and $\sigma : \mathbb{R}^n \times A \to \mathbb{R}^{n\times d}$ satisfy a uniform Lipschitz condition in A, in other words, $\exists\, K \geq 0, \forall\, x, y \in \mathbb{R}^n, \forall\, a \in A$ we have

$$|b(x, a) - b(y, a)| + |\sigma(x, a) - \sigma(y, a)| \leq K|x - y|. \tag{2.3}$$

In the case of finite horizon problems we can consider coefficients $b(t, x, a)$ and $\sigma(t, x, a)$ depending also on time t. However, in the case of infinite horizon problems the coefficients cannot be time-dependent in order to get the stationarity of the problem, that is the solution is independent on the initial time at which the optimisation problem is considered.

In the next two sections the finite and infinite horizon problems are formulated.

2.1.1 Finite horizon problems

For the finite horizon problem, with terminal time $T \in (0, \infty)$, $\mathcal{A}$ denotes the set of control processes α, which satisfy

$$E\left[\int_0^T |b(0, \alpha_t)|^2 + |\sigma(0, \alpha_t)|^2 dt\right] < \infty. \tag{2.4}$$

With conditions (2.3) and (2.4) on b, σ we have that for all $\alpha \in \mathcal{A}$ and for any initial condition $(t, x) \in [0, T] \times \mathbb{R}^n$ a unique strong solution to equation (2.1) starting from x at $s = t$ exists, which

is denoted by $\{X_s^{t,x}, t \leq s \leq T\}$.

Take $f : [0,T] \times \mathbb{R}^n \times A \to \mathbb{R}$ and $g : \mathbb{R}^n \to \mathbb{R}$ two measurable functions with:
(i) g has a lower bound, or
(ii) g satisfies a quadratic growth condition: $|g(x)| \leq C(1 + |x|^2)$, $\forall x \in \mathbb{R}^n$, for some constant C independent of x.

For $(t,x) \in [0,T] \times \mathbb{R}^n$ the subset $\mathcal{A}(t,x) \subset \mathcal{A}$ contains controls α such that

$$E\left[\int_t^T |f(s, X_s^{t,x}, \alpha_s)|ds\right] < \infty \tag{2.5}$$

and we assume that this set is not empty for all $(t,x) \in [0,T] \times \mathbb{R}^n$.

The *gain function* on the finite domain is defined as

$$J(t,x,\alpha) := E\left[\int_t^T f(s, X_s^{t,x}, \alpha_s)ds + g(X_T^{t,x})\right], \tag{2.6}$$

for all $(t,x) \in [0,T] \times \mathbb{R}^n$ and $\alpha \in \mathcal{A}(t,x)$. The function f is a so-called *running profit function* and g is a *terminal reward function*. The objective of the finite horizon problem is to maximise the gain function over all admissible controls $\mathcal{A}(t,x)$. We introduce the so-called *value function*:

$$v(t,x) := \sup_{\alpha \in \mathcal{A}(t,x)} J(t,x,\alpha). \tag{2.7}$$

For an initial state $(t,x) \in [0,T) \times \mathbb{R}^n$ we say that $\hat{\alpha} \in \mathcal{A}(t,x)$ is an optimal control if $v(t,x) = J(t,x,\hat{\alpha})$. A control process α is called a Markovian control if it has the form $\alpha_s = a(s, X_s^{t,x})$ for some measurable function $a : [0,T] \times \mathbb{R}^n \to A$.

2.1.2 Infinite horizon problems

In this section the previous conditions are adjusted to the infinite horizon case. $\mathcal{A}_0$ denotes the set of control processes α, which satisfy

$$E\left[\int_0^T |b(0,\alpha_t)|^2 + |\sigma(0,\alpha_t)|^2 dt\right] < \infty, \qquad \forall T > 0. \tag{2.8}$$

For any initial condition $x \in \mathbb{R}^n$ at $t = 0$ and for all $\alpha \in \mathcal{A}_0$ a unique strong solution to equation (2.1) exists, which is denoted by $\{X_s^x, s \geq 0\}$.

Let $f : \mathbb{R}^n \times A \to \mathbb{R}$ be a measurable function and $\rho > 0$ be a discount factor. For $x \in \mathbb{R}^n$ the subset $\mathcal{A}(x) \subset \mathcal{A}_0$ contains controls α such that

$$E\left[\int_0^\infty e^{-\rho s}|f(X_s^x, \alpha_s)|ds\right] < \infty \tag{2.9}$$

and we assume that this set is not empty for all $x \in \mathbb{R}^n$. Again we define a *gain function*:

$$J(x,\alpha) := E\left[\int_0^\infty e^{-\rho s} f(X_s^x, \alpha_s)ds\right] \tag{2.10}$$

for all $x \in \mathbb{R}^n$ and $\alpha \in \mathcal{A}(x)$. In this case the *value function* is defined by:

$$v(x) := \sup_{\alpha \in \mathcal{A}(x)} J(x,\alpha). \tag{2.11}$$

The above equation formulates the infinite horizon problem. Given an initial state $x \in \mathbb{R}^n$, we say that $\hat{\alpha} \in \mathcal{A}(x)$ is an optimal control if $v(x) = J(x,\hat{\alpha})$. Here it is important to assume that the function $f(x,a)$ does not depend on time in order to get the stationarity of the problem.

2.2 Dynamic programming principle

A fundamental principle in the theory of stochastic control is Bellman's optimality principle, also called the dynamic programming principle and already mentioned in Section 1.2. It means that if one has taken an optimal control decision path until some arbitrary observation time θ, then, given this information, it remains optimal to use it after that observation time. With this principle we derive the Hamilton-Jacobi-Bellman equation in Section 2.3, but first we give a formal definition.

For $t \in [0,T]$, $T \leq \infty$, we denote by $\mathcal{T}_{t,T}$ the set of stopping times valued in $[t,T]$. When $t = 0$ and $T = \infty$ we use the notation $\mathcal{T} = \mathcal{T}_{0,\infty}$. In the context of controlled diffusion processes described in the previous section, but valid more generally for controlled Markov processes, the dynamic programming principle is stated as follows:

Theorem 2.1. *(Dynamic programming principle (DPP))*
Finite horizon: Let $(t,x) \in [0,T] \times \mathbb{R}^n$. Then we have

$$\begin{aligned} v(t,x) &= \sup_{\alpha \in \mathcal{A}(t,x)} \sup_{\theta \in \mathcal{T}_{t,T}} E\left[\int_t^\theta f(s, X_s^{t,x}, \alpha_s) ds + v(\theta, X_\theta^{t,x})\right] \\ &= \sup_{\alpha \in \mathcal{A}(t,x)} \inf_{\theta \in \mathcal{T}_{t,T}} E\left[\int_t^\theta f(s, X_s^{t,x}, \alpha_s) ds + v(\theta, X_\theta^{t,x})\right]. \end{aligned} \tag{2.12}$$

Infinite horizon: Let $x \in \mathbb{R}^n$. Then we have

$$\begin{aligned} v(x) &= \sup_{\alpha \in \mathcal{A}(x)} \sup_{\theta \in \mathcal{T}} E\left[\int_0^\theta e^{-\rho s} f(X_s^x, \alpha_s) ds + e^{-\rho\theta} v(X_\theta^x)\right] \\ &= \sup_{\alpha \in \mathcal{A}(x)} \inf_{\theta \in \mathcal{T}} E\left[\int_0^\theta e^{-\rho s} f(X_s^x, \alpha_s) ds + e^{-\rho\theta} v(X_\theta^x)\right], \end{aligned} \tag{2.13}$$

with the convention that $\exp(-\rho\theta) = 0$ when $\theta = \infty$.

The dynamic programming principle splits the optimisation problem in two parts. For the finite domain problem an optimal control may be obtained by first searching for an optimal control from a time θ given the state value $X_\theta^{t,x}$, in other words, compute $v(\theta, X_\theta^{t,x})$. Then the quantity $E\left[\int_t^\theta f(s, X_s^{t,x}, \alpha_s) ds + v(\theta, X_\theta^{t,x})\right]$ is maximised over all controls on $[t,\theta]$.

For some derivations in the sequel we will use a stronger version of the dynamic programming principle:

Theorem 2.2. *(Stronger version DPP (finite horizon))*
For all $\alpha \in \mathcal{A}(t,x)$ and $\theta \in \mathcal{T}_{t,T}$

$$v(t,x) \geq E\left[\int_t^\theta f(s, X_s^{t,x}, \alpha_s) ds + v(\theta, X_\theta^{t,x})\right]. \tag{2.14}$$

For all $\epsilon > 0$, there exists $\alpha \in \mathcal{A}(t,x)$ such that for all $\theta \in \mathcal{T}_{t,T}$

$$v(t,x) - \epsilon \leq E\left[\int_t^\theta f(s, X_s^{t,x}, \alpha_s) ds + v(\theta, X_\theta^{t,x})\right]. \tag{2.15}$$

The DPP has a clear intuitive meaning, but its rigorous proof is technical and has been studied by several authors and by different methods. The proof in [31] uses, among other things, the tower property of conditional expectations:

Theorem 2.3. *(Tower property of conditional expectations)[36]*
Let $(\Omega, \mathcal{F}, P)$ be a probability space and $\mathcal{G}$ a sub-σ-algebra of $\mathcal{F}$. If $\mathcal{H}$ is a sub-σ-algebra of $\mathcal{G}$ ($\mathcal{H}$ contains less information than $\mathcal{G}$) and X is an integrable random variable, then

$$E[E[X|\mathcal{G}]|\mathcal{H}] = E[X|\mathcal{H}]. \tag{2.16}$$

By this theorem of iterated conditional expectation we have for a given admissible control $\alpha \in \mathcal{A}(t,x)$ and for any stopping time θ in $[t,T]$:

$$J(t,x,\alpha) = E\left[\int_t^\theta f(s, X_s^{t,x}, \alpha_s)ds + J(\theta, X_\theta^{t,x}, \alpha)\right]. \tag{2.17}$$

This forms the beginning of the proof of the DPP.

2.3 Hamilton-Jacobi-Bellman equation

With the dynamic programming principle we can derive the Hamilton-Jacobi-Bellman (HJB) equation, see [31]. This second order, nonlinear partial differential equation is the infinitesimal version of the dynamic programming principle. In short, the HJB equation is derived by assuming that the value function is smooth enough, by applying Itô's formula to $v(s, X_s^{t,x})$ between $s = t$ and $s = t + h$ and then taking h to zero in the dynamic programming principle.

We start with the finite horizon problem and use the relation of the dynamic programming principle (2.14) with $\theta = t + h$ and a constant control $\alpha_s = a$, for some arbitrary a in A:

$$v(t,x) \geq E\left[\int_t^{t+h} f(s, X_s^{t,x}, a)ds + v(t+h, X_{t+h}^{t,x})\right]. \tag{2.18}$$

Assume that the value function v is sufficiently smooth, $v \in C^{1,2}([0,T] \times \mathbb{R}^n)$. Itô's formula ([36]) then reads

$$v(t+h, X_{t+h}^{t,x}) = v(t,x) + \int_t^{t+h} \left(\frac{\partial v}{\partial t} + \mathcal{L}^a v\right)(s, X_s^{t,x})ds + \text{ (local) martingale}, \tag{2.19}$$

with differential operator of second order

$$\begin{aligned} \mathcal{L}^a v(t,x) &= b(x,a).D_x v(t,x) + \frac{1}{2}\text{tr}(\sigma\sigma'(x,a)D_x^2 v(t,x)) \\ &= \sum_{i=1}^n b_i(x,a)\frac{\partial v}{\partial x_i}(t,x) + \frac{1}{2}\sum_{i,j=1}^n (\sigma\sigma')_{ij}(x,a)\frac{\partial^2 v}{\partial x_i \partial x_j}(t,x), \end{aligned} \tag{2.20}$$

where $\sigma\sigma'(x,a)$ is an $n \times n$ matrix with components $(\sigma\sigma')_{ij}(x,a) = \sum_{k=1}^d \sigma_{ik}(x,a)\sigma_{jk}(x,a)$. $\mathcal{L}^a$ is called the infinitesimal generator associated to the diffusion X_t with constant control a. The vector D_x denotes the gradient of a function and matrix D_x^2 consists of its the second derivatives. Substituting equation (2.19) into equation (2.18) gives

$$\begin{aligned} v(t,x) &\geq E\left[\int_t^{t+h} f(s, X_s^{t,x}, a)ds + v(t,x) + \int_t^{t+h} \left(\frac{\partial v}{\partial t} + \mathcal{L}^a v\right)(s, X_s^{t,x})ds\right] \\ &= v(t,x) + E\left[\int_t^{t+h} f(s, X_s^{t,x}, a)ds + \int_t^{t+h} \left(\frac{\partial v}{\partial t} + \mathcal{L}^a v\right)(s, X_s^{t,x})ds\right] \end{aligned} \tag{2.21}$$

and we get

$$0 \geq E\left[\int_t^{t+h} f(s, X_s^{t,x}, a)ds + \int_t^{t+h} \left(\frac{\partial v}{\partial t} + \mathcal{L}^a v\right)(s, X_s^{t,x})ds\right]. \tag{2.22}$$

Dividing by h, taking the limit $h \to 0$ and interchanging limit and expectation results, according to the mean-value theory, in

$$0 \geq \frac{\partial v}{\partial t}(t,x) + \mathcal{L}^a v(t,x) + f(t,x,a). \tag{2.23}$$

Since $a \in A$ was arbitrary we obtain the inequality:

$$-\frac{\partial v}{\partial t}(t,x) - \sup_{a \in A}[\mathcal{L}^a v(t,x) + f(t,x,a)] \geq 0. \tag{2.24}$$

Now suppose that α^* is an optimal control with X_t^* the associated state solution to equation (2.1) starting from x at time t. Using this control we have equality signs instead of the preceding inequality signs and we find by similar arguments

$$-\frac{\partial v}{\partial t}(t,x) - \mathcal{L}^{\alpha_t^*} v(t,x) + f(t,x,\alpha_t^*) = 0. \tag{2.25}$$

The equations (2.24) and (2.25) result, if the above supremum in a is finite, in the *regular* case

$$-\frac{\partial v}{\partial t}(t,x) - \sup_{a \in A}[\mathcal{L}^a v(t,x) + f(t,x,a)] = 0, \qquad \forall (t,x) \in [0,T) \times \mathbb{R}^n. \tag{2.26}$$

This is often written as:

$$-\frac{\partial v}{\partial t}(t,x) - H(t,x,D_x v(t,x), D_x^2 v(t,x)) = 0, \qquad \forall (t,x) \in [0,T) \times \mathbb{R}^n, \tag{2.27}$$

where for $(t,x,p,M) \in [0,T] \times \mathbb{R}^n \times \mathbb{R}^n \times \mathcal{S}_n$ ($\mathcal{S}_n$ is the set of symmetric $n \times n$ matrices)

$$H(t,x,p,M) = \sup_{a \in A}[b(x,a).p + \frac{1}{2}\mathrm{tr}(\sigma\sigma'(x,a)M) + f(t,x,a)]. \tag{2.28}$$

The function H is called the *Hamiltonian* of the associated control problem. Equation (2.27) is the *Hamilton-Jacobi-Bellman (HJB) equation*, also called the dynamic programming equation. The a priori regular terminal condition reads $v(T,x) = g(x)$, $\forall x \in \mathbb{R}^n$, resulting from the definition of the value function.

In the examples described at the end of Section 2 the running profit function f and a terminal reward function g are often multiplied by a discount factor and the gain function J has the general form

$$J(t,x,\alpha) = E\left[\int_t^T \Gamma(t,s) f(s, X_s^{t,x}, \alpha_s) ds + \Gamma(t,T) g(X_T^{t,x})\right] \tag{2.29}$$

$$\text{with } \Gamma(t,s) = \exp\left(-\int_t^s \rho(u, X_u^{t,x}, \alpha_u) du\right), \qquad t \leq s \leq T,$$

where ρ is a measurable function on $[0,T] \times \mathbb{R}^n \times A$. Then the Hamiltonian associated to the stochastic control problem is

$$H(t,x,v,p,M) = \sup_{a \in A}[-\rho(t,x,a)v + b(x,a).p + \frac{1}{2}\mathrm{tr}(\sigma\sigma'(x,a)M) + f(t,x,a)]. \tag{2.30}$$

Control space unbounded

The Hamiltonian $H(t,x,p,M)$ is typically finite when the control set A is bounded. When the control space A is unbounded the Hamiltonian $H(t,x,p,M)$ may take the value ∞ in some domain of (t,x,p,M). Assume there exists a continuous function $G(t,x,p,M)$ on $[0,T] \times \mathbb{R}^n \times \mathbb{R}^n \times \mathcal{S}_n$ such that

$$H(t,x,p,M) < \infty \Longleftrightarrow G(t,x,p,M) \geq 0. \tag{2.31}$$

From the derivation of HJB equation (2.27) we must have

$$G(t,x,D_x v(t,x),D_x^2 v(t,x)) \geq 0, \tag{2.32}$$

$$\text{and} \quad -\frac{\partial v}{\partial t}(t,x) - H(t,x,D_x v(t,x),D_x^2 v(t,x)) \geq 0. \tag{2.33}$$

If the first inequality, (2.32), is strict at some $(t,x) \in [0,T) \times \mathbb{R}^n$, we should have equality in the second equation. We thus obtain a *variational inequality* for the Hamilton-Jacobi-Bellman equation (HJB-VI):

$$\min\left[-\frac{\partial v}{\partial t}(t,x) - H(t,x,D_x v(t,x),D_x^2 v(t,x)),\, G(t,x,D_x v(t,x),D_x^2 v(t,x))\right] = 0. \tag{2.34}$$

In this case we say that the control problem is *singular*. The value function is generally discontinuous at T, so that $v(T,x) = g(x)$ is not the relevant terminal condition. In [31] the HJB equation is discussed in the weak viscosity sense where we do not need a priory regularity of the value function. There also the correct terminal condition is derived.

Minimisation problem
The HJB equation to the minimisation problem on the finite horizon,

$$v(t,x) = \inf_{\alpha \in \mathcal{A}(t,x)} E\left[\int_t^T f(s,X_s^{t,x},\alpha_s)ds + g(X_T^{t,x})\right], \tag{2.35}$$

can be derived by looking at the maximisation problem of the value function $-v$. We arrive at the equation

$$-\frac{\partial v}{\partial t}(t,x) - H(t,x,D_x v(t,x),D_x^2 v(t,x)) = 0, \qquad \forall (t,x) \in [0,T) \times \mathbb{R}^n, \tag{2.36}$$

with Hamiltonian function

$$H(t,x,p,M) = \inf_{a \in A}[b(x,a).p + \frac{1}{2}\text{tr}(\sigma\sigma'(x,a)M) + f(t,x,a)]. \tag{2.37}$$

Infinite horizon problem
The Hamilton-Jacobi-Bellman equation for value function (2.11) on the infinite domain is derived using similar arguments:

$$\rho v(x) - H(x,D_x v(x),D_x^2 v(x)) = 0, \qquad \forall x \in \mathbb{R}^n, \tag{2.38}$$

with for $(x,p,M) \in \mathbb{R}^n \times \mathbb{R}^n \times \mathcal{S}_n$

$$H(t,x,p,M) = \sup_{a \in A}[b(x,a).p + \frac{1}{2}\text{tr}(\sigma\sigma'(x,a)M) + f(x,a)]. \tag{2.39}$$

The classical approach to solving optimal control problems starts by showing the existence of a smooth solution to the Hamilton-Jacobi-Bellman equation by partial differential equation (PDE) techniques. Then the Verification Theorem shows that the smooth solution is indeed the value function. This approach, and the viscosity solutions approach, are briefly discussed in the next section.

2.3.1 Verification Theorem and viscosity approach

The classical verification approach consists of finding a smooth solution to the HJB equation and to check by means of the Verification Theorem that this candidate, under suitable sufficient conditions, coincides with the value function $v(t,x)$. As a byproduct, we obtain an optimal Markovian control. The following Verification Theorem on the finite domain can be found in [31], with $v(t,x)$ as in equation (2.7):

Theorem 2.4. *(Verification Theorem (finite horizon))*
Let w be a function in $C^{1,2}([0,T)\times\mathbb{R}^n)\cap C^0([0,T]\times\mathbb{R}^n)$ satisfying a quadratic growth condition, i.e., there exists a constant C such that

$$|w(t,x)| \leq C(1+|x|^2), \qquad \forall (t,x)\in[0,T]\times\mathbb{R}^n. \tag{2.40}$$

(i) Suppose that

$$\begin{aligned} -\frac{\partial w}{\partial t}(t,x) - \sup_{a\in A}[\mathcal{L}^a w(t,x) + f(t,x,a)] &\geq 0, \qquad (t,x)\in[0,T)\times\mathbb{R}^n, &(2.41)\\ w(T,x) &\geq g(x), \qquad x\in\mathbb{R}^n. &(2.42)\end{aligned}$$

Then $w\geq v$ on $[0,T]\times\mathbb{R}^n$.
(ii) Suppose further that $w(T,.)=g(.)$ and there exists a measurable function $\hat{\alpha}(t,x)$, $(t,x)\in[0,T)\times\mathbb{R}^n$, valued in A such that

$$\begin{aligned} -\frac{\partial w}{\partial t}(t,x) - \sup_{a\in A}[\mathcal{L}^a w(t,x) + f(t,x,a)] &= -\frac{\partial w}{\partial t}(t,x) - [\mathcal{L}^{\hat{\alpha}(t,x)} w(t,x) + f(t,x,\hat{\alpha}(t,x))]\\ &= 0, &(2.43)\end{aligned}$$

and the SDE

$$dX_s = b(X_s,\hat{\alpha}(s,X_s))ds + \sigma(X_s,\hat{\alpha}(s,X_s))dW_s \tag{2.44}$$

admits a unique solution, denoted by $\hat{X}_s^{t,x}$, given an initial condition $X_t=x$, and the process $\{\hat{\alpha}(s,\hat{X}_s^{t,x}), t\leq s\leq T\}$ lies in $\mathcal{A}(t,x)$. Then $w=v$ on $[0,T]\times\mathbb{R}^n$ and $\hat{\alpha}$ is an optimal Markovian control.

The proof of this theorem relies mainly on Itô's formula. The Verification Theorem for the infinite case is defined likewise. The classical Verification Theorem allows us to solve control problems where one can find, or at least there exists, a smooth solution to the associated HJB equation. The first and most famous application in finance of this Verification Theorem for stochastic control problems is Merton's portfolio allocation problem, which we will discuss in Section 2.6.

Before this we derived the Hamilton-Jacobi-Bellman equation using the dynamic programming principle and we just discussed the classical verification approach, which has its limitations. The main drawback of this method is the assumption of an a priori existence of a smooth solution to the HJB equation. This is not necessarily true, not even in very simple cases. Then, the classical verification approach does not work and we need to relax the notion of solution to the HJB equation. A suitable class of weak solutions is the one of *viscosity solutions*. The notion of viscosity solutions was introduced by P.L. Lions ([24]).

For a general introduction to viscosity solutions and some general uniqueness and existence results we refer to [6]. Reference [31] explains that we do not need a priory the continuity of the value function in the viscosity approach, since we work with the lower and upper semi-continuous envelopes. They prove that the value function from the stochastic optimisation problems satisfies the associated HJB equation in the viscosity sense and determine the relevant terminal condition. It is not always easy to know *a priori* details about the continuity of the value function. Therefore one often works with the notion of viscosity solutions.

We will not pay attention to the verification and viscosity solutions approaches in the other sections (except for Section 2.6), because later on we will consider another method, based on the dynamic programming principle.

2.4 Optimal stopping and impulse control problems

In this section we extend the notion of stochastic optimisation problems with the concepts of optimal stopping and impulse control problems. Now the controller does not only have the disposal of control α

to optimise his objective, but he can also determine the terminal time or can add extra impulses to the state process. We discuss only the finite horizon cases, but similar theory holds for the infinite horizon problems.

2.4.1 Optimal stopping problems

We define the optimal stopping problem, where the controller may also decide directly the terminal time of his objective ([31]). This field of stochastic control received renewed interest due to its application in finance and economy, from asset pricing (e.g., American options, Section 2.7) to firm investment and also to real options.

We start with the case where there is no control α and the controller only has control over his terminal time. Consider the diffusion process on $\mathbb{R}^n$ given by

$$dX_t = b(X_t)dt + \sigma(X_t)dW_t, \tag{2.45}$$

with W a d-dimensional Brownian motion on the filtered probability space $(\Omega, \mathcal{F}, \mathbb{F} = (\mathcal{F}_t)_{t\geq 0}, P)$. The coefficients b and σ satisfy the same Lipschitz conditions as before. For $t \in [0,T]$ we denote by $\mathcal{T}_{t,T}$ the set of stopping times valued in $[t,T]$. The finite horizon optimal stopping problem is then formulated as

$$v(t,x) = \sup_{\tau \in \mathcal{T}_{t,T}} E\left[\int_t^\tau e^{-\rho(s-t)} f(s, X_s^{t,x})ds + e^{-\rho(\tau-t)} g(X_\tau^{t,x})\right], \qquad (t,x) \in [0,T] \times \mathbb{R}^n. \tag{2.46}$$

Note that we incorporate a discount factor $\rho \geq 0$. The value function v is related to the HJB variational inequality (HJB-VI):

$$\min[-v_t + \rho v - \mathcal{L}v - f,\, v - g] = 0, \tag{2.47}$$

with $\mathcal{L}v = b(x).D_x v + \frac{1}{2}\text{tr}(\sigma\sigma'(x)D_x^2 v)$. This means that $-v_t + \rho v - \mathcal{L}v - f = 0$ holds in the domain $\mathcal{C} = \{(t,x) \in [0,T] \times \mathbb{R}^n : v(t,x) > g(x)\}$ with $v = g$ on the boundary of $\mathcal{C}$. The problem is called a *free boundary problem*, since the boundary is unknown. $\mathcal{C}$ is called the continuation region, since it coincides with the state values for which it is optimal to let the process continue. The complement set $\mathcal{S} = \{(t,x) \in [0,T] \times \mathbb{R}^n : v(t,x) = g(x)\}$ is called the *stopping*, or *exercise region*. This region matches with the state values for which it is optimal to stop the process and receive the reward g.

Consider now the case in which the controller also has the disposal of a control α and the state process dX_t depends on α as in (2.1). The value function of the mixed control, composed of the pair control and stopping time (α, τ), may be written as

$$v(t,x) = \sup_{\tau \in \mathcal{T}_{t,T}, \alpha \in \mathcal{A}(t,x)} E\left[\int_t^\tau e^{-\rho(s-t)} f(s, X_s^{t,x}, \alpha_s)ds + e^{-\rho(\tau-t)} g(X_\tau^{t,x})\right], \qquad (t,x) \in [0,T] \times \mathbb{R}^n. \tag{2.48}$$

Then the associated HJB-VI equation reads

$$\min[-v_t + \rho v - \sup_{a \in A}[\mathcal{L}^a v + f(t,x,a)],\, v - g] = 0. \tag{2.49}$$

2.4.2 Stochastic impulse control problems

In the previous sections the state process changes continuously in time in response to the control effort. However, in practice this may be discontinuous. For example, an investor cannot invest continuously in assets or stocks, but only at discrete times. In the stochastic impulse control problem we can act on the state process X_t by choosing stopping times t_m at which the current state is immediately modified by an additive impulse ξ_m. Information about impulse control problems can be found in [21] and [2].

At every stopping time $t_m \in [0,T)$, $m \in \mathbb{N}$, there is an impulse ξ_m and the state process reads

$$\begin{aligned} dX_t &= b(X_t,\alpha_t)dt + \sigma(X_t,\alpha_t)dW_t, && \text{for } t \in (t_m, t_{m+1}), \\ X_{t_m} &= X_{t_m^-} + \xi_m, && m \in \mathbb{N}. \end{aligned} \tag{2.50}$$

Here X_{t^-} is the value of the process as it approaches t from the left. The stochastic process is càdlàg, that is right continuous with left limits. This is different from the stochastic control problem in the previous sections, where the controller could only influence the drift and/or diffusion terms of the state process and the resulting controlled diffusion remains a continuous process. Here the controlled process has a jump of size ξ_m at control time t_m, but the drift and diffusion terms remain unchanged by the impulses. The impulse control strategy is given by the triplet $\beta = (\alpha, \{t_m\}, \{\xi_m\})$ and $\mathcal{B}$ is the set of all β such that $\alpha \in \mathcal{A}(t,x)$ and

$$t_m \in [0,T),\ t_{m+1} \geq t_m,\ \xi_m \in \mathbb{R}^n. \tag{2.51}$$

The sequence $(\xi_m)_{m\geq 1}$ consists of $\mathcal{F}_{t_m}$-measurable random variables and t_m is a stopping time with respect to the filtration $\mathbb{F}$. Often there are practical restrictions on the size of impulses and $\xi_m \in B \subset \mathbb{R}^n$. Performing an impulse involves certain costs c. The term 'costs' can be confusing, because it can also represent revenues. The impulse costs $c : \mathbb{R}^n \times \mathbb{R}^n \to \mathbb{R}$ are assumed to satisfy the inequality $c(x,\xi_i+\xi_j) \geq c(x,\xi_i) + c(x,\xi_j), \forall \xi_i, \xi_j \in \mathbb{R}^n$. This states that it is more profitable to perform directly two impulses rather than execute them in two steps.

The objective function is represented by

$$J(t,x,\beta) = E^{t,x}\left[\int_t^T e^{-\rho(s-t)} f(s,X_s,\alpha_s)ds + \sum_{t\leq t_m<T} c(X_{t_m^-},\xi_m)e^{-\rho(t_m-t)} + e^{-\rho(T-t)}g(X_T)\right], \tag{2.52}$$

$\forall (t,x) \in [0,T]\times\mathbb{R}^n$. For ease of notation we use the form $E^{t,x}[X_s]$ instead of $E[X_s^{t,x}]$. The objective is to maximise this gain function over all controls $\beta \in \mathcal{B}$ and the value function is

$$v(t,x) = \sup_{\beta\in\mathcal{B}} J(t,x,\beta). \tag{2.53}$$

We define the intervention operator $\mathcal{M}$ via:

$$\mathcal{M}v(t,x) := \sup_{\xi}(v(t,x+\xi) + c(x,\xi)). \tag{2.54}$$

This represents the value of the strategy that consists of performing the best immediate action and behaving optimally afterwards. There could be states x for which it is not optimal to have an immediate action, this yields $v(t,x) \geq \mathcal{M}v(t,x)$. At the first time after t when it is optimal to execute an impulse, v and $\mathcal{M}v$ must coincide and the optimal action is equal to the optimal immediate action. We get the following variant of the dynamic programming principle:

$$v(t,x) = \sup_{\tau\in[t,T],\alpha\in\mathcal{A}(t,x)} E^{t,x}\left[\int_t^\tau e^{-\rho(s-t)} f(s,X_s,\alpha_s)ds + e^{-\rho(\tau-t)}\mathcal{M}v(\tau,X_{\tau^-})\right]. \tag{2.55}$$

We see that the impulse control problem is reduced to an optimal stopping problem, but this is not very helpful since the reward function $\mathcal{M}v(\tau,X_{\tau^-}^{t,x})$ is still unknown. However, this version of the dynamic programming principle helps us to derive a HJB equation heuristically. We find that the impulse control problem is associated to a Hamilton-Jacobi-Bellman *quasi-variational inequality* (HJB-QVI):

$$\min\left[-v_t(t,x) + rv(t,x) - \sup_{a\in A}[\mathcal{L}^a v(t,x) + f(t,x,a)],\ v(t,x) - \mathcal{M}v(t,x)\right] = 0,\ (t,x) \in [0,T)\times\mathbb{R}^n, \tag{2.56}$$

with terminal condition

$$v(T,x) = g(x), \qquad \forall x \in \mathbb{R}^n. \tag{2.57}$$

Verification theorems for the impulse control problem can be found in [39]. Under certain conditions for σ, b and f the value function v is a viscosity solution to the HJB-QVI (see [21]).

The minimisation problem with $v(t,x) = \inf_{\beta\in\mathcal{B}} J(t,x,\beta)$ is quite similar. Then we assume $c(x,\xi_i + \xi_j) \leq c(x,\xi_i) + c(x,\xi_j), \forall \xi_i, \xi_j \in \mathbb{R}^n$ and get maximum and infimum statements instead of minimum and supremum, respectively.

2.4.3 Impulse control problems under jump diffusions

In the previous sections we used the diffusion process dX_t from equation (2.1). Here we extend the impulse control theory to *jump diffusion processes* with one jump process, without control α:

$$X_t = X_0 + \int_0^t b(s,X_s)ds + \int_0^t \sigma(s,X_s)dW_s + \int_0^t z(s,X_{s^-},\Upsilon_s)dq_s, \tag{2.58}$$

or in differential notation

$$dX_t = b(t,X_t)dt + \sigma(t,X_t)dW_t + z(t,X_{t^-},\Upsilon_t)dq_t, \tag{2.59}$$

where q_t is an independent Poisson process with intensity rate λ and measures the number of jumps that took place before time t. $z(t,X_{t^-},\Upsilon_t)$ is the magnitude of a jump realisation, which is a function depending on t, X_{t^-} and random variable Υ_t that can have some arbitrarily specified distribution independent of both dW_t and dq_t. The integrals are assumed to exist. The first integral is interpreted as a Riemann integral, the second is an Itô integral, and the last one in (2.58) is notation for:

$$\int_0^t z(s,X_{s^-},\Upsilon_s)dq_s = \sum_{j=1}^{q_t} z(\tau_j, X_{\tau_j^-},\Upsilon_{\tau_j}), \tag{2.60}$$

where τ_j for $j = 1,...,q_t$ are the times when a jump takes place and Υ_{τ_j} are i.i.d. variables. Itô's formula reads

Theorem 2.5. *(Itô's formula for jump diffusion processes)[36]*
Let X be a diffusion process with jumps,

$$X_t = X_0 + \int_0^t b(s,X_s)ds + \int_0^t \sigma(s,X_s)dW_s + \int_0^t z(s,X_{s^-},\Upsilon_s)dq_s, \tag{2.61}$$

where b and σ are continuous non-anticipating processes with

$$E\left[\int_0^T \sigma(t,X_t)^2 dt\right] < \infty.$$

Then, for any $C^{1,2}$ function $f : [0,T]\times\mathbb{R} \to \mathbb{R}$, the process $f(t,X_t)$ can be represented as:

$$f(t,X_t) = f(0,X_0) + \int_0^t \left(\frac{\partial f}{\partial t} + \mathcal{L}f\right)(s,X_s)ds + \int_0^t \frac{\partial f}{\partial x}\sigma(s,X_s)dW_s + \sum_{0<s\leq t}[f(s,X_s) - f(s,X_{s^-})], \tag{2.62}$$

with $f(s,X_s) = f\Big(s, X_{s^-} + z(s,X_{s^-},\Upsilon_s)dq_s\Big)$. In differential notation:

$$\begin{aligned} df(t,X_t) &= \frac{\partial f}{\partial t}(t,X_t)dt + \frac{\partial f}{\partial x}b(t,X_t)dt \\ &+ \frac{1}{2}\frac{\partial^2 f}{\partial x^2}\sigma^2(t,X_t)dt + \frac{\partial f}{\partial x}\sigma(t,X_t)dW_t + [f(t,X_t) - f(t,X_{t^-})]dq_t. \end{aligned} \tag{2.63}$$

We consider the value function of the impulse control problem as before, but now without control α,

$$v(t,x) = \sup_{\beta\in\mathcal{B}} E^{t,x}\left[\int_t^T e^{-\rho(s-t)}f(s,X_s)ds + \sum_{t\le t_m<T} c(X_{t_m^-},\xi_m)e^{-\rho(t_m-t)} + e^{-\rho(T-t)}g(X_T)\right], \quad (2.64)$$

where $\mathcal{B}$ is the set of admissible control times and impulses $\{t_m, \xi_m\}$.

In the derivation of the Hamilton-Jacobi-Bellman equation in Section 2.3 Itô's formula for diffusion processes was used to calculate $E[v(t+h, X_{t+h}^{t,x})]$. Now we use Itô formula for jump diffusion processes and get:

$$E[v(t+h,X_{t+h}^{t,x})] = v(t,x) + E\left[\int_t^{t+h}(v_t+\mathcal{L}v)(s,X_s^{t,x})ds + \sum_{t<s\le t+h}[v(s,X_s)-v(s,X_{s^-})]\right]. \quad (2.65)$$

The theorem about the mean of stochastic jump integrals in [13] gives

$$E\left[\int_t^{t+h}(v(s,X_s)-v(s,X_{s^-}))dq_s\right] = \lambda\int_t^{t+h}E\left[v(s,X_s)-v(s,X_{s^-})\right]ds. \quad (2.66)$$

Dividing by h and sending h to zero gives:

$$\lim_{h\to 0}\frac{1}{h}E[v(t+h,X_{t+h}^{t,x})] = v(t,x) - \frac{\partial v}{\partial t}(t,x) + \mathcal{L}v(t,x) + \lambda E[v(t,x+z(t,x,\Upsilon))-v(t,x)], \quad (2.67)$$

where the expectation is taken with respect to stochastic variable Υ. The associated HJB equation is

$$\min\Big[-v_t(t,x)+\rho v(t,x)-\mathcal{L}v(t,x)-\lambda E[v(t,x+z(t,x,\Upsilon))-v(t,x)]-f(t,x), \\ v(t,x)-\mathcal{M}v(t,x)\Big] = 0, \qquad (t,x)\in[0,T)\times\mathbb{R}^n, \quad (2.68)$$

with terminal condition

$$v(T,x) = g(x), \qquad \forall x\in\mathbb{R}^n. \quad (2.69)$$

The above can easily be extended with a control process α. In [28] and [35] a broader class of stochastic optimisation problems under the more general jump diffusion processes is discussed. An impulse control problem under jump diffusion with a delayed reaction is studied in [29]. This means that there is a delay between the time when a decision for intervention is taken and the time when the intervention is actually carried out.

2.4.4 Impulse control problems including 'extreme events'

Suppose that instead of the running profit function f in gain function (2.64) we have so-called *extreme events* at times τ_i, modelled by a Poisson process with intensity rate λ, at which a certain amount is added to the gain function. Examples of extreme events in Section 2.8 and Section 3 are forest fires and floods. The value function is written as

$$v(t,x) = \sup_{\beta\in\mathcal{B}} E^{t,x}\left[\sum_{\tau_i\in[t,T]} e^{-\rho(\tau_i-t)}\eta(\tau_i,X_{\tau_i^-},\Theta_{\tau_i}) + \sum_{t\le t_m<T} c(X_{t_m^-},\xi_m)e^{-\rho(t_m-t)} + e^{-\rho(T-t)}g(X_T)\right], \quad (2.70)$$

where $\eta(t,X_{t^-},\Theta_t)$ is a function depending on t, X_{t^-} and random variable Θ_t. The values Θ_{τ_i} are i.i.d. and represent the costs of an extreme event. $\mathcal{B}$ is the set of all $\beta = (\{t_m\},\{\xi_m\})$ without control process α, which can easily be added to the results. In the derivation of the HJB equation we get the term

$$E^{t,x}\left[\sum_{\tau_i\in[t,t+h]} e^{-\rho(\tau_i-t)}\eta(\tau_i,X_{\tau_i^-},\Theta_{\tau_i})\right] = E^{t,x}\left[\int_t^{t+h} e^{-\rho(s-t)}\eta(s,X_{s^-},\Theta_s)dq_s\right]. \quad (2.71)$$

Dividing this by h, sending h to zero and interchanging limit and expectation gives (by [13]):

$$\begin{aligned}\lim_{h\to 0}\frac{1}{h}E^{t,x}\left[\sum_{\tau_i\in[t,t+h]} e^{-\rho(\tau_i-t)}\eta(\tau_i, X_{\tau_i^-}, \Theta_{\tau_i})\right] &= \lim_{h\to 0}\frac{1}{h}\lambda\int_t^{t+h} e^{-\rho(s-t)}E^{t,x}[\eta(s, X_{s^-}, \Theta_s)]ds \\ &= \lambda E[\eta(t,x,\Theta)]. \end{aligned} \tag{2.72}$$

We end this section with the HJB equation associated to value function (2.70):

$$\min\Big[-v_t(t,x)+\rho v(t,x)-\mathcal{L}v(t,x)-\lambda E[\eta(t,x,\Theta)],\ v(t,x)-\mathcal{M}v(t,x)\Big]=0, \qquad (t,x)\in[0,T)\times\mathbb{R}^n. \tag{2.73}$$

with terminal condition

$$v(T,x)=g(x), \qquad \forall x\in\mathbb{R}^n. \tag{2.74}$$

2.5 Examples of stochastic optimisation problems

In the next sections we discuss three examples of stochastic optimisation problems. The first example is the well-known portfolio allocation problem of Merton, where the Verification Theorem is applied to verify a candidate solution. The second example is also a financial problem. There the price of European options is derived, whereby the holder tries to maximise his expected payoff. The third example does not stem from the financial world but there are obvious similarities. Namely, in the harvesting problem optimal forest harvesting decisions have to be made. This problem can be viewed in the context of the real options approach, where we try to calculate the real option value by representing it as a value function. In Section 3 we will consider a similar problem, the dike height problem, where the costs of land protection against floods are minimised.

For the derivation of partial differential equations for the option values in the last two examples we discuss two different methods. In the first method the option price is formulated as a stochastic optimisation problem. With the theory from the previous sections the associated HJB equations can be derived. This is called the *dynamic programming approach*, referring to the dynamic programming principle which is used to derive the HJB equations. The second method is called the *contingent claims approach*. For this we assume that the asset markets are rich enough to hedge the risks and that the market will not reward the investor for holding his risky asset. This approach, together with the complete market assumption, is sometimes preferred to the dynamic programming approach, because no risk adjusted discount rate needs to be determined.

2.6 Example 1: Merton's portfolio allocation problem

The portfolio allocation problem is originally formulated and studied by Merton ([27]) and we solve it by using the classical verification method. Merton considered a portfolio consisting of riskless bonds and risky stocks. The value of the wealth at time t is denoted by X_t. At any time t the agent invests a proportion $\alpha_t\in A$, with A a closed convex subset of $\mathbb{R}$, of his wealth in risky stocks of price S_t and $1-\alpha_t$ in bonds of price S_t^0 with riskless interest rate r. The stock price follows a geometric Brownian motion $dS_t=\mu S_t dt+\sigma S_t dW_t$. The dynamics of his wealth are given by

$$\begin{aligned} dX_t &= \frac{X_t\alpha_t}{S_t}dS_t+\frac{X_t(1-\alpha_t)}{S_t^0}dS_t^0 \\ &= \frac{X_t\alpha_t}{S_t}(\mu S_t dt+\sigma S_t dW_t)+\frac{X_t(1-\alpha_t)}{S_t^0}rS_t^0 dt \\ &= X_t(\alpha_t\mu+(1-\alpha_t)r)dt+X_t\alpha_t\sigma dW_t. \end{aligned} \tag{2.75}$$

The agent wants to maximise his expected utility from terminal wealth X_T at terminal time $T<\infty$. The utility function $U(.)$ is nondecreasing and concave on $\mathbb{R}_+$. This formulates the risk aversion of the

agent. The objective is given by the value function

$$v(t,x) = \sup_{\alpha \in \mathcal{A}(t,x)} J(t,x,\alpha) = \sup_{\alpha \in \mathcal{A}(t,x)} E[U(X_T^{t,x})], \qquad (t,x) \in [0,T] \times \mathbb{R}. \tag{2.76}$$

The problem is equivalent to an optimal control problem with gain function (2.6), with $f \equiv 0$ and $g(X_T^{t,x}) = U(X_T^{t,x})$. The associated HJB equation for this stochastic control problem is

$$-\frac{\partial w}{\partial t} - \sup_{a \in A}[\mathcal{L}^a w(t,x)] = 0 \quad \text{with terminal condition} \quad w(T,x) = U(x), \qquad x \in \mathbb{R}. \tag{2.77}$$

The diffusion generator reads $\mathcal{L}^a w(t,x) = (a\mu + (1-a)r)xw_x + \frac{1}{2}x^2\sigma^2 a^2 w_{xx}$. We switched to a notation with w to stay in line with the Verification Theorem 2.4. Next we will show that $w = v$.

Merton considered power utility functions of constant relative risk aversion (CRRA) type:

$$U(x) = \frac{x^p}{p}, \qquad x \geq 0,\ p < 1,\ p \neq 0. \tag{2.78}$$

For this utility function one can find explicitly a smooth solution to problem (2.77). To find this solution we start with a candidate solution of the form $w(t,x) = \phi(t)U(x)$, for some positive function ϕ. Substituting this into equation (2.77) we derive the following ordinary differential equation for ϕ

$$\phi'(t) + q\phi(t) = 0, \quad \phi(T) = 1, \tag{2.79}$$

$$\text{with } q = p \sup_{a \in A}[a(\mu - r) + r - \frac{1}{2}a^2(1-p)\sigma^2] := p \sup_{a \in A} y(a).$$

We obtain $\phi(t) = \exp(q(T-t))$. The value function $w(t,x) = \exp(q(T-t))U(x)$ is a smooth solution to equation (2.77) and it is strictly increasing and concave in x. The function $a \in A \mapsto y(a)$ is strictly concave on the closed convex set A and thus attains its maximum at some constant $\hat{a}$. It follows that $\hat{a}$ attains the supremum of $\sup_{a \in A}[\mathcal{L}^a w(t,x)]$. The wealth processes X_t associated with this constant control $\hat{a}$ admits a unique solution given an initial condition. The Verification Theorem 2.4 tells us that the value function to the portfolio allocation maximisation problem (2.76) is equal to $w(t,x)$ and $\hat{a}$ is an optimal Markovian control. In other words, the optimal proportion of wealth to invest in stock is constant given by $\hat{a}$. Finally, when $A = \mathbb{R}$ we can find explicitly the optimal control:

$$\hat{\alpha} = \frac{\mu - r}{\sigma^2(1-p)}. \tag{2.80}$$

2.7 Example 2: European call and put options

In the financial markets, traders buy and sell stocks and options. An option is a contract between a buyer and a seller that gives the buyer the right, but not the obligation, to buy or to sell a particular asset on or before the option's expiration date, at an agreed price. Many different options exist, the most well-known options being the European call and put options.

Definition 2.1. *(European call (put) option)*
A European call (put) option gives its holder the right, but not the obligation, to buy from (sell to) the writer a prescribed asset for a prescribed price at a prescribed time in the future.

The prescribed asset is called the underlying asset with value X_t at time t, the agreed price is the strike price K and the prescribed time is the expiration time T. The price of an option at time t is denoted by value function $v(t,x)$. We consider the price of a European put option with payoff at expiration time T equal to $g(X_T) = (K - X_T)^+$. A similar analysis holds for call options for which the payoff reads $g(X_T) = (X_T - K)^+$. The asset price is as usually described by a geometric Brownian motion:

$$dX_t = \mu X_t dt + \sigma X_t dW_t. \tag{2.81}$$

We use the dynamic programming approach and the contingent claims approach to price the option.

2.7.1 Dynamic programming approach

The first way to derive the European put option price is by using the dynamic programming, or the expected value approach. This approach can be used if the market is not complete and it is not possible to hedge the option. The option price is then calculated as the discounted expected payoff with respect to the true state process (2.81), that is under the true world measure $\mathbb{P}$. The value function is denoted by:

$$v(t,x) = E^{\mathbb{P}}[e^{-\rho(T-t)}(K - X_T^{t,x})^+], \qquad (t,x) \in [0,T] \times \mathbb{R}. \tag{2.82}$$

The risk adjusted discount rate ρ reflects the return required by the holder to hold the risky option. The control space A is reduced to a singleton $\{a_0\}$, since there is no control on the asset price X_t. There are no decisions to be made by the holder of the option, he just has to wait to expiration time T. Compared with gain function (2.29) we find that for $f \equiv 0$, $g(X_T^{t,x}) = (K - X_T^{t,x})^+$ and $\Gamma(t,s) = e^{-\rho(s-t)}$ the HJB equation is reduced to the linear Cauchy problem:

$$-\frac{\partial v}{\partial t}(t,x) + \rho v(t,x) - \mathcal{L}^{a_0} v(t,x) = 0, \tag{2.83}$$

or

$$-\frac{\partial v}{\partial t} + \rho v - \mu x \frac{\partial v}{\partial x} - \frac{1}{2}\sigma^2 x^2 \frac{\partial^2 v}{\partial x^2} = 0, \qquad \forall (t,x) \in [0,T) \times \mathbb{R}, \tag{2.84}$$

with terminal condition $v(T,x) = g(x)$.

Unlike the European options an *American put option* gives the holder the right, but not the obligation, to sell a prescribed asset for a prescribed price *at any time* between the starting date and a prescribed expiration time. The price of an American put option can be expressed by an optimal stopping problem:

$$v(t,x) = \sup_{\tau \in \mathcal{T}_{t,T}} E[e^{-\rho(\tau-t)}(K - X_\tau^{t,x})^+], \qquad (t,x) \in [0,T] \times \mathbb{R}. \tag{2.85}$$

This is analogous to optimal stopping problem (2.46) with $f \equiv 0$ and $g(X_\tau^{t,x}) = (K - X_\tau^{t,x})^+$. The following partial differential equation is found

$$\min[-\frac{\partial v}{\partial t} + \rho v - \mu x \frac{\partial v}{\partial x} - \frac{1}{2}\sigma^2 x^2 \frac{\partial^2 v}{\partial x^2},\, v - g] = 0, \qquad \forall (t,x) \in [0,T) \times \mathbb{R}. \tag{2.86}$$

In the continuation region $\mathcal{C}$ it is optimal to hold the option and the left-hand side equals zero. The payoff in the stopping region $\mathcal{S}$ is $g(x)$.

2.7.2 Contingent claims approach

Now assume that the market is complete and there is a risk-free interest rate r. In such a case we can use the contingent claims approach to calculate the put option price. With a portfolio consisting of the option v and $\Delta = \frac{\partial v}{\partial x}$ underlying assets we can derive the risk-neutral price which satisfies the Black-Scholes equation (see [33]):

$$-\frac{\partial v}{\partial t} + rv - rx \frac{\partial v}{\partial x} - \frac{1}{2}\sigma^2 x^2 \frac{\partial^2 v}{\partial x^2} = 0, \qquad \forall (t,x) \in [0,T) \times \mathbb{R}, \tag{2.87}$$

with terminal condition $v(T,x) = g(x)$. This equation has an analytical solution, called the Black-Scholes price. If we compare this equation with equation (2.84) the term $-\rho v$ is replaced by $-rv$ and μx is replaced by rx. According to the Feynman-Kac formula ([31]) we have

$$v(t,x) = E^{\mathbb{Q}}[e^{-r(T-t)}(K - X_T^{t,x})^+], \qquad (t,x) \in [0,T] \times \mathbb{R}. \tag{2.88}$$

This formulation looks like equation (2.82) from the dynamic programming approach. However, now the expectation is taken with respect to the risk-neutral measure $\mathbb{Q}$ under which $dX_t = rX_t dt + \sigma X_t dW_t$. Note that the drift term μ is reduced to r. Furthermore, discounting is done using the risk-free interest

rate instead of the risk adjusted discount rate.

The option prices can be calculated by solving equation (2.87) with PDE methods or by means of equation (2.88). The last one is employed in Fourier pricing methods such as the CONV method ([25]) and the COS method ([10]), which we will discuss in Section 6.3.

In [14] the following equation is found for the risk-neutral price of American put options using the non-arbitrage principle:

$$\min[-\frac{\partial v}{\partial t} + rv - rx\frac{\partial v}{\partial x} - \frac{1}{2}\sigma^2 x^2 \frac{\partial^2 v}{\partial x^2},\, v - g] = 0. \tag{2.89}$$

2.8 Example 3: Harvesting forest problem

In [17] and [16] the valuation of forest land is studied. This topic has been a concern in academic literature for over 150 years. Uncertainty concerning land valuation is for example due to volatile prices for timber and production risks. Another aspect is the problem of optimal harvesting under the risk of a forest fire. We describe the real options approach to investigate the value of the forest land. First the tree harvesting model, including fire risk, is defined. This model can be adjusted to other agricultural harvesting problems, such as cereal harvests, and the risk of fire might be replaced by the risk of, for example, pests. After this, equations for the value of land are derived using both the dynamic programming and the contingent claims approach, as in [17].

The harvesting model describes the optimal harvesting problem and it accounts for the risk of fire. The stand of trees is assumed to be even-aged and will be used for commercial forestry. The aim is to find the value of a stand of trees depending on P_t, the price of timber at time t, and the age of the stand ζ_t. The stand value under optimal harvesting is denoted by $v = v(t, P_t, \zeta_t) = v(t, X_t)$, with $X_t = [P_t, \zeta_t]'$ ($'$ represents the transpose of a matrix or vector).

The price of timber follows a stochastic diffusion process:

$$dP_t = a(t, P_t)dt + b(t, P_t)dW_t. \tag{2.90}$$

We assume that an accurate description of this process is a mean reverting process with $a(t, P_t) = \eta(\overline{P} - P_t)$ and $b(t, P_t) = \sigma P_t$. The price level tends to revert to the long run mean $\overline{P}$. The volume of timber on the stand is given by the deterministic function $Q = Q(\zeta_t)$ depending on the stand age.

The return of harvesting and selling the timber will give a profit of $(P_t - C_h)Q(\zeta_t)$, where constant C_h includes the harvesting costs per cubic meter and the value of the bare land $v(t, P_t, 0)$. If harvesting is delayed there is a capital gain or loss due to the change in timber volume, price change and the possible occurrence of fire. Contrary to [17] we do not incorporate management costs to maintain the stand, because this may make the problem formulation more involved, but not necessarily more difficult.

The age of the stand ζ_t is a stochastic variable which depends on the time of the last harvest t_h and the occurrence of fire. If no fire has occurred we have $\zeta_t = t - t_h$, but if a fire occurs the stand age will jump to zero. The occurrence of fire is modelled by a Poisson process q_t with intensity rate λ. By this the stand age is modelled as a simplified jump diffusion process.

In short, the uncontrolled state process reads

$$dX_t = \begin{bmatrix} dP_t \\ d\zeta_t \end{bmatrix} = \begin{bmatrix} a(t, P_t)dt + b(t, P_t)dW_t \\ dt - \zeta_t dq_t \end{bmatrix}. \tag{2.91}$$

It is assumed that a fire consumes the entire stand, although some timber may be salvaged. Let S be the value of salvaged timber net of harvesting costs per hectare and assume this value to be a constant propor-

tion γ of the value of the stand if it was harvested immediately before the fire: $S(X_{t^-}) = (P_t - C_h)Q(\zeta_{t^-})\gamma$. The loss in the case of a fire is $v(t, P_t, 0) - v(t, X_{t^-}) + S(X_{t^-})$.

The problem of optimal harvesting is defined on a finite horizon $[0, T]$. At each time the land owner has to decide whether or not to harvest and he will weigh up the profit from harvesting immediately versus delaying until the next period. Clearly there is a trade-off between the returns of harvesting immediately and waiting, which bears the risk of a fire. In the next sections partial differential equations for the value of land are derived under different assumptions about hedging the risk of price changes and the fire risk.

2.8.1 Dynamic programming approach

For the derivation of the first equation we assume that neither the risks from price changes nor from fire can be hedged. Then the value of the land must be estimated as an expected value with respect to the true price process and the risk of fire. It is assumed that the holder of the asset makes the optimal choice between harvesting the stand or waiting, in other words holding the option or not, which is the control. In order to hold the option the investor would require a constant risk adjusted discount rate ρ. We can formulate the harvesting problem as an optimal stopping problem or an impulse control problem (without control process α). Both are discussed below.

Optimal stopping problem
The owner of the forest land wants to value his stand of trees under the assumption that he makes an optimal decision about the harvesting time τ. The land is valued as the expected losses from fire plus the revenues from harvesting at time τ:

$$\begin{aligned} v(t,x) &= \sup_{\tau \in \mathcal{T}_{t,T}} J(t,x,\tau) \\ &= \sup_{\tau \in \mathcal{T}_{t,T}} E^{t,x}\left[\sum_{\tau_i \in [t,\tau]} e^{-\rho(\tau_i - t)} S(X_{\tau_i^-}) + e^{-\rho(\tau - t)} g(X_\tau) \right], \quad (t,x) = (t,p,\zeta) \in [0,T] \times \mathbb{R}^2, \end{aligned} \tag{2.92}$$

with reward on the harvesting time $g(X_\tau) = (P_\tau - C_h)Q(\zeta_\tau) + v(\tau, P_\tau, 0)$. The times τ_i denote the fire times and these extreme events give a deterministic revenue $S(X_{\tau_i^-})$. The problem is similar to the optimal stopping problem (2.46) with $f \equiv 0$, but now under a jump diffusion process (Section 2.4.3) and including extreme events (Section 2.4.4). If we compare this we arrive at the associated Hamilton-Jacobi-Bellman equation variational inequality:

$$\min\Big[-v_t + \rho v - \mathcal{L}v - \lambda[v(t,p,0) - v] - \lambda S,\, v - g \Big] = 0, \tag{2.93}$$

or

$$\begin{aligned} \min\Big[&-v_t + (\rho + \lambda)v - a(t,p)v_p - v_\zeta - \frac{1}{2}b^2(t,p)v_{pp} - \lambda[v(t,p,0) + S], \\ &v - (p - C_h)Q(\zeta) - v(t,p,0) \Big] = 0, \qquad \forall (t,x) = (t,p,\zeta) \in [0,T) \times \mathbb{R}^2. \end{aligned} \tag{2.94}$$

Impulse control problem
The harvesting problem can also be formulated by an impulse control problem on the finite domain $[0, T]$, with harvesting times t_m, $m \in \mathbb{N}$. At the harvesting times an impulse $\xi_m = [0, -\zeta_{t_m^-}]'$ is added to the state process. To be precise, the price of timber remains the same, but the age of the stand jumps to zero. The 'costs' of an impulse are $c(X_{t_m^-}, \xi_m) = (P_{t_m} - C_h)Q(\zeta_{t_m^-})$. At each time there is only one possible impulse, namely harvesting everything, so the intervention operator is

$$\mathcal{M}v(t, X_t) = v(t, X_t + \xi_t) + c(X_{t^-}, \xi_t) = v(t, P_t, 0) + (P_t - C_h)Q(\zeta_{t^-}). \tag{2.95}$$

The following dynamics hold:

$$\begin{aligned} dP_t &= a(t,P_t)dt + b(t,P_t)dW_t, && \text{for } t \in (t_m, t_{m+1}), \\ d\zeta_t &= dt - \zeta dq_t, && \text{for } t \in (t_m, t_{m+1}), \\ \zeta_{t_m} &= \zeta_{t_m^-} - \zeta_{t_m^-}, && m \in \mathbb{N}. \end{aligned} \tag{2.96}$$

Denote by $\mathcal{B}$ the set of possible harvesting times. The value of the stand can be expressed by the value function

$$\begin{aligned} v(t,x) &= \sup_{\beta\in\mathcal{B}} J(t,x,\beta) \\ &= \sup_{\beta\in\mathcal{B}} E^{t,x}\left[\sum_{\tau_i\in[t,T]} e^{-\rho(\tau_i-t)} S(X_{\tau_i^-}) + \sum_{t\le t_m<T} e^{-\rho(t_m-t)}(P_{t_m} - C_h)Q(\zeta_{t_m^-})\right], \\ &\quad (t,x) = (t,p,\zeta) \in [0,T]\times\mathbb{R}^2. \end{aligned} \tag{2.97}$$

This is comparable with the impulse control problem under jump diffusion (2.64) combined with the case of extreme events (Section 2.4.4). If a fire occurs, that means a jump in the Poisson process q_s, the value function v changes to $v(s, P_s, 0)$. The associated Hamilton-Jacobi-Bellman variational inequality reads:

$$\min\Big[- v_t + \rho v - \mathcal{L}v - \lambda[v(t,p,0) - v] - \lambda S,\, v - \mathcal{M}v\Big] = 0, \tag{2.98}$$

or

$$\begin{aligned} \min\Big[&- v_t + (\rho+\lambda)v - a(t,p)v_p - v_\zeta - \frac{1}{2}b^2(t,p)v_{pp} - \lambda[v(t,p,0) + S], \\ &v - (p - C_h)Q(\zeta) - v(t,p,0)\Big] = 0, \qquad (t,x) = (t,p,\zeta) \in [0,T)\times\mathbb{R}^2, \end{aligned} \tag{2.99}$$

with terminal condition $v(T,x) = 0$.

Not surprisingly, the optimal stopping time and the impulse control formulations lead to the same HJB-VI equation. Equality to zero of the first equation in the minimisation operator (2.99) describes the value of the forested land when it is optimal not to harvest. Equality to zero of the second equation represents the value at an optimal harvesting time. Due to the possibility of fire a risk premium λ is added to the risk adjusted discount rate ρ. The drawback of this dynamic programming approach is the fact that it is difficult to determine the appropriate discount rate ρ. Besides, it is generally not correct to assume a constant discount rate. Because of that we recommend to use, if possible, the contingent claims approach from the next section.

2.8.2 Contingent claims approach

In this section we use the contingent claims or risk-neutral valuation approach to derive two other partial differential equations for the optimal harvesting problem, following the analysis in [17]. For the first one we assume that the asset markets are sufficiently rich to be able to hedge the risks of price changes and fire and the market will not reward the investor for holding his risky asset. The advantage is that it is not necessary to choose a risk adjusted discount rate and it is consistent with financial options theory.

Denote the value of the stand of trees from the previous section by v_1. We construct a portfolio π consisting of this value v_1 and two other assets v_2 and v_3. Asset $v_2 = v_2(t, P_t, \zeta_t)$ depends only on timber price and not on fire and asset $v_3 = v_3(t, P_t, \zeta_t)$ depends on the risk of fire alone. Using Itô's formula the

dynamics of v_1 are derived as

$$\begin{aligned} dv_1(t,X_t) &= \frac{\partial v_1}{\partial t}(t,X_t)dt + \frac{\partial v_1}{\partial p}(t,X_t)[a(t,P_t)dt + b(t,P_t)dW_t] + \frac{\partial v_1}{\partial \zeta}(t,X_t)dt \\ &+ \frac{1}{2}\frac{\partial^2 v_1}{\partial p^2}(t,X_t)b^2(t,P_t)dt + [v_1(t,P_t,0) - v_1(t,X_{t^-})]\,dq_t \\ &= \left((v_1)_t + a(t,P_t)(v_1)_p + (v_1)_\zeta + \frac{1}{2}b^2(t,P_t)(v_1)_{pp}\right)dt \\ &+ b(t,P_t)(v_1)_p dW_t + [v_1(t,P_t,0) - v_1(t,X_{t^-})]dq_t, \end{aligned} \tag{2.100}$$

and likewise we find in shorthand notation:

$$\begin{aligned} dv_1(t,X_t) &= \mu_1 v_1 dt + s_1 v_1 dW_t + [v_1(t,P_t,0) - v_1(t,X_{t^-})]dq_t, \\ dv_2(t,X_t) &= \mu_2 v_2 dt + s_2 v_2 dW_t, \\ dv_3(t,X_t) &= \mu_3 v_3 dt + [v_3(t,P_t,0) - v_3(t,X_{t^-})]dq_t, \end{aligned} \tag{2.101}$$

with

$$\begin{aligned} \mu_j &:= \left((v_j)_t + a(t,P_t)(v_j)_p + (v_j)_\zeta + \tfrac{1}{2}b^2(t,P_t)(v_j)_{pp}\right)\tfrac{1}{v_j}, \quad j=1,2, \\ s_j &:= \tfrac{b(t,P_t)}{v_j}(v_j)_p, \qquad\qquad\qquad\qquad\qquad\qquad j=1,2, \\ \mu_3 &:= ((v_3)_t + (v_3)_\zeta)\tfrac{1}{v_3}. \end{aligned} \tag{2.102}$$

In the hedging portfolio we take, at time t, n_1, n_2 and n_3 numbers of v_1, v_2 and v_3, respectively. So,

$$\pi(t,X_t) = n_1 v_1(t,X_t) + n_2 v_2(t,X_t) + n_3 v_3(t,X_t). \tag{2.103}$$

Assume it is optimal not to harvest and we consider the value of the portfolio a small time dt later. Over the hedging interval dt the amounts n_1, n_2 and n_3 are held constant. A time dt later we have n_1 times the value of forest land at time $t+dt$ and likewise for assets v_2 and v_3. Also the cashflow of the salvage value of timber $n_1 S dq_t$, due to a possible fire in the small time interval, has entered the portfolio. For simplicity we assume that the salvage value for asset v_3 equals zero. The change in the portfolio value is:

$$d\pi(t,X_t) = n_1 dv_1(t,X_t) + n_1 S(X_{t^-})dq_t + n_2 dv_2(t,X_t) + n_3 dv_3(t,X_t). \tag{2.104}$$

The risk of the hedging portfolio is reflected by changes dW_t and dq_t. To eliminate these risks we choose n_1, n_2 and n_3 so that

$$n_1 s_1 v_1 + n_2 s_2 v_2 = 0 \quad \text{and} \quad n_1[v_1(t,P_t,0) - v_1(t,X_{t^-}) + S(X_{t^-})] + n_3[v_3(t,P_t,0) - v_3(t,X_{t^-})] = 0. \tag{2.105}$$

Because of this, the dW_t and dq_t terms are eliminated, which results in

$$d\pi = n_1\mu_1 v_1 dt + n_2\mu_2 v_2 dt + n_3\mu_3 v_3 dt. \tag{2.106}$$

There is no risk, to first order, and thus this portfolio must earn the risk-free rate r, in other words we set $d\pi = r\pi dt$. With this we get a system of 3 equations with 3 unknowns:

$$\begin{bmatrix} s_1 v_1 & s_2 v_2 & 0 \\ v_1(t,P_t,0) - v_1(t,X_{t^-}) + S(X_{t^-}) & 0 & v_3(t,P_t,0) - v_3(t,X_{t^-}) \\ v_1(\mu_1 - r) & v_2(\mu_2 - r) & v_3(\mu_3 - r) \end{bmatrix} \begin{bmatrix} n_1 \\ n_2 \\ n_3 \end{bmatrix} = \begin{bmatrix} 0 \\ 0 \\ 0 \end{bmatrix}. \tag{2.107}$$

In order to have a nontrivial solution the determinant of this matrix must equal zero. This will happen if the rows of the matrix are linearly dependent. So there must be two parameters λ_P and λ_F such that (multiply the first row by λ_P and the second row by λ_F):

$$\begin{aligned} (\mu_1 - r)v_1 &= \lambda_P s_1 v_1 - \lambda_F[v_1(t,P_t,0) - v_1(t,X_{t^-}) + S(X_{t^-})], \\ (\mu_2 - r)v_2 &= \lambda_P s_2 v_2, \\ (\mu_3 - r)v_3 &= -\lambda_F[v_3(t,P_t,0) - v_3(t,X_{t^-})]. \end{aligned} \tag{2.108}$$

Working out the first row gives:

$$-v_t + (r+\lambda_F)v - [a(t,p) - \lambda_P b(t,p)]\, v_p - v_\zeta - \frac{1}{2}b^2(t,p)v_{pp} - \lambda_F[v(t,p,0)+S] = 0,$$
$$(t,x) = (t,p,\zeta) \in [0,T) \times \mathbb{R}^2, \qquad (2.109)$$

with

$$\lambda_P = \frac{\mu_2 - r}{s_2} \text{ and } \lambda_F = \frac{\mu_3 - r}{[v_3(t,p,0) - v_3]/v_3}. \qquad (2.110)$$

The above equation holds while it is optimal to refrain from harvesting. Parameter λ_P is called the market price of timber price risk and λ_F the market price of fire risk. They reflect the extra return over the risk-free rate r per unit of variability. The variability of price is measured by the instantaneous standard deviation for $v_2(t, P_t, \zeta_t)$: s_2. The variability for fire is measured by $-[v_3(t,P_t,0) - v_3]/v_3$, which is the proportional loss in asset value if a fire occurs. In theory λ_P and λ_F could be estimated using historical data on prices and timberland sales, as discussed in [17].

Equation (2.99) was derived assuming that the risks could not be hedged, but the asset v would earn a risk adjusted return ρ. Comparing equations (2.99) and (2.109) we see that in the second equation the risk adjusted discount rate ρ is replaced by the risk-free interest rate r and the true probability of fire λ is replaced by market price of fire λ_F. Furthermore, the term $a(t,p)v_p$ is replaced by $[a(t,p) - \lambda_P b(t,p)]v_p$.

Contingent claims approach under imperfect hedging
For the derivation of the final partial differential equation we will assume that it is possible to hedge price risk but not fire risk, so the investor will not be rewarded with extra return for taking on price risk. The hedging portfolio consists of n_1 assets v_1 and n_2 assets v_2, as defined before. The price risk is hedged by choosing n_1 and n_2 so that

$$n_1 s_1 v_1 + n_2 s_2 v_2 = 0. \qquad (2.111)$$

There remains:

$$d\pi = n_1\mu_1 v_1 dt + n_1[v_1(t,P_t,0) - v_1(t,X_{t^-}) + S(X_{t^-})]dq_t + n_2\mu_2 v_2 dt. \qquad (2.112)$$

Now it is not possible to perform a perfect hedge with $d\pi = r\pi dt$, but we require $E[d\pi] = r\pi dt$. This is called imperfect hedging, since no perfect replicate of the real option value can be made. In other words

$$\begin{aligned} &E[n_1\mu_1 v_1 dt + n_1[v_1(t,P_t,0) - v_1(t,X_{t^-}) + S(X_{t^-})]dq_t + n_2\mu_2 v_2 dt] \\ &\quad = \quad n_1\mu_1 v_1 dt + \lambda[v_1(t,P_t,0) - v_1(t,X_{t^-}) + S(X_{t^-})]dt + n_2\mu_2 v_2 dt \\ &\quad = \quad r\pi dt. \end{aligned} \qquad (2.113)$$

This results in the following system of 2 equations with 2 unknowns:

$$\begin{bmatrix} s_1 v_1 & s_2 v_2 \\ v_1(\mu_1 - r) + \lambda[v_1(t,P_t,0) - v_1(t,X_{t^-}) + S(X_{t^-})] & v_2(\mu_2 - r) \end{bmatrix} \begin{bmatrix} n_1 \\ n_2 \end{bmatrix} = \begin{bmatrix} 0 \\ 0 \end{bmatrix}. \qquad (2.114)$$

For a nontrivial solution there must be a parameter λ_P such that:

$$\begin{aligned} (\mu_1 - r)v_1 + \lambda[v_1(t,P_t,0) - v_1(t,X_{t^-}) + S(X_{t^-})] &= \lambda_P s_1 v_1, \\ (\mu_2 - r)v_2 &= \lambda_P s_2 v_2. \end{aligned} \qquad (2.115)$$

Now we arrive at

$$-v_t + (r+\lambda)v + [a(t,p) - \lambda_P b(t,p)]\, v_p - v_\zeta - \frac{1}{2}b^2(t,p)v_{pp} - \lambda[v(t,p,0)+S] = 0,$$
$$(t,x) = (t,p,\zeta) \in [0,T) \times \mathbb{R}^2, \qquad (2.116)$$

with

$$\lambda_P = \frac{\mu_2 - r}{s_2}. \tag{2.117}$$

Here λ_F in equation (2.109) is replaced by the true probability of fire λ. In equation (2.99) λ was added as a risk premium to the risk adjusted discount rate ρ. In equation (2.116) the fire probability λ is added to the risk-free rate r, due to the assumption that it is possible to hedge the price risk, but not the fire risk.

In [17] an interesting discussion takes place about the risk-neutral price and the estimation of the market price of risk. It is noticed that the risk-neutral price is given by its expected discounted value, where discounting is done at the risk-free rate r and the expectation is taken with respect to a risk adjusted process. This is achieved by reducing the expect growth rate $a(t,p)$ by the risk premium $\lambda_P b(t,p)$. The term $[a(t,p) - \lambda_P b(t,p)]$ is often referred to as the risk-neutral drift rate. This is comparable with the option price (2.88), where the risk-neutral price is calculated with a risk-free discount rate and under a process with reduced drift r.

3 The dike height stochastic optimisation problem

Another example of stochastic optimisation problems considers the dike height problem. A significant part of the Netherlands lies below the sea level and flood prevention has always been a major concern for this country. The water level is predicted to rise so it may be necessary to increase the dike height in the future. A pioneer in investigating the economic-decision problem of optimal dike height is Prof. D. van Dantzig, after the flood disaster in the southwestern part of the Netherlands in 1953. Van Dantzig ([7]) suggested a strategy where each dike is increased if the probability of the water level exceeding the dike level is above a certain threshold. A recent alternative strategy is based on the expected loss due to flooding instead of the exceedance probability (see [9]). With this the construction costs are balanced against the expected flooding costs.

In Section 3.1 a basic model is explained, for which we will develop a numerical solution method in Section 4. The relation and the differences between the harvesting and dike height problems are discussed in Section 3.2. After this, improved models for the dike height problem are proposed in Section 3.3. We end this section with a discussion about the models.

3.1 First model for the dike height problem

The problem posed is when to increase the dikes and also by which amount. The goal is to minimise the future expected costs, consisting of the investment costs of dike level increases, losses due to flooding and the terminal costs. We put this in the form of a stochastic impulse control problem, which leads up to a second order Hamilton-Jacobi-Bellman equation. We start by defining the model, in accordance to [32]. Later on this model will be extended.

Process $X_t^{(1)}$ represents the dike level. We have the possibility to control this value. $Y_t^{(2)} = w(t)$ is a deterministic average water level. In [22] and [32] a piecewise linear process of the form $dY_t^{(2)} = \mu_w(t)dt$ was used.

Remark 3.1. *We use $Y_t^{(2)}$ instead of the obvious $X_t^{(2)}$ for ease of notation in Section 8, where a surplus water level $X_t^{(2)}$ is defined. The superscript (2) denotes the second process instead of a square root.*

The economic value of endangered goods is modelled by a geometric Brownian motion,

$$dY_t^{(3)} = \mu_3 Y_t^{(3)} dt + \sigma_3 Y_t^{(3)} dW_t^{(3)}, \tag{3.1}$$

where μ_3 is the predicted economic growth factor and σ_3 the economic volatility. The mean of this process reads $E^{t,y}[Y_s^{(3)}] = ye^{\mu_3(s-t)}$. We consider the log-process of the economic value:

$$X_t^{(3)} := \log(Y_t^{(3)}), \tag{3.2}$$

where log denotes the natural logarithm. We use Itô calculus to find

$$\begin{aligned} X_t^{(3)} &= X_0^{(3)} + \int_0^t \frac{1}{Y_s^{(3)}} dY_s^{(3)} + \frac{1}{2}\frac{-1}{(Y_s^{(3)})^2}(dY_s^{(3)})^2 \\ &= X_0^{(3)} + \int_0^t (\mu_3 - \frac{1}{2}\sigma_3^2)ds + \int_0^t \sigma_3 dW_s^{(3)}. \end{aligned} \tag{3.3}$$

So, we have

$$X_t^{(3)} = X_0^{(3)} + (\mu_3 - \frac{1}{2}\sigma_3^2)t + \sigma_3 dW_t^{(3)} \sim \mathcal{N}(X_0^{(3)} + (\mu_3 - \frac{1}{2}\sigma_3^2)t,\, \sigma_3^2 t), \tag{3.4}$$

where $\mathcal{N}(\mu, \sigma^2)$ represents a normally distributed random variable with mean μ and standard deviation σ. From now on we use this stochastic **log**-economic value of endangered goods. This Brownian motion

is a Lévy process and its characteristic function reads

$$\varphi_{X_t^{(3)}}(u) = e^{iX_0^{(3)}u} \exp\left(i(\mu_3 - \frac{1}{2}\sigma_3^2)tu - \frac{1}{2}\sigma_3^2 t u^2 \right). \tag{3.5}$$

The state variable of the first model is $X_t = [X_t^{(1)}, X_t^{(3)}]'$. Note that the process $Y_t^{(2)} = w(t)$ is omitted, because it is a deterministic function of time t. In the model the dikes can be increased at stopping times t_m, $m \in \mathbb{N}$, by an amount $u_m \in U$. The set U can either be continuous or discrete, for example, $U = \{0, 5, 10, \ldots\}$ cm as in [22]. The other state variables remain the same, so the impulse on the state process is $\xi_m = [u_m, 0]'$. There is no control α on the drift and diffusion terms of the process. Denote by $\mathbf{u} = (\{t_m\}, u_m)$ the impulse control strategy and by $\mathcal{U}$ the set of all $\mathbf{u}$ such that,

$$t_m \in [0, T), \quad t_{m+1} \geq t_m, \quad u_m \in U. \tag{3.6}$$

The dynamics of the state process X_t is summarised by

$$\begin{aligned} dX_t^{(1)} &= 0, && \text{for } t \in (t_m, t_{m+1}), \\ dX_t^{(3)} &= (\mu_3 - \tfrac{1}{2}\sigma_3^2)dt + \sigma_3 dW_t^{(3)}, && \text{for } t \in (t_m, t_{m+1}), \\ X_{t_m} &= X_{t_m^-} + [u_m, 0]', && m \in \mathbb{N}. \end{aligned} \tag{3.7}$$

Note that $Y_t^{(2)}$ is an *average water level*. Occurrences of extreme water level are added to this level, modelled by a Poisson process q_t with intensity rate λ. If a jump in the Poisson process occurs the average water level jumps instantaneously by an amount $\mathcal{J}_t$, which is a random variable with probability density function

$$f_{\mathcal{J}}(y) = k_1 e^{k_1(k_2 - y) - e^{k_1(k_2 - y)}}. \tag{3.8}$$

The extreme water level size $\mathcal{J}$ is Gumbel distributed with scale parameter $1/k_1 > 0$ and location parameter $k_2 \in \mathbb{R}$ ([26]). The mean is $k_2 + \gamma_{EM}/k_1$, with $\gamma_{EM} \approx 0.58$ the Euler-Mascheroni constant, and the variance $(\pi/k_1)^2/6$.

The total water level is a summation of the average water level $w(t)$ and a possible jump:

$$w(t) + \mathcal{J}_t dq_t. \tag{3.9}$$

After an occurence of extreme water level, the total water level returns to $w(t)$. The fraction of the economic value that is lost if the total water level exceeds the dike height by an amount y is given by the function $l_p(y)$, where

$$l_p(y) = \max(1 - e^{-\lambda_p y}, 0), \tag{3.10}$$

with $\lambda_p > 0$ a rate parameter. The losses at time t due to flooding are proportional to the economic value of endangered goods and are given by

$$\exp(X_t^{(3)}) l_p(w(t) + \mathcal{J}_t - X_t^{(1)}) dq_t. \tag{3.11}$$

3.1.1 Dynamic programming approach

For the dynamic programming approach we assume that it is not possible to hedge the risks from flooding and from changes in the state process X_t. We use a discount factor ρ to measure the expected discounted costs.

Let τ_i denote the times of extreme water levels with sizes $\mathcal{J}_{\tau_i}$ i.i.d. variables. The discounted future flood losses at time t are given by

$$\int_t^T e^{-\rho(s-t)} \exp(X_s^{(3)}) l_p(w(s) + \mathcal{J}_s - X_s^{(1)})\, dq_s = \sum_{\tau_i \in [t,T]} e^{-\rho(\tau_i - t)} \exp(X_{\tau_i}^{(3)}) l_p(w(\tau_i) + \mathcal{J}_{\tau_i} - X_{\tau_i}^{(1)}) \tag{3.12}$$

The terminal costs at time T are called b_T and they express the total discounted expected costs after the terminal time T. For this it is assumed that the dike and water level remain constant beyond this time and we have:

$$b_T(x_1, x_3) = E^{T,x}\left[\sum_{\tau_i \in [T,\infty)} e^{-\rho(\tau_i - T)} \exp(X^{(3)}_{\tau_i}) l_p(w(T) + \mathcal{J}_{\tau_i} - x_1)\right]. \tag{3.13}$$

The construction costs of a dike increase at time t_m by an amount u_m are denoted by $b(X^{(1)}_{t_m^-}, u_m)$, with

$$b(x_1, u) = \begin{cases} 0, & \text{for } u = 0, \\ b^+(x_1, u), & \text{for } u > 0, \end{cases} \tag{3.14}$$

where $b^+(x_1, u)$ is a smooth function, increasing in x_1 and u, and $b^+(x_1, 0) \neq 0$.

At any time t one has to decide whether to increase the dike height, and if so by which amount, or to do nothing and wait until the next time. There is a trade-off between increasing the dike level immediately at certain costs and waiting, which bears the risk of flooding. The total discounted expected flooding and construction costs, which are called the flood protection costs, for a control $\mathbf{u}$ are given by the gain function:

$$\begin{aligned} J(t, x_1, x_3, \mathbf{u}) &= E^{t,x}\Bigg[\sum_{\tau_i \in [t,T]} e^{-\rho(\tau_i - t)} \exp(X^{(3)}_{\tau_i}) l_p(w(\tau_i) + \mathcal{J}_{\tau_i} - X^{(1)}_{\tau_i}) \\ &\quad + \sum_{t \le t_m < T} e^{-\rho(t_m - t)} b(X^{(1)}_{t_m^-}, u_m) + e^{-\rho(T-t)} b_T(X^{(1)}_T, X^{(3)}_T)\Bigg], \\ &\quad (t, x) = (t, x_1, x_3) \in [0, T] \times \mathbb{R}^2. \end{aligned} \tag{3.15}$$

The average water level is not included as variable in the function J since it is a deterministic function of time t. The aim is to minimise these costs of flood protection. For this we define the value function, representing the minimum costs, by

$$v(t, x_1, x_3) = \inf_{\mathbf{u} \in \mathcal{U}} J(t, x_1, x_3, \mathbf{u}). \tag{3.16}$$

This stochastic impulse control problem, about when and by which amount to increase the dike height, represents a trade-off between investment costs of the heightenings and the expected costs due to floods. It coincides with impulse control problem (2.70) with $c(X_{t_m^-}, \xi_m) = b(X^{(1)}_{t_m^-}, u_m)$ and $\eta(\tau_i, X_{\tau_i^-}, \Theta_{\tau_i}) = \exp(X^{(3)}_{\tau_i}) l_p(w(\tau_i) + \mathcal{J}_{\tau_i} - X^{(1)}_{\tau_i})$. This results in the associated HJB quasi-variational inequality:

$$\begin{aligned} \max\Big[-v_t(t,x) + \rho v(t,x) - \mathcal{L}v(t,x) - \lambda E[\exp(x_3) l_p(w(t) + \mathcal{J} - x_1)],\, v(t,x) - \mathcal{M}v(t,x)\Big] = 0, \\ (t, x) = (t, x_1, x_3) \in [0, T) \times \mathbb{R}^2, \end{aligned} \tag{3.17}$$

with terminal condition

$$v(T, x) = b_T(x), \qquad x \in \mathbb{R}^2. \tag{3.18}$$

The intervention operator is $\mathcal{M}v(t,x) = \inf_{u \in U} v(t, x + (u, 0)) + b(x_1, u)$ and

$$\begin{aligned} E[\exp(x_3) l_p(w(t) + \mathcal{J} - x_1)] &= \exp(x_3) E[l_p(w(t) + \mathcal{J} - x_1)] \\ &= \exp(x_3) \int_{-\infty}^{\infty} l_p\Big(y - (x_1 - w(t))\Big) f_{\mathcal{J}}(y) dy \\ &:= \exp(x_3) \beta(x_1 - w(t)), \end{aligned} \tag{3.19}$$

where $\beta(h)$ is a function that is decreasing in h.

We can rewrite the HJB-QVI as

$$\max\Big[-v_t(t,x)+\rho v(t,x)-\mathcal{L}v(t,x)-\lambda\exp(x_3)\beta(x_1-w(t)),v(t,x)-\inf_{u\in U}[v(t,x+(u,0))+b(x_1,u)]\Big] = 0, \qquad (t,x)=(t,x_1,x_3)\in[0,T)\times\mathbb{R}^2. \qquad (3.20)$$

The left-hand side in the maximum statement is equal to zero when it is *not* optimal to increase the dike height and the right-hand side is equal to zero in case it is optimal to increase dike height. Under the first model we have

$$\mathcal{L}v(t,x)=(\mu_3-\frac{1}{2}\sigma_3^2)\frac{\partial v}{\partial x_3}(t,x)+\frac{1}{2}\sigma_3^2\frac{\partial^2 v}{\partial x_3^2}(t,x). \qquad (3.21)$$

3.1.2 Contingent claims approach

Assume that it is possible to hedge the flood risk and risks from changes in the economic value with, for example, an asset of a company that is included in the economic value of endangered goods or an asset that is related to a company which delivers barricade sandbags or rebuilds destructed houses. Then repeating the arguments in the contingent claims approach as done for the harvesting problem in Section 2.8.2 results in another partial differential equation. Since no information about possible hedge instruments is available, we omit this analysis and refer to [34] for a detailed derivation.

In the derivation of the last partial differential equation in Section 2.8.2 it was assumed that it was possible to hedge price risk but not fire risk. Analogous in the case of the dike height problem, we may consider societal risks which cannot be hedged, for example, the risk that people who live in the flooded area cannot move back to their destructed houses.

3.2 The relation between the harvesting and dike height problems

In the previous sections we studied the harvesting and dike height problems. First we defined the stochastic models. Then two methods have been discussed to derive partial differential equations for the problems, the dynamic programming and the contingent claims approach. In this section we discuss the similarities and differences between both models, under the dynamic programming approach, and in Section 3.3 we construct some alternatives to the first basic model of the dike height problem. First we summarise both stochastic impulse control problems:

Harvesting problem
State dynamics

$$\begin{aligned} dP_t &= a(t,P_t)dt+b(t,P_t)dW_t, && \text{for } t\in(t_m,t_{m+1}),\\ d\zeta_t &= dt-\zeta dq_t, && \text{for } t\in(t_m,t_{m+1}),\\ X_{t_m} &= X_{t_m^-}+[0,-\zeta_{t_m^-}]', && m\in\mathbb{N}. \end{aligned} \qquad (3.22)$$

Value function

$$v(t,x) = \sup_{\beta\in\mathcal{B}}E^{t,x}\left[\sum_{\tau_i\in[t,T]}e^{-\rho(\tau_i-t)}S(X_{\tau_i^-})+\sum_{t\le t_m<T}e^{-\rho(t_m-t)}(P_{t_m}-C_h)Q(\zeta_{t_m^-})\right]. \qquad (3.23)$$

Associated Hamilton-Jacobi-Bellman variational inequality

$$\min\Big[-v_t+\rho v(t,x)-\mathcal{L}v(t,x)-\lambda[v(t,p,0)-v+S],v-[v(t,p,0)+(p-C_h)Q(\zeta)]\Big]=0, \qquad (t,x)=(t,p,\zeta)\in[0,T)\times\mathbb{R}^2, \qquad (3.24)$$

with terminal condition $v(T,x)=0$.

Dike height problem
State dynamics

$$\begin{aligned} dX_t^{(1)} &= 0, && \text{for } t \in (t_m, t_{m+1}), \\ dX_t^{(3)} &= (\mu_3 - \tfrac{1}{2}\sigma_3^2)dt + \sigma_3 dW_t^{(3)}, && \text{for } t \in (t_m, t_{m+1}), \\ X_{t_m} &= X_{t_m^-} + [u_m, 0]', && m \in \mathbb{N}. \end{aligned} \tag{3.25}$$

Value function

$$\begin{aligned} v(t,x) = \inf_{\mathbf{u}\in\mathcal{U}} E^{t,x}\Bigg[& \sum_{\tau_i\in[t,T]} e^{-\rho(\tau_i - t)} \exp(X_{\tau_i}^{(3)}) l_p(w(\tau_i) + \mathcal{J}_{\tau_i} - X_{\tau_i}^{(1)}) \\ & + \sum_{t\le t_m < T} e^{-\rho(t_m - t)} b(X_{t_m^-}^{(1)}, u_m) + e^{-\rho(T-t)} b_T(X_T^{(1)}, X_T^{(3)}) \Bigg]. \end{aligned} \tag{3.26}$$

Associated Hamilton-Jacobi-Bellman quasi-variational inequality

$$\begin{aligned} \max\Big[& -v_t(t,x) + \rho v(t,x) - \mathcal{L}v(t,x) - \lambda \exp(x_3)\beta(x_1 - w(t)), v(t,x) - \inf_{u\in U}[v(t, x + (u,0)) + b(x_1, u)]\Big] \\ & = 0, \qquad (t,x) = (t, x_1, x_3) \in [0,T) \times \mathbb{R}^2. \end{aligned} \tag{3.27}$$

with terminal condition $v(T,x) = b_T(x_1, x_3)$.

In both problems the occurrence of disasters is modelled, in the first problem there is a risk of fire and in the second problem the risk of floods. We called the times of a disaster τ_i and there are obvious differences between both models concerning the occurrence and times of a disaster. A disaster in the harvesting problem has a direct effect on the revenues, that are changed by an amount $S(X_{\tau_i^-})$. Besides the state dynamics are changed, to be precise, ζ_t is send to zero and so is v to $v(t, P_t, 0)$. So, the total loss due to fire is $v(t, P_t, 0) - v + S$. However, there is also an indirect effect because a disaster in the harvesting model also affects the possible revenues $(P_{t_m} - C_h)Q(\zeta_{t_m^-})$, by means of the function Q. The longer the time that has past after a disaster, the higher $Q(\zeta_t)$, hence the faster a harvest would be profitable. On the other hand the occurrence of a flood has only a direct effect on the change of the costs of flood protection by an amount $\exp(X_{\tau_i}^{(3)}) l_p(w(\tau_i) + \mathcal{J}_{\tau_i} - X_{\tau_i}^{(1)})$. This is comparable with the salvage revenues S in the harvesting problem. The flood does also not affect the state dynamics X_t because they are independent of a disaster. Because of that, a disaster does not influence the construction costs $b(X_{t_m^-}^{(1)}, u_m)$. Consequently the occurrence and time of a disaster do not influence the choice whether to increase the dike level now or later. However, the expectation of the flood losses influences the control and higher expected flood losses advance the heightening.

Harvesting the forest as well as increasing the dikes, that is carrying out an impulse ξ_m, causes a change in the value function and in the state process. It influences v since it is changed to $v(t_m, P_{t_m}, 0)$ with revenues $(P_{t_m} - C_h)Q(\zeta_{t_m^-})$ and to $v(t_m, X_{t_m}^{(1)} + u_m, X_{t_m}^{(3)})$ with costs $b(X_{t_m^-}^{(1)}, u_m)$, respectively. The state processes are changed by an amount $\xi_m = [0, -\zeta_{t_m}^-]'$ and $\xi_m = [u_m, 0]'$, respectively. So in the harvesting problem an impulse affects only the stand age ζ_t, in other words the time of last impulse or disaster. There is only one possible impulse, namely harvesting everything. In the dike height problem a minimisation problem must be performed to decide the best immediate dike increase level. This results in a quasi-variational inequality instead of a variational inequality.

Finally we compare the effects of timber volume growth $Q(\zeta_t)$ and timber price increase on harvesting and the growth of the economic value of endangered goods and the relative dike height $X_t^{(1)} - w(t)$ on heightening. The volume of timber depends only on the stand age ζ_t and the price P_t is exogenous. An increase in the timber volume, as well as a price increase, increases the revenues of harvesting, which thus delays the harvesting. However, also the possible losses of a disaster are increased by them, which

advances harvesting. There is a trade-off between the returns of harvesting immediately and waiting, which bears the risk of a fire. In the dike height problem a similar trade-off exists. An increase in economic value does not affect the decision of raising the dikes now or later by means of the construction costs which are independent of $X^{(3)}_{t_m}$. However, these costs are affected positively by dike level $X^{(1)}_t$ and the increase level u_m, which can delay a certain heightening. A higher economic value leads to higher costs of possible disasters and a lower difference between the dike level and average water level as well. In this way a higher log-economic value $X^{(3)}_t$, as well as a lower relative dike height $X^{(1)}_t - w(t)$, shortens the time before increasing the dikes.

Another clear difference between both models is the presence of a terminal reward function in the dike height problem. In the harvesting problem in [17] they assume that $v(T, x) = 0$ and the terminal time T is made large enough such that this assumption has a negligible effect on the actual value function. In the dike height problem we set $v(T, x) = b_T(x)$. However, the addition of a terminal condition not equal to zero has no interesting effects on the model or the associated HJB equation.

3.3 Alternative dike height models

In the previous sections we studied a dike height model, which is mainly based on [32]. In the next sections we develop alternative models for the dike height problem. These models incorporate concepts such as stochastic water level, the dike age, a recovery rate or a soil compression and deterioration function. The additional state dynamics are coloured in blue.

3.3.1 Stochastic water level

Due to global warming, the water level is expected to rise considerably in the next centuries. The future water level rise is uncertain and scientific predictions distinct from each other. Different models for a stochastic average water level, instead of a deterministic one, may be used.

In general the state dynamics may be modelled by:

$$\begin{aligned} dX^{(1)}_t &= 0, && \text{for } t \in (t_m, t_{m+1}), \\ dY^{(2)}_t &= b_w(t, X_t)dt + \sigma_w(t, X_t)dW^{(2)}_t, && \text{for } t \in (t_m, t_{m+1}), \\ dX^{(3)}_t &= (\mu_3 - \tfrac{1}{2}\sigma_3^2)dt + \sigma_3 dW^{(3)}_t, && \text{for } t \in (t_m, t_{m+1}), \\ X_{t_m} &= X_{t_m^-} + [u_m, 0, 0]', && m \in \mathbb{N}. \end{aligned} \tag{3.28}$$

b_w is the drift term of the average water level and σ_w the volatility. Now the value function depends also on an average water level variable:

$$\begin{aligned} v(t, x_1, y_2, x_3) = \inf_{\mathbf{u}\in\mathcal{U}} E^{t,x} \Bigg[& \sum_{\tau_i \in [t,T]} e^{-\rho(\tau_i - t)} \exp(X^{(3)}_{\tau_i}) l_p(Y^{(2)}_{\tau_i} + \mathcal{J}_{\tau_i} - X^{(1)}_{\tau_i}) \\ & + \sum_{t \le t_m < T} e^{-\rho(t_m - t)} b(X^{(1)}_{t_m^-}, u_m) + e^{-\rho(T-t)} b_T(X^{(1)}_T, Y^{(2)}_T, X^{(3)}_T) \Bigg]. \end{aligned} \tag{3.29}$$

The associated Hamilton-Jacobi-Bellman quasi-variational inequality reads

$$\max\left[-v_t + \rho v(t,x) - \mathcal{L}v(t,x) - \lambda x_3 \beta(x_1 - y_2),\ v(t,x) - \inf_{u\in U}[v(t, x + (u,0,0)) + b(x_1, u)]\right] = 0,$$
$$(t, x) = (t, x_1, y_2, x_3) \in [0, T) \times \mathbb{R}^3, \tag{3.30}$$

with terminal condition $v(T,x) = b_T(x)$ and

$$\mathcal{L}v(t,x) = b_w(t,x)\frac{\partial v}{\partial y_2}(t,x) + (\mu_3 - \frac{1}{2}\sigma_3^2)\frac{\partial v}{\partial x_3}(t,x) + \frac{1}{2}\sigma_w^2(t,x)\frac{\partial^2 v}{\partial y_2^2}(t,x) + \frac{1}{2}\sigma_3^2\frac{\partial^2 v}{\partial x_3^2}(t,x). \tag{3.31}$$

In Section 8 we will use the following model for the stochastic average water level process

$$Y_t^{(2)} = w(t) + \sigma_w W_t^{(2)}, \tag{3.32}$$

with $\sigma_w > 0$ a constant. In other words, a scaled Wiener process is added to the deterministic function $w(t)$.

3.3.2 The dike age

In an attempt to take concepts from the harvesting problem and include them in the dike height model, we incorporate the *dike age* ζ_t. This variable is comparable with the stand age and depends on the time of the last dike increase t_{di} and the occurence of floods. If no flooding has occurred we have $\zeta_t = t - t_{di}$ and a flood lets ζ_t jump to zero. The new dynamics of the state process $X_t = [X_t^{(1)}, X_t^{(3)}, \zeta_t]'$ read:

$$\begin{aligned} dX_t^{(1)} &= 0, && \text{for } t \in (t_m, t_{m+1}), \\ dX_t^{(3)} &= (\mu_3 - \tfrac{1}{2}\sigma_3^2)dt + \sigma_3 dW_t^{(3)}, && \text{for } t \in (t_m, t_{m+1}), \\ d\zeta_t &= dt - \zeta_t dq_t, && \text{for } t \in (t_m, t_{m+1}), \\ X_{t_m} &= X_{t_m^-} + [u_m, 0, -\zeta_{t_m^-}]', && m \in \mathbb{N}. \end{aligned} \tag{3.33}$$

In this case we have a jump diffusion state process and a disaster changes the state process by an $\mathcal{F}_t$-measurable value ζ_t. An important difference between the harvesting and dike height problem is the positive influence of the stand age on the revenues in the harvesting problem and the independence of the dike age on the construction costs in the dike height problem. We might wonder whether it is realistic to postpone an increase of the dike level when ζ_t is small. Construction costs that are increasing in the dike age may model the effect of dike deterioration, since this advances the dike reinforcements for a longer time that has past after the last dike increase or disaster. We propose to use the construction costs $b(x_1, \zeta, u)$, which are increasing in ζ. The value function reads:

$$\begin{aligned} v(t,x) = \inf_{\mathbf{u}\in\mathcal{U}} E^{t,x}\Bigg[&\sum_{\tau_i \in [t,T]} e^{-\rho(\tau_i - t)} \exp(X_{\tau_i}^{(3)}) l_p(w(\tau_i) + \mathcal{J}_{\tau_i} - X_{\tau_i}^{(1)}) \\ &+ \sum_{t \le t_m < T} e^{-\rho(t_m - t)} b(X_{t_m^-}^{(1)}, \zeta_{t_m^-}, u_m) + e^{-\rho(T-t)} b_T(X_T^{(1)}, X_T^{(3)}) \Bigg]. \end{aligned} \tag{3.34}$$

The Hamilton-Jacobi-Bellman equation associated to this value function is:

$$\begin{aligned} \max\Big[&- v_t + rv(t,x) - \mathcal{L}v(t,x) - \lambda[v(t,x_1,x_3,0) - v] - \lambda \exp(x_3)\beta(x_1 - w(t)), \\ &v(t,x) - \inf_{u\in U}[v(t,x_1+u,x_3,0) + b(x_1,\zeta,u)]\Big] = 0, \\ &(t,x) = (t,x_1,x_3,\zeta) \in [0,T) \times \mathbb{R}^3, \end{aligned} \tag{3.35}$$

with terminal condition $v(T,x) = b_T(x)$. Remark that the operator $\mathcal{L}v(t,x)$ now includes the derivative v_ζ.

Now a disaster affects the state dynamics by sending ζ_t to zero. This also affects the new construction costs $b(x,\zeta,u)$. A higher dike age, to be precise a longer time that has past after a disaster or dike increase, will advance the next heightening. Although this may reasonably model the deterioration of dikes, it seems not realistic that the construction costs are really increasing in the dike age. Besides, it might be difficult to find an appropriate model for the construction costs depending on the dike age. The modelling of dike deterioration is also discussed in Section 3.3.3.

3.3.3 Soil compression and deterioration

In the harvesting problem the longer time that has past after a disaster or a harvest, the higher the revenues from harvesting and the earlier a harvest is profitable. We ask ourselves again whether it is realistic to add something similar to the dike height problem. In the previous model the dike age, which is determined by the last dike increase or disaster, positively affects the construction costs b and models dike deterioration by that. It is realistic to assume that the longer the time that has past after a dike increase, the earlier a next dike increase is necessary. In this section we want to adapt the state dynamics to account for this.

This new model is based on the discrete dike height model in [22] where soil compression factors affect the dike height in the following way:

$$X^{(1)}(t+1) = X^{(1)}(t) + u(t) - \gamma_1 u(t-1) - \gamma_2 u(t-2) - \gamma_3 u(t-3). \tag{3.36}$$

$\{\dots, t-3, t-2, t-1, t, t+1, \dots\}$ are the discrete times, $X^{(1)}(t)$ is the dike height at time t, $u(t)$ is the dike increase at time t and $\gamma_1, \gamma_2, \gamma_3 \in [0,1)$ are the soil compression factors in the first, second and third year after a dike increase. In an example for an island the factors $\gamma_1 = 0.05$, $\gamma_2 = 0.03$ and $\gamma_3 = 0.01$ are used. With this a dike increase is assumed to reduce by 9% after three years.

We suggest to incorporate a *rate of soil compression and deterioration* of the dikes by a function γ. We assume that only the time of last raising and not the time of the last disaster affects this rate. For this we introduce ς_t as the time of the last dike increase, which is independent of floods. The proposed state dynamics are:

$$\begin{aligned}
dX_t^{(1)} &= -\gamma(t,\varsigma_t) X_t^{(1)} dt, && \text{for } t \in (t_m, t_{m+1}),\\
dX_t^{(3)} &= (\mu_3 - \tfrac{1}{2}\sigma_3^2)dt + \sigma_3 dW_t^{(3)}, && \text{for } t \in (t_m, t_{m+1}),\\
d\varsigma_t &= dt, && \text{for } t \in (t_m, t_{m+1}),\\
X_{t_m} &= X_{t_m^-} + [u_m, 0, -\varsigma_{t_m^-}]', && m \in \mathbb{N},
\end{aligned} \tag{3.37}$$

where $\gamma(t,\varsigma_t) \in [0,1)$ models the soil compression and deterioration of the dikes and depends on ς_t. We use the same value function as in equation (3.26) including an additional state variable ς. The associated HJB equation for this model is

$$\begin{aligned}
\max\Big[&- v_t + rv(t,x) - \mathcal{L}v(t,x) - \lambda \exp(x_3)\beta(x_1 - w(t)),\ v(t,x) - \\
&\inf_{u \in U}[v(t, x_1 + u, x_3, 0) + b(x_1, u)]\Big] = 0, \quad (t,x) = (t, x_1, x_3, \varsigma) \in [0,T) \times \mathbb{R}^3,
\end{aligned} \tag{3.38}$$

where

$$\mathcal{L}v(t,x) = -\gamma(t,\varsigma)x_1 \frac{\partial v}{\partial x_1}(t,x) + (\mu_3 - \frac{1}{2}\sigma_3^2)\frac{\partial v}{\partial x_3}(t,x) + \frac{\partial v}{\partial \varsigma}(t,x) + \frac{1}{2}\sigma_3^2 \frac{\partial^2 v}{\partial x_3^2}(t,x). \tag{3.39}$$

3.3.4 A recovery rate

In the dike height problems discussed so far we assumed that the economic value is recovered immediately in case of a flood. However, it seems more realistic to assume an immediate loss of economic value if a flood occurs, but a certain recovery time with a *recovery rate* before all losses are recovered. We wish to remember the flood losses made, but still maintain a Markovian state process. For this we introduce a new process $X_t^{(4)}$ which keeps track of the flood losses that are not yet recovered. These losses are recovered with a positive recovery rate $R(t, X_t)$, which is zero if there are no flooding costs remaining.

We model the economic value of endangered goods by:

$$dY_t^{(3)} = \mu_3 Y_t^{(3)} dt + \sigma_3 Y_t^{(3)} dW_t^{(3)} - Y_t^{(3)} l_p(w(t) + \mathcal{J}_t - X_t^{(1)}) dq_t + Y_t^{(3)} R(t, X_t) dt. \tag{3.40}$$

The first two terms are the same as in equation (3.1). The third term represents the flood losses and the last term denotes the recovery of the economic value in time. Then the dynamics of the flood losses that are not yet recovered read

$$dX_t^{(4)} = -Y_t^{(3)} R(t, X_t)dt + Y_t^{(3)} l_p(w(t) + \mathcal{J}_t - X_t^{(1)})dq_t. \tag{3.41}$$

We use Itô calculus to find

$$\begin{aligned}
\log(Y_t^{(3)}) &= \log(Y_0^{(3)}) + \int_0^t \mu_3 - \frac{1}{2}\sigma_3^2 + R(s, X_s)ds + \int_0^t \sigma_3 dW_s^{(3)} \\
&+ \sum_{0<s\leq t} [\log\left(Y_{s^-}^{(3)} - Y_{s^-}^{(3)} l_p(w(s) + \mathcal{J}_s - X_s^{(1)})\right) - \log(Y_{s^-}^{(3)})]dq_s \\
&= \log(Y_0^{(3)}) + \int_0^t \mu_3 - \frac{1}{2}\sigma_3^2 + R(s, X_s)ds + \int_0^t \sigma_3 dW_s^{(3)} \\
&+ \sum_{0<s\leq t} \log\left(1 - l_p(w(s) + \mathcal{J}_s - X_s^{(1)})\right)dq_s.
\end{aligned} \tag{3.42}$$

So, for the log-economic value of endangered goods we have

$$dX_t^{(3)} = d\log(Y_t^{(3)}) = \left(\mu_3 - \frac{1}{2}\sigma_3^2 + R(t, X_t)\right)dt + \sigma_3 dW_t^{(3)} + \log\left(1 - l_p(w(t) + \mathcal{J}_t - X_t^{(1)})\right)dq_t. \tag{3.43}$$

The state dynamics can be expressed by

$$\begin{aligned}
dX_t^{(1)} &= 0, && t \in (t_m, t_{m+1}), \\
dX_t^{(3)} &= \left(\mu_3 - \tfrac{1}{2}\sigma_3^2 + R(t, X_t)\right)dt + \sigma_3 dW_t^{(3)} + \log\left(1 - l_p(w(t) + \mathcal{J}_t - X_t^{(1)})\right)dq_t, && t \in (t_m, t_{m+1}), \\
dX_t^{(4)} &= -\exp(X_t^{(3)})R(t, X_t)dt + \exp(X_t^{(3)})l_p(w(t) + \mathcal{J}_t - X_t^{(1)})dq_t, && t \in (t_m, t_{m+1}), \\
X_{t_m} &= X_{t_m^-} + [u_m, 0, 0]', && m \in \mathbb{N}.
\end{aligned} \tag{3.44}$$

Using the stochastic control theory from Section 2.4 we obtain the HJB equation associated to value function (3.26), with additional state variable x_4:

$$\begin{aligned}
\max\Big[&- v_t + rv(t,x) - \mathcal{L}v(t,x) - \lambda E[v(t, x_1, x_3 + \Theta_1, x_4 + \Theta_2) - v] - \lambda x_3 \beta(x_1 - w(t)), \\
&v(t,x) - \inf_{u \in U}[v(t, x + (u, 0, 0)) + b(x_1, u)]\Big] = 0, \quad (t,x) = (t, x_1, x_3, x_4) \in [0,T) \times \mathbb{R}^3,
\end{aligned} \tag{3.45}$$

where the expectation is taken with respect to the size of the extreme water level $\mathcal{J}$, with the jumps $\Theta_1 = \log\left(1 - l_p(w(t) + \mathcal{J} - x_1)\right)$ and $\Theta_2 = \exp(x_3) l_p(w(t) + \mathcal{J} - x_1)$. The operator $\mathcal{L}$ is given by

$$\mathcal{L}v(t,x) = (\mu_3 - \frac{1}{2}\sigma_3^2 + R(t,x))\frac{\partial v}{\partial x_3}(t,x) - e^{x_3} R(t,x)\frac{\partial v}{\partial x_4}(t,x) + \frac{1}{2}\sigma_3^2 \frac{\partial^2 v}{\partial x_3^2}(t,x). \tag{3.46}$$

The recovery rate $R(t, X_t)$ depends on the time t and state process X_t and must be equal to zero if all losses are recovered. We can model for example the case where the recovery rate is higher when the flood losses that are not recovered yet are high, for example

$$R(t, X_t) = \begin{cases} 0.5X_t^{(4)} + 0.2, & \text{for } X_t^{(4)} > 0, \\ 0, & \text{for } X_t^{(4)} \leq 0. \end{cases} \tag{3.47}$$

The recovery rate model shows some interesting similarities with the harvesting problem. If a fire in the forest happens the stand age jumps to zero and recovers in time. The stand age affects the harvesting revenues and the possible losses from a fire. In the above model a flood causes a sudden decrease in the economic value, which recovers hereafter at a certain rate. The economic value of endangered goods does not affect the construction costs, but it influences the possible losses from a next flood and in this way the dike increase time is delayed.

3.4 Discussion

The model extensions we proposed in the previous sections make the dimension of the state dynamics higher and thus also the dimension of the HJB equation. In this discussion we wonder whether these extensions are really useful and which model is best to use in the sequel.

A model we did not discuss until now is a model with deterministic log-economic value of endangered goods: $X_t^{(3)} = X_0^{(3)} + \mu_3 t$. This model is used in [32] and in discrete form in [22] and reduces the space dimension of the HJB equation to one. Although this model is not very realistic and there are no stochastic processes, it represents a basic model and is easy to start with. However, this model is not interesting with respect to the stochastic solution method that we will develop in Section 4.

Instead of one stochastic process, the economic value of endangered goods, we can consider the average water level as a stochastic process too. As there is a lot of discussion about the future water level rise, this seems a relevant extension.

In the third dike model, Section 3.3.2, we aimed to resemble concepts from the harvesting problem by introducing the dike age ζ_t, similar to the forest stand age. If the dike age does not influence the construction costs or the losses from flooding this addition does not seem very useful. On the other hand, construction costs which are increasing in the dike age may model the dike deterioration. However, it might be difficult to find an appropriate model for the construction costs depending on the dike age and it does not seem realistic that the construction costs are increasing in the dike age.

We think that the use of a soil compression and deterioration rate is realistic, because the quality of dikes gets worse over time. The longer the time that has past after the last dike increase, the earlier the next increase may become necessary. However, if this rate is almost zero it will not affect the problem greatly.

Also incorporating a recovery rate for the economy in the dike model is realistic. Now the losses from flooding are not recovered immediately and economic recovery happens at a certain recovery rate, which can depend on, for example, the losses that are not yet recovered or the economic value remaining. This is comparable with the stand age in the harvesting problem, which becomes zero if a fire takes place and increases over time afterwards. Most easy is the case of a constant recovery rate until there are no flood losses left.

A disadvantage of the models with stochastic water level, dike age, soil compression and deterioration rate and recovery rate, is the dimensionality that we get, since this results in three-space-dimensional partial differential equations.

In the remainder of the Master Thesis we firstly focus on the basic model from Section 3.1. Secondly, the extended version with stochastic average water level comes up in Section 8. We discuss computational difficulties of the models with recovery rate and with a soil compression and deterioration rate in Section 8.4.1. We will not use the model with the dike age.

4 The dike-COS method: A Fourier-cosine valuation method for one-factor Lévy processes

In [10] an option pricing method for European options based on Fourier-cosine series was developed. This method was called the COS method and was extended in [11] to pricing Bermudan, barrier and American options. In this section we explain the generalisation to the *dike-COS method* to solve the dike height problem for the first model (Section 3.1) with only **one** stochastic process, namely the economic value of endangered goods. This problem is a stochastic impulse control problem, as we explained in Section 3.1.1.

We start discussing the dynamic programming principle for a discrete time lattice. Then the COS formula, which can help with the approximation of expectations, is explained in Section 4.1. In Section 4.2 a recursive algorithm is developed.

Let t_0 denote the initial time and $t_M = T$ the terminal time. At these times no dike increase is prescribed. We take a finite number of fixed control times $\{t_1, t_2, \ldots, t_m, \ldots, t_{M-1}\}$ with $\Delta t := t_m - t_{m-1}$ and $t_0 < t_1 < \ldots < t_M$. At the control times one can increase the dike level. The set of possible dike level increases is $U = \{u^0, u^1, u^2, \ldots, u^K\}$, with K a finite number, $u^0 = 0$ and $u^0 < u^1 < u^2 < \ldots < u^K$. For example, $U = \{0,\ 40,\ 60,\ 80\}$ cm. At each control time one has to decide whether or not to increase the dike level and by which amount.

Value function $v(t,x) = v(t, x_1, x_3)$ denotes the expected costs of flood protection at time t, with dike level x_1 and log-economic value of endangered goods x_3, under optimal heightenings. Note that the process $Y_t^2 = w(t)$ is omitted as variable as before, because it is a deterministic function of time t. The following impulse control problem to formulate the dike height problem is obtained as in Section 3.1.1:

$$\begin{aligned} v(t,x) &= \min_{\mathbf{u}\in\mathcal{U}} E^{t,x}\Bigg[\sum_{\tau_i\in[t,T]} e^{-\rho(\tau_i - t)} \exp(X^{(3)}_{\tau_i}) l_p(w(\tau_i) + \mathcal{J}_{\tau_i} - X^{(1)}_{\tau_i}) \\ &\quad + \sum_{t\le t_m<T} e^{-\rho(t_m - t)} b(X^{(1)}_{t_m^-}, u_m) + e^{-\rho(T-t)} b_T(X^{(1)}_T, X^{(3)}_T)\Bigg]. \end{aligned} \tag{4.1}$$

This value can be seen as a real option value. The set $\mathbf{u} = (\{t_m\}, u_m)$ denotes the impulse control and $\mathcal{U}$ is the set of all $\mathbf{u}$ such that $u_m \in U = \{u^0, u^1, u^2, \ldots\ u^K\}$. In this notation a subscript indicates the control time and a superscript the size of the dike increase. Note that the dike level remains constant within the intervals $[t_{m-1}, t_m^-]$. The dynamic programming principle gives, for $m = 1, \ldots, M$:

$$\begin{aligned} v(t_{m-1}, x_1, x_3) &= E^{t_{m-1},x}\Bigg[\sum_{\tau_i\in[t_{m-1},t_m]} e^{-\rho(\tau_i - t_{m-1})} \exp(X^{(3)}_{\tau_i}) l_p\left(w(\tau_i) + \mathcal{J}_{\tau_i} - x_1\right)\Bigg] \\ &\quad + E^{t_{m-1},x}\left[e^{-\rho\Delta t} v(t_m^-, x_1, X^{(3)}_{t_m})\right], \end{aligned} \tag{4.2}$$

followed by

$$\begin{aligned} v(t_m^-, x_1, y) &= \mathcal{M} v(t_m, x_1, y) \\ &= \min_{u^i\in U}\left[v(t_m, x_1 + u^i, y) + b(x_1, u^i)\right], \qquad (m \neq 0, M). \end{aligned} \tag{4.3}$$

After terminal time T the dike height and average water level are assumed to remain constant and the

terminal costs are given by the expected flooding costs hereafter:

$$\begin{aligned} v(T, x_1, x_3) &= b_T(x_1, x_3) \\ &= E^{T,x}\left[\sum_{\tau_i \in [T,\infty)} e^{-\rho(\tau_i - T)} \exp(X^{(3)}_{\tau_i}) l_p(w(T) + \mathcal{J}_{\tau_i} - x_1)\right] \\ &= \lambda \int_T^\infty e^{-\rho(s-T)} E^{T,x}[\exp(X^{(3)}_s)]\beta(x_1 - w(T))ds \\ &= \lambda\beta(x_1 - w(T)) \exp(x_3) \int_T^\infty e^{(\mu_3 - \rho)(s-T)} ds \\ &= \frac{\lambda\beta(x_1 - w(T))}{\rho - \mu_3} \exp(x_3). \end{aligned} \tag{4.4}$$

The terminal costs are decreasing in x_1 and increasing in x_3.

The first part of equation (4.2) is the expected running costs from flooding in $[t_{m-1}, t_m]$:

$$\begin{aligned} & E^{t_{m-1},x}\left[\sum_{\tau_i \in [t_{m-1}, t_m]} e^{-\rho(\tau_i - t_{m-1})} \exp(X^{(3)}_{\tau_i}) l_p\left(w(\tau_i) + \mathcal{J}_{\tau_i} - x_1\right)\right] \\ &\quad = \lambda \int_{t_{m-1}}^{t_m} e^{-\rho(s - t_{m-1})} E^{t_{m-1},x}[\exp(X^{(3)}_s)] E^{t_{m-1},x}[l_p\left(w(s) + \mathcal{J} - x_1\right)] ds \\ &\quad = \exp(x_3)\lambda \int_{t_{m-1}}^{t_m} e^{(s - t_{m-1})(\mu_3 - \rho)} \beta(x_1 - w(s)) ds \\ &\quad := \exp(x_3) d(t_{m-1}, t_m, x_1). \end{aligned} \tag{4.5}$$

Function d is called the *proportional damage function*. Function β admits an analytical solution for the Gumbel distributed extreme water level sizes, as shown in Section 4.3. The above time integral is approximated by applying the Composite Trapezoidal rule with N_t integration steps. The approximated value is denoted by $\hat{d}(t_{m-1}, t_m, x_1)$.

The second part of equation (4.2) represents the expected costs of flood protection at the next time step, t_m^-, denoted as the *continuation value* $c(t_{m-1}, x_1, x_3)$. The expectation is taken with respect to the stochastic log-economic value of endangered goods. In Section 4.1 we explain a method to estimate this value. With the above notation, the real option value can be written as

$$v(t_{m-1}, x_1, x_3) = \exp(x_3) d(t_{m-1}, t_m, x_1) + c(t_{m-1}, x_1, x_3). \tag{4.6}$$

4.1 COS formula for the continuation value

The expectation $c(t_{m-1}, x_1, x_3)$ can be approximated by the COS method. The COS method is based on the Fourier-cosine series expansion of the density function of the stochastic process. It relies on the insight that the characteristic function is closely related to the series coefficients of this expansion. We assume that the reader is familiar with these concepts. The following theory is derived from [10] and [11].

From now on function f denotes a density function instead of a running profit function as we saw in, for example, equation (2.6). We start with

$$c(t_{m-1}, x_1, x_3) = e^{-\rho\Delta t} E^{t_{m-1},x}\left[v(t_m^-, x_1, X^{(3)}_{t_m})\right] = e^{-\rho\Delta t} \int_{\mathbb{R}} v(t_m^-, x_1, y) f(y|x_3) dy. \tag{4.7}$$

The conditional density function $f(y|x_3)$ decays to zero rapidly as $y \to \pm\infty$. Because of that we can truncate the infinite integration range of the expectation to some interval $[a, b] \subset \mathbb{R}$ without loosing

significant accuracy. We obtain the approximation

$$\begin{aligned} c_1(t_{m-1}, x_1, x_3) &= e^{-\rho\Delta t} \int_a^b v(t_m^-, x_1, y) f(y|x_3) dy \\ &= e^{-\rho\Delta t} \int_a^b v(t_m^-, x_1, y) \sum_{k=0}^{+\infty}{}' G_k(x_3) \cos\left(k\pi \frac{y-a}{b-a}\right) dy. \end{aligned} \tag{4.8}$$

In the second line of equation (4.8) the conditional density is replaced by its Fourier-cosine expansion in y on $[a, b]$, with series coefficients $\{G_k(x_3)\}_{k=0}^{+\infty}$ defined by

$$G_k(x_3) := \frac{2}{b-a} \int_a^b f(y|x_3) \cos\left(k\pi \frac{y-a}{b-a}\right) dy. \tag{4.9}$$

The notation c_i is used for the different approximations of c and keeps track of the numerical errors that set in from each step. We interchange summation and integration and insert the definition

$$V_k(t_m^-, x_1) := \frac{2}{b-a} \int_a^b v(t_m^-, x_1, y) \cos\left(k\pi \frac{y-a}{b-a}\right) dy, \tag{4.10}$$

which are the Fourier-cosine series coefficients of $v(t_m^-, x_1, y)$ on $[a, b]$. This results in

$$c_1(t_{m-1}, x_1, x_3) = \frac{b-a}{2} e^{-\rho\Delta t} \sum_{k=0}^{+\infty}{}' G_k(x_3) V_k(t_m^-, x_1). \tag{4.11}$$

Note that the product of $f(y|x_3)$ and $v(t_m^-, x_1, y)$ is transformed to a product of their Fourier-cosine series coefficients. Truncation of the series summation gives the approximation

$$c_2(t_{m-1}, x_1, x_3) = \frac{b-a}{2} e^{-\rho\Delta t} \sum_{k=0}^{N-1}{}' G_k(x_3) V_k(t_m^-, x_1). \tag{4.12}$$

The coefficients $G_k(x_3)$ can be approximated as follows

$$\begin{aligned} G_k(x_3) &\approx \frac{2}{b-a} \int_{\mathbb{R}} f(y|x_3) \cos\left(k\pi \frac{y-a}{b-a}\right) dy \\ &= \frac{2}{b-a} \Re\left[\int_{\mathbb{R}} f(y|x_3) e^{ik\pi \frac{y}{b-a}} dy e^{-ik\pi \frac{a}{b-a}}\right] \\ &= \frac{2}{b-a} \Re\left[\varphi\left(\frac{k\pi}{b-a}\middle| x_3\right) e^{-ik\pi \frac{a}{b-a}}\right] := F_k(x_3). \end{aligned} \tag{4.13}$$

$\varphi(.|x_3)$ is the conditional characteristic function of $X_{t_m}^{(3)}$, given that $X_{t_{m-1}}^{(3)} = x_3$. The density function of a stochastic process is usually not known, whereas the characteristic function is known. Inserting the above gives the *COS formula* for approximation of $c(t_{m-1}, x_1, x_3)$:

$$\begin{aligned} \hat{c}(t_{m-1}, x_1, x_3) &= e^{-\rho\Delta t} \sum_{k=0}^{N-1}{}' \Re\left[\varphi\left(\frac{k\pi}{b-a}\middle| x_3\right) e^{-ik\pi \frac{a}{b-a}}\right] V_k(t_m^-, x_1) \\ &= e^{-\rho\Delta t} \sum_{k=0}^{N-1}{}' \Re\left[\varphi_{levy}\left(\frac{k\pi}{b-a}\right) e^{ik\pi \frac{x_3-a}{b-a}}\right] V_k(t_m^-, x_1), \end{aligned} \tag{4.14}$$

where the last equality holds for Lévy processes, with $\varphi_{levy}(u) := \varphi(u|0)$. The process used for the log-economic value of endangered goods is indeed a Lévy process. Finally, we end up with

$$\hat{v}(t_{m-1}, x_1, x_3) = \exp(x_3)\hat{d}(t_{m-1}, t_m, x_1) + e^{-\rho\Delta t} \sum_{k=0}^{N-1}{}' \Re\left[\varphi_{levy}\left(\frac{k\pi}{b-a}\right) e^{ik\pi \frac{x_3-a}{b-a}}\right] V_k(t_m^-, x_1). \tag{4.15}$$

Since the terms $V_k(t_m^-, x_1)$ are independent of x_3, we can calculate the real option value for many log-economic values x_3 simultaneously. It is even possible to calculate the option value for many different dike levels simultaneously:

$$\hat{v}(t_{m-1}, \mathbf{x_1}, \mathbf{x_3}) = \exp(\mathbf{x_3})\hat{d}(t_{m-1}, t_m, \mathbf{x_1}) + e^{-\rho\Delta t}{\sum_{k=0}^{N-1}}' \Re\left[\varphi_{levy}\left(\frac{k\pi}{b-a}\right) e^{ik\pi\frac{\mathbf{x_3}-a}{b-a}}\right] \mathbf{V}_k(t_m^-, \mathbf{x_1}). \quad (4.16)$$

4.2 Recursion formula for coefficients V_k

In this section a recursive algorithm for the dike height problem is explained. First we choose a grid for the dike level x_1, for example $x_1 \in [425, 505, 585, 665, 745]$ cm. It is important for the algorithm that this grid coincides with the grid points of $x_1 + u^i$, $\forall\, i$, except for the first and last entries. Let D denote the *number of dike level grid points*.

Coefficients at time t_M^-
For approximating the option prices at time t_{M-1} we need the coefficients $V_k(t_M^-, x_1)$. Their exact representation reads:

$$\begin{aligned} V_k(t_M^-, x_1) &= \frac{2}{b-a}\int_a^b v(T, x_1, y)\cos\left(k\pi\frac{y-a}{b-a}\right)dy \\ &= \frac{2}{b-a}\int_a^b \frac{\lambda\beta(x_1 - w(T))}{\rho - \mu_3}\exp(y)\cos\left(k\pi\frac{y-a}{b-a}\right)dy \\ &= \frac{\lambda\beta(x_1 - w(T))}{\rho - \mu_3}\frac{2}{b-a}\chi_k(a,b), \end{aligned} \quad (4.17)$$

where the analytical solution of $\chi_k(z_1, z_2)$ can be found in Appendix A.

Next we consider the coefficients that are used to estimate the real option values at times $t_0, \ldots, t_{M-2}$. In the terms $V_k(t_m^-, x_1)$ the option value appears:

$$v(t_m^-, x_1, y) = \min_{u^i \in U}\left[v(t_m, x_1 + u^i, y) + b(x_1, u^i)\right]. \quad (4.18)$$

The construction costs are given by

$$b(x_1, u) = \begin{cases} 0, & \text{for } u = 0, \\ b^+(x_1, u), & \text{for } u > 0, \end{cases} \quad (4.19)$$

where $b^+(x_1, u)$ is a smooth function, increasing in x_1 and u, and $b^+(x_1, 0) \neq 0$.

We suppose that, for a fixed dike level, a higher economic value of endangered goods leads to a higher, or equal, optimal reinforcement level (see results in [32]). Assume that we can find intervals $A_m^i(x_1) \subset [a, b]$, such that for a log-economic value $y \in A_m^i(x_1)$ it is optimal to increase the dike level x_1 at control time t_m by an amount u^i. These intervals are named the *construction domains*. We will explain an algorithm to determine these domains in Section 4.2.1. For $x_1 + u^i$ higher than the largest dike level grid point we take $A_m^i(x_1)$ empty, implying that the dike heightening involved is not allowed anymore.

With the construction domains we can split the integral in the definition of V_k into parts, independent

of k:

$$\begin{aligned} V_k(t_m^-, x_1) &= \frac{2}{b-a}\int_a^b v(t_m^-, x_1, y)\cos\left(k\pi\frac{y-a}{b-a}\right)dy \\ &= \frac{2}{b-a}\int_a^b \min_{u^i\in U}\left[v(t_m, x_1+u^i, y)+b(x_1,u^i)\right]\cos\left(k\pi\frac{y-a}{b-a}\right)dy \\ &= \frac{2}{b-a}\sum_{i=0}^{K}\int_{A_m^i(x_1)} v(t_m, x_1+u^i, y)\cos\left(k\pi\frac{y-a}{b-a}\right)dy \\ &+ \frac{2}{b-a}\sum_{i=1}^{K}\int_{A_m^i(x_1)} b(x_1,u^i)\cos\left(k\pi\frac{y-a}{b-a}\right)dy \\ &:= \sum_{i=0}^{K} C_k(A_m^i(x_1), t_m, x_1+u^i) + \sum_{i=1}^{K} B_k(A_m^i(x_1), x_1, u^i), \qquad (m\neq 0, M). \end{aligned} \tag{4.20}$$

Next, the backward recursion of the coefficients V_k will be explained.

Coefficients at time t_{M-1}^-
For approximation of the option prices at time t_{M-2} we need the exact coefficients $V_k(t_{M-1}^-, x_1)$. We will use the approximated option value $\hat{v}(t_{M-1}, y_1, y)$ to approximate the terms $C_k(z_1, z_2, t_{M-1}, y_1)$, where the variables z_1 and z_2 denote the boundaries of the construction domain. This approximation is denoted by $\hat{C}_k(z_1, z_2, t_{M-1}, y_1)$. This results in the approximated coefficient:

$$\hat{V}_k(t_{M-1}^-, x_1) := \sum_{i=0}^{K}\hat{C}_k(A_{M-1}^i(x_1), t_{M-1}, x_1+u^i) + \sum_{i=1}^{K} B_k(A_{M-1}^i(x_1), x_1, u^i). \tag{4.21}$$

Note that the terms B_k are time-independent and known analytically:

$$\begin{aligned} B_k(z_1, z_2, x_1, u^i) &= \frac{2}{b-a}\int_{z_1}^{z_2} b(x_1,u^i)\cos\left(k\pi\frac{y-a}{b-a}\right)dy \\ &= \frac{2}{b-a}b(x_1,u^i)\int_{z_1}^{z_2}\cos\left(k\pi\frac{y-a}{b-a}\right)dy \\ &= \frac{2}{b-a}b(x_1,u^i)\psi_k(z_1,z_2), \end{aligned} \tag{4.22}$$

with $\psi_k(z_1, z_2)$ as defined in Appendix A. On the integrants of terms $\hat{C}_k$ we can apply again the Fourier-

cosine expansion by inserting equation (4.15). This reads

$$\begin{aligned}
\hat{C}_k(z_1,z_2,t_{M-1},y_1) &= \frac{2}{b-a}\int_{z_1}^{z_2}\hat{v}(t_{M-1},y_1,y)\cos\left(k\pi\frac{y-a}{b-a}\right)dy \\
&= \frac{2}{b-a}\int_{z_1}^{z_2}\exp(y)\hat{d}(t_{M-1},t_M,y_1)\cos\left(k\pi\frac{y-a}{b-a}\right)dy \\
&+ e^{-\rho\Delta t}\frac{2}{b-a}\int_{z_1}^{z_2}\left(\sum_{j=0}^{N-1}{}'\Re\left[\varphi_{levy}\left(\frac{j\pi}{b-a}\right)e^{ij\frac{y-a}{b-a}}\right]V_j(t_M^-,y_1)\right)\cos\left(k\pi\frac{y-a}{b-a}\right)dy \\
&= \frac{2}{b-a}\hat{d}(t_{M-1},t_M,y_1)\int_{z_1}^{z_2}\exp(y)\cos\left(k\pi\frac{y-a}{b-a}\right)dy \\
&+ e^{-\rho\Delta t}\Re\left\{\sum_{j=0}^{N-1}{}'\varphi_{levy}\left(\frac{j\pi}{b-a}\right)V_j(t_M^-,y_1)\frac{2}{b-a}\int_{z_1}^{z_2}e^{ij\frac{y-a}{b-a}}\cos\left(k\pi\frac{y-a}{b-a}\right)dy\right\} \\
&= \frac{2}{b-a}\hat{d}(t_{M-1},t_M,y_1)\chi_k(z_1,z_2) \\
&+ e^{-\rho\Delta t}\Re\left\{\sum_{j=0}^{N-1}{}'\varphi_{levy}\left(\frac{j\pi}{b-a}\right)V_j(t_M^-,y_1)\cdot M_{k,j}(z_1,z_2)\right\}, \qquad (4.23)
\end{aligned}$$

where the coefficients $M_{k,j}(z_1,z_2)$ are given by:

$$M_{k,j}(z_1,z_2) := \frac{2}{b-a}\int_{z_1}^{z_2}e^{ij\pi\frac{y-a}{b-a}}\cos\left(k\pi\frac{y-a}{b-a}\right)dy. \qquad (4.24)$$

Finally we end up with the vector form

$$\begin{aligned}
\hat{V}(t_{M-1}^-,x_1) &= \sum_{i=0}^{K}\frac{2}{b-a}\hat{d}(t_{M-1},t_M,x_1+u^i)\chi(A_{M-1}^i(x_1)) + \sum_{i=0}^{K}e^{-\rho\Delta t}\Re\{M(A_{M-1}^i(x_1))\mathbf{w^i}\} \\
&+ \sum_{i=1}^{K}\frac{2}{b-a}b(x_1,u^i)\psi(A_{M-1}^i(x_1)), \qquad (4.25)
\end{aligned}$$

where

$$\mathbf{w^i} := \{w_j^i\}_{j=0}^{N-1} \quad \text{with} \quad w_j^i := \varphi\left(\frac{j\pi}{b-a}\right)V_j(t_M^-,x_1+u^i), \;\; w_0^i = \frac{1}{2}\varphi(0)V_0(t_M^-,x_1+u^i). \qquad (4.26)$$

The inputs of the functions χ, ψ and M represent the boundary values of their integration range.

Coefficients at time t_m^-, $1 \le m < M-1$
For the other coefficients the approximations $\hat{v}(t_m,y_1,y)$ **and** $\hat{V}_k(t_{m+1}^-,y_1)$ will be used to approximate the terms $C_k(z_1,z_2,t_m,y_1)$. The same arguments as before give the following numerical approximation of the Fourier-cosine coefficients at time t_m^-:

$$\begin{aligned}
\hat{V}(t_m^-,x_1) &= \sum_{i=0}^{K}\frac{2}{b-a}\hat{d}(t_m,t_{m+1},x_1+u^i)\chi(A_m^i(x_1)) + \sum_{i=0}^{K}e^{-\rho\Delta t}\Re\{M(A_m^i(x_1))\hat{\mathbf{w}}^{\mathbf{i}}\} \\
&+ \sum_{i=1}^{K}\frac{2}{b-a}b(x_1,u^i)\psi(A_m^i(x_1)), \qquad (m=1,\ldots,M-2), \qquad (4.27)
\end{aligned}$$

where

$$\hat{\mathbf{w}}^{\mathbf{i}} := \{\hat{w}_j^i\}_{j=0}^{N-1} \quad \text{with} \quad \hat{w}_j^i := \varphi\left(\frac{j\pi}{b-a}\right)\hat{V}_j(t_{m+1}^-,x_1+u^i), \;\; \hat{w}_0^i = \frac{1}{2}\varphi(0)\hat{V}_0(t_{m+1}^-,x_1+u^i). \qquad (4.28)$$

An extra error is introduced because the real option values are approximated by using $\hat{V}_k$. We will discuss this propagating error in Section 5.2.

Fast Fourier Transform
The matrix-vector product $M\mathbf{w}$ in the terms $\hat{C}$ can be computed by an Fourier-based algorithm, as stated in the following theorem.

Theorem 4.1. *(Efficient computation of $\hat{C}(z_1, z_2, t_m, y_1)$)[11]*
The matrix-vector product $M(z_1, z_2)\mathbf{w}$ in equations (4.25) and (4.27) can be computed in $O(N \log_2 N)$ operations with the help of the Fast Fourier Transform (FFT) algorithm.

The key insight of this efficient computation is the equality

$$M_{k,j}(z_1, z_2) = -\frac{i}{\pi}\left(M^c_{k,j}(z_2, z_2) + M^s_{k,j}(z_1, z_2)\right), \tag{4.29}$$

and the fact that the matrix M^c is a Hankel matrix and M^s is a Toeplitz matrix ($M^c_{i,j} = M^c_{i-1,j+1}$ and $M^s_{i,j} = M^s_{i+1,j+1}$). The matrices $M^c_{k,j}$ and $M^s_{k,j}$ can be found in Appendix D. These special structures make the calculation of the matrix-vector products efficient using FFT algorithms, as described in [11] and [5].

Algorithm
We can recover the terms $\hat{V}_k(t_m^-, x_1)$ recursively, starting at $V_k(t_M^-, x_1)$. The algorithm to solve the dike height problem backwards in time reads:

Algorithm 1. *(Dike-COS method)*

Initialisation:
Calculate coefficients $V_k(t_M^-, x_1)$ for $k = 0, 1, \ldots, N-1$ and all possible dike levels x_1.

Main loop to recover $\hat{V}(t_m^-, x_1)$:
For $m = M-1$ to 1:

- *Determine the construction domains $A^i_m(x_1)$ with the Bisection method (see Section 4.2.1).*
- *Compute $\hat{V}(t_m^-, x_1)$ for all possible dike levels (with the help of the FFT algorithm).*

Final step:
Compute $\hat{v}(t_0, x_1, x_3)$ by inserting $\hat{V}_k(t_1^-, x_1)$ into equation (4.15).

Computational complexity
The computational complexity of the dike-COS method depends on the following six parameters:

$M-1$,	the number of control times,
N,	the number of coefficients in the series expansion,
K,	the number of possible dike increase levels unequal to zero,
D,	the number of dike level grid points,
N_t,	the number of integration steps for the Trapezoidal rule,
N_{bis},	the number of iterations of the Bisection method to locate $A^i_m(x_1)$ (see Section 4.2.1).

(4.30)

The initialisation of the above algorithm takes $O(ND)$ operations. Location of all domains $A^i_m(x_1)$ at each time lattice has complexity $O(DKN_{bis})$. The computation of a vector $\hat{C}(z_1, z_2, t_m, y_1)$ has complexity $O(N_t + N \log_2 N)$ with the help of the Trapezoidal rule and the FFT algorithm. This dominates the

computation of $B(z_1, z_2, x_1, u^i)$, which is linear in N. So, the work needed to compute $\hat{V}(t_m^-, x_1)$ for all possible dike levels is $O(DK(N_t + N\log_2 N))$. Then the total work required for the main loop is

$$O\Big((M-1)DK(N_{bis} + N_t + N\log_2 N)\Big). \tag{4.31}$$

The computation complexity of the final step is $O(N_t + N)$.

Comparison with financial options and authors contribution
We discuss some similarities between our real option problem and the Bermudan and the swing options, which are financial options. The holder of a *Bermudan option* can exercise his option at a finite number of fixed exercise dates, comparable with the finite number of fixed control times in the dike height problem. However, a Bermudan option can be exercised only once, whereas the real option here remains valid after a dike heightening and the dikes can be increased more than once. A *swing option* gives the right to order extra units of a commodity. The amount of commodity at each swing action can be chosen from a certain set, for example $\{-2, -1, 0, 1, 2\}$, where a negative amount implies back delivery and a positive amount means ordering. Similarly, the dike increase levels are in the set $U = \{u^0, u^1, \ldots, u^K\}$.

The main difference between these two financial options and the real option here is the possible change in the state dynamics by an impulse at the control times in the dike height problem. That is, the dike height jumps to a higher level if a reinforcement is performed. Because of that we need to keep track of the dike level. Besides there is a kind of cashflow from flooding costs in the dike height problem, which is represented by the proportional damage function d. In practice, a terminal time of the order $T \simeq 0.1 - 10$ is used for pricing financial options. However, in our numerical example of the dike height problem in Section 7 there is a much larger terminal time, $T = 300$. This results in a much larger computational domain, which may give difficulties as we will show in Section 6.3 and Section 7.1.

The dike-COS method is mainly based on the COS pricing method for Bermudan and swing options ([11] and [41]). Since we need to keep track of the dike level in our stochastic impulse control, the problem dimension is increased. Furthermore the estimation of the additional proportional damage function can take much computation time if not implemented efficiently. However, we found an analytical representation of the function $\beta(h)$, see Section 4.3, which appears to by useful and efficient. We propose an algorithm for determination of the construction domains in Section 4.2.1. Uniqueness results to justify this algorithm are assumed on the basis of the results in [32].

4.2.1 Construction domains $A_m^i(x_1)$

The determination of the domains $A_m^i(x_1)$ needs to be done carefully. It may be possible that, for example, the domain $A_m^1(x_1)$ is an empty set, whereas $A_m^0(x_1)$ and $A_m^2(x_1)$ are not. Then there exists a value y^* for which it is not optimal to heighten the dike if the log-economic value is less than y^* and it is optimal to increase the dike level by an amount u^2 if the log-economic value is higher than y^*. This is due to the fact that the function $b(x_1, u)$ is discontinuous in $u = 0$, see [32]. We explain an algorithm to determine the domains $A_m^i(x_1)$.

Suppose we are on time lattice $m \neq 0, M$. Keep in mind that $A_m^i(x_1)$ is empty for $x_1 + u^i$ higher than the largest dike level grid point. First we only consider the set of strictly positive dike increments $U^+ := U \backslash \{u^0\}$ and the corresponding option value

$$v^+(t_m^-, x_1, y) := \min_{u^i \in U^+} \left[v(t_m, x_1 + u^i, y) + b(x_1, u^i) \right]. \tag{4.32}$$

We determine the values $y_m^i(x_1)$ such that:

$$v(t_m, x_1 + u^i, y_m^i(x_1)) + b(x_1, u^i) = v(t_m, x_1 + u^{i+1}, y_m^i(x_1)) + b(x_1, u^{i+1}). \tag{4.33}$$

In other words, $y_m^i(x_1)$ represents the log-economic value at which the optimal dike increase level changes from u^i to u^{i+1} if only the set U^+ is taken into account. We assume that the values $y_m^i(x_1)$ are unique

and increasing in i, in accordance with the results of [32].

It follows that

$$v(t_m^-, x_1, y) = \min\left[v(t_m, x_1, y),\, v^+(t_m^-, x_1, y)\right]. \tag{4.34}$$

We proceed by finding the value $y_m^0(x_1)$, which is supposed to be unique, such that

$$v(t_m, x_1, y_m^0(x_1)) = v^+(t_m^-, x_1, y_m^0(x_1)). \tag{4.35}$$

This value represents the change from the case of no dike increase to the case where dike reinforcement is optimal. Now the construction domains can be found as follows:

$$A_m^i(x_1) = [a,b] \cap \begin{cases} [-\infty, y_m^0(x_1)] & \text{for } i = 0, \\ \left[-\infty, y_m^i(x_1)\right] \cap [y_m^0(x_1), \infty] & \text{for } i = 1, \\ \left[y_m^{i-1}(x_1), y_m^i(x_1)\right] \cap [y_m^0(x_1), \infty] & \text{for } 1 < i < K, \\ \left[y_m^{K-1}(x_1), \infty\right] \cap [y_m^0(x_1), \infty] & \text{for } i = K. \end{cases} \tag{4.36}$$

The preceding procedure is repeated for all possible dike levels x_1. Uniqueness of the points $y_m^0(x_1)$ and $y_m^i(x_1)$ needs to be proved formally, but we accept unicity based on the results in [32].

Examples

The previous algorithm is illustrated by two examples with $U = \{u^0, u^1, u^2\}$, $u^1 = 30$ cm, $u^2 = 60$ cm and $[a,b] = [-1.03, 30.15]$. The parameter values used are the same as introduced for the experiments with an island in Section 7.

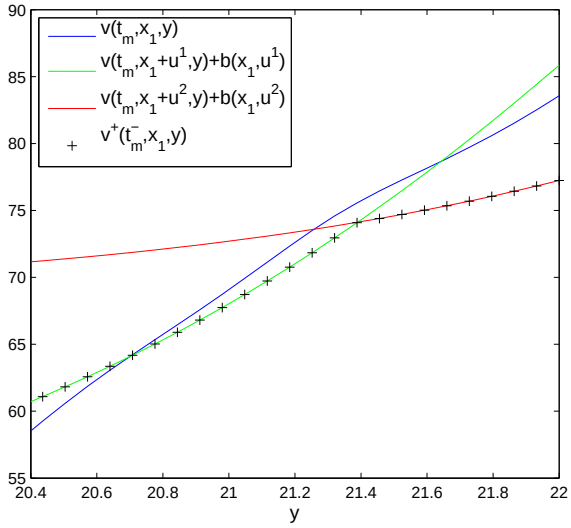

Figure 4.1: Overview of construction domains $A_m^i(x_1)$ for example 1 ($t_m = 200, x_1 = 545$).

Example 1: Figure 4.1 shows the option values for $t_m = 200$ years and $x_1 = 545$ cm. The intersection of the red and green line gives $y_m^1(x_1) \approx 21.39$. Then from the blue and dotted line, which represents $v^+(t_m^-, x_1, y)$, it follows that $y_m^0(x_1) \approx 20.70$. We deduce that

$$A_m^0(x_1) = [-1.03, 20.70], \quad A_m^1(x_1) = [20.70, 21.39], \quad A_m^2(x_1) = [21.39, 30.15]. \tag{4.37}$$

Example 2: The second example considers the construction domains for $t_m = 100$ years and $x_1 = 455$ cm. Figure 4.2 shows that $y_m^1(x_1) \approx 19.86$ and $y_m^0(x_1) \approx 20.06$. We find

$$A_m^0(x_1) = [-1.03, 20.06], \quad A_m^1(x_1) = \varnothing, \quad A_m^2(x_1) = [20.06, 30.15]. \tag{4.38}$$

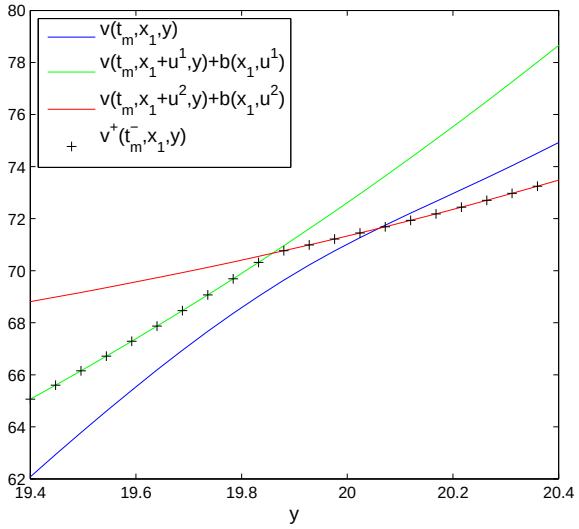

Figure 4.2: Overview of construction domains $A_m^i(x_1)$ for example 2 ($t_m = 100, x_1 = 455$).

Bisection method
We may use Newton's method to determine the points $y_m^i(x_1)$ and $y_m^0(x_1)$. However, Newton's method requires a 'good' initial value. Since the derivative of the curve concerned can change rapidly this method does not always show a proper convergence in our test cases. Because of that we use the robust Bisection method, with N_{bis} iterations, to find the construction domains.

4.3 Expected loss fraction function β

In [32] the integral in the function $\beta(h)$, see equation (4.42) below, is approximated by the Composite Trapezoidal rule with integration interval $[-500, 500]$ and $N_y = 1000$ integration steps. There the parameter values $k_1 = 8.16299 \cdot 10^{-1}$ and $k_2 = 1.88452 \cdot 10^2$ are used. We will show that we can evaluate this function also analytically.

The extreme water level size $\mathcal{J}$ is Gumbel distributed with density function

$$f_{\mathcal{J}}(y) = k_1 e^{k_1(k_2-y)-e^{k_1(k_2-y)}}, \tag{4.39}$$

with scale parameter $1/k_1 > 0$ and location parameter $k_2 \in \mathbb{R}$. Its distribution function reads

$$F_{\mathcal{J}}(y) = e^{-e^{k_1(k_2-y)}}. \tag{4.40}$$

The fraction of economic value lost, if the difference between the dike height and the average water level is h and the extreme water level size is y, is

$$l_p(y-h) = (1-e^{-\lambda_p(y-h)})^+ = \begin{cases} 0, & \text{for } y < h, \\ 1-e^{-\lambda_p(y-h)}, & \text{for } y > h. \end{cases} \tag{4.41}$$

The expectation of this loss fraction if an extreme water level occurs reads:

$$\begin{aligned} \beta(h) &= E[l_p(\mathcal{J}-h)] \\ &= \int_{-\infty}^{\infty} l_p(y-h) f_{\mathcal{J}}(y) dy \\ &= \int_h^{\infty} f_{\mathcal{J}}(y) dy - \int_h^{\infty} e^{-\lambda_p(y-h)} f_{\mathcal{J}}(y) dy. \end{aligned} \tag{4.42}$$

We calculate these two integrals separately. First of all,

$$\begin{aligned}\int_h^\infty f_{\mathcal{J}}(y)dy &= 1 - \int_{-\infty}^h f_{\mathcal{J}}(y)dy \\ &= 1 - F_{\mathcal{J}}(h) \\ &= 1 - \exp\left(-e^{k_1(k_2-h)}\right) \end{aligned} \tag{4.43}$$

and secondly

$$\begin{aligned}\int_h^\infty e^{-\lambda_p(y-h)} f_{\mathcal{J}}(y)dy &= e^{\lambda_p h} k_1 \int_h^\infty e^{-\lambda_p y} e^{k_1(k_2-y)} e^{-e^{k_1(k_2-y)}} dy \\ &= e^{\lambda_p h} k_1 \int_{h-k_2}^\infty e^{-\lambda_p(k_2+x)} e^{-k_1 x} e^{-e^{-k_1 x}} dx \\ &= e^{\lambda_p(h-k_2)} k_1 \int_{h-k_2}^\infty (e^{-k_1 x})^{\lambda_p/k_1+1} e^{-(e^{-k_1 x})} dx \\ &= -e^{\lambda_p(h-k_2)} \int_{\exp(-k_1(h-k_2))}^0 z^{\lambda_p/k_1+1-1} e^{-z} dz \\ &= e^{\lambda_p(h-k_2)} \gamma(\exp(-k_1(h-k_2)), \lambda_p/k_1+1). \end{aligned} \tag{4.44}$$

Adding up the two parts yields the analytical representation:

$$\beta(h) = 1 - \exp\left(-e^{k_1(k_2-h)}\right) - e^{\lambda_p(h-k_2)} \gamma(\exp(-k_1(h-k_2)), \lambda_p/k_1+1). \tag{4.45}$$

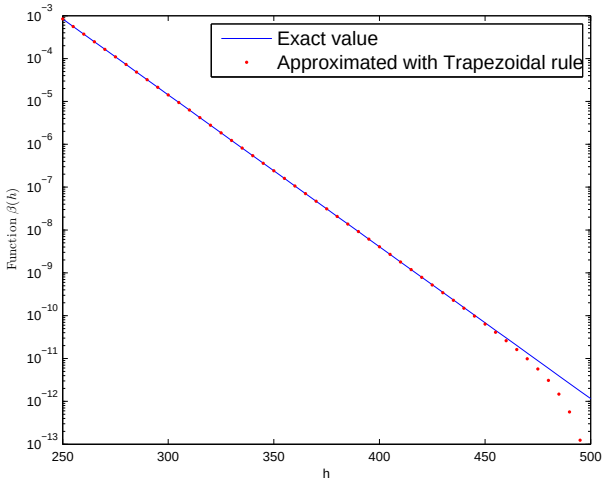

Figure 4.3: Function $\beta(h)$ on logarithmic scale.

γ is the lower incomplete gamma function, $\gamma(x,s) = \int_0^x z^{s-1} e^{-z}\, dz$. This function can be evaluated by using the Matlab functions `gammainc(x,s)` and `gamma(s)`. However, using Matlab results in a negative value $\beta(h)$ for large values h (e.g., $h > 646$), due to inaccuracy. This is undesirable, since it points to negative costs. It is important to be aware of this inaccuracy and to correct for it. In Figure 4.3 the exact values and the approximated values using the Trapezoidal rule are shown. The latter ones take more computation time. The values received by the Composite Trapezoidal rule are too low for h close to 500, because then the integration interval $[-500, 500]$ is too small. The absolute error is at most $3.00 \cdot 10^{-5}$ on the grid $[0 : 0.01 : 800]$. The function $\beta(h)$ is decreasing in h and convex for $h > 200$. We will use the exact representation of function $\beta(h)$ and set this value equal to zero if the obtained value is negative, so no significant errors are introduced by its computation.

5 Error analysis

In this section we analyse the error of the dike-COS-method, based on the error analysis in [10] and [11]. Errors are introduced by using the Composite Trapezoidal rule, the COS formula and by evolution through time via the coefficients $\hat{V}_k$. In Section 5.1 we start with the local error where no control and no backward recursion of the terms $\hat{V}_k$ are taken into account. This corresponds to the case of a European option. After that the error propagation in the backward recursion is studied in Section 5.2 and Section 5.3.

5.1 Local error dike-COS method

We consider the error of the Composite Trapezoidal integration rule and the error in the derivation of the COS formula. The local error reads:

$$\begin{aligned}\epsilon_{Loc}(t_{m-1},x_1,x_3|N,[a,b],N_t) &:= v(t_{m-1},x_1,x_3)-\hat{v}(t_m,x_1,x_3|N,[a,b],N_t)\\ &= \exp(x_3)(d(t_{m-1},t_m,x_1)-\hat{d}(t_{m-1},t_m,x_1|N_t))\\ &+ c(t_{m-1},x_1,x_3)-\hat{c}(t_{m-1},x_1,x_3|N,[a,b]).\end{aligned} \tag{5.1}$$

The above notation includes the method parameters used for the approximations, namely $N,[a,b]$ and N_t.

The time integral in the function $d(t_{m-1},t_m,x_1)$ is approximated by applying the Composite Trapezoidal rule with N_t integration steps. The error is given by

$$\begin{aligned}\epsilon_{Trap}(t_{m-1},t_m,x_1|N_t) &:= d(t_{m-1},t_m,x_1)-\hat{d}(t_{m-1},t_m,x_1|N_t)\\ &= -\frac{(t_m-t_{m-1})^3}{12N_t^2}G''(t^*)\\ &= O(1/N_t^2),\end{aligned} \tag{5.2}$$

with analytical function $G(s)=\lambda e^{(s-t_{m-1})(\mu_3-\rho)}\beta(x_1-w(s))\in C^2([t_{m-1},t_m])$ and $t^*\in[t_{m-1},t_m]$.

We define the local error of the COS formula as

$$\epsilon_{COS}(t_{m-1},x_1,x_3|N,[a,b]) := c(t_{m-1},x_1,x_3)-\hat{c}(t_{m-1},x_1,x_3|N,[a,b]). \tag{5.3}$$

Let assume that the terms $V_k(t_m^-,x_1)$ are exact. Errors are introduced in three steps: the truncation of the integration range, the substitution of the density by its cosine series expansion on the truncated range and the substitution of the series coefficients by the characteristic function approximation. An upper bound for the error of the European pricing option COS method with respect to the truncation range and the convergence rate in dependence of N have been derived in [10]. The key to bound the error lies in the decay rate of the Fourier-cosine series coefficients. We will discuss the three errors one after the other:

1. The integration range truncation error:

$$\epsilon_1(t_{m-1},x_1,x_3|[a,b]) := c(t_{m-1},x_1,x_3)-c_1(t_{m-1},x_1,x_3|[a,b]) = e^{-\rho\Delta t}\int_{\mathbb{R}\setminus[a,b]} v(t_m^-,x_1,y)f(y|x_3)dy > 0. \tag{5.4}$$

If $v(t_m^-,x_1,y)f(y|x_3)$ is very small outside the interval $[a,b]$, then the error ϵ_1 can be ignored.

2. The series truncation error on $[a,b]$:

$$\begin{aligned}\epsilon_2(t_{m-1},x_1,x_3|N,[a,b]) &:= c_1(t_{m-1},x_1,x_3|[a,b])-c_2(t_{m-1},x_1,x_3|N,[a,b])\\ &= \frac{b-a}{2}e^{-\rho\Delta t}\sum_{k=N}^{+\infty}G_k(x_3)V_k(t_m^-,x_1).\end{aligned} \tag{5.5}$$

The convergence rate of Fourier-cosine series depends on the properties of the approximated functions in the expansion interval. The following definitions and propositions can be found in [5]. These definitions are all asymptotic definitions based on the behaviour of the series coefficients for large k. They may be misleading if applied for small or moderate values of k. We start with classifying the rate of convergence:

Definition 5.1. *(Algebraic Index of Convergence)*
The algebraic index of convergence n is the largest number for which

$$\lim_{k\to\infty} |a_k| k^n < \infty, \qquad k >> 1, \tag{5.6}$$

where the a_k are the coefficients of the series.
Alternative definition: If the coefficients of a series are a_k and if

$$a_k \sim O(1/k^n), \qquad k >> 1, \tag{5.7}$$

(decay asymptotically) then n is the algebraic index of convergence.

Definition 5.2. *(Exponential Index of Convergence)*
*If the algebraic index of convergence n is unbounded - in other words, if the coefficients a_k decrease faster than $1/k^n$ for **any** finite n - then the series is said to have the property of "infinite order", or "exponential" convergence.*
Alternative definition: If

$$a_k \sim O(\exp(-qk^{\varrho})), \qquad k >> 1, \tag{5.8}$$

with q a constant for some $\varrho > 0$, then the series has "infinite order" or "exponential" convergence. The exponent ϱ is the exponential index of convergence.

We can distinguish three rates of exponential convergence by the following definition.

Definition 5.3. *(Rates of Exponential Convergence)*
A series whose coefficients are a_k is said to have the property of "supergeometric", "geometric" or "subgeometric" convergence depending upon whether

$$\lim_{k\to\infty} \log(|a_k|)/k = \begin{cases} -\infty & \textit{supergeometric,} \\ \textit{constant} & \textit{geometric,} \\ 0 & \textit{subgeometric.} \end{cases} \tag{5.9}$$

Alternative definitions:
1. If $a_k \sim O([\,]\exp(-(k/j)\log(k)))$ (for some $j > 0$), convergence is supergeometric.
2. If $a_k \sim O([\,]\exp(-qk))$ ($\varrho = 1$), convergence is geometric.
3. If the exponential index of convergence $\varrho < 1$, then the convergence is subgeometric.
(The empty brackets $[\,]$ denote factors that vary more slowly with k than the exponentials.)

The convergence concepts become clear with Figure 5.1. On the left log-linear plot, with the logarithm of the absolute value of a_k versus k, the coefficients of a geometrically converging series will asymptotically resemble a straight line. Supergeometric convergence can be defined as coefficients whose curve has an increasingly negative slope. Similarly, subgeometric and algebraic convergence rates produce curves which bend upward away from the straight line of geometric convergence. On the right log-log plot in Figure 5.1, the curve of coefficients with algebraic convergence, with algebraic index of convergence n, resembles asymptotically a straight line with slope $-n$. Exponential convergence results in an unbounded negative slope.

The normal density function is a typical function that has a supergeometrically converging cosine series expansion (see right side plot of Figure 6.2 in Section 6.1). The convergence type can be derived from the following proposition.

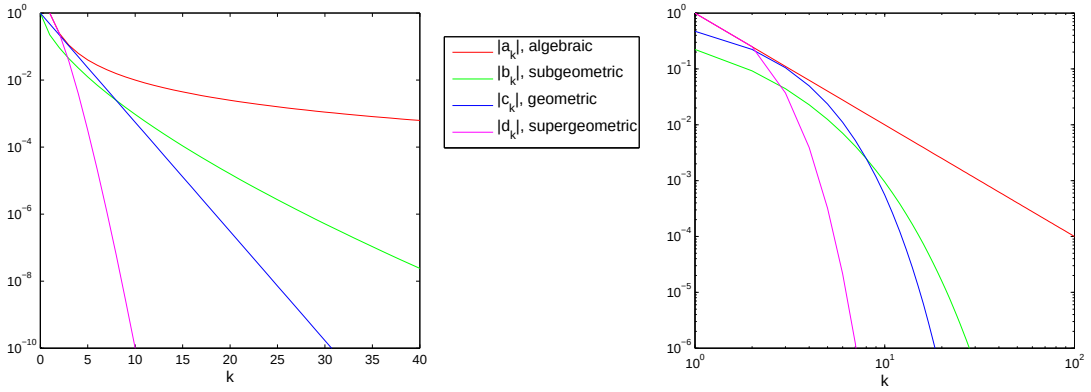

Figure 5.1: Convergence rates coefficients ([5]) ($a_k = 1/k^2$ (algebraic index of convergence $n = 1$),
$b_k = \exp(-1.5k^{2/3})$ $(\log(|b_k|)/k = 0)$,
$c_k = \exp(0.75k)$ $(\log(|c_k|)/k = 0.75)$,
$d_k = \exp(-k \log k))$ $(\log(|d_k|)/k = -\infty)$.

Proposition 5.1. *(Convergence of Fourier-cosine series)[10]*
If $h(x) \in C^\infty([a, b] \subset \mathbb{R})$, then its Fourier-cosine series expansion on $[a, b]$ has (at least) geometric convergence. The constant q in equation (5.8) is determined by the location in the complex plane of the singularities nearest to the expansion interval. Exponent ϱ is determined by the type and strength of the singularity.

If a function $h(x)$, or any of its derivatives, is discontinuous, its Fourier-cosine series coefficients show algebraic convergence. Integration-by-parts shows that the algebraic index of convergence, n, is at least as large as n', with the n'-th derivative of $h(x)$ integrable.

The absolute error of truncation of the expansion after N terms is denoted by $E_{Tr}(N)$. The following proposition allows to bound the series truncation error of an algebraically and geometrically converging series.

Proposition 5.2. *(Last coefficient error estimate)*
The truncation error is the same order of magnitude as the last coefficient retained in the truncation for a series with (at least) geometric convergence. Since the truncation error is a quantity we can only estimate anyway (in the absence of a known, exact solution), we can loosely speak of the last retained coefficient as being the truncation error, that is:

$$E_{Tr}(N) \sim O(|a_N|) = O\left([\,]\exp(-N\nu)\right). \tag{5.10}$$

Here, constant $\nu > 0$ is called the asymptotic rate of geometric convergence of the series, which satisfies

$$\nu = \lim_{k\to\infty} \frac{-\log(|a_k|)}{k}, \tag{5.11}$$

and $[\,]$ denotes a factor which varies less than exponentially with N.

Extension: if the series has algebraic convergence index n, i.e., if $a_k \sim O(1/k^n)$ for large k, then

$$E_{Tr}(N) \sim O(|Na_N|). \tag{5.12}$$

(Note that an algebraically converging series behaves like ([4])

$$\sum_{k=N+1}^{+\infty} \frac{1}{k^n} \sim O\left(\frac{1}{(n-1)N^{n-1}}\right) = O\left(N\frac{1}{N^n}\right), \qquad N >> 1.) \tag{5.13}$$

Now we return to the series truncation error ϵ_2. For N so large that $|V_k(t_m^-, x_1)| \leq 1$ for $k \geq N$, the error can be bounded by

$$\begin{aligned} |\epsilon_2(t_{m-1}, x_1, x_3|N, [a,b])| &= \left| \frac{b-a}{2} e^{-\rho\Delta t} \sum_{k=N}^{+\infty} G_k(x_3) V_k(t_m^-, x_1) \right| \\ &\leq \frac{b-a}{2} e^{-\rho\Delta t} \sum_{k=N}^{+\infty} |G_k(x_3)|. \end{aligned} \tag{5.14}$$

The error is dominated by the series truncation error of the coefficients G_k. We can also bound the error with a summation over the coefficients $V_k(t_m^-, x_1)$. However, we assume that the coefficients G_k decay faster than V_k as the density function is typically smoother than the 'payoff' function, which makes the above bound tighter.

With Proposition 5.2 we find that the error converges exponentially for density functions in the class $C^\infty([a,b])$:

$$|\epsilon_2(t_{m-1}, x_1, x_3|N, [a,b])| < P(x_3, N) \exp(-(N-1)\nu(x_3)), \tag{5.15}$$

where $\nu(x_3) > 0$ is a constant and P is a factor that varies less than exponentially with N. A density function with discontinuity in one of its derivatives results in an algebraic convergence of the Fourier-cosine expansion:

$$|\epsilon_2(t_{m-1}, x_1, x_3|N, [a,b])| < \frac{\overline{P}(x_3)}{(N-1)^{n(x_3)-1}}, \tag{5.16}$$

where $\overline{P}$ is a function depending on x_3 and $n(x_3)$ the algebraic index of convergence of the series coefficients $G_k(x_3)$.

3. The error related to approximating $G_k(x_3)$ by $F_k(x_3)$ (equation (4.13)):

$$\begin{aligned} \epsilon_3(t_{m-1}, x_1, x_3|N, [a,b]) &:= c_2(t_{m-1}, x_1, x_3|N, [a,b]) - \hat{c}(t_{m-1}, x_1, x_3|N, [a,b]) \\ &= \frac{b-a}{2} e^{-\rho\Delta t} {\sum_{k=0}^{N-1}}' (G_k(x_3) - F_k(x_3)) V_k(t_m^-, x_1) \\ &= -e^{-\rho\Delta t} \int_{\mathbb{R}\setminus[a,b]} \left[{\sum_{k=0}^{N-1}}' \cos\left(k\pi \frac{y-a}{b-a}\right) V_k(t_m^-, x_1) \right] f(y|x_3) dy \\ &= -e^{-\rho\Delta t} \int_{\mathbb{R}\setminus[a,b]} \left[v(t_m^-, x_1, y) - \sum_{k=N}^{+\infty} \cos\left(k\pi \frac{y-a}{b-a}\right) V_k(t_m^-, x_1) \right] f(y|x_3) dy \\ &= -\epsilon_1(t_{m-1}, x_1, x_3|[a,b]) \\ &+ e^{-\rho\Delta t} \int_{\mathbb{R}\setminus[a,b]} \left[\sum_{k=N}^{+\infty} \cos\left(k\pi \frac{y-a}{b-a}\right) V_k(t_m^-, x_1) \right] f(y|x_3) dy. \end{aligned} \tag{5.17}$$

We define

$$\begin{aligned} \epsilon_5(t_{m-1}, x_1, x_3|N, [a,b]) &:= e^{-\rho\Delta t} \int_{\mathbb{R}\setminus[a,b]} \left[\sum_{k=N}^{+\infty} \cos\left(k\pi \frac{y-a}{b-a}\right) V_k(t_m^-, x_1) \right] f(y|x_3) dy \\ &= \epsilon_1(t_{m-1}, x_1, x_3|[a,b]) + \epsilon_3(t_{m-1}, x_1, x_3|N, [a,b]). \end{aligned} \tag{5.18}$$

Error ϵ_5 is the integral over the domain $\mathbb{R}\setminus[a,b]$ of the density function $f(y|x_3)$ times the error resulting from approximation of the discounted payoff function

$$e^{-\rho\Delta t} v(t_m^-, x_1, y) \tag{5.19}$$

by

$$e^{-\rho\Delta t}\sum_{k=0}^{N-1}{}'\cos\left(k\pi\frac{y-a}{b-a}\right)V_k(t_m^-,x_1). \tag{5.20}$$

The function $f(y|x_3)$ is large for y close to x_3. Besides, the Fourier-cosine expansion of $v(t_m^-,x_1,y)$ is less accurate close to b compared to boundary a for call-like payoff functions. Together they can result in a significant error for x_3 in the vicinity of b. In Section 6.3.2 we investigate a case where ϵ_5 is estimated using a numerical integration rule. It also shows how the local error may be reduced by error ϵ_3 compared to error ϵ_1.

Now we can write the local error of the COS method as

$$\begin{aligned}\epsilon_{COS}(t_{m-1},x_1,x_3|N,[a,b]) &= \epsilon_1(t_{m-1},x_1,x_3|[a,b])+\epsilon_2(t_{m-1},x_1,x_3|N,[a,b])+\epsilon_3(t_{m-1},x_1,x_3|N,[a,b])\\ &= \epsilon_2(t_{m-1},x_1,x_3|N,[a,b])+\epsilon_5(t_{m-1},x_1,x_3|N,[a,b]).\end{aligned} \tag{5.21}$$

We end up with

$$|\epsilon_{Loc}(t_{m-1},x_1,x_3|N,[a,b],N_t)|\leq e^{x_3}|\epsilon_{Trap}(t_{m-1},t_m,x_1|N_t)|+|\epsilon_{COS}(t_{m-1},x_1,x_3|N,[a,b])|. \tag{5.22}$$

If the integration interval $[a,b]$ is chosen sufficiently wide and N_t sufficiently large, then the series truncation error ϵ_2 dominates the overall local error. This implies that for smooth density functions the error ϵ_{Loc} converges exponentially, otherwise it goes algebraically. However, roundoff errors may give difficulties in the convergence of Fourier-cosine series expansions as we will show in Section 6.

Remark 5.1. *In [10] another bound for the local error has been obtained as follows. The function $v(t_m^-,x_1,y)$ has an integrable derivative and according to Proposition 5.1 the Fourier-cosine coefficients show at least algebraic convergence. This gives the following estimate*

$$\begin{aligned}e^{-\rho\Delta t}\left|\sum_{k=N}^{+\infty}\cos\left(k\pi\frac{y-a}{b-a}\right)V_k(t_m^-,x_1)\right| &\leq e^{-\rho\Delta t}\sum_{k=N}^{+\infty}|V_k(t_m^-,x_1)|\\ \leq\frac{Q(t_m^-,x_1)}{(N-1)^{n-1}} &\leq Q(t_m^-,x_1),\qquad \text{for } N>>1, n\geq 1,\end{aligned} \tag{5.23}$$

for some positive constant Q independent of N. This allows to bound the error related to approximating $G_k(x_3)$ by $F_k(x_3)$ by

$$\begin{aligned}|\epsilon_3(t_{m-1},x_1,x_3|N,[a,b])| &\leq |\epsilon_1(t_{m-1},x_1,x_3|[a,b])|+Q(t_m^-,x_1)\left|\int_{\mathbb{R}\setminus[a,b]}f(y|x_3)dy\right|\\ &:= |\epsilon_1(t_{m-1},x_1,x_3|[a,b])|+Q(t_m^-,x_1)\epsilon_4(x_3|[a,b]),\end{aligned} \tag{5.24}$$

with $0\leq\epsilon_4(x_3|[a,b])\leq 1$. Then we get

$$|\epsilon_{COS}(t_{m-1},x_1,x_3|N,[a,b])|\leq 2|\epsilon_1(t_{m-1},x_1,x_3|[a,b])|+|\epsilon_2(t_{m-1},x_1,x_3|N,[a,b])|+Q(t_m^-,x_1)|\epsilon_4(x_3|[a,b])|. \tag{5.25}$$

This contains an error ϵ_4, which includes the density function f. In [10] it has been proposed to let the characteristics of the stochastic process prescribe the integration interval $[a,b]$ such that, for example,

$$\epsilon_4(x|[a,b])<10^{-5}. \tag{5.26}$$

We will show in Section 6.3 and Section 8.5.3 that this is not always accurate and that in some cases it is better to take the properties of the payoff function into account too when choosing the integration interval.

5.2 Error propagation in the backward recursion

The coefficients $V_k(t_m^-, x_1)$ are recovered recursively, backwards in time. The local error ϵ_{Loc} may propagate through time. In this section we study the error in the Fourier coefficients,

$$\varepsilon_k(t_m^-, x_1) := V_k(t_m^-, x_1) - \hat{V}_k(t_m^-, x_1) \tag{5.27}$$

and

$$|\varepsilon(t_m^-)|_\infty := \max_{k,x_1} |\varepsilon_k(t_m^-, x_1)|. \tag{5.28}$$

For ease of notation we consider the case of only two possible dike increase levels, u^0 and u^1. The results can easily be extended to the case of more possible dike increase levels.

We introduce the *construction points* $y_m^*(x_1)$, which represent the log-economic value for which the optimal dike increase level changes from zero to the positive amount u^1. In other words, they represent the right side boundary of the intervals $A_m^0(x_1)$. We assume that the construction points $y_m^*(x_1)$ are exact, in other words, the error resulting from applying the Bisection method is not significant. The error propagation caused by an incorrect construction point is discussed in Section 5.3 and examples are given in Section 7.1.

Theorem 5.1. *With N_t sufficiently large, $[a,b] \subset \mathbb{R}$ sufficiently wide and a probability density function f in $C^\infty([a,b])$, the error $\varepsilon_k(t_m^-, x_1)$ converges exponentially in N for all $1 \le m \le M-1$.*

Proof by induction:
A similar proof for the problem of pricing Bermudan options can be found in [11]. However, here we explicitly discuss the error of the COS formula close the boundaries of the domain. It can also be proved that if the local error converges algebraically, then so does ε.

Step 1: Base case
The terms B_k are exact, see equation (4.22). So, on time lattice $M-1$ we have

$$\begin{aligned}
\varepsilon_k(t_{M-1}^-, x_1) &= C_k(a, y_{M-1}^*(x_1), t_{M-1}, x_1) - \hat{C}_k(a, y_{M-1}^*(x_1), t_{M-1}, x_1) \\
&+ C_k(y_{M-1}^*(x_1), b, t_{M-1}, x_1 + u^1) - \hat{C}_k(y_{M-1}^*(x_1), b, t_{M-1}, x_1 + u^1) \\
&:= \varepsilon_k(a, y_{M-1}^*(x_1), t_{M-1}, x_1) + \varepsilon_k(y_{M-1}^*(x_1), b, t_{M-1}, x_1 + u^1),
\end{aligned} \tag{5.29}$$

where

$$\begin{aligned}
\varepsilon_k(z_1, z_2, t_{M-1}, y_1) &= \frac{2}{b-a} \int_{z_1}^{z_2} (v(t_{M-1}, y_1, y) - \hat{v}(t_{M-1}, y_1, y)) \cos\left(k\pi \frac{y-a}{b-a}\right) dy \\
&= \frac{2}{b-a} (d(t_{M-1}, t_M, y_1) - \hat{d}(t_{M-1}, t_M, y_1 | N_t) \chi(z_1, z_2) \\
&+ \frac{2}{b-a} \int_{z_1}^{z_2} (c(t_{M-1}, y_1, y) - \hat{c}(t_{M-1}, y_1, y)) \cos\left(k\pi \frac{y-a}{b-a}\right) dy.
\end{aligned} \tag{5.30}$$

Coefficients $V_k(t_M^-, y_1)$ are exact, see equation (4.17), so the only error introduced by the COS formula is the local error $\epsilon_{COS}(t_{M-1}, y_1, y | N, [a,b])$. Assuming that N_t is set sufficiently large, so that the error resulting from the Trapezoidal rule can be neglected, we obtain:

$$\varepsilon_k(z_1, z_2, t_{M-1}, y_1) = \frac{2}{b-a} \int_{z_1}^{z_2} \epsilon_{COS}(t_{M-1}, y_1, y | N, [a,b]) \cos\left(k\pi \frac{y-a}{b-a}\right) dy. \tag{5.31}$$

The absolute error can be bounded by

$$\begin{aligned}
|\varepsilon_k(z_1, z_2, t_{M-1}, y_1)| &\le \frac{2}{b-a} \int_{z_1}^{z_2} \left| \epsilon_{COS}(t_{M-1}, y_1, y | N, [a,b]) \cos\left(k\pi \frac{y-a}{b-a}\right) \right| dy \\
&\le \frac{2}{b-a} \int_{z_1}^{z_2} |\epsilon_{COS}(t_{M-1}, y_1, y | N, [a,b])| dy.
\end{aligned} \tag{5.32}$$

This is less than two times the average of $|\epsilon_{COS}(t_{M-1}, y_1, y|N, [a,b])|$ over the interval $[a,b]$. The error ϵ_{COS} may be large close to the boundaries a and b. However, assuming that the integration range $[a,b]$ is chosen sufficiently wide the series truncation error ϵ_2 will dominate the average. The series truncation error ϵ_2 converges exponentially with respect to N according to Proposition 5.1. This allows to bound the error:

$$|\varepsilon_k(z_1, z_2, t_{M-1}, y_1)| \quad \leq \quad \frac{2}{b-a}(z_2 - z_1)P(N)e^{-(N-1)\nu}, \tag{5.33}$$

where we use the notation $P(N) := \max_{y\in[a,b]} P(y,N)$ and $\nu := \min_{y\in[a,b]} \nu(y)$, where $P(y,N) > 0$ is a function which varies less than exponentially in N and $\nu(y) > 0$ is a function not depending on N.

Adding up the terms results in

$$\begin{aligned} |\varepsilon_k(t_{M-1}^-, x_1)| &\leq \frac{2}{b-a}\left[(y_{M-1}^*(x_1) - a)P(N)e^{-(N-1)\nu} + (b - y_{M-1}^*(x_1))P(N)e^{-(N-1)\nu}\right], \\ |\varepsilon(t_{M-1}^-)|_\infty &\leq 2P(N)e^{-(N-1)\nu}. \end{aligned} \tag{5.34}$$

It follows that the convergence of $\varepsilon_k(t_{M-1}^-, x_1)$ is exponential in N, like the series truncation error ϵ_2.

Step 2: Inductive step
If

$$|\varepsilon(t_{m+1}^-)|_\infty \leq R(N)e^{-(N-1)\nu}, \qquad \text{(Induction Hypothesis)} \tag{5.35}$$

where $R(N)$ varies less than exponentially in N, then

$$|\varepsilon(t_m^-)|_\infty \sim O\left(e^{-(N-1)\nu}\right). \tag{5.36}$$

Proof: Take $m \in \{1, \ldots, M-2\}$ fixed. For the estimation of $v(t_m, x_1, x_3)$ the COS formula with approximations $\hat{V}_k(t_{m+1}^-, y_1)$ is used. The estimated value is denoted by $\overline{v}(t_m, x_1, x_3)$. The use of the approximations $\hat{V}_k(t_{m+1}^-, y_1)$ introduces an additional error to $V_k(t_m^-, x_1)$:

$$\begin{aligned} \varepsilon_k(t_m^-, x_1) &= C_k(a, y_m^*(x_1), t_m, x_1) - \hat{C}_k(a, y_m^*(x_1), t_m, x_1) \\ &+ C_k(y_m^*(x_1), b, t_m, x_1 + u^1) - \hat{C}_k(y_m^*(x_1), b, t_m, x_1 + u^1) \\ &:= \varepsilon_k(a, y_m^*(x_1), t_m, x_1) + \varepsilon_k(y_m^*(x_1), b, t_m, x_1 + u^1), \end{aligned} \tag{5.37}$$

where

$$\begin{aligned} \varepsilon_k(z_1, z_2, t_m, y_1) &= \frac{2}{b-a}\int_{z_1}^{z_2} (v(t_m, y_1, y) - \overline{v}(t_m, y_1, y)) \cos\left(k\pi\frac{y-a}{b-a}\right) dy \\ &= \frac{2}{b-a}(d(t_m, t_{m+1}, y_1) - \hat{d}(t_m, t_{m+1}, y_1|N_t))\chi(z_1, z_2) \\ &+ \frac{2}{b-a}\int_{z_1}^{z_2} (c(t_m, y_1, y) - \overline{c}(t_m, y_1, y)) \cos\left(k\pi\frac{y-a}{b-a}\right) dy, \end{aligned} \tag{5.38}$$

with $\overline{c}$ obtained by inserting $\hat{V}_k(t_{m+1}^-, y_1)$ in the COS formula:

$$\begin{aligned} \overline{c}(t_m, y_1, y) &= e^{-\rho\Delta t}{\sum_{j=0}^{N-1}}' \Re\left[\varphi_{levy}\left(\frac{j\pi}{b-a}\right)e^{ij\pi\frac{y-a}{b-a}}\right]\hat{V}_j(t_{m+1}^-, y_1) \\ &= e^{-\rho\Delta t}{\sum_{j=0}^{N-1}}' \Re\left[\varphi_{levy}\left(\frac{j\pi}{b-a}\right)e^{ij\pi\frac{y-a}{b-a}}\right](V_j(t_{m+1}^-, y_1) - \varepsilon_j(t_{m+1}^-, y_1)) \\ &= \hat{c}(t_m, y_1, y) - e^{-\rho\Delta t}{\sum_{j=0}^{N-1}}' \Re\left[\varphi_{levy}\left(\frac{j\pi}{b-a}\right)e^{ij\pi\frac{y-a}{b-a}}\right]\varepsilon_j(t_{m+1}^-, y_1). \end{aligned} \tag{5.39}$$

Assuming that N_t is sufficiently large, the error ϵ_{COS} resulting from the Trapezoidal rule can be neglected. Next $\varepsilon_k(z_1, z_2, t_m, y_1)$ can be separated into two parts:

$$\begin{aligned}\varepsilon_k(z_1, z_2, t_m, y_1) &= \frac{2}{b-a}\int_{z_1}^{z_2}(c(t_m, y_1, y) - \hat{c}(t_m, y_1, y) + \hat{c}(t_m, y_1, y) - \overline{c}(t_m, y_1, y))\cos\left(k\pi\frac{y-a}{b-a}\right)dy \\ &= \frac{2}{b-a}\int_{z_1}^{z_2}(\epsilon_{COS}(t_m, y_1, y|N, [a,b]) + \overline{\epsilon}(t_{m+1}^-, y_1, y))\cos\left(k\pi\frac{y-a}{b-a}\right)dy, \qquad (5.40)\end{aligned}$$

where

$$\overline{\epsilon}(t_{m+1}^-, y_1, y) = e^{-\rho\Delta t}\sum_{j=0}^{N-1}{}'\,\Re\left[\varphi_{levy}\left(\frac{j\pi}{b-a}\right)e^{ij\pi\frac{y-a}{b-a}}\right]\varepsilon_j(t_{m+1}^-, y_1). \qquad (5.41)$$

The first part is related to the local error ϵ_{COS} and the second part is related to the terms $\varepsilon_j(t_{m+1}^-, y_1)$. Assuming that $[a,b]$ is chosen sufficiently wide, the first part can be bounded as before:

$$\left|\frac{2}{b-a}\int_{z_1}^{z_2}\epsilon_{COS}(t_m, y_1, y|N, [a,b])\cos\left(k\pi\frac{y-a}{b-a}\right)dy\right| \le \frac{2}{b-a}(z_2 - z_1)P(N)e^{-(N-1)\nu}. \qquad (5.42)$$

For the second part we start with

$$\left|\frac{2}{b-a}\int_{z_1}^{z_2}\overline{\epsilon}(t_{m+1}^-, y_1, y)\cos\left(k\pi\frac{y-a}{b-a}\right)dy\right| \le \frac{2}{b-a}\int_{z_1}^{z_2}\left|\overline{\epsilon}(t_{m+1}^-, y_1, y)\right|dy. \qquad (5.43)$$

Next we find

$$\begin{aligned}\left|\overline{\epsilon}(t_{m+1}^-, y_1, y)\right| &= \left|e^{-\rho\Delta t}\sum_{j=0}^{N-1}{}'\,\Re\left[\varphi_{levy}\left(\frac{j\pi}{b-a}\right)e^{ij\pi\frac{y-a}{b-a}}\right]\varepsilon_j(t_{m+1}^-, y_1)\right| \\ &\le e^{-\rho\Delta t}\sum_{j=0}^{N-1}{}'\left|\Re\left[\varphi_{levy}\left(\frac{j\pi}{b-a}\right)e^{ij\pi\frac{y-a}{b-a}}\right]\right|\left|\varepsilon_j(t_{m+1}^-, y_1)\right| \\ &\le e^{-\rho\Delta t}R(N)e^{-(N-1)\nu}\sum_{j=0}^{N-1}{}'\left|\Re\left[\varphi_{levy}\left(\frac{j\pi}{b-a}\right)e^{ij\pi\frac{y-a}{b-a}}\right]\right|. \qquad (5.44)\end{aligned}$$

For the last step we used the Induction Hypothesis. With the definition of G_k, equation (4.9), follows that

$$\begin{aligned}\sum_{j=0}^{N-1}{}'\left|\Re\left[\varphi_{levy}\left(\frac{j\pi}{b-a}\right)e^{ij\pi\frac{y-a}{b-a}}\right]\right| &= \sum_{j=0}^{N-1}{}'\left|\frac{b-a}{2}G_j(y) + \int_{\mathbb{R}\setminus[a,b]}f(z|y)\cos\left(j\pi\frac{z-a}{b-a}\right)dz\right| \\ &\le \frac{b-a}{2}\sum_{j=0}^{N-1}{}'|G_j(y)| + \sum_{j=0}^{N-1}{}'\int_{\mathbb{R}\setminus[a,b]}f(z|y)dz \qquad (f \ge 0) \\ &\le \frac{b-a}{2}\sum_{j=0}^{N-1}{}'|G_j(y)| + N. \qquad (5.45)\end{aligned}$$

We define

$$W(N) := \max_{y\in[a,b]}\frac{b-a}{2}\sum_{j=0}^{N-1}{}'|G_j(y)| = O\left(\max_{y\in[a,b]}\sum_{j=0}^{N-1}{}'(e^{-\nu(y)})^j\right), \qquad (5.46)$$

which represents the sum of a geometric series and convergences in N. We end up with

$$\left|\overline{\epsilon}(t_{m+1}^-, y_1, y)\right| \le e^{-\rho\Delta t}R(N)e^{-(N-1)\nu}(W(N) + N) \qquad (5.47)$$

and

$$\left|\frac{2}{b-a}\int_{z_1}^{z_2}\overline{\epsilon}(t_{m+1}^-,y_1,y)\cos\left(k\pi\frac{y-a}{b-a}\right)dy\right| \leq \frac{2}{b-a}(z_2-z_1)e^{-\rho\Delta t}R(N)e^{-(N-1)\nu}(W(N)+N). \quad (5.48)$$

Adding up the parts gives

$$|\varepsilon_k(t_m^-,x_1)| \quad \leq \quad \Big[2P(N)+2e^{-\rho\Delta t}R(N)(W(N)+N)\Big]e^{-(N-1)\nu}. \quad (5.49)$$

This completes the proof. □

5.3 Error propagation with incorrect construction points

In Section 5.2 we made the assumption of exactly determined construction points $y_m^*(x_1)$. However, the function $\hat{v}(t_m,x_1,x_3)$ is not always accurate, especially not in the vicinity of the boundaries of the computational domain. This may result in finding incorrect construction points, which may have a significant impact on the error propagation.

Suppose that construction point $y_m^*(x_1)$ is estimated by the incorrect value $\tilde{y}_m^*(x_1)$. This introduces an additional error in the estimation of $V_k(t_m^-,x_1)$:

$$\begin{aligned}
&\tilde{V}_k(t_m^-,x_1)\\
&:= \frac{2}{b-a}\int_a^{\tilde{y}_m^*(x_1)}\hat{v}(t_m,x_1,y)\cos\left(k\pi\frac{y-a}{b-a}\right)dy\\
&+ \frac{2}{b-a}\int_{\tilde{y}_m^*(x_1)}^{b}\hat{v}(t_m,x_1+u^i,y)\cos\left(k\pi\frac{y-a}{b-a}\right)dy + \frac{2}{b-a}\int_{\tilde{y}_m^*(x_1)}^{b}b(x_1,u^i)\cos\left(k\pi\frac{y-a}{b-a}\right)dy\\
&= \frac{2}{b-a}\int_a^{y_m^*(x_1)}\hat{v}(t_m,x_1,y)\cos\left(k\pi\frac{y-a}{b-a}\right)dy + \frac{2}{b-a}\int_{y_m^*(x_1)}^{\tilde{y}_m^*(x_1)}\hat{v}(t_m,x_1,y)\cos\left(k\pi\frac{y-a}{b-a}\right)dy\\
&+ \frac{2}{b-a}\int_{\tilde{y}_m^*(x_1)}^{y_m^*(x_1)}\hat{v}(t_m,x_1+u^i,y)\cos\left(k\pi\frac{y-a}{b-a}\right)dy + \frac{2}{b-a}\int_{y_m^*(x_1)}^{b}\hat{v}(t_m,x_1+u^i,y)\cos\left(k\pi\frac{y-a}{b-a}\right)dy\\
&+ \frac{2}{b-a}\int_{\tilde{y}_m^*(x_1)}^{y_m^*(x_1)}b(x_1,u^i)\cos\left(k\pi\frac{y-a}{b-a}\right)dy + \frac{2}{b-a}\int_{y_m^*(x_1)}^{b}b(x_1,u^i)\cos\left(k\pi\frac{y-a}{b-a}\right)dy\\
&= \hat{V}_k(t_m^-,x_1) + \frac{2}{b-a}\int_{y_m^*(x_1)}^{\tilde{y}_m^*(x_1)}[\hat{v}(t_m,x_1,y)-\hat{v}(t_m,x_1+u^i,y)-b(x_1,u^i)]\cos\left(k\pi\frac{y-a}{b-a}\right)dy. \quad (5.50)
\end{aligned}$$

We get the error

$$\begin{aligned}
\tilde{\varepsilon}_k(t_m^-,x_1) &:= V_k(t_m^-,x_1)-\tilde{V}_k(t_m^-,x_1)\\
&= \varepsilon_k(t_m^-,x_1) - \frac{2}{b-a}\int_{y_m^*(x_1)}^{\tilde{y}_m^*(x_1)}[\hat{v}(t_m,x_1,y)-\hat{v}(t_m,x_1+u^i,y)-b(x_1,u^i)]\cos\left(k\pi\frac{y-a}{b-a}\right)dy. \quad (5.51)
\end{aligned}$$

The error depends on value $\tilde{y}_m^*(x_1)$ and the difference between $\hat{v}(t_m,x_1,y)$ and $\hat{v}(t_m,x_1+u^i,y)+b(x_1,u^i)$ over the integration range. It is clear that the effect of this error can be disastrous in the backward recursion, starting by the calculation of $\hat{v}(t_{m-1},x_1,x_3)$. However, the difference between $\hat{v}(t_m,x_1,y)$ and $\hat{v}(t_m,x_1+u^i,y)+b(x_1,u^i)$ is usually small for y close to $\tilde{y}_m^*(x_1)$ and because of that the error will be bounded in practice. Moreover, if the interval $[a,b]$ is sufficiently wide, then the incorrect construction domains at the boundaries will not significantly affect the real option prices in the middle of the computational domain. We will demonstrate examples where the incorrect construction points are found in Section 7.1.

6 Numerical experiments error

In this section we perform numerical tests to confirm the error analysis of the COS method by means of the COS formula for pricing European options, for which a similar error analysis as in Section 5.1 holds. In that section an exponential error convergence for density functions that belong to $C^\infty([a,b])$ was found. However, the tests will show that the error convergence can be spoilt by roundoff errors, especially for large values of T as we have them with real options. We start with the COS density recovery and the Fourier-cosine series expansion of the European call and put payoff functions. Thereafter the COS formula for pricing European call and put options is tested. Finally methods using Fourier-sine or modified Fourier series expansions are discussed. In this section we use the abbreviations call and put options to denote European call and European put options.

6.1 COS density recovery

In [10] the first step to explain the COS method for pricing call and put options consists of showing how a density function $f(y)$ can be recovered from its characteristic function, starting by

$$f(y) = \sum_{k=0}^{+\infty}{}' G_k \cos\left(k\pi \frac{y-a}{b-a}\right), \tag{6.1}$$

with

$$G_k = \frac{2}{b-a}\int_a^b f(y)\cos\left(k\pi\frac{y-a}{b-a}\right)dy. \tag{6.2}$$

The *COS density recovery* gives the approximation

$$\hat{f}(y) = \sum_{k=0}^{N-1}{}' F_k \cos\left(k\pi \frac{y-a}{b-a}\right), \tag{6.3}$$

where

$$F_k := \frac{2}{b-a}\Re\left[\varphi\left(\frac{k\pi}{b-a}\right)e^{-ik\pi\frac{a}{b-a}}\right] \approx G_k. \tag{6.4}$$

We investigate the error of the density recovery for the standard normal density function

$$f(y) = \frac{1}{\sqrt{2\pi}}\, e^{-\frac{1}{2}y^2}, \tag{6.5}$$

with characteristic function $\varphi(u) = e^{-\frac{1}{2}u^2}$. We take $[a,b] = [-10,10]$ and $N = 2^5$. The results are shown in Figure 6.1. An absolute error lower than 10^{-6} is achieved, which is highly satisfactorily.

Next, the dependence of N and the size of the interval $[a,b]$ are analysed. We take interval $[a,b] = [-L,\, L]$, with L =10, 100 and 1000, and calculate the maximal absolute errors for y on the integer grid $[-6:6]$. The error introduced by the approximation of G_k by F_k can be neglected for these intervals. The left side plot of Figure 6.2 indicates that it takes significant larger values of N to reach the same level of accuracy for larger values L. Besides, the minimal error obtained is somewhat larger for larger L, probably because the series expansion over a larger interval hinders the recovery, although the density function is close to zero in the additional domain. The part where the minimal error is reached, is the so-called *roundoff plateau*. In [5] the following is stated:

Let $a_{\max}$ denote the maximum absolute value of the spectral coefficients a_k for all k. Let e denote a constant proportional to the roundoff error or 'machine epsilon', typically around 10^{-16} on most computers, but somewhat larger, perhaps by a factor of 100 or more. Then when the exact coefficients fall below $ea_{\max}$, spectral algorithms including interpolation will compute roundoff-corrupted coefficients that will

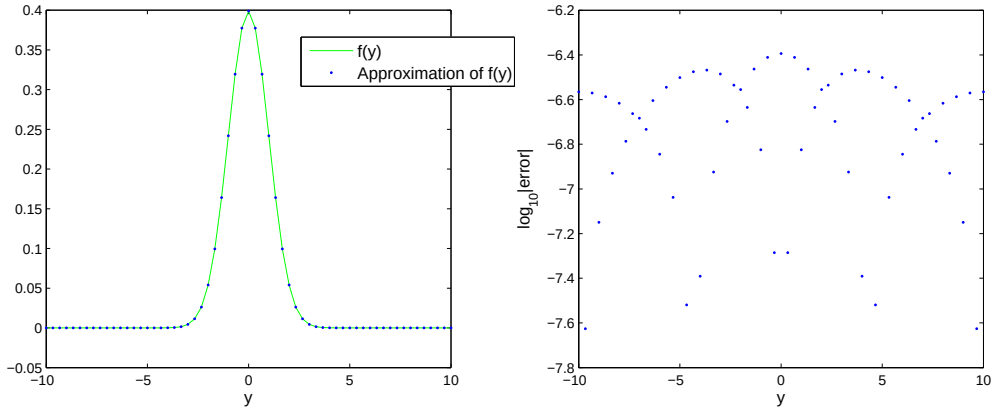

Figure 6.1: Left: COS density recovery, right: the error ($[a, b] = [-10, 10]$ and $N = 2^5$).

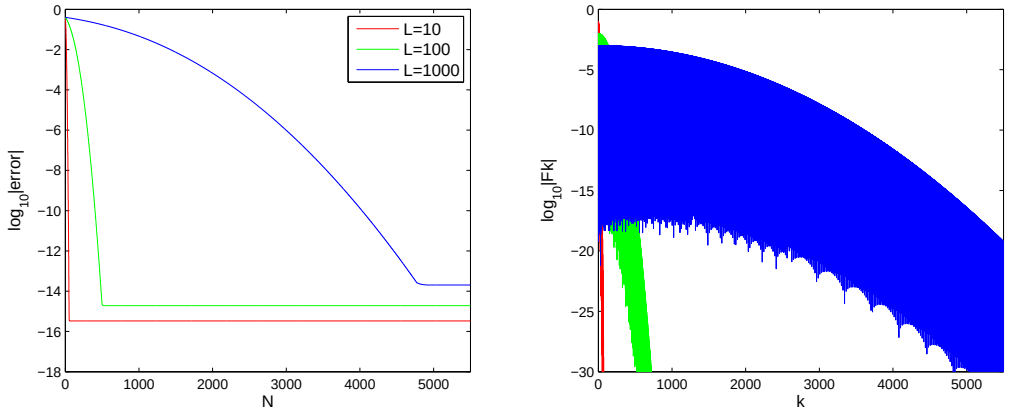

Figure 6.2: Left: max. error on integer grid $[-6 : 6]$, right: coefficients F_k.

flatten out at roughly $a_k \sim ea_{\max}$ for all sufficiently large k. ("Roughly" means that coefficients in the "Roundoff Plateau" fluctuate randomly about the indicated magnitude.).

The right plot in Figure 6.2 shows the values of the coefficients F_k. The more detailed left plot in Figure 6.3 shows that, for $L = 10$, the roundoff plateau is reached around $N = 50$. The coefficients F_k are shown in the right plot and we have $F_{\max} = F_2 \approx 9.52 \cdot 10^{-2}$. The odd coefficients are much lower than the even coefficients, because the density function is even ($G_k = 0$ for k odd). We have: $F_{50}/F_{\max} \approx 4.23 \cdot 10^{-14}$. When all coefficients fall below $eF_{\max}$ the plateau is reached. From this we can conduct that $e \approx 10^{-14}$, which is indeed about a factor 100 times the 'machine epsilon'.

For $L = 1000$ the roundoff plateau is reached at $N \approx 4800$. The corresponding coefficients thus decrease much slower. We have $F_{4800}/F_{\max} \approx 4.52 \cdot 10^{-13}$.

The limit $\lim_{k\to\infty} \log(|F_k|)/k$ goes to minus infinity and the convergence of the coefficients is supergeometric in k (see Definition 5.3). The error has the same supergeometric convergence rate in N, until the roundoff plateau is attained. The decreasing coefficients F_k have a big impact on when the roundoff plateau with pricing options is reached as we will demonstrate in Section 6.3.1.

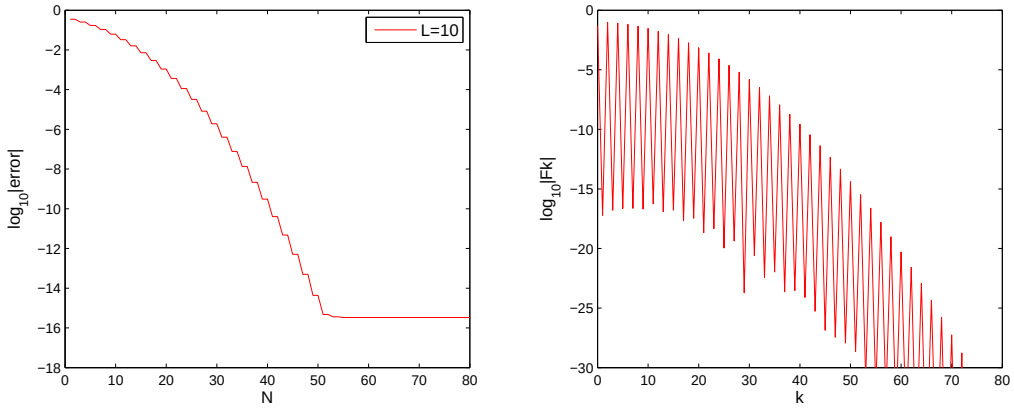

Figure 6.3: Left: max. error on integer grid $[-6:6]$, right: coefficients F_k $(L = 10)$.

Multiple Precision
The awareness of the fact that loss of significance can occur is useful. Sometimes the solution to roundoff errors consists of changing the order of operations ([40]). However, as long as the large coefficients are not sufficiently accurate, we will not reach a better accuracy. An obvious solution seems to be the use of higher precision calculations. For that reason we use the Multiple Precision Toolbox for Matlab to investigate the influence of precision on the error of the density recovery.

Numbers are in general represented approximately as a fixed number and scaled using an exponent:

$$\pm d_0.d_1d_2\ldots d_{p-1} \times \beta^E, \tag{6.6}$$

where $d_0.d_1d_2\ldots d_{p-1}$ is the value of the significand, β is the base, usually 2, 10 or 16, and E is the exponent ([40]). The number of digits in the significand is as usually called the precision p.

Single precision is a binary format that is 32 bits long and its significand has a precision of $p = 24$ bits (about 7 decimal digits). Double precision occupies 64 bits and its significand has a precision of $p = 53$ bits (about 16 decimal digits). Matlab's default precision is double precision. In the tests with the Multiple Precision Toolbox we use the significand precision p with $p = 24, 53$ and 100 bits.

We take $[a, b] = [-10, 10]$ and repeat the preceding error analysis. The results are shown in Figure 6.4. The upper plot shows the values of the coefficients F_k (black) and the lines indicate the values $2^{-p}F_{\max}$. Error convergence for the various precisions is shown in the lower plot. The figure shows that single precision is indeed less accurate than double precision. With single precision, $p = 24$ bits, the roundoff plateau is reached when roughly all coefficients are below $2^{-24}F_{\max} \approx 10^{-8}F_{\max}$ times a factor about 100. With higher precision, for example $p = 100$ bits, the results are the same for low N compared to double precision, but this higher precision gives smaller errors for large values N, where double precision has already reached the roundoff plateau. So, the roundoff plateau is 'delayed' by higher precision calculations and the minimal attainable error is lower. The computation time is linear in N and besides the use of the Multiple Precision Toolbox for Matlab takes much more time (more than a factor 100 in our computations). Because of that, we advise to use higher precision calculations only if results using double precision are not sufficiently accurate.

6.2 Fourier-cosine series expansion of payoff function

In this section we discuss the Fourier-cosine series expansion of the option payoff function, which is an important approximation in the COS method for pricing option. Both call and put payoff functions are

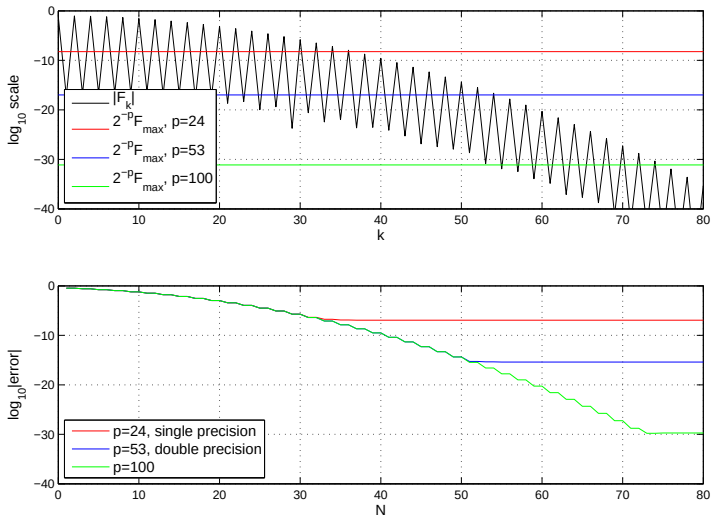

Figure 6.4: Higher precision calculations, max. error on integer grid $[-6:6]$ for $p = 24, 53, 100$.

studied. The definitions of call and put options are given in Theorem 2.1. The asset price at time t is denoted by S_t, the agreed price is the strike price K and the prescribed time is the expiration time T.

Call option
The payoff of a call option at the terminal time, with scaled log-asset price $y = \log(S_T/K)$, is given by the function

$$g^{call}(y) := K(e^y - 1)^+. \tag{6.7}$$

Fourier-cosine series expansion gives the approximation:

$$\hat{g}^{call}(y) = \sum_{k=0}^{N-1}{}' V_k \cos\left(k\pi\frac{y-a}{b-a}\right), \tag{6.8}$$

where

$$V_k = \frac{2}{b-a}\int_a^b g^{call}(y)\cos\left(k\pi\frac{y-a}{b-a}\right)dy = \frac{2}{b-a}K(\chi(0,b) - \psi(0,b)), \qquad (a \le 0 \le b). \tag{6.9}$$

We take strike price $K = 100$, interval $[a, b] = [-2, 2]$ and $N = 2^5$. The results are shown in Figure 6.5. We see a peak in the error around $y = 0$, probably due to the discontinuous derivative at that point. For larger intervals $[a, b]$, the error around b dominates. In the next test we measure the error at $y = 0$ for different values of N and different intervals $[a, b]$. From the results in Figure 6.6 it follows that a larger interval $[a, b]$ gives rise to a larger error. The coefficients V_k decrease algebraically (right side plot). The slope on the log-log graph is -2, so the algebraic index of convergence is 2. The error decreases with order $O(|NV_N|)$ in accordance with Proposition 5.2. The call payoff function is unbounded for $y \to \infty$, which gives much larger coefficients for larger intervals and with that also larger errors. The roundoff plateau is not yet reached and the results will thus not be improved by using higher precision calculations.

Put option
The payoff of a put option reads

$$g^{put}(y) := K(1 - e^y)^+, \tag{6.10}$$

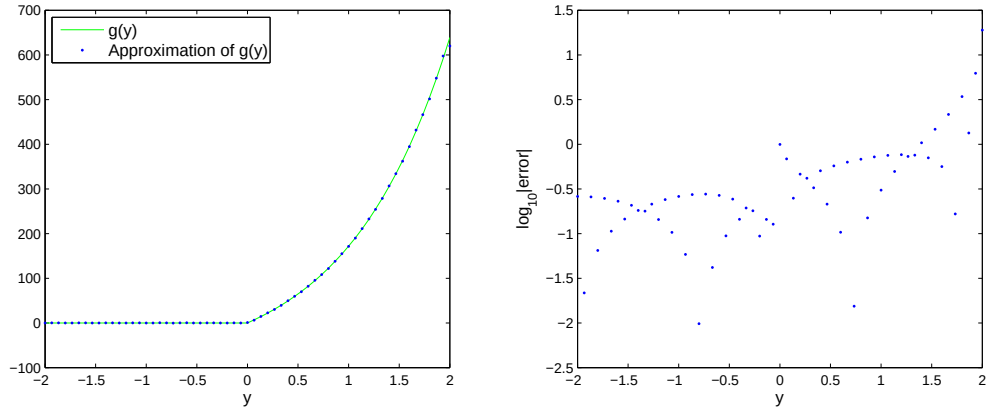

Figure 6.5: Left: Fourier-cosine expansion $g^{call}(y)$, right: the error ($K = 100$, $[a, b] = [-2, 2]$ and $N = 2^5$).

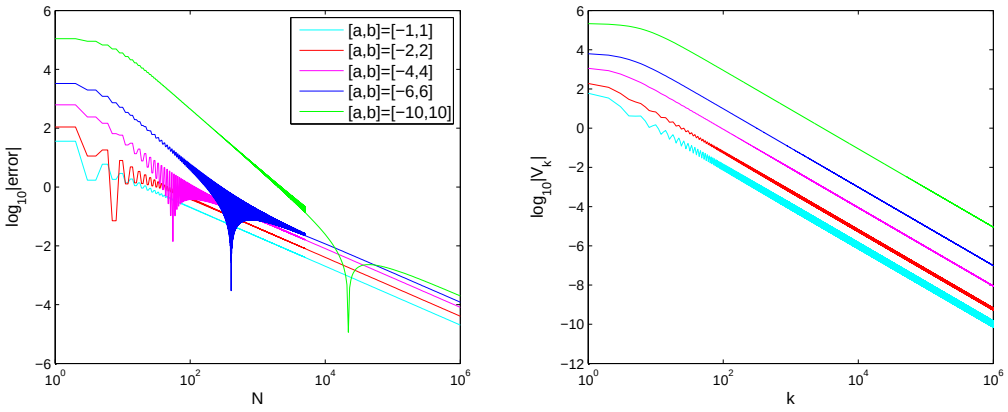

Figure 6.6: Left: convergence error of $\hat{g}^{call}(0)$, right: coefficients V_k, ($K = 100$).

with Fourier-cosine series expansion

$$\hat{g}^{put}(y) = \sum_{k=0}^{N-1}{}' V_k \cos\left(k\pi \frac{y-a}{b-a}\right), \tag{6.11}$$

where

$$V_k = \frac{2}{b-a}\int_a^b g^{put}(y)\cos\left(k\pi\frac{y-a}{b-a}\right)dy = \frac{2}{b-a}K(-\chi(a,0)+\psi(a,0)), \qquad (a \leq 0 \leq b). \tag{6.12}$$

The put payoff function is bounded by strike price K. Because of that the Fourier coefficients do not become as large as their sister call payoff coefficients for larger intervals $[a, b]$, which has a positive effect on the error especially for low values N. Error results for different values of N and different intervals $[a, b]$ are shown in Figure 6.7.

Comparison of the error results for the call and put payoff functions shows that about the same error is achieved for high N ($N \approx 10^6$). If one has only dispose of hundred coefficients for the approximation, then the call payoff series expansion performs less satisfactorily. Because of this the COS pricing method may give better results for pricing put options compared to call options, as we will discuss in the next section.

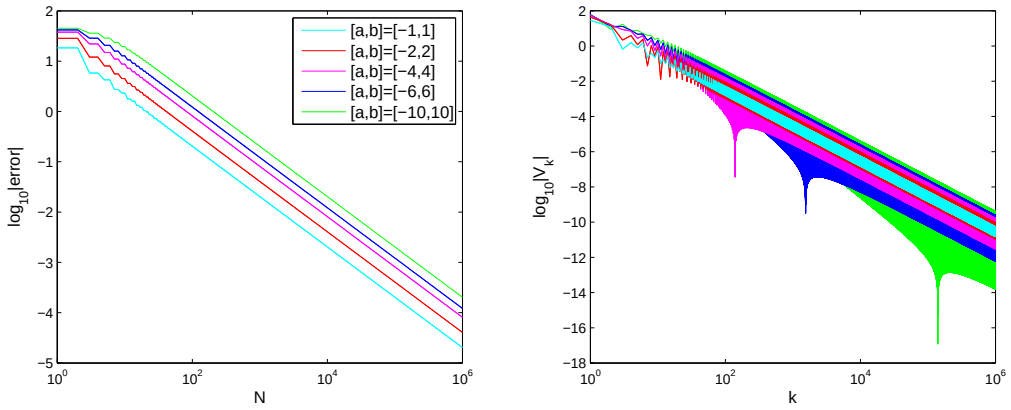

Figure 6.7: Left: convergence error details of $\hat{g}^{put}(0)$, right: coefficients V_k, $(K = 100)$.

6.3 COS method for call and put option prices

In [10] numerical experiments were performed to test the COS method and European call and put prices were calculated. We perform here extensive tests to further analyse the error of this method.

The underlying asset has value S_t at time t and the strike price is K. We switch to the scaled log-asset price process:

$$X_t = \log(S_t/K). \tag{6.13}$$

The asset price is modelled by a geometric Brownian motion. In accordance with Section 2.7.2 there holds

$$v(t,x) = E^{t,x}[e^{-r(T-t)}g(X_T)], \tag{6.14}$$

with expectation taken with respect to the risk-neutral measure under which $dX_t = (r - \frac{1}{2}\sigma^2)dt + \sigma dW_t$. We study the results for the parameters

$$r = 0.1,\ \sigma = 0.25,\ t_0 = 0,\ S_0 = 100. \tag{6.15}$$

Next we define $\Delta t := T - t_0$. The exact solutions for the call and put prices are given by their Black-Scholes prices (see Appendix E):

$$\begin{aligned} v_{BScall}(t_0,x) &= Ke^x N(d_2) - Ke^{-r\Delta t}N(d_1), \\ v_{BSput}(t_0,x) &= Ke^{-r\Delta t} - Ke^x + v_{BScall}(t_0,x), \end{aligned} \tag{6.16}$$

where $N(.)$ denotes the standard normal distribution function and with

$$d_1 = \frac{x + (r - \frac{1}{2}\sigma^2)\Delta t}{\sigma\sqrt{\Delta t}} \qquad \text{and} \qquad d_2 = d_1 + \sigma\sqrt{\Delta t}. \tag{6.17}$$

The approximation by the COS method is a combination of the Fourier-cosine series coefficients of the payoff function and the estimated coefficients of the density function:

$$\hat{v}(t_0,x) = e^{-r\Delta t}\frac{b-a}{2}\sum_{k=0}^{N-1}{}' F_k(x)V_k, \tag{6.18}$$

$$\text{where} \qquad \frac{b-a}{2}F_k(x) = \Re\left[\varphi_{levy}\left(\frac{k\pi}{b-a}\right)e^{ik\pi\frac{x-a}{b-a}}\right], \tag{6.19}$$

and with Fourier coefficients V_k of the corresponding payoff function $g(y)$. We obtain:

$$\begin{aligned} V_k^{call} &= \frac{2}{b-a}K(\chi_k(0,b) - \psi_k(0,b)), \\ V_k^{put} &= \frac{2}{b-a}K(-\chi_k(a,0) + \psi_k(a,0)). \end{aligned} \tag{6.20}$$

In Section 5.1 we found that the error of the COS method consists of three parts. Two of them are related to the integration domain $[a,b]$. Using the same error notation for the COS option pricing formula as in Section 5.1, there holds

$$\epsilon_1(x|[a,b]) = e^{-r\Delta t}\int_{\mathbb{R}\setminus[a,b]} v(T,y)f(y|x)dy, \tag{6.21}$$

$$\epsilon_3(x|N,[a,b]) = \frac{b-a}{2}e^{-r\Delta t}{\sum_{k=0}^{N-1}}'(G_k(x) - F_k(x))V_k, \tag{6.22}$$

$$\epsilon_5(x|N,[a,b]) = \epsilon_1(x|[a,b]) + \epsilon_3(x|N,[a,b]). \tag{6.23}$$

The series truncation error, which converges exponentially in N for the underlying Brownian motion, reads

$$\epsilon_2(x|N,[a,b]) = \frac{b-a}{2}e^{-r\Delta t}\sum_{k=N}^{+\infty} G_k(x)V_k. \tag{6.24}$$

It consists of a combination of both Fourier-cosine coefficients G_k and V_k. This error dominates if the integration range is sufficiently wide for given x. This error, for its part, is dominated by roundoff errors for N sufficiently large.

The integration range truncation error can be calculated exactly, see Appendix E. We find for a call option ($a \le 0 \le b$)

$$\epsilon_1(x|[a,b]) = e^x K(1 - N(b_2)) - Ke^{-r\Delta t}(1 - N(b_1)), \tag{6.25}$$

where

$$b_1 = \frac{b - x - (r - \frac{1}{2}\sigma^2)\Delta t}{\sigma\sqrt{\Delta t}} \qquad \text{and} \qquad b_2 = b_1 - \sigma\sqrt{\Delta t}. \tag{6.26}$$

For a put option we obtain ($a \le 0 \le b$):

$$\epsilon_1(x|[a,b]) = -e^x K N(a_2) + Ke^{-r\Delta t}N(a_1), \tag{6.27}$$

where

$$a_1 = \frac{a - x - (r - \frac{1}{2}\sigma^2)\Delta t}{\sigma\sqrt{\Delta t}} \qquad \text{and} \qquad a_2 = a_1 - \sigma\sqrt{\Delta t}. \tag{6.28}$$

In Section 5.1 we defined

$$\epsilon_4(x|[a,b]) = \int_{\mathbb{R}\setminus[a,b]} f(y|x)dy. \tag{6.29}$$

This error is used in equation (5.25) to bound the error of the COS method. The error ϵ_4 for both financial options reads

$$\epsilon_4(x|[a,b]) = N(a_1) + (1 - N(b_1)). \tag{6.30}$$

Integration range $[a,b]$
The following integration range was proposed in [10]:

$$[a,b] := \left[c_1 - L\sqrt{c_2 + \sqrt{c_4}},\ c_1 + L\sqrt{c_2 + \sqrt{c_4}}\right], \qquad L = 10, \tag{6.31}$$

where c_1, c_2 and c_4 are the first, second and fourth cumulant of X_T, given that $X_0 = x_0$. For the underlying Brownian motion we have $c_1 = x_0 + (r - \frac{1}{2}\sigma^2)T$, $c_2 = \sigma^2 T$ and $c_4 = 0$. We will make critical

comments on this integration range, which in only based on the characteristics of the stochastic process and not on the payoff function. According to [10] the above range, with $L = 10$, is accurate in the range $T = 0.1$ to $T = 10$. We investigate whether something goes wrong for $T = 100$.

In the next sections we perform various numerical tests to analyse the convergence of the series truncation error (Section 6.3.1) and the integration range truncation error (Section 6.3.2).

6.3.1 Convergence and the roundoff plateau

In this section we take $K = 100$ ($x_0 = 0$) and integration interval (6.31) with L equal to or larger than 10. For these values of L the errors ϵ_1 and ϵ_3 are not relevant. This gives the opportunity to investigate the convergence of the series truncation error ϵ_2. We calculate the error of the option prices, compared to the exact Black-Scholes prices. Besides the error of the COS density recovery

$$\hat{f}(y) = \sum_{k=0}^{N-1}{}' F_k \cos\left(k\pi\frac{y-a}{b-a}\right), \tag{6.32}$$

and the error of the payoff approximation

$$\hat{g}(y) = \sum_{k=0}^{N-1}{}' V_k \cos\left(k\pi\frac{y-a}{b-a}\right), \tag{6.33}$$

in the point $y = 0$, are determined.

Terminal time $T = 0.1$
The exact Black-Scholes prices for $K = 100$ and terminal time $T = 0.1$ are 3.66 for the call option and 2.67 for the put option. Results of the calculations are shown in Figure 6.8, on a logarithmic scale. The left side plots correspond to the call option and the right plots to the put option. The option prices are converging in N, but the error of the approximated option prices reaches a roundoff plateau (upper plots). This happens just before the error of the density recovery reaches its roundoff plateau (middle plots). At that moment the Fourier-cosine series approximation of payoff function has not yet reached its roundoff plateau and the call payoff expansion is less accurate compared to the put payoff (lowest plots).

It takes more terms N to reach the same level of accuracy for the option prices for larger integration intervals, because the series expansions of the functions are worse for larger integration intervals. By that also the value of the roundoff plateau for the error of call options prices is higher. Since a Fourier-cosine expansion of the payoff function works out better for the put option payoff, especially for larger intervals $[a, b]$, the error results for large L are better for put option prices.

In the Figure 6.9 the Fourier-cosine coefficients V_k, $F_k(x_0)$ and the product

$$\mathsf{a}_k := e^{-r\Delta t}\frac{b-a}{2}F_k(x_0)V_k, \tag{6.34}$$

associated to the call option, for $L = 10$, are shown. When the coefficients a_k are below their maximal absolute value $\mathsf{a}_{\max}$ times $e \approx 10^{-14}$ the roundoff plateau is reached. Mainly the fast decreasing coefficients F_k determine how fast the plateau is reached. They decrease a little bit slower than the terms a_k, therefore the roundoff plateau for the error of the option prices is reached somewhat earlier than the roundoff plateau of the COS density recovery. The option price error has the same convergence rate as the coefficients F_k, namely supergeometric. The roundoff plateau has a value around 10^{-14}.

Terminal time $T = 100$
Next we examine whether the COS pricing method is also accurate for a very large terminal time $T = 100$.

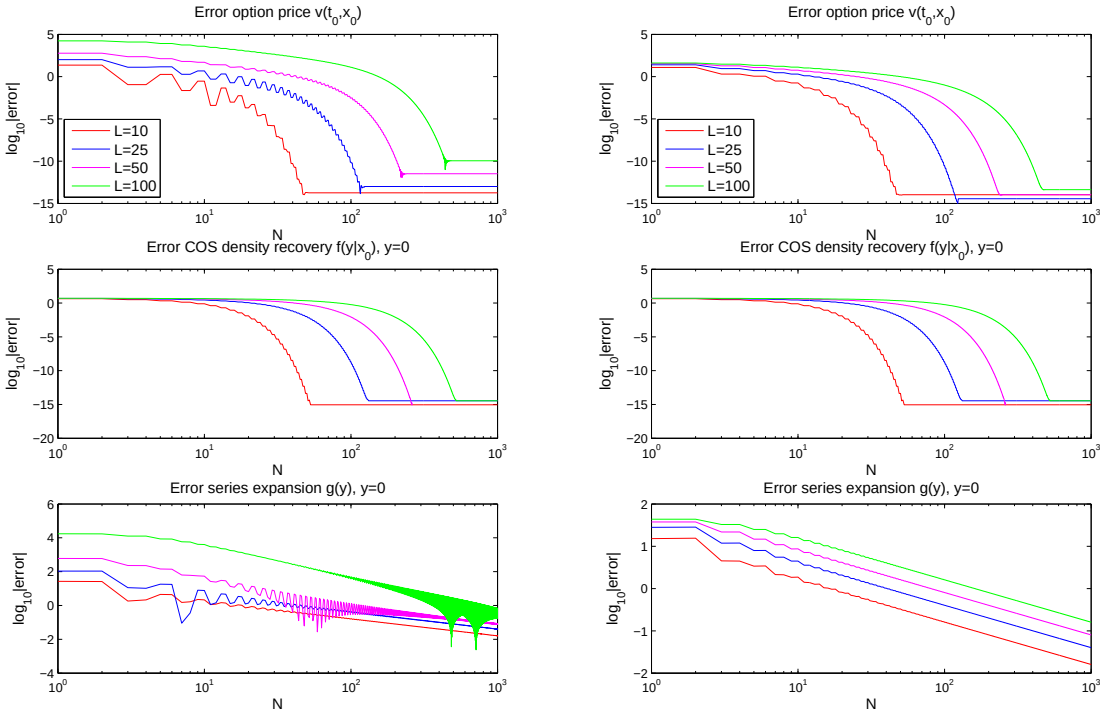

(a) Call option.

(b) Put option.

Figure 6.8: Errors of Fourier-cosine expansions, $T = 0.1$ ($x_0 = 0$).

Although this is not very realistic in the case of pricing financial options, the analysis will give insight into possible difficulties using the COS method in the real options context, by which large terminal times may be used. The exact Black-Scholes prices for $K = 100$ and $T = 100$ are about 99.996 for the call option and $5.92 \cdot 10^{-6}$ for the put option.

According to equation (6.31), a larger terminal time leads to a larger integration interval $[a, b]$, because then the stochastic value X_T can cover a wider range. So, the interval for the call payoff expansion gets larger, which worsens the error of its series expansion. Because of that, the error of the call option prices is less accurate for terminal time $T = 100$, see the left plots in Figure 6.10. The put payoff recovery works well for large intervals $[a, b]$, as the function is bounded by value K. Because of that, the error of the put option prices does not suffer significantly from a larger terminal T (right plots). Note that the absolute errors, instead of the relative errors, are measured. The roundoff plateaus are reached for the same values of N as for terminal time $T = 0.1$.

Remark 6.1. *Reference [10] has priced call options using the corresponding European put option prices and the put-call parity, which leads to the same accuracy of the puts, namely of order* 10^{-15} *for terminal time* $T = 100$. *However, in the real options context for control problems a likewise parity does not (yet) exist and therefore we do not use it here.*

We examine the call option price error further. Again the coefficients V_k, $F_k(x_0)$ and their product a_k, for $L = 10$, are explored, see Figure 6.11(a). When the coefficients a_k are below their maximal absolute value $\mathsf{a}_{\max}$ times e the roundoff plateau is reached. Increasing the number of coefficients N in the series expansion gives an error which is at most a factor 10^{15} smaller, but at least only of order 10^{-5}.

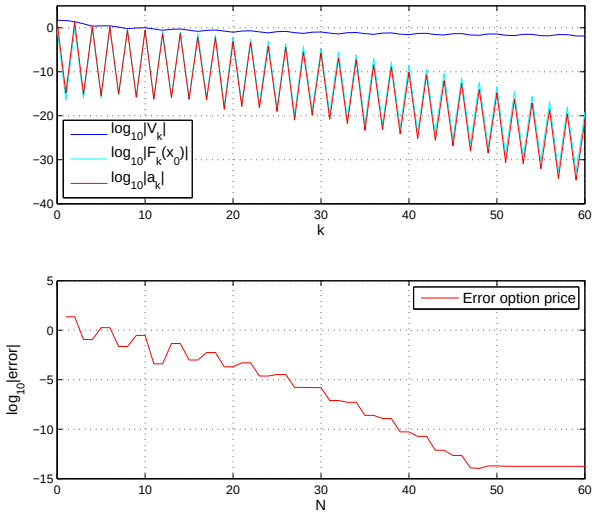

Figure 6.9: Convergence coefficients V_k, F_k, a_k and the call option price error, $T = 0.1$, ($x_0 = 0$, $L = 10$).

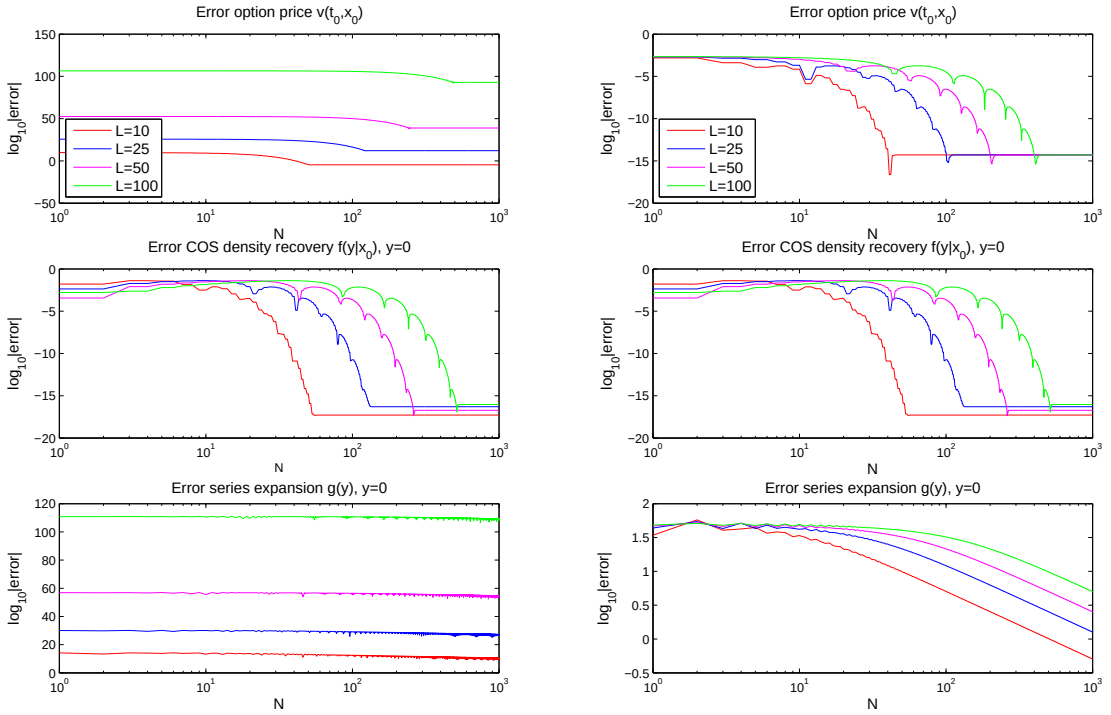

(a) Call option.

(b) Put option.

Figure 6.10: Errors of Fourier-cosine expansions, $T = 100$ ($x_0 = 0$).

In order to make more clear how the first, large coefficients influence the option price, we show the development of the approximated call option prices in the number of terms N by an example for $L = 10$. The first coefficients a_k are very large, of order 10^{10}, and positive coefficients alternates with negative

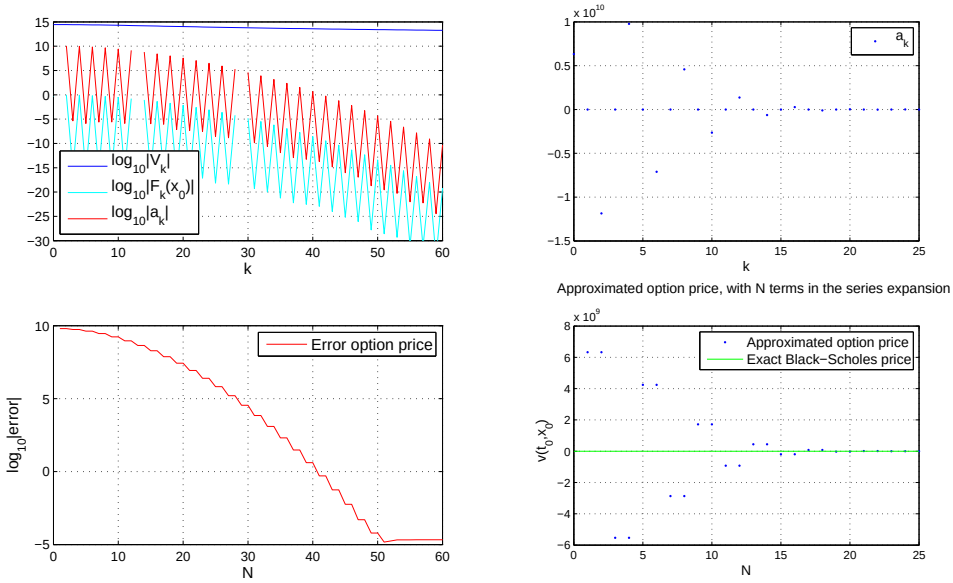

(a) Convergence coefficients V_k, F_k, a_k and the call option price error.

(b) Development approximated call option price.

Figure 6.11: Convergence coefficients, error and approximated call option price, $T = 100$ ($x_0 = 0$, $L = 10$).

ones, see upper plot in Figure 6.11(b). The lower plot illustrates how the summation over the coefficients a_k develops in N. There holds $\mathsf{a}_{\max} \approx 10^{10}$, which is, using double precision, accurate up to about six decimals places. This affects the attainable accuracy. Indeed this corresponds closely to the roundoff plateau with value 10^{-5}. This shows how the first, large coefficients affect the accuracy that can be reached.

We demonstrated how the large coefficients affect the attainable accuracy. Suppose that the maximum absolute value of the coefficients, $\mathsf{a}_{\max}$, has accuracy 10^q for some value q. We set the following rule-of-thumb:

The summation $\sum_{k=0}^{N-1} \mathsf{a}_k$ *can reach an accuracy of at most* 10^q.

Multiple Precision

Again we use the Multiple Precision Toolbox for Matlab to investigate the error convergence with higher precision calculations. This enables us to use more accurate coefficients a_k, so that the roundoff plateau can be lowered, as illustrated in Figure 6.12. The value $\mathsf{a}_{\max}$ has an accuracy of thirteen decimals using precision $p = 75$ and the corresponding roundoff plateau has value 10^{-12}. However, using the Multiple Precision Toolbox takes much more computation time (more than a factor 100 in our computations). Again we recommend the use of higher precision calculations only if the results of double precision are not accurate enough.

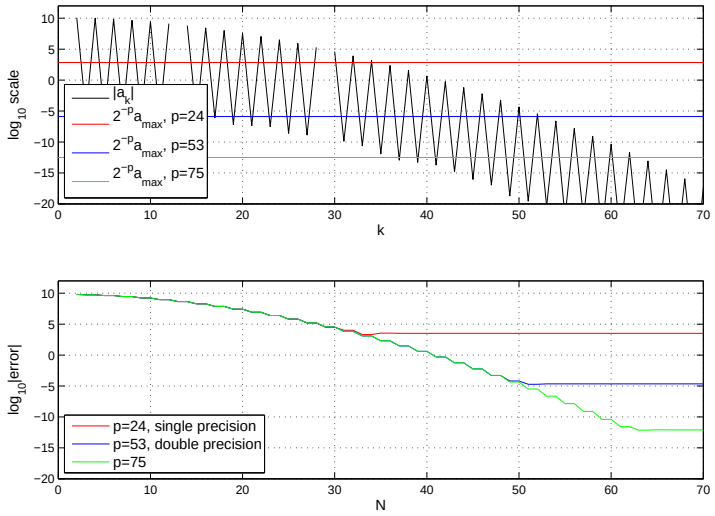

Figure 6.12: Higher precision calculations call option price for $p = 24, 53, 75$, $T = 100$.

6.3.2 Error close to the boundaries of the domain

The COS method can be used to calculate the European option prices for many different values x simultaneously. However, the integration range (6.31) is defined based on only one of their values, x_0. We investigate the error for different values $x \in [a, b]$. The truncation error ϵ_1 and ϵ_3 may be large close to the boundary values a and b. These errors may give difficulties when determining the construction domains in the more involved dike-height problem, or the early-exercise points for pricing Bermudan options, if they are located in the vicinity of the boundaries. In this section we first investigate the influence of a low value L, for which the errors ϵ_1 and ϵ_3 dominate even for x_0.

The integration range $[a, b]$ suggested by equation (6.31) is based on the cumulants of the normally distributed log-asset price X_T. We may require, for example, $\epsilon_4 < TOL$ for some given tolerance TOL. The probability that a normally distributed random variable is within L standard deviations of its mean, to be precise in the interval $[c_1 - L\sqrt{c_2}, c_1 + L\sqrt{c_2}]$, is given by

$$N(c_1 + L\sqrt{c_2}) - N(c_1 - L\sqrt{c_2}) = \operatorname{erf}\left(L/\sqrt{2}\right). \tag{6.35}$$

For example, $\operatorname{erf}(4/\sqrt{2}) \approx 0.999937$ and $\operatorname{erf}(6/\sqrt{2}) \approx 0.999999998$. So, for $L = 4$ we have $\epsilon_4(x|[a, b]) = 1 - \operatorname{erf}\left(L/\sqrt{2}\right) \approx 6.33 \cdot 10^{-5}$.

Reference [10] proposed to take value $L = 10$. A slightly smaller value L will not cause a very large error ϵ_4. However, the error

$$\epsilon_1(x|[a, b]) = e^{-r\Delta t} \int_{\mathbb{R}\setminus[a,b]} g(y) f(y|x) dy > 0, \tag{6.36}$$

which also takes into account the characteristics of the payoff function, may become too large, especially for call options.

Figure 6.3.2 demonstrates the effects of a small value $L = 4$ for $x_0 = 0$ and terminal times $T = 0.1$ (upper plots) and $T = 100$ (lower plots). The density functions are given in the left side plots and the functions $e^{-r\Delta t} g(y) f(y|x_0)$ in the middle (call options) and right plot (put options). The error ϵ_4 has value $6.33 \cdot 10^{-5}$ in both cases. The integration range truncation error ϵ_1 is represented by the red coloured areas

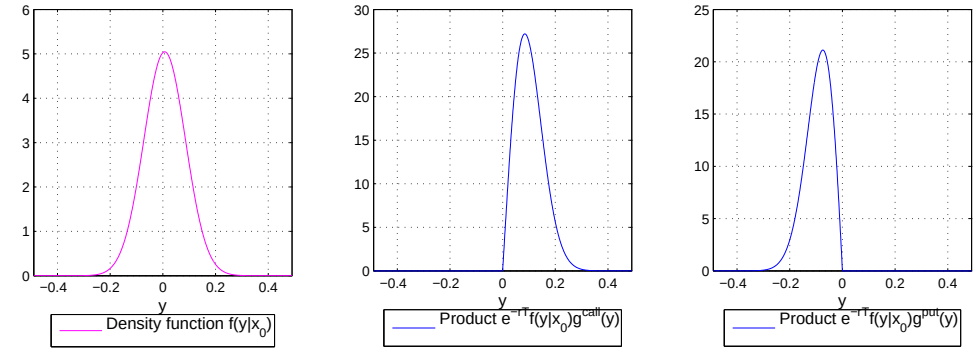

(a) Terminal time $T = 0.1, L = 4, [a, b] = [-0.31, 0.32]$.

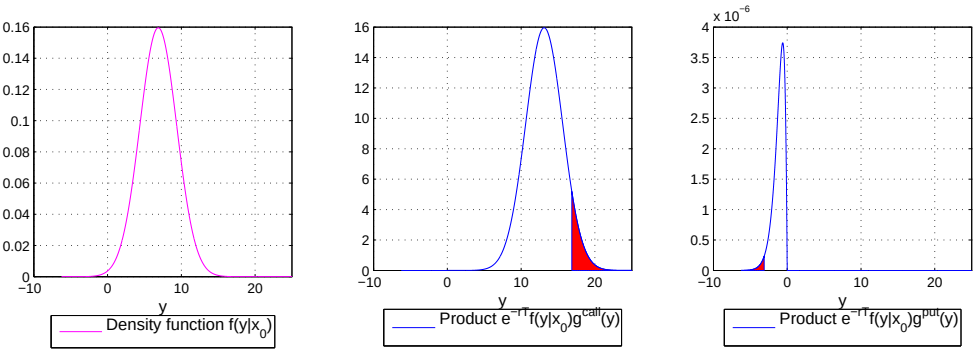

(b) Terminal time $T = 100, L = 4, [a, b] = [-3.13, 16.88]$.

Figure 6.13: Functions $f(y|x_0)$ (left) and $e^{-r\Delta t}g(y)f(y|x_0)$ for call (middle) and put options (right), $x_0 = 0$. The red area represents ϵ_1.

and has value $1.27 \cdot 10^{-3}$ and 6.68 for the call options for $T = 0.1$ and $T = 100$, respectively. The put payoff function is bounded and therefore the truncation error ϵ_1 for put options is much lower, $8.75 \cdot 10^{-4}$ and $1.40 \cdot 10^{-4}$ for $T = 0.1$ and $T = 100$, respectively. Especially the errors for the large terminal time $T = 100$ are unacceptable. Multiplying the density function by the payoff shifts the mass. This shows that an integration range that is defined only based on the density function is not always accurate, which we will also illustrate by an example in Section 8.5.3. We will show that the error ϵ_1 may be partly reduced by ϵ_3.

Next we measure the error on the whole domain $x \in [a, b]$. Again two terminal times are considered, $T = 0.1$ and $T = 100$. We start with the call option prices for terminal time $T = 0.1$. Figure 6.14 shows the total error ϵ, the integration range truncation error ϵ_1, the error ϵ_3 related to approximating $G_k(x)$ by $F_k(x)$, and the sum of both errors:

$$\begin{aligned} \epsilon_5(x|N,[a,b]) &= \epsilon_1(x|[a,b]) + \epsilon_3(x|N,[a,b]) \\ &= e^{-r\Delta t}\int_{\mathbb{R}\setminus[a,b]} \left[\sum_{k=N}^{+\infty} \cos\left(k\pi\frac{y-a}{b-a}\right) V_k\right] f(y|x)dy \\ &= e^{-r\Delta t}\int_{\mathbb{R}\setminus[a,b]} \left[g(y) - \hat{g}(y)\right] f(y|x)dy. \end{aligned} \tag{6.37}$$

The exact Black-Scholes prices are used to calculate the total error ϵ. The integration range truncation error is given by equation (6.25) and the error ϵ_3 is estimated using a numerical integration rule. We set $N = 2^{12}$, so that the roundoff plateau is reached. The overview confirms that the series truncation error ϵ_2 can be neglect since the total error equals error ϵ_5 nearly. The error is large in the vicinity of

boundary value b.

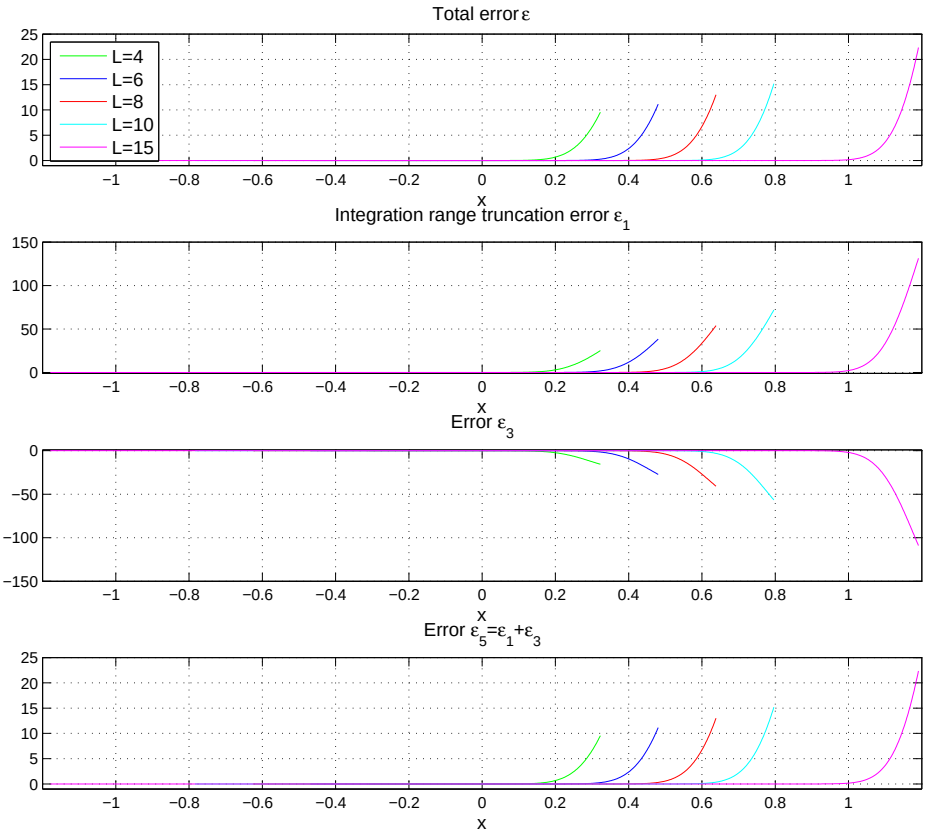

Figure 6.14: Errors approximated call option price for different values x and L, $T = 0.1$ ($x_0 = 0$).

For $L = 10$, there holds for $x = b$:

$$\epsilon_1 \approx 73.00, \quad \epsilon_3 \approx -57.54, \quad \epsilon_5 \approx 15.46. \tag{6.38}$$

The error ϵ_3 is negative at the b-side and compensates for the large truncation error ϵ_1. This is illustrated by Figure 6.15, where we take $L = 10$ ($[a, b] = [-0.78, 0.80]$). The upper plot shows the discounted payoff function and its Fourier-cosine series expansion, which is symmetric in a and b. The error is large outside the interval $[a, b]$. The density function $f(y|x = b)$ is given in the middle plot. The product of both functions, this is the integrand of

$$v(t_0, x = b) = \int_{\mathbb{R}} e^{-r\Delta t} g(y) f(y|x = b) dy, \tag{6.39}$$

appears in the third plot. The integration range truncation error ϵ_1 enters by truncation of the above integration interval $\mathbb{R}$ to $[a, b]$, which is represented by the sum of the pink and light green area. Note that the error ϵ_5 equals the light green area, so the pink part only represents the error $-\epsilon_3$. This demonstrates how the first error is compensated by the third error for x close to b. Computing the areas gives:

$$\begin{array}{rcll} \epsilon_1 & = & \text{pink} + \text{light green} & \approx & 73.00, \\ -\epsilon_3 & = & \text{pink} & \approx & 57.54, \\ \epsilon_5 & = & \text{light green} & \approx & 15.46, \end{array} \tag{6.40}$$

which corresponds to the results in Figure 6.14. We remark that the integration range truncation error is close to zero for x in the vicinity of a. Then the error ϵ_3 and the series truncation error ϵ_2 remain. The error reaches a roundoff plateau in the middle of the computational domain. Although not visible from the figure, this plateau is a little bit higher for larger integration domains $[a, b]$. Results for the put options prices are quite similar, except that the error is large at the left-hand side instead of the right-hand side of the computational domain. Moreover, the put option errors are smaller compared to the call errors, because their payoff function is bounded by K.

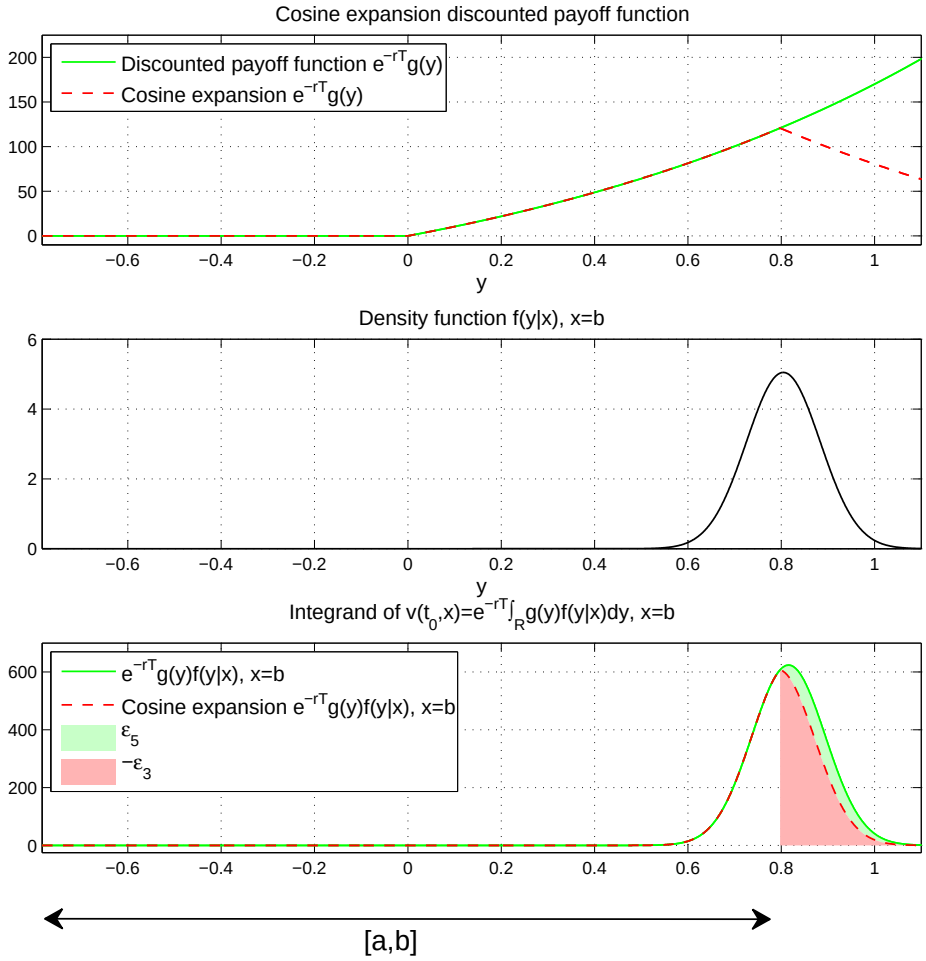

Figure 6.15: Truncation range error $\epsilon_1(x|[a, b])$ compensated by $\epsilon_3(x|N, [a, b])$ for $x = b$.

The error results for the large terminal time $T = 100$ are shown in Figure 6.16. Only the total errors ϵ for call (upper plot) and put options (lower plot) are given, on a logarithmic scale.

Firstly we discuss the error results for the call prices. The roundoff plateau is represented by the horizontal parts. Outside this plateau the error ϵ_5, which is the sum of the integration range truncation error ϵ_1 and ϵ_3, dominates. The value of the roundoff plateau is higher for larger values of L as the Fourier-cosine series expansion of the call payoff is less accurate for larger intervals. For $x = 0$ the value $L = 10$ is just large enough in order to stay outside the part where the error ϵ_5 dominates. By varying the value L we see a trade-off between a smaller error ϵ_5 and smaller roundoff errors. The optimal value L for $x = 0$ is $L = 8$. However, if the density function and the exact solution are not known, it is more difficult to

determine the optimal interval $[a, b]$.

Secondly we take a look at the errors of the put option prices. They do not suffer from a larger value L in the middle of the computational domain. This follows from the fact that the value of the roundoff plateau, where the roundoff errors dominate, does not depend on L. Surprisingly, the plateau shows a 'bump' in the middle of the computational domain. Possibly this is due to the Gibbs phenomenon, which is illustrated by Figure 6.17. There the Fourier-cosine series expansion of the put payoff function, for $[a, b] = [-10, 10]$ and $N = 2^5$, is shown. The error is highest for $y = 0$. The derivative of the function $g(y)$ increases if y approaches zero from the left side and there holds

$$\lim_{y \uparrow 0} \frac{dg^{put}(y)}{dy} = K. \tag{6.41}$$

The derivative is not continuous in $y = 0$, which may cause the so-called Gibbs phenomenon.

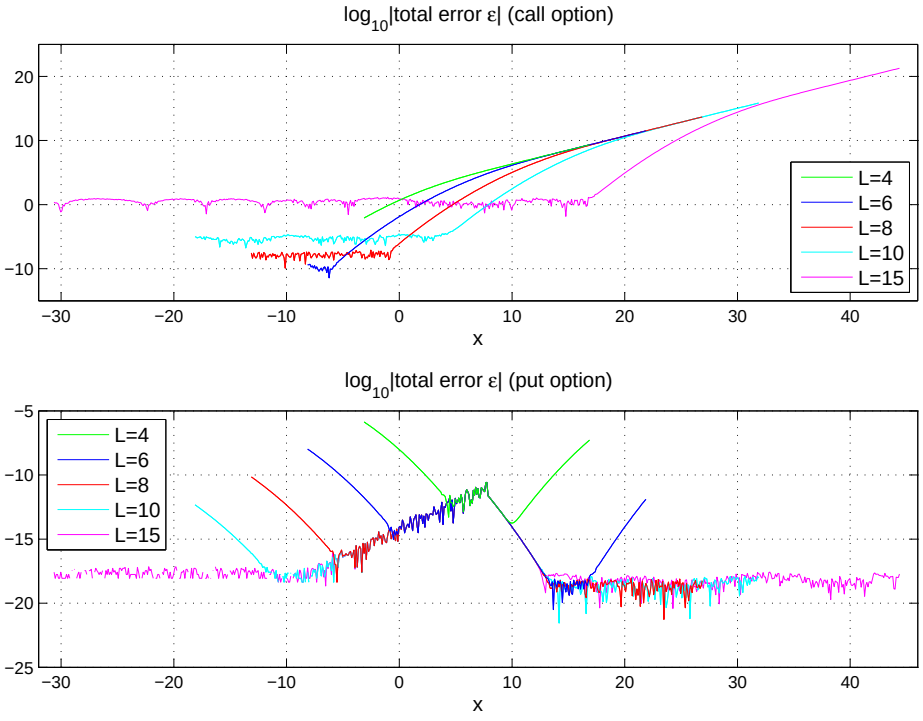

Figure 6.16: Errors approximated option prices for different values x and L, $T = 100$ ($x_0 = 0$).

Remark 6.2. *At last we change the proposed interval (6.31) by*

$$[a, b] = \left[c_1 - L_l \sqrt{c_2 + \sqrt{c_4}},\ c_1 + L_r \sqrt{c_2 + \sqrt{c_4}} \right]. \tag{6.42}$$

With this we will confirm that one of the boundary of interval (6.31) is more significant. Repeating the previous tests with $L_l = \frac{1}{2}L$ and $L_r = L$ does not show different errors for the call option prices. The coefficients are of the same order and the same accuracy is reached. However, the coefficients F_k decrease faster on the smaller interval, so that the roundoff plateau is reached earlier. The results for put options are less satisfactorily since most part of the mass in the integral represented by equation (6.14) is located at the left side of the integration domain. This leads up to a larger error ϵ_5. The results for $L_l = L$ and $L_r = \frac{1}{2}L$ give a higher roundoff plateau for call option because the coefficients are lowered by this, but the

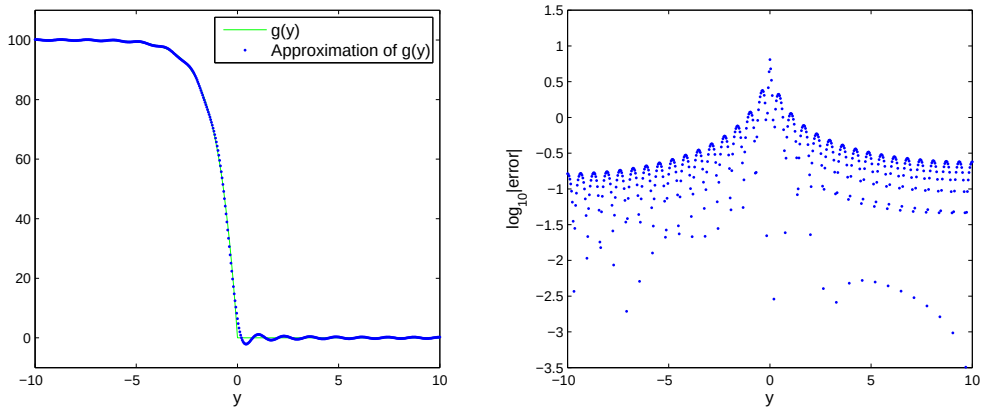

Figure 6.17: Possible explanation 'bump' error put prices ($K = 100, [a, b] = [-10, 10], N = 2^5$).

error ϵ_5 is much higher. The put option price errors remain the same in the middle of the computational domain. This establishes that multiplying the density function by the payoff shifts the mass and that an integration range which only based on the density function is not always accurate.

6.3.3 SIN method

One might wonder why we use the COS method instead of a similar SIN method. Indeed a function can also be represented by its Fourier-sine series expansion. The error results of a SIN density recovery and the COS density recovery are similar for sufficiently large domains $[a, b]$. However, the Fourier-sine series expansion of the call payoff function shows less satisfactorily results, as we present in this section.

We start with a moral principle cited from [5]:
"MORAL PRINCIPLE 1
(i) When in doubt, use Chebyshev polynomials unless the solution is spatially periodic, in which case an ordinary Fourier series is better.
(ii) Unless you're sure another set of basis functions is better, use Chebyshev polynomials.
(iii) Unless you're really, really sure that another set of basis functions is better, use Chebyshev polynomials."

For a finite interval, which can always be rescaled and translated to $[-1, 1]$, Chebyshev or Legendre polynomials are optimal. The complete Fourier series expansion is better if a function is periodic. An important feature of Chebyshev series is that their convergence properties are not affected by the values of the approximated function or its derivatives at the boundaries.

The Chebyshev series expansion of a function $H(\theta)$ supported on the finite interval $[-1, 1]$ reads

$$H(\theta) = \sum_{k=0}^{+\infty}{}' a_k T_k(\theta), \quad \text{where} \quad T_k(\theta) = \cos(k \cos^{-1}(\theta)), \tag{6.43}$$

and with coefficients

$$a_k = \frac{2}{\pi} \int_{-1}^{1} \frac{1}{\sqrt{1-\theta^2}} H(\theta) T_k(\theta) d\theta. \tag{6.44}$$

There holds $T_k(\cos x) = \cos(kx)$ and the transformation $\theta = \cos(x)$ gives

$$\begin{aligned} a_k &= -\frac{2}{\pi}\int_{\pi}^{0} \frac{\sin(x)}{\sqrt{1-\cos^2(x)}} H(\cos x)\cos(kx)dx \\ &= \frac{2}{\pi}\int_{0}^{\pi} H(\cos x)\cos(kx)dx. \end{aligned} \tag{6.45}$$

The coefficients of $H(\theta)$ of a Chebyshev series are identical with the Fourier-cosine coefficients of $H(\cos x)$ on the interval $[0, \pi]$ and so both series expansions are equivalent under transformation. For functions supported on any other finite interval $[a, b]$ the Fourier-cosine series expansion can easily by obtained via a change of variables.

Although the insistent advice in [5] to use the Chebyshev, or the equivalent Fourier-cosine series, we test the Fourier-sine series expansion. The Fourier-sine series expansion for the call payoff function $g^{call}(y)$ reads

$$\hat{g}^{call}_{SIN}(y) = \sum_{k=1}^{N-1} W_k \sin\left(k\pi\frac{y-a}{b-a}\right), \tag{6.46}$$

where

$$W_k = \frac{2}{b-a}\int_a^b g^{call}(y)\sin\left(k\pi\frac{y-a}{b-a}\right)dy = \frac{2}{b-a}K(\chi^{SIN}_k(0,b) - \psi^{SIN}_k(0,b)), \tag{6.47}$$

with $\chi^{SIN}_k(z_1, z_2)$ and $\psi^{SIN}_k(z_1, z_2)$ as defined in Appendix B.

The Fourier-sine expansion always has value zero at the boundaries of the expansion interval, which may affect the convergence rate. Results for $[a, b] = [-2, 2]$, $K = 100$ and $N = 2^3$ are shown in Figure 6.18. The errors are worse for the Fourier-sine series expansion, compared to the Fourier-cosine expansion. Furthermore, the errors of the Fourier-cosine expansion decrease at a faster rate than the errors of the sine expansion.

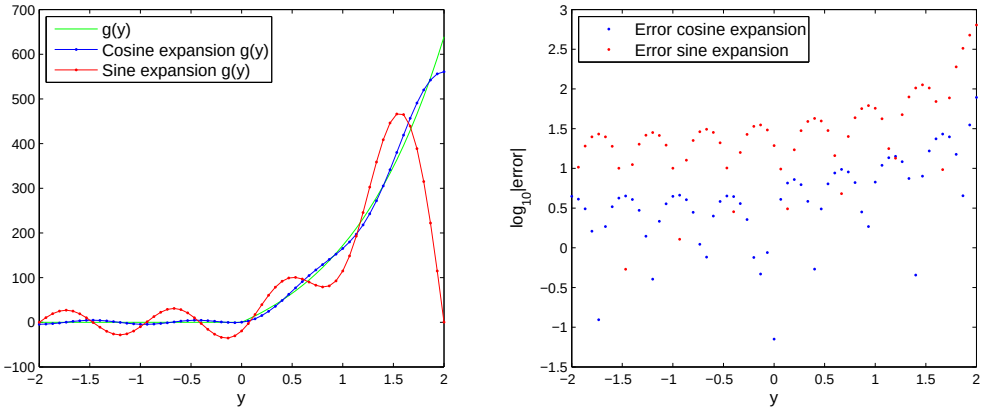

Figure 6.18: Fourier-cosine and Fourier-sine expansion $g^{call}(y)$ and the error ($K = 100$, $[a, b] = [-2, 2]$ and $N = 2^3$).

The sine functions $\sin(k\pi\frac{y-a}{b-a})$ are equal to zero for $y = a$ and $y = b$, and so is the series expansion at the boundary points. Because of that, the error of the sine expansion at boundary point $b = 2$ remains equal to $g^{call}(b) \approx 639$. Difficulties of the Fourier-sine expansion arise from their boundary values.

The COS formula for pricing options, equation (6.18), is a combination of the estimated density recovery coefficients and the payoff coefficients. A similar SIN formula does not work satisfactorily, because it is

hampered by the Fourier-sine expansion of the call payoff function. Valuation of put options using a SIN formula faces the same problems.

6.3.4 Modified Fourier method

Recently modifications of the classical Fourier series expansions are developed. In [19] the $\sin(k\pi\theta)$ functions (on $[-1,1]$) are replaced by $\sin((k-\frac{1}{2})\pi\theta)$, whereas the cosine terms remain the same. They showed that this modified Fourier expansion converges pointwise at a faster rate than the Fourier expansion for nonperiodic functions. The modified Fourier series expansion can by used to approximate the density and payoff functions. In this section we explain a method to pricing option using this series expansion and we perform tests to analyse the error.

The modified Fourier series expansion of a function $H(\theta)$ supported on the finite interval $[-1,1]$ reads ([19]):

$$H(\theta) \sim \sum_{k=0}^{+\infty}{}' c_k \cos(k\pi\theta) + \sum_{k=1}^{+\infty} s_k \sin\left((k-\tfrac{1}{2})\pi\theta\right), \qquad \theta \in [-1,1], \tag{6.48}$$

with

$$c_k = \int_{-1}^{1} H(\theta)\cos(k\pi\theta)\,d\theta \quad \text{and} \quad s_k = \int_{-1}^{1} H(\theta)\sin\left((k-\tfrac{1}{2})\pi\theta\right)d\theta. \tag{6.49}$$

For a function h supported on the finite interval $[a,b] \in \mathbb{R}$ the modified series expansion can be obtained via a change of variables:

$$x = \frac{a+b}{2} + \frac{b-a}{2}\theta. \tag{6.50}$$

We get

$$h(x) \sim \sum_{k=0}^{+\infty}{}' c_k \cos\left(k\pi\frac{2x-(b+a)}{b-a}\right) + \sum_{k=1}^{+\infty} s_k \sin\left((k-\tfrac{1}{2})\pi\frac{2x-(b+a)}{b-a}\right), \qquad x \in [a,b], \tag{6.51}$$

with

$$c_k = \int_a^b h(x)\cos\left(k\pi\frac{2x-(b+a)}{b-a}\right)dx \quad \text{and} \quad s_k = \int_a^b h(x)\sin\left((k-\tfrac{1}{2})\pi\frac{2x-(b+a)}{b-a}\right)dx. \tag{6.52}$$

In Section 4.1 the Fourier-cosine series expansion of the density function and the payoff function are used to estimate an expected value. In [10] a similar COS method for pricing call and put options was derived, see equation (6.18). Now we use the modified Fourier series expansion to develop the so-called Mod-4 method. The option price approximation reads

$$\begin{aligned} v(t_0,x) &= e^{-r\Delta t}\int_{\mathbb{R}} g(y)f(y|x)dy \\ &\approx e^{-r\Delta t}\int_a^b g(y)f(y|x)dy \\ &\approx e^{-r\Delta t}\int_a^b g(y)\left[\sum_{k=0}^{+\infty}{}' G_k^c(x)\cos\left(k\pi\frac{2y-(b+a)}{b-a}\right) + \sum_{k=1}^{+\infty} G_k^s(x)\sin\left((k-\tfrac{1}{2})\pi\frac{2y-(b+a)}{b-a}\right)\right]dy. \end{aligned} \tag{6.53}$$

The conditional density is replaced by its modified Fourier expansion in y on $[a,b]$, with series coefficients

$\{G_k^c(x)\}_{k=0}^{+\infty}$ and $\{G_k^s(x)\}_{k=1}^{+\infty}$ defined by

$$\begin{aligned} G_k^c(x) &:= \frac{2}{b-a}\int_a^b f(y|x)\cos\left(k\pi\frac{2y-(b+a)}{b-a}\right)dy, \\ G_k^s(x) &:= \frac{2}{b-a}\int_a^b f(y|x)\sin\left((k-\tfrac{1}{2})\pi\frac{2y-(b+a)}{b-a}\right)dy. \end{aligned} \tag{6.54}$$

We interchange summation and integration and insert the definitions

$$\begin{aligned} V_k^c &:= \frac{2}{b-a}\int_a^b g(y)\cos\left(k\pi\frac{2y-(b+a)}{b-a}\right)dy, \\ V_k^s &:= \frac{2}{b-a}\int_a^b g(y)\sin\left((k-\tfrac{1}{2})\pi\frac{2y-(b+a)}{b-a}\right)dy, \end{aligned}$$

which are the modified Fourier series coefficients of the payoff function. Truncation of the series results in

$$v(t_0,x) \approx \frac{b-a}{2}e^{-r\Delta t}\left[\sum_{k=0}^{N-1}{}' G_k^c(x)V_k^c + \sum_{k=1}^{N-1} G_s^c(x)V_k^s\right]. \tag{6.55}$$

The coefficients G_k^c and G_k^c can be approximated in a similar way as in equation (4.13):

$$\begin{aligned} G_k^c(x) &\approx \frac{2}{b-a}\int_{\mathbb{R}} f(y|x)\cos\left(k\pi\frac{2y-(b+a)}{b-a}\right)dy \\ &= \frac{2}{b-a}\Re\left[\int_{\mathbb{R}} f(y|x)e^{\frac{i2k\pi}{b-a}y}dy e^{-ik\pi\frac{(b+a)}{b-a}}\right] \\ &= \frac{2}{b-a}\Re\left[\varphi_{levy}\left(\frac{2k\pi}{b-a}\right)e^{ik\pi\frac{2x-(b+a)}{b-a}}\right] := F_k^c(x). \\ G_k^s(x) &\approx \frac{2}{b-a}\Im\left[\varphi_{levy}\left(\frac{2(k-\frac{1}{2})\pi}{b-a}\right)e^{i(k-\frac{1}{2})\pi\frac{2x-(b+a)}{b-a}}\right] := F_k^s(x). \end{aligned} \tag{6.56}$$

We end up with the *Mod-4 formula*:

$$\begin{aligned} \hat{v}(t_0,x) &:= e^{-r\Delta t}\Big(\sum_{k=0}^{N-1}{}'\Re\left[\varphi_{levy}\left(\frac{2k\pi}{b-a}\right)e^{ik\pi\frac{2x-(b+a)}{b-a}}\right]V_k^c. \\ &+ \sum_{k=1}^{N-1}\Im\left[\varphi_{levy}\left(\frac{2(k-\frac{1}{2})\pi}{b-a}\right)e^{i(k-\frac{1}{2})\pi\frac{2x-(b+a)}{b-a}}\right]V_k^s\Big). \end{aligned} \tag{6.57}$$

The modified Fourier coefficients of a call payoff function read

$$\begin{aligned} V_k^c &= \frac{2}{b-a}K(\chi_k^c(0,b)-\psi_k^c(0,b)), \\ V_k^s &= \frac{2}{b-a}K(\chi_k^s(0,b)-\psi_k^s(0,b)), \end{aligned} \tag{6.58}$$

where the analytical solution of functions $\chi_k^c(z_1,z_2)$, $\chi_k^s(z_1,z_2)$, $\psi_k^c(z_1,z_2)$, $\psi_k^s(z_1,z_2)$ can be found in Appendix C.

The error convergence of the Mod-4 method is analysed for a call option with terminal time $T = 100$. Figure 6.19 shows the results, for which the same parameter values as for Figure 6.11(a) are used. The roundoff plateau is reached about two times faster in N, compared to the COS method. However, two summations need to be calculated which doubles the computation time. Possibly the implementation can be done efficiently in order to reduce the computation time, which is important in financial applications. The largest modified Fourier coefficients and cosine-Fourier coefficients are of the same order of magnitude and have the same accuracy. Because of that, the minimal error reached by the mod-FOUR method is about the same as by the COS method.

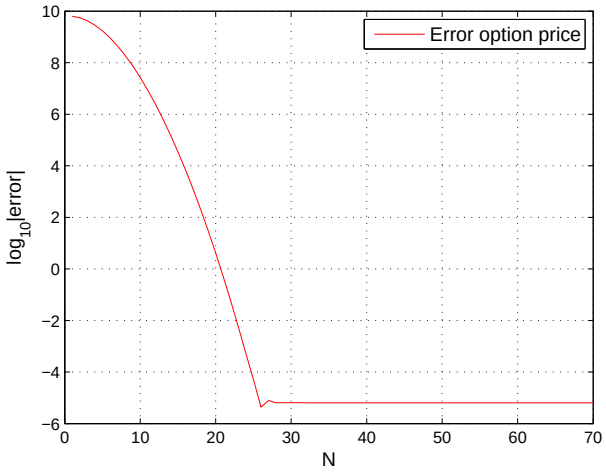

Figure 6.19: Convergence error call option price by Mod-4 method, $T = 100$ ($x_0 = 0, L = 10$).

6.4 Conclusion and discussion

We started in Section 6.1 with the COS density recovery of the standard normal distribution function. The estimated Fourier-cosine coefficients and the error of the recovery converge supergeometrically. However, the errors have a minimal attainable value, represented by the roundoff plateau. Higher precision calculations enable us to decrease the attainable error, but this takes much more time.

After that the payoff function of the call and put options were considered in Section 6.2. The series expansion with a small number of coefficients N is less accurate for the call payoff function compared to the put payoff, because the call payoff function is unbounded whereas the put payoff is bounded by K. Besides, a larger integration interval $[a, b]$, which results in larger coefficients for the call payoff function, has a negative effect on the error.

The estimated Fourier-cosine coefficients of the density function and the coefficients of the payoff expansion were combined in the COS option pricing formula in Section 6.3. First the series truncation error ϵ_2 was studied. The error convergence is supergeometric, until a roundoff plateau is reached. The attainable error is determined by the accuracy of the largest coefficient $\mathsf{a}_{\max}$. Since a larger interval $[a, b]$ results in larger coefficients for the call payoff series expansion, the call options error is not accurate for large terminal time $T = 100$.

After this the integration range truncation error ϵ_1 and ϵ_3 were explored. We showed that an interval $[a, b]$ which is defined only based on the density function, the error ϵ_4, or the characteristics of the stochastic process may be inaccurate. A larger integration interval lowers the error ϵ_5 for given x. However, by this also the roundoff plateau for the call option error is higher. There is a trade-off between a smaller truncation error and smaller roundoff errors. Put option do not suffer from this as their payoff function is bounded, which results in smaller payoff series coefficients.

For the choice of the integration interval $[a, b]$ we recommend, if possible, to take into account the characteristics of the payoff function too. A smaller interval gives rise to a larger error ϵ_5. However, a larger interval has two drawbacks. Firstly, convergence takes longer for larger intervals since the series expansion is hampered by this. Secondly, the minimal attainable error may be higher if the coefficients are larger. Since the value of the coefficients is known, we are able to estimate this accuracy. We advice to carefully consider the pros and cons of possible integration intervals.

Higher precision calculations have a positive effect on the error if the number of coefficients N is sufficiently large, because the computed coefficients are more accurate. The main disadvantage is the longer computation time this takes. Possibly the Mod-4 method, which we developed in Section 6.3.4, may reduce the computation time. However, this method did not result in a lower call option price error because the coefficients have the same order of accuracy.

The tests gave insight into possible difficulties we may face using the more involved dike-COS method, which we will discuss in the next section.

7 Numerical experiments with dike-COS method

The dike-COS method is tested on a model for a small island from [32]. This model is simplified and not yet for practical use. However, this model will show that the method can be applied to a stochastic impulse control problem. The numerical computations are done using Matlab 7.7.0. The computer used has a Core2Duo 2.33 GHz CPU with 2 GB RAM.

For the numerical experiments the following parameters are used:

- Time lattice details:
$$t_0 = 0 \text{ yr}, T = 300 \text{ yr}, M = 300 \ (\Delta t = 1 \text{ yr}). \tag{7.1}$$
- Process parameters:
$$\mu_3 = 0.025, \sigma_3 = 0.15, \rho = 0.05, X_0^{(1)} = 425 \text{ cm}, X_0^{(3)} = \text{ mln€} \log(3.4 \cdot 10^4). \tag{7.2}$$
- Extreme water level occurrences:
$$\lambda = 1 \text{ yr}^{-1}, k_1 = 8.16299 \cdot 10^{-1}\text{cm}^{-1}, k_2 = 1.88452 \cdot 10^2\text{cm}, \lambda_p = 1.2 \cdot 10^{-2}\text{cm}^{-1}. \tag{7.3}$$

We use an average water level process of the form $dY_t^{(2)} = \mu_w(t)dt$. Reference [22] has based this model on the predicted increase of water level over all climate scenarios proposed by the KNMI ([23]). The drift μ_w is time-dependent and is given by

$$\mu_w(t) = \begin{cases} 0.5 & \text{for } t \in [0, 50), \\ 0.7 & \text{for } t \in [50, 100), \\ 0.9 & \text{for } t \in [100, 150), \\ 0.7 & \text{for } t \in [150, 200), \\ 0.5 & \text{for } t \in [200, 250), \\ 0.3 & \text{for } t \in [250, 300]. \end{cases} \tag{7.4}$$

Further we use the following model for the construction costs

$$b^+(x_1, u) = k_f + k_u\Big(u^2 \tan(\phi) + u(2x_1 \tan(\phi) + z - H \tan(\phi))\Big), \tag{7.5}$$

with constants $k_f = \text{mln€}22.975$, $k_u = 1.921 \cdot 10^{-4}\text{mln€/cm}^2$, $\phi = 1.25$, $H = 0$ cm and $z = 500$ cm. The costs $b^+(x_1, u)$ are increasing in x_1 and u, as can be seen in Figure 7.1.

A justification of the parameter values and the functions $f_{\mathcal{J}}(y)$, $l_p(y)$, $w(t)$ and $b^+(x_1, u)$ can be found in [22] and [32]. For more information about the discount rate for climate change analysis we refer to [20].

Integration range $[a, b]$
In Section 6.3.2 and 6.4 we concluded that we need to choose the integration interval $[a, b]$ carefully. An interval defined only based on the density function is not always accurate and it is advised to consider the characteristics of the payoff function too. The payoff at terminal time T, $v(T, x_1, x_3)$, is known and is a call-like function in x_3. However, we do not have much information about the 'payoff functions' $v(t_m^-, x_1, x_3)$ at the other time levels, except that these functions are call-like too. Furthermore, the behaviour of the option values in the recursive algorithm is involved and it is difficult to determine a priori a correct interval $[a, b]$. [32] based his computational domain on the expectation of the economic value and we partly adopt this. Although the awareness that an interval based only on the characteristics of the density function is not necessarily accurate, we start with

$$[a, b] = \left[c_1 - L\sqrt{c_2 + \sqrt{c_4}}, c_1 + L\sqrt{c_2 + \sqrt{c_4}}\right], \tag{7.6}$$

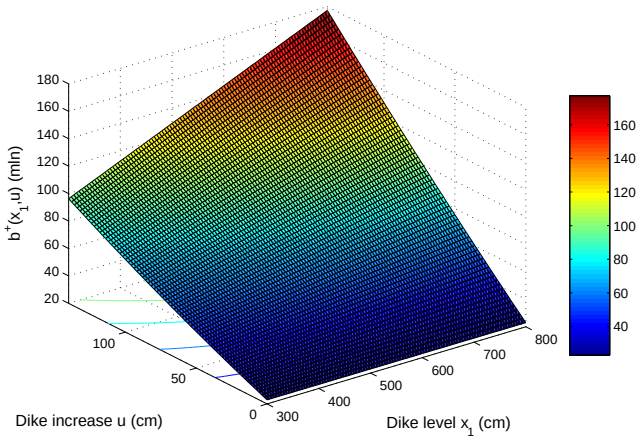

Figure 7.1: Construction costs $b^+(x_1, u)$.

where c_1, c_2 and c_4 are the first, second and fourth cumulant of $X_T^{(3)}$, conditioned on $X_0^{(3)}$, respectively. For the underlying Brownian motion we have $c_1 = X_0^{(3)} + (\mu_3 - \frac{1}{2}\sigma_3^2)T$, $c_2 = \sigma_3^2 T$ and $c_4 = 0$. We will vary the value L in Section 7.2 and determine a good estimate for interval $[a, b]$. The interval for $L = 2$ is like the interval used in [32], which was found sufficiently large. However, we will use at least value $L = 3$ in Section 7.2 since we think that our method suffers more from boundary errors.

An advantage of the proposed interval is the ability to determine the portion of the possible log-economic value paths $X_t^{(3)}$ that is covered. As we saw before, the probability that the normally distributed random variable $X_T^{(3)}$ is in the interval $[c_1 - L\sqrt{c_2},\, c_1 + L\sqrt{c_2}]$, is $1 - \mathrm{erf}(L/\sqrt{2})$.

The contents of the remainder of this section are as follows. Firstly, the approximated real option prices and construction domains are compared to their exact solution at time t_{M-1}. Then we discuss the results for the dike height problem with six possible dike increase levels. Finally a discussion, including the validation of the method, is presented in Section 7.3.

7.1 Exact solution at time t_{M-1}

We can find the continuation value at time t_{M-1} analytically. This gives, assuming that the error resulting from the Trapezoidal rule can be neglected, exact option values $v(t_{M-1}, x_1, x_3)$ and exact construction domains $A_{M-1}^i(x_1)$. So, we have the possibility to compare the solution from the dike-COS-method with the exact solution at that time lattice.

There holds

$$X_{t_{m+1}} | X_{t_m} \sim \mathcal{N}\left(X_{t_m} + (\mu_3 - \frac{1}{2}\sigma_3^2)\Delta t, \sigma_3^2 \Delta t \right), \tag{7.7}$$

and with equation (7.7) the continuation value at time t_{M-1} reads:

$$\begin{aligned} c(t_{M-1},x_1,x_3) &= e^{-\rho\Delta t}\int_{\mathbb{R}} v(t_M,x_1,y)f(y|x_3)dy \\ &= \frac{\lambda\beta(x_1-w(T))}{\rho-\mu_3}\frac{e^{-\rho\Delta t}}{\sqrt{2\pi}\sigma_3\sqrt{\Delta t}}\int_{\mathbb{R}} e^y e^{-\frac{1}{2}\left(\frac{y-x_3-(\mu_3-\frac{1}{2}\sigma_3^2)\Delta t}{\sigma_3\sqrt{\Delta t}}\right)^2}dy \\ &= e^{(\mu_3-\rho)\Delta t+x_3}\frac{\lambda\beta(x_1-w(T))}{\rho-\mu_3}. \end{aligned} \tag{7.8}$$

The COS method gives the approximation

$$\hat{c}(t_{M-1},x_1,x_3) = e^{-\rho\Delta t}\sum_{k=0}^{N-1}{}'\,\Re\left[\varphi_{levy}\left(\frac{k\pi}{b-a}\right)e^{ik\pi\frac{x_3-a}{b-a}}\right]V_k(t_M^-,x_1). \tag{7.9}$$

Similar as in Section 6.3 the truncation error can be found analytically:

$$\epsilon_1(t_{M-1},x_1,x_3|[a,b]) = e^{(\mu_3-\rho)\Delta t+x_3}\frac{\lambda\beta(x_1-w(T))}{\rho-\mu_3}\left[N(a_1-\sigma_3\sqrt{\Delta t})+(1-N(b_1-\sigma_3\sqrt{\Delta t}))\right], \tag{7.10}$$

with

$$a_1=\frac{a-x_3-(\mu_3-\frac{1}{2}\sigma_3^2)\Delta t}{\sigma_3\sqrt{\Delta t}} \quad \text{and} \quad b_1=\frac{b-x_3-(\mu_3-\frac{1}{2}\sigma_3^2)\Delta t}{\sigma_3\sqrt{\Delta t}}. \tag{7.11}$$

In Figure 7.2 the errors obtained for $x_1 = 425$ cm and various values of L, are shown. The upper plot in the figure shows the logarithmic absolute value of the exact continuation value and the approximated solutions $\hat{c}(t_{M-1},x_1,x_3)$. The inaccuracies at the left side of the computational domain are due to roundoff errors in the terms $V_k(t_M^-,x_1)$. The second plot represents the error compared to the exact solution. We set $N = 2^{12}$ and the roundoff plateau is reached, so no further improvement is found for higher values of N. The integration range truncation errors ϵ_1 are shown in the third plot. This error is largest close to the boundary b, but the total error is reduced by error ϵ_3 in the same way as we explained in Section 6.3.2. The roundoff errors dominate in the middle of the computational domain. The roundoff plateau is lower for smaller sized integration intervals, because then the Fourier-cosine series expansion of the call-like function $v(t_M,x_1,y)$ is more accurate (as discussed in Section 6.2). The continuation value is lower for a higher dike level and a smaller error will be obtained, since the expansion of a lower function $v(t_M,x_1,y)$ is more accurate.

The expected value of the economic value at time t_{M-1} is about mln€e^{18}. For the log-economic value $x_3 = 18$ the error is of order 10^{-3}. It is difficult to tell in advance whether this is accurate enough for the remainder of the dike-COS method. However, the tests of this algorithm in Section 7.2 show convergence up to eight decimals, which is accurate enough for practical use.

Multiple Precision

In Figure 7.2 we see that the roundoff plateau for $L = 6$ and $x_1 = 425$ cm has value about 10^{-3}. The exact continuation value for a log-economic value $x_3 = 18$ is $c(t_{M-1},425,18) \approx 3.24\cdot 10^6$. Also here higher precision calculations can lower the roundoff plateau and improve the attainable error, see Figure 7.3.

The upper plot shows the coefficients

$$\mathsf{b}_k := e^{-\rho\Delta t}\frac{b-a}{2}F_k(x_3)V_k(t_M^-,x_1) \tag{7.12}$$

and the lines indicate the values $2^{-p}\mathsf{b}_{\max}$. Error convergence for various precisions is shown in the lower plot. The roundoff plateau is reached when all coefficients are below $e\mathsf{b}_{\max}$, with e a constant proportional to the 'machine epsilon' 2^{-p}, by a factor about 100. For the last time in this thesis we showed

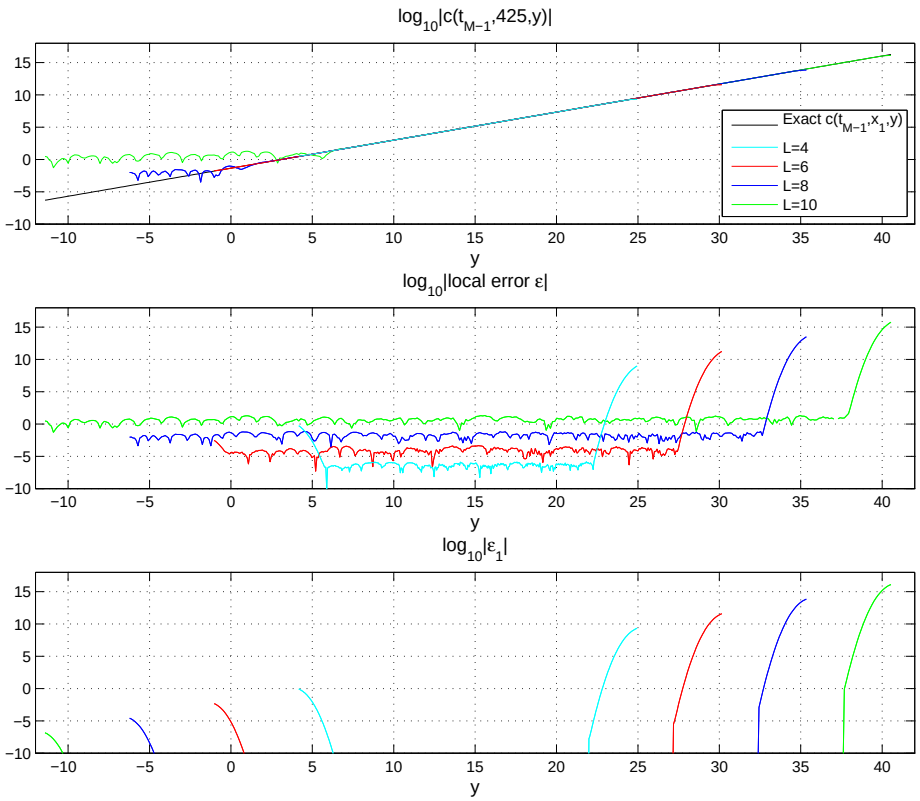

Figure 7.2: Error approximated continuation value $\hat{c}(t_{M-1}, x_1, y)$, $x_1 = 425$ ($N = 2^{12}$).

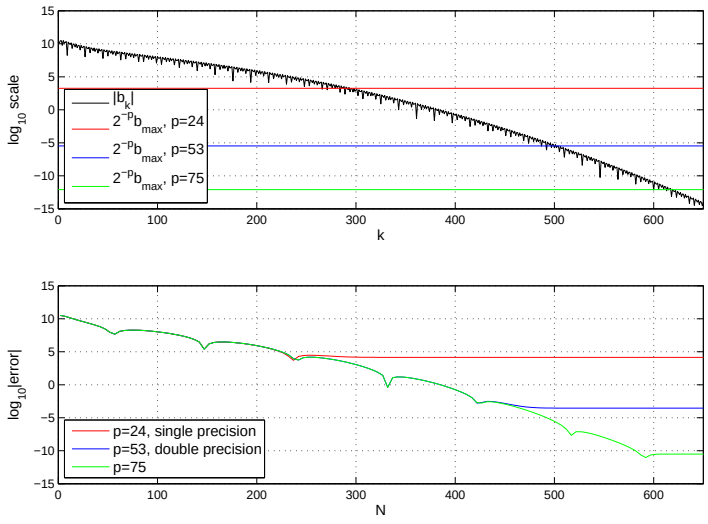

Figure 7.3: Higher precision calculations $\hat{c}(t_{M-1}, x_1, x_3)$, $x_1 = 425, x_3 = 18$ for $p = 24, 53, 75$ ($L = 6$).

how higher precision calculations can 'delay' the roundoff plateau and lower the minimal attainable error.

Exact construction points

Next we will analyse the estimated construction domains at time lattice $M-1$. We consider the case of only two possible dike increase levels, $u^0 = 0$ cm and $u^1 = 40$ cm. In Section 5.2 the corresponding construction points $y_m^*(x_1)$ were introduced. They represent the log-economic values for which the optimal dike increase changes from u^0 to u^1. The construction points at time t_{M-1} can be determined analytically. Solving the root of

$$k(y) := v(t_{M-1}, x_1, y) - v(t_{M-1}, x_1 + u^1, y) - b(x_1, u^1) \tag{7.13}$$

results in:

$$y_{M-1}^*(x_1) = \log\left(\frac{b(x_1,u^1)}{d(t_{M-1},t_M,x_1) - d(t_{M-1},t_M,x_1+u^1) + e^{(\mu_3-\rho)\Delta t}\frac{\lambda}{\rho-\mu_3}(\beta(x_1-w(T)) - \beta(x_1+u^1-w(T)))}\right). \tag{7.14}$$

In the dike-COS method we determine the root of

$$\hat{k}(y) := \hat{v}(t_{M-1}, x_1, y) - \hat{v}(t_{M-1}, x_1 + u^1, y) - b(x_1, u^1). \tag{7.15}$$

In test cases we saw that the algorithm from Section 4.2.1 did not always converge to the correct construction points. This may be due to the inaccuracy of the COS formula around the boundaries a and b or due to the roundoff errors. Both will be illustrated by an example below.

In Table 7.1 the exact construction points are shown. The approximated construction points, which are found using the approximated real option prices, are also calculated. The incorrect values are coloured in red. The error resulting from the Trapezoidal rule can be neglected, because N_t was set to 2000. Besides we used $N = 2^{12}$, for which the roundoff plateau is reached, and the results are the same as for a higher number of coefficients in the series expansion.

$y_{M-1}^*(x_1)$ \ x_1	425	465	505	665	705	745
exact	6.8823	10.1832	13.4851	26.6812	29.9774	33.2661
approx. ($L = 6$, $b = 30.1476$)	6.8823	10.1832	13.4851	26.6812	30.0208	30.1476
approx. ($L = 10$)	6.5956	10.1826	13.4854	26.6812	29.9774	33.2661

Table 7.1: Exact and approximated construction points.

First we discuss the construction points found using $L = 6$. Note that $y_{M-1}^*(745)$ is set equal to boundary point b. The approximated construction point $y_{M-1}(705)$ is too high, because the functional $\hat{k}(y)$ is lower than the exact solution close to boundary b, see Figure 7.4. This can be explained as follows. Assume that N_t and N are chosen sufficiently large, so that the errors ϵ_{Trap} and ϵ_2 are not relevant and that the roundoff error is not significant. The error ϵ_5 is positive in the vicinity of boundary b. Then the error resulting from approximation of $k(y)$ by $\hat{k}(y)$ is dominated by

$$\begin{aligned} k(y) - \hat{k}(y) &\approx \epsilon_5(t_{M-1}, x_1, y) - \epsilon_5(t_{M-1}, x_1 + u, y) \\ &= e^{-\rho\Delta t}\int_{\mathbb{R}\setminus[a,b]}\left[\sum_{k=N}^{+\infty}\cos\left(k\pi\frac{z-a}{b-a}\right)\left(V_k(t_M^-, x_1) - V_k(t_M^-, x_1+u)\right)\right] f(z|y)dz > 0. \end{aligned} \tag{7.16}$$

Since the function $v(t_M, x_1, z)$ is larger than $v(t_M, x_1 + u, z)$, the above error is positive for y close to b. It follows that the estimated function $\hat{k}$ is lower than the true function for values y close to b. From that we can deduce that the use of function $\hat{k}$ can result in a larger construction point. Since the area where the integration range truncation error occurs is small, the difference between the estimated and exact construction point is at most as large as the size of that area. Besides, the function $k(y)$ is small for y close to the construction point, which will reduce the propagating error from using the incorrect construction point.

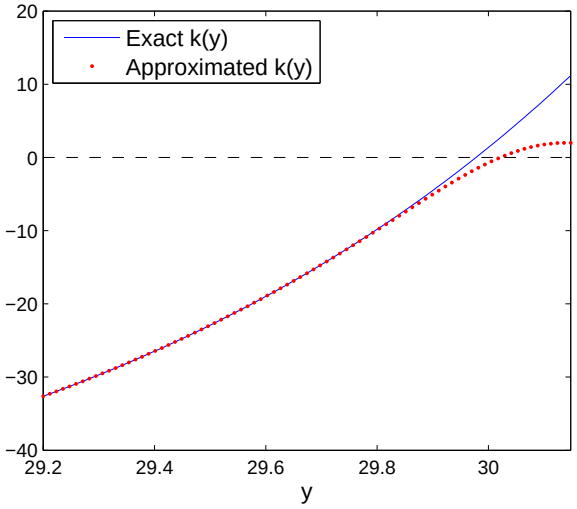

Figure 7.4: Incorrect construction point $y^*_{M-1}(705)$, $L = 6$, due to truncation errors.

Incorrect construction points $y^*_{M-1}(425)$, $y^*_{M-1}(465)$ and $y^*_{M-1}(505)$, which are found with $L = 10$, have another origin. These errors are caused by the roundoff errors in the COS formula. From Figure 7.2 we can deduce that the roundoff plateau is of order 10 for dike level $x_1 = 425$ cm and $L = 10$. This error results in a completely incorrect construction point, as shown in Figure 7.5. The use of higher precision calculations would improve the approximation of the option values and by that also help to find the correct construction points. Since the roundoff plateau is lower for the higher dike levels, the corresponding estimated construction points are more accurate.

The dike-COS method results in incorrect construction points if they are located in the vicinity of the boundary points, no matter what the size of the interval is. However, in Section 5.3 we concluded that the error propagation due to an incorrect construction point is not necessarily large. Since the area where integration range truncation errors occur is small, the difference between the estimated and true construction domains is at most as large as the size of that area. A larger integration interval resembles the original domain beter, but results in a higher roundoff plateau and so the construction points are less accurate for higher values of L. Besides, error convergence takes longer for larger values of L.

We try to find a compromise between those inaccuracies. Based on the results we recommend to choose an interval $[a, b]$ as small as possible, but the integration interval should not become too small. Then the remaining question is: "When is the integration interval too small?" If the real option value increases significantly with larger interval, then the interval is too small since this indicates that the truncation error is still large. However, be aware of the fact that also larger roundoff errors, introduced by a larger interval, may give rise to a larger option value. In Section 7.2 we will carefully choose the interval $[a, b]$.

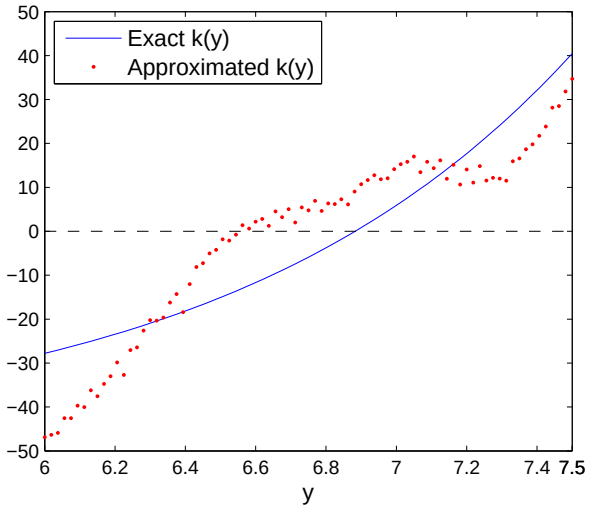

Figure 7.5: Incorrect construction point $y^*_{M-1}(425)$, $L = 10$, due to roundoff errors.

7.2 Tests dike-COS method for an island

Tests for six possible dike increase levels are performed in this section. We take $U = \{0, 20, 40, 60, 80, 100\}$ cm. The selection of this set is relevant according to the corresponding results of [32] and [22]. In our tests we calculate the costs of flood protection at time $t_0 = 0$ with initial dike level $X_0^{(1)} = 425$ cm and initial log-economic value of endangered goods $X_0^{(3)} = \log(3.4 \cdot 10^4)$, that is the real option value $\hat{v}(t_0, X_0^{(1)}, X_0^{(3)})$. We also calculate the control for an economic value of endangered goods equal to its expected value:

$$E^{t_0,x}[\exp(X_t^{(3)})] = e^{X_0^{(3)}} e^{\mu_3 t}. \tag{7.17}$$

The corresponding optimal dike re-informcement times are named the *construction times*.

Dike level grid x_1
The initial dike level is $X_0^{(1)} = 425$ cm and for efficiency reasons we take $x_1 \in [425, 445, 465, 485, \ldots]$ cm. In the formulation of the stochastic impulse control problem an infinite number of dike increases is in principle possible. In our discrete problem 299 dike heightenings would be possible, which suggests a number of dike level grid points $D > 300$. However, in the computations a much smaller grid size D is sufficiently in order to receive the same results as for a larger grid size, which takes more computation time. On the other hand, too few grid points restricts the number of possible dike reinforcements and affects the real option price. So, there is a kind of convergence of the real option value in D, which ends for a sufficiently large value D. We set the following requirement:

Requirement 1. *(Number of dike level grid points D)*
The number of dike level grid points, D, is chosen so that a larger grid size than D does not change the real option price anymore.

For a larger interval $[a, b]$ for the stochastic log-economic process, a larger number of dike level grid points is found to be necessary. In the computations with $L = 10$ the smallest grid size that satisfies Requirement 1 is $D = 22$.

Different values N and L
For the first test we take $D = 22$, $N_t = 2000$ and $N_{bis} = 80$ and we vary the values L and dd, with $N = 2^{dd}$. Table 7.2 shows the real option values, which are converging in N. It takes longer to reach

a certain level of accuracy for larger L, because a larger integration domain $[a, b]$ is considered and this hampers the Fourier-cosine series expansion. The roundoff plateau is reached for a value $dd = 9$ or higher. Then the approximated real option values are determined up to order 10^{-12}. We find that it is optimal to increase the dikes by amount $u^1 = 40$ cm at times 146, 185, 232 and 293 year if the economic value follows its expected value. A star behind the option values denotes incorrect construction times.

dd \ L	3	4	5	6
7	0.054641240657122	0.054639775446674	0.054692112772278	0.054792918686524
8	0.054641228170803	0.054639394656118	0.054639397409261	0.054640233884875
9	0.054641228170836	0.054639394656626	0.054639393884868	0.054639393888552
10	0.054641228170837	0.054639394656630	0.054639393884868	0.054639393888602
11	0.054641228170845	0.054639394656578	0.054639393884862	0.054639393888611
12	0.054641228170843	0.054639394656622	0.054639393884867	0.054639393888628

dd \ L	7	8	9	10
7	0.05881685976427*	0.15771593001764*	0.26737494457923*	-7.27116764048778*
8	0.054642533152485	0.05522974047843*	0.08394024278452*	0.08594733953757*
9	0.054639393888217	0.054639393597885	0.054639854708965	0.054671755101117
10	0.054639393888749	0.054639393888550	0.054639394116050	0.054639393902084
11	0.054639393888760	0.054639393888599	0.054639394115560	0.054639393869343
12	0.054639393888802	0.054639393888803	0.054639394115929	0.054639393883667

Table 7.2: Real option values $\hat{v}(t_0, X_0^{(1)}, X_0^{(3)})$, effect of dd and L ($D = 22, N_t = 2000, N_{bis} = 80$).

dd \ L	3	4	5	6	7	8	9	10
7	49	56	64	72	80	90	98	104
8	65	75	87	98	111	124	137	147
9	96	113	132	152	173	196	216	231
10	159	190	223	258	295	339	373	402
11	302	371	411	477	551	626	697	752
12	563	691	822	968	1131	1301	1470	1453

Table 7.3: CPU times (s), effect of dd and L ($D = 22, N_t = 2000, N_{bis} = 80$).

A higher value L implies a larger integration interval $[a, b]$ and this resembles the original domain better. Therefore, we would expect a kind of convergence in L. However, the method is affected by the roundoff errors especially for higher values L, see Section 7.1. This may lead up to incorrect construction domains. So, there is a trade-off between a smaller truncation error and smaller roundoff errors. The results in the table are satisfactorily, but we suppose that for higher values L the roundoff errors have an increasing influence. An accuracy about eight decimals is obtained, which is sufficiently accurate in practice. We decide to use $L = 6$ ($[a, b] = [-1.03, 30.15]$) in the sequel of Section 7.2. Then a dike level grid size $D = 16$ suffices to fulfil Requirement 1. We did not find that one of the boundaries affects the option value more significantly, which we did in the case of pricing European options in the end of Section 6.3.2. Because of that we hold on to the proposed interval (7.6).

Computation time has order $O(N \log_2 N)$, which fits in with the computation times in Table 7.3. We will use $dd = 10$ hereafter. The method takes longer for larger L, because then there are fewer construction domains outside the interval $[a, b]$. The Bisection method is not used if the root is not in the interval

considered.

Number of Bisection iterations
Next the influence of the number of iterations of the Bisection method is analysed. The Bisection method gives only a domain in which the root of an equation is present. Without using any other information, the optimal estimate for the location of the root is the midpoint of the smallest range found. In that case, the absolute error of the values $y_m^i(x_1)$ and $y_m^0(x_1)$ from Section 4.2.1, after N_{bis} iterations, is at most

$$\epsilon_{Bis} := \frac{b-a}{2^{N_{bis}+1}}, \tag{7.18}$$

assuming that the approximated real option values are accurate enough.

The option prices converge in N_{bis} and only fifteen Bisection iterations already give an accuracy of eight decimals, see second column of Table 7.4. Also the maximal absolute error of the construction domains $A_m^i(x_1)$ is calculated, with the construction domains for $N_{bis} = 80$ as reference values. The error is decreasing in N_{bis} and matches to ϵ_{Bis} for small values N_{bis}. The computation time is linear in the number of Bisection iterations. To save computation time we take $N_{bis} = 30$ in the computations to follow.

N_{bis}	$\hat{v}(t_0, X_0^{(1)}, X_0^{(3)})$	max. |error| $A_m^i(x_1)$	ϵ_{Bis}	CPU time (s)
10	0.054639898069154	$1.540 \cdot 10^{-2}$	$1.522 \cdot 10^{-2}$	80
15	0.054639394346814	$4.756 \cdot 10^{-4}$	$4.757 \cdot 10^{-4}$	93
20	0.054639393889160	$1.486 \cdot 10^{-5}$	$1.487 \cdot 10^{-5}$	106
30	0.054639393888593	$3.566 \cdot 10^{-8}$	$1.451 \cdot 10^{-8}$	132
40	0.054639393888570	$1.366 \cdot 10^{-7}$	$1.417 \cdot 10^{-11}$	158
50	0.054639393888573	$9.191 \cdot 10^{-8}$	$1.385 \cdot 10^{-14}$	183
60	0.054639393888602	0	$1.352 \cdot 10^{-17}$	202
80	0.054639393888602	ref. values	$1.289 \cdot 10^{-23}$	236

Table 7.4: Effect number of Bisection iterations N_{bis}, reference value $N_{bis} = 80$ ($D = 16, N_t = 2000, L = 6, dd = 10$).

Damage function
While solving the dike height problem, the proportional damage function $\hat{d}(t_{m-1}, t_m, x_1|N_t)$ is invoked $(M-1)D+1$ times. For the estimation of the time integral in equation (4.5), N_t integration steps are used. According to Table 7.5, the option values are decreasing in N_t, due to the convexity of the integrand $G(s) = \lambda e^{(s-t_{m-1})(\mu_3-\rho)}\beta(x_1 - w(s))$ for many parameter values. Then the expected flooding costs are overestimated for low N_t. This is confirmed by the value $\exp(X_0^{(3)})\hat{d}(0, 140, 425)$, which represents the expected flooding costs, at time $t = 0$, until time $t = 140$ for a constant dike level of 425 cm. We take 140 time N_t integration steps for the estimation. This value is also decreasing in N_t, see the third column in the table. The computational complexity is linear in N_t, but this is not clearly visible from the computation times since the computations of the proportional damage function do not take much time. We use $N_t = 500$ in the sequel of this section.

Control law
Figure 7.6 shows the optimal control law at different time levels. Note that the y-axis represents the economic value of endangered goods instead of its logarithmic value. The combination of a dike level and economic value prescribes the optimal dike increase level. This control law resembles the results in [32] and validates the dike-COS method by that.

Computational issues
The Matlab function to determine the construction domains took most time. In every Bisection iteration

N_t	$\hat{v}(t_0, X_0^{(1)}, X_0^{(3)})$	$\exp(X_0^{(3)})\hat{d}(0, 140, 425\|140.N_t)$	CPU time (s)
1	0.054643980565217	0.030464763124572	125
5	0.054639577366423	0.030459784657939	125
10	0.054639439756035	0.030459629074051	125
25	0.054639401227439	0.030459585512857	126
50	0.054639395721874	0.030459579288269	126
100	0.054639394345947	0.030459577732698	126
250	0.054639393960807	0.030459577297203	127
500	0.054639393905492	0.030459577234736	128
1000	0.054639393891919	0.030459577219379	129
2000	0.054639393888593	0.030459577215585	131

Table 7.5: Effect integration steps N_t ($D = 16, L = 6, dd = 10, N_{bis} = 30$).

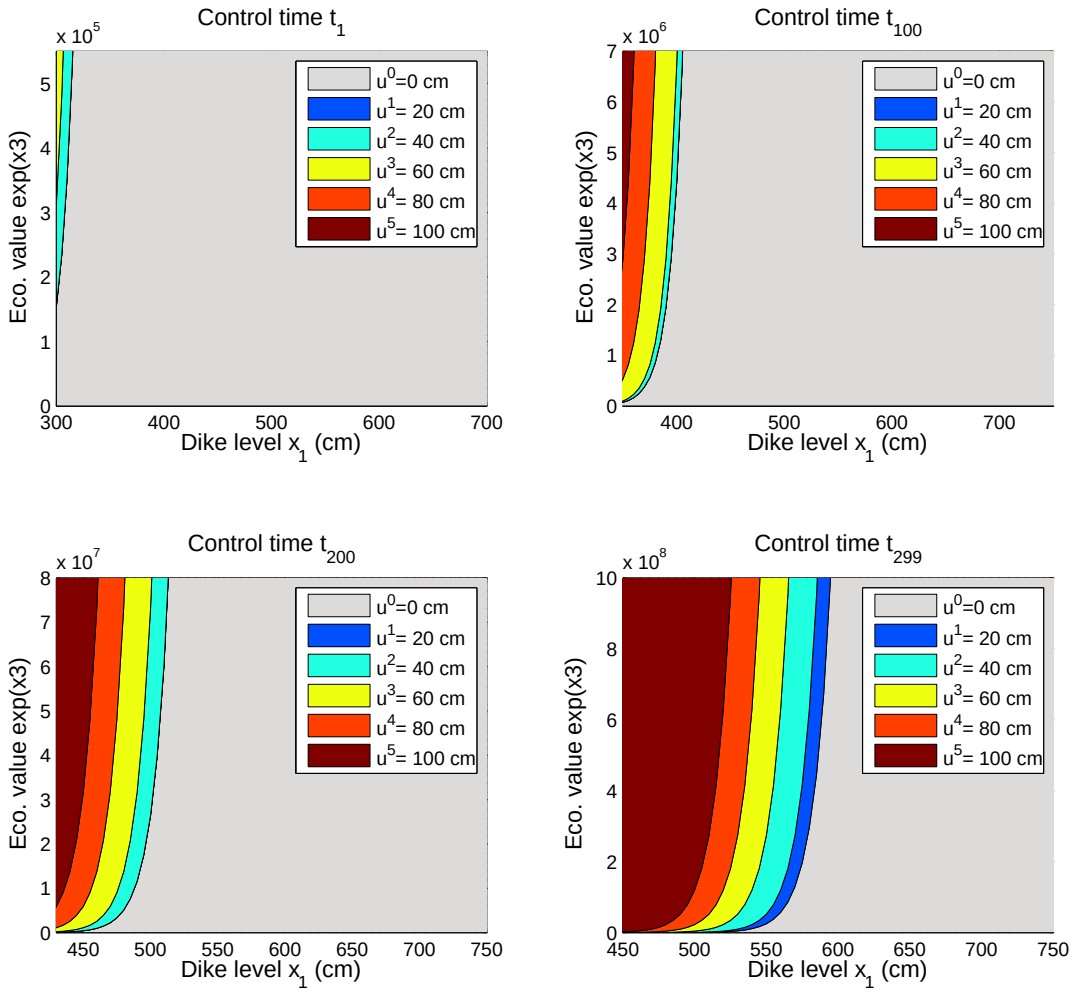

Figure 7.6: Dike height control law ($N_t = 500, N_{bis} = 30, dd = 10, L = 6$).

two option values $\hat{v}(t_m, x_1, y)$ need to be evaluated. Perhaps the algorithm can be speed up by implementation of a faster method to determine the construction domains. As we remarked before, Newton's method is faster, but less robust, compared to the Bisection method. Also a combination of these two methods, by which the Bisection method is used to determine a 'good' initial value for Newton's method, did not work satisfactorily, because it needed 'trial and error' to discover how accurate the initial value had to be. Moreover, calculation of the matrix-vector products $M\mathbf{w}$, although done efficiently by the FFT algorithm, takes a significant part of the computation time.

7.2.1 Variation of parameters

So far, we only varied the method parameters L, dd, N_{bis} and N_t. Next we study the variation in the model parameters. Firstly the time lattice parameters are changed. Then the effect of the process parameters, and finally the effect of the water level parameters, is studied. The following fixed parameters are used:

$$L = 6,\ dd = 10,\ N_{bis} = 30,\ N_t = 500. \tag{7.19}$$

The dike level grid size is changed during the parameter variation in order to satisfy Requirement 1. Since parameter variation investigates the effect on the real option values and not longer the convergence is studied, we round off the real option values to six decimal places. Also the construction times, which are the optimal dike reinforcement times corresponding to an economic value of endangered goods equal to its expected value, are calculated. The values between brackets after the construction times denote the corresponding optimal dike increase levels. When this is omitted, a heightening by amount 40 cm is optimal.

Number of control times $M - 1$
In practice not a fixed discrete time grid at which the dikes can be increased is prescribed. However, decreasing the number of control times makes the problem not very unrealistic as the true decision making process is not continuous. Since the computational complexity is linear in M, a lower value M will reduce the computation time significantly, as appears from Table 7.6. The real option values are decreasing in M, because an increasing number of control times gives more flexibility, which is profitable and lowers the expected costs in this model.

M	dt	Construction times	$\hat{v}(t_0, X_0^{(1)}, X_0^{(3)})$	CPU time (s)
300	1	146 185 232 293	0.054639	127
250	1.2	145.2 184.8 231.6 292.8	0.054653	106
200	1.5	145.5 184.5 231 292.5	0.054674	84
150	2	146 184 232 292	0.054712	63
100	3	144 186 231 291	0.054795	42
50	6	144 186 234 294	0.055101	21
30	10	150 180 230 290	0.055637	13
10	30	150 180 240 270	0.060753	4

Table 7.6: Effect number of control times M ($D = 16$).

Terminal time T
The dike height problem is modelled on a finite horizon. It is assumed that the dike and water level remain constant after the terminal time. In [22] these assumptions are justified because all arctic and mountain ice is predicted to melt in the foreseeable future and the sea level will stay constant once all ice has melted. A lowered terminal time does not effect the solution greatly, see Table 7.7, and we deduce that the terminal time $T = 300$ was chosen large enough so that the terminal condition has a negligible effect on the present value function. Then the discount factor is $e^{-\rho T} \approx 3.06 \cdot 10^{-7}$, which almost neglects the costs at the end of the time horizon.

T	Construction times	$\hat{v}(t_0, X_0^{(1)}, X_0^{(3)})$
300	146 185 232 293	0.054639
275	146 185 232	0.054638
250	146 185 232	0.054633
225	146 185	0.054570
200	146 185	0.054355

Table 7.7: Effect terminal time T, $\Delta t = 1$ $(M = T)$.

Different discount rates ρ
If the economic value follows its expected value it is optimal to increase the dikes in 146, 185, 232 and 293 years. This is in line with the dike reinforcement times in [32]. In that research a continuous set of possible dike increase levels was used and construction times 148, 190, 239 and 296 year were found with dike increase levels varying from 33.89 to 42.80 cm.

At first sight, performing the first dike reinforcement after 146 years seems very late. The construction costs of the first reinforcement are mln€47.40. However, the discount factor $e^{-\rho \cdot 146} \approx 6.76 \cdot 10^{-4}$ highly diminishes the discounted costs at the present and delays heightening. It is clear that discounting has a huge impact on the costs. Because of that we investigate the effect of the risk adjusted discount factor.

ρ	Construction times	$\hat{v}(t_0, X_0^{(1)}, X_0^{(3)})$
0.03	142(60) 199 250 299	0.991676
0.04	143 182 229 289	0.223078
0.05	146 185 232 293	0.054639
0.06	147 187 235 297	0.014958
0.08	150 191 239 298	0.001890
0.10	153 193 242 299	0.000597

Table 7.8: Effect risk adjusted discount factor ρ.

The risk adjusted discount factor has a significant influence on the expected flood protection costs and the construction times, see Table 7.8. The real option values are affected significantly if ρ is only changed from 0.05 to 0.04 or 0.06. A lower discount rate values the discounted future flooding costs higher and gives, although the discounted construction costs are higher, rise to earlier dike construction times. Contrary, a higher discount rate values the discounted future costs lower and delays the heightenings. Choosing the risk adjusted discount factor ρ is often difficult and not objective, which is a main drawback of using the dynamic programming approach when risks cannot be hedged.

μ_3	Construction times	$\hat{v}(t_0, X_0^{(1)}, X_0^{(3)})$
0.015	165 215 285	0.024604
0.020	154 197 253	0.037313
0.025	146 185 232 293	0.054639
0.030	138 174 215 266	0.077522
0.035	132 165 201 245 298	0.106959

Table 7.9: Effect expected economic growth rate μ_3.

Economic value of endangered goods
Next we change the expected economic growth rate μ_3 and economic volatility σ_3. The results are shown

in Table 7.9 and Table 7.10. Not surprisingly, the costs of flood protection are increasing in μ_3 and this advances the heightenings. The real option values are decreasing in σ_3, because less volatility reduces the change on a realisation with very high costs. This is apparently more significant than the reduced probability on a realisation with low costs. The expected economic value is independent of the economic volatility, therefore the volatility does not significantly affect the construction times.

σ_3	Construction times	$\hat{v}(t_0, X_0^{(1)}, X_0^{(3)})$
0.05	145 184 231 291	0.080049
0.10	145 185 231 292	0.069289
0.15	146 185 232 293	0.054639
0.20	146 186 233 294	0.039675
0.30	148 168 237 296	0.017664

Table 7.10: Effect economic volatility σ_3.

Worst-case scenario

The average water level process $w(t)$ we used in the previous tests, was based on the predicted increase of water level over all climate scenarios proposed by the KNMI ([23]). [22] states that the drift $\mu_w(t)$ in equation (7.4) is around 25% higher for all t in the worst-case scenario. This worst-case scenario water level is denoted by

$$w^{extr}(t) := \int_0^t 1.25\mu_w(s)ds = 1.25w(t). \tag{7.20}$$

We define a third scenario, with lower water level, by $w^{low}(t) := 0.75w(t)$. Figure 7.7 shows the three piecewise linear average water levels and Table 7.11 gives the construction times and real option values for the three different scenarios. The worst-case scenario rises flood protection costs by a factor 2.3.

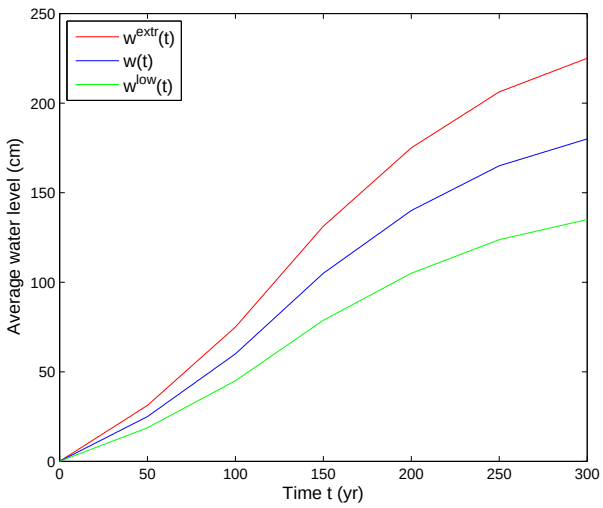

Figure 7.7: Deterministic average water level scenarios $w^{low}(t)$, $w(t)$ and $w^{extr}(t)$.

Extreme water level parameters

Scenario	Construction times	$\hat{v}(t_0, X_0^{(1)}, X_0^{(3)})$
$w^{low}(t)$	176 230 299	0.017674
$w(t)$	146 185 232 293	0.054639
$w^{extr}(t)$	128 157 192 233 287	0.130315

Table 7.11: Effect average water level $w(t)$.

The extreme water levels occurrences are modelled by four parameters:

$$\begin{array}{ll} \lambda, & \text{the intensity rate of the extreme water level process } q_t, \\ k_1, & \text{reciprocal of scale parameter of the Gumbel distribution for extreme water level sizes,} \\ k_2, & \text{location parameter of the Gumbel distribution for extreme water level sizes,} \\ \lambda_p, & \text{rate parameter in fraction lost function } l_p. \end{array} \tag{7.21}$$

We vary these parameters one after the other. Firstly, the intensity rate λ, in which the real option value is increasing according to the results in Table 7.12.

λ	Construction times	$\hat{v}(t_0, X_0^{(1)}, X_0^{(3)})$
0.5	153 194 243 299	0.036494
1	146 185 232 293	0.054639
1.5	141 180 226 285	0.069113
2	138 177 221 279	0.081640
3	134 172 215 271	0.103264

Table 7.12: Effect intensity rate λ.

Variables k_1 and k_2 are the parameters of the Gumbel distribution. The mean of the extreme water level sizes is $k_2 + \gamma_{EM}/k_1$, with $\gamma_{EM} \approx 0.58$ the Euler-Mascheroni constant. Not surprisingly, the flood protection costs are increasing in k_2, see Table 7.13. The variance of the extreme water level sizes, $(\pi/k_1)^2/6$, is decreasing in k_1, like the mean. Both cut down the costs of flood protection if k_1 is raised, see Table 7.14.

k_2	Construction times	$E[\mathcal{J}]$	$\hat{v}(t_0, X_0^{(1)}, X_0^{(3)})$
$1.68452 \cdot 10^2$	165 207 260	175.52	0.020966
$1.78452 \cdot 10^2$	155 195 244 299(20)	185.52	0.033955
$1.88452 \cdot 10^2$	146 185 232 293	195.52	0.054639
$1.98452 \cdot 10^2$	137 175 220 277	205.52	0.087676
$2.08452 \cdot 10^2$	129 165 207 260	215.52	0.140872

Table 7.13: Effect Gumbel distribution parameter k_2.

At last we consider the effect of rate parameter λ_p. The function l_p is chosen to match the geographical distribution of the economic goods on the island and the flow patterns of water on the island due to differences in altitude (see [22]). This is difficult and requires large amounts of data. The lives of the inhabitants of the island are modelled as part of the economic value. Since people's lives can nowadays often be rescued during a flood, l_p was chosen to approach one only slowly:

$$l_p(y) = \max(1 - e^{-\lambda_p y}, 0). \tag{7.22}$$

A larger rate parameter λ_p implies higher flood losses and a higher real option value (Table 7.15).

k_1	Construction times	$E[\mathcal{J}]$	$\mathrm{Var}(\mathcal{J})$	$\hat{v}(t_0, X_0^{(1)}, X_0^{(3)})$
$7.16299 \cdot 10^{-2}$	130 164 204 253 299	196.51	320.60	0.163881
$7.66299 \cdot 10^{-2}$	138 175 219 274	195.98	280.13	0.091717
$8.16299 \cdot 10^{-2}$	146 185 232 293	195.52	246.86	0.054639
$8.66299 \cdot 10^{-2}$	153 194 244 299	195.12	219.19	0.034222
$9.16299 \cdot 10^{-2}$	161 203 258	194.75	195.92	0.022285

Table 7.14: Effect Gumbel distribution parameter k_1.

λ_p	Construction times	$\hat{v}(t_0, X_0^{(1)}, X_0^{(3)})$
$0.6 \cdot 10^{-2}$	152 193 242 299	0.037935
$1.2 \cdot 10^{-2}$	146 185 232 293	0.054639
$2.4 \cdot 10^{-2}$	140 178 223 282	0.076134
$4.8 \cdot 10^{-2}$	135 172 216 272	0.101033
$9.6 \cdot 10^{-2}$	131 168 210 264	0.125851
$12.0 \cdot 10^{-2}$	130 166 209 262	0.133119

Table 7.15: Effect rate parameter λ_p.

Initial dike level
Finally, we investigate the effect of the initial dike level. Not surprisingly, Table 7.16 shows that that the construction times are advanced when the initial dike level is lower. The value function for an initial dike level of 575 cm matches to $\exp(X_0^{(3)})d(0, 300, 575) \approx 0.0000114$, which represents the expected flooding costs, at time $t = 0$, over the whole time horizon when the dike level remains equal to 575 cm.

$X_0^{(1)}$ (cm)	Construction times	$\hat{v}(t_0, X_0^{(1)}, X_0^{(3)})$
300	24 69 108 141 180 226 285	27.31634
325	54 94 129 165 207 260	7.988053
375	104 137 175 219 277	0.599131
425	146 285 232 293	0.054639
475	195 245	0.004717
525	260	0.000288
575	-	0.000011

Table 7.16: Effect initial dike level $X_0^{(1)}$.

7.3 Discussion

This discussion consists of two parts, the first part is about the validation of the dike-COS method and the second part about the contingent claims approach.

Validation
Tests of the dike-COS method are worked out one after the other. We started with a comparison between the approximated real options values and their exact solution at time t_{M-1}. After that we made some critical notes on the estimation of the construction domains. However, we suppose that the possible incorrect construction domains in the vicinity of the boundaries a and b do not significantly affect the real options values in the middle of the computational domain. The results in Tables 7.2, 7.4 and 7.5 show satisfactory convergence in the method parameters N, $[a, b]$, N_{bis} and N_t. Validation of the dike-COS method is mainly based on the control law in [32], on page 31, Figure 7. Our Figure 7.6 resembles these

results closely. Validation has also taken place for the COS formula for pricing call and put options.

The processes are modelled on a large time horizon, $T = 300$, but it is difficult to predict, for example, the water level rise after the next century. Besides, we may doubt whether the geometric Brownian motion used to model the economic value of endangered goods is realistic, especially on the long term. However, the real option value is not significantly affected by the characteristics of the processes in the distant future.

Hedging risk, contingent claims approach
As we discussed before it is better to use the contingent claims approach (CCA) than the dynamic programming principle approach (DPPA) if information about possible hedge instruments is available. The partial differential equation resulting from the CCA can be converted back to a value function. Then a risk-free interest rate is used for discounting and the expectation is taken under a risk-neutral measure, see, for example, Section 2.7.

In our example with the island no information about possible hedge instruments was available and a risk adjusted discount rate was used. Suppose that hedge instruments exist to hedge the risks of floods or the economic uncertainty and discounting is done with the risk-free interest rate. The risk-free rate is usually lower than the risk adjusted discount rate and the results in Table 7.8 show that this leads to a higher real option value. However, the drift of the stochastic process is reduced under the risk-neutral measure, which reduces the option value (Table 7.9). We wonder when the option values resulting from the dynamic programming approach and the contingent claims approach are similar. The same question can be asked for the real option values in the harvesting problem, Section 2.8.1 and Section 2.8.2. In [18] necessary and sufficient conditions for the DPPA price equal to the CCA price are derived. If there exist hedge instruments to hedge the risks of floods or the economic uncertainty, then probably a same analysis applies for the dike height problem. Then all costs of risk factors like societal risk should be carefully taken into account.

8 The dike-Q-COS method: A Fourier-cosine valuation method for two-factor Lévy processes

In this part the dike height model with **two** stochastic processes is considered. The economic value of endangered goods is stochastic. Furthermore, we use a stochastic average water level, instead of a deterministic one. The dike-COS method from Section 4 is extended to handle this problem. We start in Section 8.1 with the formulation of the model. Then we explain the COS convolution formula and the Quadrature-COS formula, in order to develop the dike-Q-COS method in Section 8.4. Tests of this recursive algorithm for an island are performed in Section 8.6.

8.1 Second model for the dike height problem

The future climate change and temperature rise, which depend mainly on the concentration green house gasses, are uncertain. Because of that there is a highly uncertain future water level, contrary to the model with deterministic water level $w(t)$ in Section 4. In an attempt to match this uncertainty, we proposed the following stochastic model for the average water level in Section 3.3.1

$$Y_t^{(2)} = w(t) + \sigma_w W_t^{(2)}, \tag{8.1}$$

where $\sigma_w \geq 0$ is the constant water level volatility. We define the *surplus water level process* by

$$X_t^{(2)} := \sigma_w W_t^{(2)} \sim \mathcal{N}(0, \sigma_w^2 t). \tag{8.2}$$

The deterministic function $w(t)$ is known and the process $X_t^{(2)}$ is a zero mean Brownian motion with variance $\sigma_w^2 t$. In Figure 8.1 simulated paths for $\sigma_w = 1$ are shown.

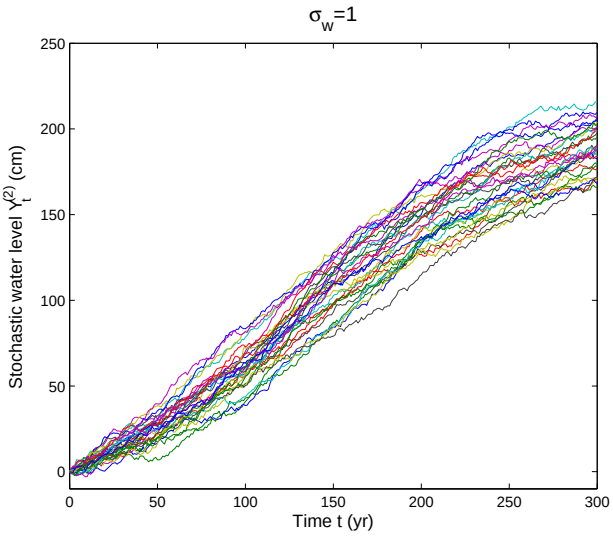

Figure 8.1: Simulated paths stochastic average water level $Y_t^{(2)} = w(t) + X_t^{(2)}$, $\sigma_w = 1$.

Let $X_t = [X_t^{(1)}, X_t^{(2)}, X_t^{(3)}]'$ denote the state process. The second model is summarised by:

$$\begin{aligned}
dX_t^{(1)} &= 0, && \text{for } t \in (t_m, t_{m+1}),\\
dX_t^{(2)} &= \sigma_w dW_t^{(2)}, && \text{for } t \in (t_m, t_{m+1}),\\
dX_t^{(3)} &= (\mu_3 - \tfrac{1}{2}\sigma_3^2)dt + \sigma_3 dW_t^{(3)}, && \text{for } t \in (t_m, t_{m+1}),\\
X_{t_m} &= X_{t_m^-} + [u_m, 0, 0]', && m \in \mathbb{N}.
\end{aligned} \tag{8.3}$$

Remark 8.1. *Under this model the water level may become negative. This is not a problem since the initial water level $Y_0^{(2)} = w(0)$ is just a reference value, whereas, in the financial world, models for asset prices do often not allow negative values.*

Again at any time t one has to decide whether to increase the dike height, and if so by which amount, or to do nothing and wait until the next time. Let $v(t,x) = v(t,x_1,x_2,x_3)$ denote the expected costs of flood protection at time t, with dike level x_1, surplus water level x_2 and log-economic value of endangered goods x_3, under optimal heightenings. This value function is represented by:

$$\begin{aligned} v(t,x_1,x_2,x_3) &= \inf_{\mathbf{u}\in\mathcal{U}} E^{t,x}\Bigg[\sum_{\tau_i\in[t,T]} e^{-\rho(\tau_i-t)}\exp(X^{(3)}_{\tau_i}) l_p(w(\tau_i)+X^{(2)}_{\tau_i}+\mathcal{J}_{\tau_i}-X^{(1)}_{\tau_i}) \\ &\quad + \sum_{t\le t_m<T} e^{-\rho(t_m-t)} b(X^{(1)}_{t_m^-},u_m) + e^{-\rho(T-t)} b_T(X^{(1)}_T,X^{(2)}_T,X^{(3)}_T)\Bigg], \\ &\quad (t,x)=(t,x_1,x_2,x_3)\in[0,T]\times\mathbb{R}^3, \end{aligned} \tag{8.4}$$

where τ_i denote the times at which an extreme water level occurs. After terminal time T the dike height and surplus water level are assumed to remain constant and the terminal costs are given by the expected flooding costs hereafter:

$$\begin{aligned} v(T,x_1,x_2,x_3) &= b_T(x_1,x_2,x_3) \\ &:= E^{T,x}\Bigg[\sum_{\tau_i\in[T,\infty)} e^{-\rho(\tau_i-T)}\exp(X^{(3)}_{\tau_i}) l_p(w(T)+x_2+\mathcal{J}_{\tau_i}-x_1)\Bigg] \\ &= \frac{\lambda\beta(x_1-w(T)-x_2)}{\rho-\mu_3}\exp(x_3). \end{aligned} \tag{8.5}$$

The associated HJB-QVI reads

$$\begin{aligned} \max\Big[&-v_t(t,x)+\rho v(t,x)-\mathcal{L}v(t,x)-\lambda\exp(x_3)\beta(x_1-x_2), \\ &v(t,x)-\inf_{u\in U}[v(t,x+(u,0,0))+b(x_1,u)]\Big]=0, \qquad (t,x)=(t,x_1,x_2,x_3)\in[0,T)\times\mathbb{R}^3, \end{aligned} \tag{8.6}$$

with

$$\mathcal{L}v(t,x) = (\mu_3-\frac{1}{2}\sigma_3^2)\frac{\partial v}{\partial x_3}(t,x)+\frac{1}{2}\sigma_w^2\frac{\partial^2 v}{\partial x_2^2}(t,x)+\frac{1}{2}\sigma_3^2\frac{\partial^2 v}{\partial x_3^2}(t,x). \tag{8.7}$$

For the extended dike-COS method we use the same discrete time grid as before, $t_0,\ldots,t_m,\ldots,t_M$, and the same finite set of dike increase levels $U=\{u^0,\ldots,u^K\}$. The dynamic programming principle gives, for $m=M,\ldots,1$

$$\begin{aligned} v(t_{m-1},x_1,x_2,x_3) &= E^{t_{m-1},x}\Bigg[\sum_{\tau_i\in[t_{m-1},t_m]} e^{-\rho(\tau_i-t_{m-1})}\exp(X^{(3)}_{\tau_i}) l_p\Big(w(\tau_i)+X^{(2)}_{\tau_i}+\mathcal{J}_{\tau_i}-x_1\Big)\Bigg] \\ &+ E^{t_{m-1},x}\Big[e^{-\rho\Delta t} v(t_m^-,x_1,X^{(2)}_{t_m},X^{(3)}_{t_m})\Big]. \end{aligned} \tag{8.8}$$

The first part, the running costs from flooding, is discussed in Section 8.2 and the continuation part comes up in Section 8.3. At the control times it holds that:

$$\begin{aligned} v(t_m^-,x_1,x_2,y) &= \mathcal{M}v(t_m,x_1,x_2,y) \\ &= \min_{u^i\in U}\left[v(t_m,x_1+u^i,x_2,y)+b(x_1,u^i)\right], \qquad (m\neq 0,M). \end{aligned} \tag{8.9}$$

8.2 COS convolution formula for the expected flood losses

In this section we use the convolution of density functions to develop the COS convolution for estimation of the flood losses during the time interval $[t_{m-1}, t_m]$. They depend on the total water level,

$$w(s) + X_s^{(2)} + \mathcal{J}_s dq_s, \tag{8.10}$$

and the expected discounted flood losses read:

$$\begin{aligned}
&E^{t_{m-1},x}\left[\sum_{\tau_i\in[t_{m-1},t_m]} e^{-\rho(\tau_i-t_{m-1})}\exp(X_{\tau_i}^{(3)})l_p\left(w(\tau_i)+X_{\tau_i}^{(2)}+\mathcal{J}_{\tau_i}-x_1\right)\right]\\
&\quad= \int_{t_{m-1}}^{t_m}\lambda e^{-\rho(s-t_{m-1})}E^{t_{m-1},x}[\exp(X_s^{(3)})l_p\left(w(s)+X_s^{(2)}+\mathcal{J}-x_1\right)]ds\\
&\quad= \int_{t_{m-1}}^{t_m}\lambda e^{-\rho(s-t_{m-1})}E^{t_{m-1},x}[\exp(X_s^{(3)})]E^{t_{m-1},x}[l_p(w(s)+X_s^{(2)}+\mathcal{J}-x_1)]ds\\
&\quad= \exp(x_3)\int_{t_{m-1}}^{t_m}\lambda e^{(s-t_{m-1})(\mu_3-\rho)}E^{t_{m-1},x}[l_p(w(s)+X_s^{(2)}+\mathcal{J}-x_1)]ds\\
&\quad:= \exp(x_3)d(t_{m-1},t_m,x_1,x_2).
\end{aligned}\tag{8.11}$$

First we approximate the time integral in the *proportional damage function* d by an integration rule. Then the expectation is approximated by a COS formula for the sum $X_s^{(2)}+\mathcal{J}$.

The time integral is approximated by applying the equidistant Composite Trapezoidal rule, with N_t integration steps:

$$d_1(t_{m-1},t_m,x_1,x_2) = \sum_{p=0}^{N_t} y_p H(t_{m-1},x_1,x_2,\vartheta_p), \tag{8.12}$$

where

$$H(t_{m-1},x_1,x_2,\vartheta_p) := \lambda e^{(\vartheta_p-t_{m-1})(\mu_3-\rho)}E^{t_{m-1},x}[l_p(w(\vartheta_p)+X_{\vartheta_p}^{(2)}+\mathcal{J}-x_1)], \tag{8.13}$$

and y_p denote the weights of the quadrature node $\vartheta_p\in[t_{m-1},t_m]$ with $p=0,1,2,\ldots,N_t$. We remark that the function H does not represent the Hamiltonian in this section. Note that the expectation can be represented by a double integral since there are two random variables, $X_s^{(2)}$ and $\mathcal{J}$. However, the convolution of both density functions enables us to reduce it to a single integral:

$$\begin{aligned}
H(t_{m-1},x_1,x_2,\vartheta_p) &= \lambda e^{(\vartheta_p-t_{m-1})(\mu_3-\rho)}E^{t_{m-1},x}[l_p(w(\vartheta_p)+X_{\vartheta_p}^{(2)}+\mathcal{J}-x_1)]\\
&= \lambda e^{(\vartheta_p-t_{m-1})(\mu_3-\rho)}\int_{\mathbb{R}}\int_{\mathbb{R}} l_p(w(\vartheta_p)+x+y-x_1)f_{X_{\vartheta_p}^{(2)}|X_{t_{m-1}}^{(2)}}(x|x_2)dx f_{\mathcal{J}}(y)dy\\
&= \lambda e^{(\vartheta_p-t_{m-1})(\mu_3-\rho)}\int_{\mathbb{R}} l_p(w(\vartheta_p)+z-x_1)\int_{\mathbb{R}} f_{X_{\vartheta_p}^{(2)}|X_{t_{m-1}}^{(2)}}(z-y|x_2)f_{\mathcal{J}}(y)dydz\\
&= \lambda e^{(\vartheta_p-t_{m-1})(\mu_3-\rho)}\int_{\mathbb{R}} l_p(w(\vartheta_p)+z-x_1)f_{Z_{\vartheta_p}|X_{t_{m-1}}^{(2)}}(z|x_2)dz,
\end{aligned}\tag{8.14}$$

where the function $f_{Z_s|X_{t_{m-1}}^{(2)}}(z|x_2)$ is the convolution of $f_{X_s^{(2)}|X_{t_{m-1}}^{(2)}}$ and $f_{\mathcal{J}}$:

$$f_{Z_s|X_{t_{m-1}}^{(2)}}(z|x_2) := \int_{\mathbb{R}} f_{X_s^{(2)}|X_{t_{m-1}}^{(2)}}(z-y|x_2)f_{\mathcal{J}}(y)dy. \tag{8.15}$$

Since the process $X_s^{(2)}$ and the extreme water level size $\mathcal{J}$ are independent, the characteristic function of $Z_s = X_s^{(2)}+\mathcal{J}$ is the product of both individual characteristic functions:

$$\begin{aligned}
\varphi_{Z_s|X_{t_{m-1}}^{(2)}}(u|x_2) &= \varphi_{X_s^{(2)}|X_{t_{m-1}}^{(2)}}(u|x_2)\varphi_{\mathcal{J}}(u)\\
&= e^{iux_2}\varphi_{X_s^{(2)}-X_{t_{m-1}}^{(2)}}(u)\varphi_{\mathcal{J}}(u).
\end{aligned}\tag{8.16}$$

In the next step the expectation in the function H is approximated by a COS formula. The COS method, for an integration domain $[a_Z, b_Z] \subset \mathbb{R}$, N_Z terms in the series expansion, and the above relation give the following formula:

$$\begin{aligned}
&\hat{H}(t_{m-1}, x_1, x_2, \vartheta_p) \\
&:= \lambda e^{(\vartheta_p - t_{m-1})(\mu_3 - \rho)} \sum_{k=0}^{N_Z - 1}{}' \Re\left[\varphi_{Z_{\vartheta_p}|X^{(2)}_{t_{m-1}}}\left(\frac{k\pi}{b_Z - a_Z}|x_2\right) e^{-ik\pi \frac{a_Z}{b_Z - a_Z}}\right] \mathcal{V}_k(x_1 - w(\vartheta_p)) \\
&= \lambda e^{(\vartheta_p - t_{m-1})(\mu_3 - \rho)} \sum_{k=0}^{N_Z - 1}{}' \Re\left[\varphi_{X^{(2)}_{\vartheta_p} - X^{(2)}_{t_{m-1}}}\left(\frac{k\pi}{b_Z - a_Z}\right) \varphi_{\mathcal{J}}\left(\frac{k\pi}{b_Z - a_Z}\right) e^{ik\pi \frac{x_2 - a_Z}{b_Z - a_Z}}\right] \mathcal{V}_k(x_1 - w(\vartheta_p)),
\end{aligned} \tag{8.17}$$

with (for $a_Z \le x \le b_Z$)

$$\begin{aligned}
\mathcal{V}_k(x) &= \frac{2}{b_Z - a_Z} \int_{a_Z}^{b_Z} l_p(z - x) \cos\left(k\pi \frac{z - a_Z}{b_Z - a_Z}\right) dz \qquad (k \neq 0) \\
&= \frac{2}{b_Z - a_Z} \int_{a_Z}^{b_Z} \max(1 - e^{-\lambda_p(z-x)}, 0) \cos\left(k\pi \frac{z - a_Z}{b_Z - a_Z}\right) dz \\
&= \frac{2}{b_Z - a_Z} \int_{x}^{b_Z} (1 - e^{-\lambda_p(z-x)}) \cos\left(k\pi \frac{z - a_Z}{b_Z - a_Z}\right) dz \\
&= \frac{2}{b_Z - a_Z} \int_{x}^{b_Z} \cos\left(k\pi \frac{z - a_Z}{b_Z - a_Z}\right) dz - e^{\lambda_p x} \frac{2}{b_Z - a_Z} \int_{x}^{b_Z} e^{-\lambda_p z} \cos\left(k\pi \frac{z - a_Z}{b_Z - a_Z}\right) dz \\
&= \frac{2}{k\pi}\left(\sin(k\pi) - \sin\left(k\pi \frac{x - a_Z}{b_Z - a_Z}\right)\right) + \frac{2e^{-\lambda_p(b_Z - x)}}{(k\pi)^2 + \lambda_p^2 (b_Z - a_Z)^2} \cdot \Big[(a_Z - b_Z)\lambda_p e^{\lambda_p(b_Z - x)} \\
&\quad \cdot \cos\left(k\pi \frac{x - a_Z}{b_Z - a_Z}\right) + \lambda_p (b_Z - a_Z)\cos(k\pi) + k\pi e^{\lambda_p(b_Z - x)} \sin\left(k\pi \frac{x - a_Z}{b_Z - a_Z}\right) - k\pi \sin(k\pi)\Big], \\
\mathcal{V}_0(x) &= 2\frac{b_Z - x}{b_Z - a_Z} - 2\frac{1 - e^{-\lambda_p(b_Z - x)}}{\lambda_p (b_Z - a_Z)}.
\end{aligned} \tag{8.18}$$

We name this the *COS convolution formula*. Other density functions than the Gumbel distribution can easily be incorporated as long as the characteristic function is known. A COS formula can also be derived to estimate the function $\beta(h)$ for the model with deterministic water level (Section 4.3) if the density function of $\mathcal{J}$ is unknown whereas the characteristic function is known.

We end up with

$$\begin{aligned}
&\hat{d}(t_{m-1}, t_m, x) := \sum_{p=0}^{N_t} y_p \hat{H}(t_{m-1}, x_1, x_2, \vartheta_p) \\
&= \lambda e^{(\vartheta_p - t_{m-1})(\mu_3 - \rho)} \sum_{p=0}^{N_t} y_p \sum_{k=0}^{N_Z - 1}{}' \Re\left[\varphi_{X^{(2)}_{\vartheta_p} - X^{(2)}_{t_{m-1}}}\left(\frac{k\pi}{b_Z - a_Z}\right) \varphi_{\mathcal{J}}\left(\frac{k\pi}{b_Z - a_Z}\right) e^{ik\pi \frac{x_2 - a_Z}{b_Z - a_Z}}\right] \mathcal{V}_k(x_1 - w(\vartheta_p)).
\end{aligned} \tag{8.19}$$

Remark 8.2. *We can rewrite the function H as*

$$\begin{aligned}
H(t_{m-1}, x_1, x_2, \vartheta_p) &= \lambda e^{(\vartheta_p - t_{m-1})(\mu_3 - \rho)} E^{t_{m-1}, x_1, x_2}[\beta(x_1 - w(\vartheta_p) - X^{(2)}_{\vartheta_p})] \\
&= \lambda e^{(\vartheta_p - t_{m-1})(\mu_3 - \rho)} \int_{\mathbb{R}} \beta(x_1 - w(\vartheta_p) - x) f_{X^{(2)}_{\vartheta_p}|X^{(2)}_{t_{m-1}}}(x|x_2) dx.
\end{aligned} \tag{8.20}$$

This is a one-dimensional integral. One might wonder why we do not apply the COS method to this

expectation. However, no analytical solution for the corresponding Fourier-cosine coefficients,

$$\int_{z_1}^{z_2} \beta(x_1 - w(\theta_p) - x) \cos\left(k\pi \frac{x - z_1}{z_2 - z_1}\right) dx, \tag{8.21}$$

was found.

8.3 Quadrature-COS formula for the continuation value

In [12] a method for pricing Bermudan and discretely monitored barrier options under the Heston stochastic volatility model has been developed. Under this two-dimensional model the variance of the logarithm of the stock price is modelled by a square-root process. The method is a combination of a Fourier-cosine series expansion and a high-order quadrature rule in the other dimension. We follow a similar way to estimate the two-factor expectation in the continuation part of the real option value in equation (8.8).

We consider the *continuation value*

$$\begin{aligned} c(t_{m-1}, x_1, x_2, x_3) &:= E^{t_{m-1},x}\left[e^{-\rho\Delta t} v(t_m^-, x_1, X_{t_m}^{(2)}, X_{t_m}^{(3)})\right] \\ &= e^{-\rho\Delta t} \int_{\mathbb{R}^2} v(t_m^-, x_1, y_2, y_3) f(\mathbf{y}|\mathbf{x}) d\mathbf{y}. \end{aligned} \tag{8.22}$$

The processes $X_t^{(2)}$ and $X_t^{(3)}$ are independent, so the conditional density function is $f(\mathbf{y}|\mathbf{x}) = f_2(y_2|x_2) f_3(y_3|x_3)$, where f_2 and f_3 are the density functions of the surplus water level process and the log-economic value, respectively. Truncation of the outer-integral yields

$$\begin{aligned} c_1(t_{m-1}, x_1, x_2, x_3) &= e^{-\rho\Delta t} \int_{a_2}^{b_2} \int_{\mathbb{R}} v(t_m^-, x_1, y_2, y_3) f_3(y_3|x_3) dy_3 f_2(y_2|x_2) dy_2 \\ &= \int_{a_2}^{b_2} G(t_m^-, x_1, y_2, x_3) f_2(y_2|x_2) dy_2, \end{aligned} \tag{8.23}$$

with

$$G(t_m^-, x_1, y_2, x_3) := e^{-\rho\Delta t} \int_{\mathbb{R}} v(t_m^-, x_1, y_2, y_3) f_3(y_3|x_3) dy_3. \tag{8.24}$$

The outer-integral is approximated by applying a J-point equidistant Composite Trapezoidal rule:

$$c_2(t_{m-1}, x_1, x_2, x_3) = \sum_{q=0}^{J-1} w_q f_2(\theta_q|x_2) G(t_m^-, x_1, \theta_q, x_3), \tag{8.25}$$

where w_q denote the weights of the quadrature node θ_q with $q = 0, 1, 2, \ldots, J-1$.. In the last step the conditional expectation that is represented by function G is replaced by a COS formula, resulting in

$$\hat{c}(t_{m-1}, x_1, x_2, x_3) = e^{-\rho\Delta t} \sum_{q=0}^{J-1} w_q f_2(\theta_q|x_2) {\sum_{k=0}^{N-1}}' \Re\left[\varphi_{3levy}\left(\frac{k\pi}{b-a}\right) e^{ik\pi\frac{x_3-a}{b-a}}\right] V_{kq}(t_m^-, x_1), \tag{8.26}$$

with

$$V_{kq}(t_m^-, x_1) = \frac{2}{b-a} \int_a^b v(t_m^-, x_1, \theta_q, y_3) \cos\left(k\pi \frac{y_3 - a}{b-a}\right) dy_3 \tag{8.27}$$

and $\varphi_{3levy}(u) = \varphi_3(u|0)$ the characteristic function of the log-economic process. Finally, we interchange the summations:

$$\begin{aligned} \hat{c}(t_{m-1}, x_1, x_2, x_3) &= e^{-\rho\Delta t} \Re\left[{\sum_{k=0}^{N-1}}' \sum_{q=0}^{J-1} w_q f_2(\theta_q|x_2) \varphi_{3levy}\left(\frac{k\pi}{b-a}\right) V_{kq}(t_m^-, x_1) e^{ik\pi\frac{x_3-a}{b-a}}\right] \\ &= e^{-\rho\Delta t} \Re\left[{\sum_{k=0}^{N-1}}' Q_k(t_{m-1}, x_2, x_1) e^{ik\pi\frac{x_3-a}{b-a}}\right], \end{aligned} \tag{8.28}$$

where

$$Q_k(t_{m-1}, x_2, x_1) := \sum_{q=0}^{J-1} w_q f_2(\theta_q|x_2)\varphi_{3levy}\left(\frac{k\pi}{b-a}\right) V_{kq}(t_m^-, x_1). \tag{8.29}$$

We call this equation the *Q(uadrature)-COS formula*. Let Φ denote the $J \times J \times N$ matrix with entries $\left[w_q f_2(\theta_q|x_2)\varphi_{3levy}\left(\frac{k\pi}{b-a}\right)\right]_{k,q,p}$. This matrix is time-independent.

Addition of the expected flood losses and the continuation value yields

$$\hat{v}(t_{m-1}, x_1, x_2, x_3) := \exp(x_3)\hat{d}(t_{m-1}, t_m, x_1, x_2) + e^{-\rho\Delta t}\Re\left[\sum_{k=0}^{N-1}{}' Q_k(t_{m-1}, x_2, x_1)e^{ik\pi\frac{x_3-a}{b-a}}\right]. \tag{8.30}$$

Remark 8.3. *The average water level process $Y_t^{(2)}$ (equation (8.1)) can cover a wider range than the surplus water level process $X_t^{(2)}$ (equation (8.2)), see Figure 8.1. Using the surplus water level instead allows to narrow the truncation of the outer integral in (8.23) more and therefore less integration points are required. This is the reason why we use the surplus water level. Other processes for the water level can easily be used, as long as the density function is known. In order to have a time-independent matrix Φ, a stationary process is preferred. If the density function is unknown, whereas the characteristic function is known, then the COS density recovery can be used to estimate the density function.*

8.4 Recursion formula for coefficients V_{kq}

Similar to the backward recursion of the coefficients in Section 4.2, we can find a recursive algorithm for the terms $V_{kq}(t_m^-, x_1)$.

Coefficients at time t_M^-
The coefficients $V_{kq}(t_M^-, y_1)$ have an analytical representation:

$$\begin{aligned} V_{kq}(t_M^-, x_1) &= \frac{2}{b-a}\int_a^b v(T, x_1, \theta_q, y)\cos\left(k\pi\frac{y-a}{b-a}\right)dy \\ &= \frac{2}{b-a}\int_a^b \frac{\lambda\beta(x_1 - w(T) - \theta_q)}{\rho - \mu_3}\exp(y)\cos\left(k\pi\frac{y-a}{b-a}\right)dy \\ &= \frac{\lambda\beta(x_1 - w(T) - \theta_q)}{\rho - \mu_3}\frac{2}{b-a}\chi_k(a,b). \end{aligned} \tag{8.31}$$

Coefficients at time t_m^-, $1 \le m \le M-1$
Assume that we can find the so-called *construction domains* $A_m^i(x_1, \theta_q) \subset [a,b]$, which represent the intervals with log-economic values for which it is optimal to perform a heightening by amount u^i at time t_m, for dike level x_1, if the surplus water level has value θ_q. We can split the integral into parts, independent of k, but in dependence of q:

$$\begin{aligned} V_{kq}(t_m^-, x_1) &= \frac{2}{b-a}\int_a^b v(t_m^-, x_1, \theta_q, y_3)\cos\left(k\pi\frac{y_3-a}{b-a}\right)dy_3 \\ &= \frac{2}{b-a}\int_a^b \min_{u^i\in U}\left[v(t_m, x_1+u^i, \theta_q, y_3) + b(x_1, u^i)\right]\cos\left(k\pi\frac{y_3-a}{b-a}\right)dy_3 \\ &= \sum_{i=0}^{K}\frac{2}{b-a}\int_{A_m^i(x_1,\theta_q)} v(t_m, x_1+u^i, \theta_q, y_3)\cos\left(k\pi\frac{y_3-a}{b-a}\right)dy_3 \\ &+ \sum_{i=1}^{K}\frac{2}{b-a}\int_{A_m^i(x_1,\theta_q)} b(x_1, u^i)\cos\left(k\pi\frac{y_3-a}{b-a}\right)dy_3 \\ &:= \sum_{i=0}^{K} C_{kq}(A_m^i(x_1,\theta_q), t_m, x_1) + \sum_{i=1}^{K} B_k(A_m^i(x_1,\theta_q), x_1, u^i) \qquad (m \neq 0, M). \end{aligned} \tag{8.32}$$

The approximation of the first parts reads

$$\begin{aligned}
&\hat{C}_{kq}(z_1, z_2, t_m, y_1) \\
&\quad = \frac{2}{b-a}\int_{z_1}^{z_2} \hat{v}(t_m, y_1, \theta_q, y_3)\cos\left(k\pi\frac{y_3-a}{b-a}\right)dy_3 \\
&\quad = \frac{2}{b-a}\int_{z_1}^{z_2} \exp(y_3)\hat{d}(t_m, t_{m+1}, y_1, \theta_q)\cos\left(k\pi\frac{y_3-a}{b-a}\right)dy_3 \\
&\quad + \frac{2}{b-a}\int_{z_1}^{z_2} e^{-\rho\Delta t}\Re\left[\sum_{j=0}^{N-1}{}' \hat{Q}_j(t_m, \theta_q, x_1)e^{ij\pi\frac{x_3-a}{b-a}}\right]\cos\left(k\pi\frac{y_3-a}{b-a}\right)dy_3 \\
&\quad = \frac{2}{b-a}\hat{d}(t_m, t_{m+1}, y_1, \theta_q)\chi_k(z_1, z_2) + e^{-\rho\Delta t}\Re\left[\sum_{j=0}^{N-1}{}' M_{k,j}(z_1, z_2)\hat{Q}_j(t_m, \theta_q, y_1)\right]. \qquad (8.33)
\end{aligned}$$

The terms B_k are known analytically, see equation (4.22). We end up with a matrix-vector product representation:

$$\begin{aligned}
\hat{V}_q(t_m^-, x_1) &= \sum_{i=0}^{L}\frac{2}{b-a}\hat{d}(t_m, t_{m+1}, x_1+u^i, \theta_q)\chi(A_m^i(x_1, \theta_q)) + \sum_{i=0}^{L} e^{-\rho\Delta t}\Re\{M(A_m^i(x_1, \theta_q))\hat{\mathbf{w}}^{\mathbf{i}}\} \\
&+ \sum_{i=1}^{L}\frac{2}{b-a}b(x_1, u^i)\psi(A_m^i(x_1, \theta_q)), \qquad (m = 1, \ldots, M-2), \qquad (8.34)
\end{aligned}$$

with

$$\hat{\mathbf{w}}^{\mathbf{i}} := \{\hat{w}_j^i\}_{j=0}^{N-1} \quad \text{with} \quad \hat{w}_j^i := \hat{Q}_j(t_m, x_1+u^i, \theta_q), \;\; \hat{w}_0^i = \frac{1}{2}\hat{Q}_0(t_m, x_1+u^i, \theta_q). \qquad (8.35)$$

At time t_{M-1}^- we use the exact vector:

$$\mathbf{w}^{\mathbf{i}} := \{w_j^i\}_{j=0}^{N-1} \quad \text{with} \quad w_j^i := Q_j(t_{M-1}, x_1+u^i, \theta_q), \;\; w_0^i = \frac{1}{2}Q_0(t_{M-1}, x_1+u^i, \theta_q). \qquad (8.36)$$

Algorithm
The algorithm the solve the dike height problem under the model with a stochastic water level now reads

Algorithm 2. *(Dike-Q-COS method)*

Initialisation:

- *Calculate coefficients $V_{kq}(t_M^-, x_1)$ for $k = 0, 1, \ldots, N-1$, $q = 0, 1, \ldots, J-1$ and all possible dike levels x_1.*
- *Prepare the matrix Φ.*

Main loop to recover $\hat{V}(t_m^-, x_1)$:
For $m = M-1$ to 1:

- *Determine the construction domains $A_m^i(x_1, \theta_q)$.*
- *Compute $\hat{V}_q(t_m^-, x_1)$ for all possible dike levels and $q = 0, 1, \ldots, J-1$ (with the help of the FFT algorithm).*
- *Compute $\hat{Q}(t_{m-1}, x_1, \theta_q)$ for all possible dike levels and $q = 0, 1, \ldots, J-1$.*

Final step:
Compute $\hat{v}(t_0, x_1, x_2, x_3)$ by inserting $\hat{V}_{kq}(t_1^-, x_1)$ into equation (8.30).

Construction domains
In [12] Newton's method is used to find the early-exercise points for pricing Bermudan options. This algorithm is applied for all θ_q simultaneously. However, here the construction domains $A_m^i(x_1, \theta_q)$ are determined for each θ_q *separately*, using the Bisection method and by the same algorithm as in Section 4.2.1. We did not discover a way to speed up the determination of the construction domains. Parallel computing may be used to perform the calculations for all θ_q simultaneously.

Computational complexity
Two extra complexity dimensions are added to the overview in (4.30):

$$\begin{array}{ll} J, & \text{number of integration points } \theta_q, \\ N_Z, & \text{the number of coefficients in the series expansion in equation (8.17).} \end{array} \tag{8.37}$$

Calculation of the first coefficients $V_{kq}(t_M^-, x_1)$ is of order $O(NJD)$. However, the computational effort in the initialisation step is dominated in J by preparation of the matrix Φ, which takes $O(NJ^2)$ operations. Determination of the construction domains and calculation of the new coefficients $\hat{V}(t_m^-, x_1)$ are both linear in J. Computation of the new terms $\hat{Q}$ has order $O(NJ^2D)$ complexity. The computational complexity of the proportional damage function is linear in N_Z. The complexity of the main loop is therefore

$$O\Big((M-1)\left[DKJ(N_{bis} + N_t N_Z + N\log_2 N) + NJ^2D\right]\Big). \tag{8.38}$$

The computational complexity of the final step has order $O(N_t N_Z + N)$.

Authors contribution
The dike-Q-COS method is mainly based on the COS method for pricing financial options under the two-dimensional Heston model ([12]) and the dike-COS method. As we discussed before we need to keep track of the dike level and a kind of cashflow from flooding costs is added, which expands the algorithm. We used the convolution of density functions to develop the COS convolution for estimation of the two-dimensional expectation in the proportional damage function d. We noticed that is useful to consider the so-called surplus water level in order to narrow the range of the process that is used to model the stochastic average water level.

8.4.1 Extensions to alternative models

In Section 3.3 we proposed some extensions of the first dike height model. A model with stochastic average water level has been employed before. Here we discuss how the dike-Q-COS method may be adapted to apply it to the models with recovery rate and soil compression and deterioration rate.

In general, these extensions add an extra space-dimension to the value function. The calculation of the expected flood losses and the continuation value gets more involved by that. The expectations with respect to the additional random variable can be estimated by using a quadrature rule, as we did in Section 8.3. However, this will significantly increase the computational complexity.

Soil compression and deterioration rate
In Section 3.3.3 we discussed the model with a soil compression and deterioration rate. The process ς_t was assigned to recall the time of the last heightening. By this an extra space dimension was added to the value function. A rate of soil compression and deterioration was added by function γ. If this function is deterministic, depending on ς_t, then the dike level process between the control times is known and the expectations do not depend on this variable. Probably much more dike level grid points are required in order to work with compressed levels, which increases the computation time significantly. Besides, the calculation of the proportional damage function is more involved when the dike level changes.

Recovery rate
A model including a recovery rate for the flood losses was proposed in Section 3.3.4. The flood losses that are not yet recovered are remembered by the additional process $X_t^{(4)}$, which adds an extra space dimension to the problem. The jumps in the processes $X_t^{(3)}$ and $X_t^{(4)}$ are time-dependent, so they do not satisfy the requirements of a Lévy process as they do not have stationary increments. The processes can be approximated by Lévy processes on the time interval $[t_m, t_{m+1}]$ by considering a time-independent recovery rate and a constant average water level during that period. The most difficult part by adapting the dike-Q-COS method to this problem is finding the appropriate characteristic functions and density functions. Maybe a PDE method to solving the associated Hamilton-Jacobi-Bellman equation will be easier to apply in this case.

8.5 Error Analysis

In this section we analyse the error of the dike-Q-COS method. There are similarities to the error analysis of the dike-COS method with deterministic water level (Section 5). We focus on the additional elements.

8.5.1 Local error dike-Q-COS method

We start with analysing the local error of the Composite Trapezoidal integration rule plus the COS convolution formula and the error in the derivation of the Quadrature-COS formula.

The error introduced by approximation of the proportional damage function with the Composite Trapezoidal rule, with N_t integration steps, is denoted by

$$\epsilon_{d1}(t_{m-1}, t_m, x_1, x_2|N_t) := d(t_{m-1}, t_m, x_1, x_2) - d_1(t_{m-1}, t_m, x_1, x_2|N_t). \tag{8.39}$$

The function H is approximated by the COS convolution formula and we define

$$\epsilon_{COSconv}(N_Z, [a_Z, b_Z]) := \sup_{m,x_1,x_2,\vartheta_p} |H(t_{m-1}, x_1, x_2, \vartheta_p) - \hat{H}(t_{m-1}, x_1, x_2, \vartheta_p|N_Z, [a_Z, b_Z])|. \tag{8.40}$$

The rate of convergence depends on the convolution of density functions f_{Z_s}, according to the analysis in Section 5.1. The error introduced by the COS convolution formula results in

$$\begin{aligned}
\epsilon_{d2}(t_{m-1}, t_m, x_1, x_2|N_t, N_Z, [a_Z, b_Z]) &:= d_1(t_{m-1}, t_m, x_1, x_2|N_t) - \hat{d}(t_{m-1}, t_m, x_1, x_2|N_Z, [a_Z, b_Z], N_t) \\
&= \sum_{p=0}^{N_t} y_p \left(H(t_{m-1}, x_1, x_2, \vartheta_p) - \hat{H}(t_{m-1}, x_1, x_2, \vartheta_p) \right) \\
&\leq \epsilon_{COSconv} \sum_{p=0}^{N_t} y_p.
\end{aligned} \tag{8.41}$$

The total local error introduced by approximation of the proportional damage function is

$$\begin{aligned}
\epsilon_d(t_{m-1}, t_m, x_1, x_2|N_Z, [a_Z, b_Z], N_t)| &:= d(t_{m-1}, t_m, x_1, x_2) - \hat{d}(t_{m-1}, t_m, x_1, x_2|N_Z, [a_Z, b_Z], N_t) \\
&\leq \epsilon_{d1}(t_{m-1}, t_m, x_1, x_2|N_t) + \epsilon_{d2}(t_{m-1}, t_m, x_1, x_2|N_Z, [a_Z, b_Z], N_t).
\end{aligned} \tag{8.42}$$

The local error of the Quadrature-COS formula is defined by

$$\epsilon_{QCOS}(t_{m-1}, x_1, x_2, x_3|N, [a, b], J, [a_2, b_2]) := c(t_{m-1}, x_1, x_2, x_3) - \hat{c}(t_{m-1}, x_1, x_2, x_3|N, [a, b], J, [a_2, b_2]). \tag{8.43}$$

Errors in approximation of c are introduced in three steps: the truncation of the integration range over the surplus water level, discretization of the surplus water level dimension and approximation of the

integral with the Composite Trapezoidal rule, and the error introduced by the COS formula. We will discuss the three errors one after the other:

1. Surplus water level integration range truncation error:

$$\begin{aligned}\epsilon_{c1}(t_{m-1},x_1,x_2,x_3|[a_2,b_2]) &:= c(t_{m-1},x_1,x_2,x_3) - c_1(t_{m-1},x_1,x_2,x_3|[a_2,b_2])\\ &= e^{-\rho\Delta t}\int_{\mathbb{R}\setminus[a_2,b_2]}\int_{\mathbb{R}} v(t_m^-,x_1,y_2,y_3)f_3(y_3|x_3)dy_3 f_2(y_2|x_2)dy_2\\ &= e^{-\rho\Delta t}\int_{\mathbb{R}\setminus[a_2,b_2]} G(t_m^-,x_1,y_2,x_3)f_2(y_2|x_2)dy_2. \end{aligned} \tag{8.44}$$

This error depends on the speed of decay to zero of the function G, which is increasing in the surplus water level, times the surplus water level density.

2. Discretization error induced by approximating the surplus water level integral with the Composite Trapezoidal rule:

$$\epsilon_{c2}(t_{m-1},x_1,x_2,x_3|J,[a_2,b_2]) := c_1(t_{m-1},x_1,x_2,x_3|[a_2,b_2]) - c_2(t_{m-1},x_1,x_2,x_3|J,[a_2,b_2]). \tag{8.45}$$

The quadrature error converges with order $O(J^{-2})$ if $G(t_m^-,x_1,x,x_3)f_2(x|x_2)\in C^2([a_2,b_2])$ ([1]).

3. The error introduced by using the COS method: The function G is approximated by

$$\hat{G}(t_m^-,x_1,\theta_q,x_3) := e^{-\rho\Delta t}\sum_{k=0}^{N-1}{}'\,\Re\left[\varphi_{3levy}\left(\frac{k\pi}{b-a}\right)e^{ik\pi\frac{x_3-a}{b-a}}\right]V_{kq}(t_m^-,x_1). \tag{8.46}$$

The error

$$\epsilon_{COS}(t_{m-1},x_3|N,[a,b]) := \sup_{x_1,\theta_q}|G(t_m^-,x_1,\theta_q,x_3) - \hat{G}(t_m^-,x_1,\theta_q,x_3|N,[a,b])| \tag{8.47}$$

converges exponentially in N for smooth densities if the integration range $[a,b]$ is sufficiently wide, as discussed in Section 5.1. The summation over the terms $\hat{G}$ results in the error:

$$\begin{aligned}\epsilon_{c3}(t_{m-1},x_1,x_2,x_3|N,[a,b],J,[a_2,b_2]) &:= c_2(t_{m-1},x_1,x_2,x_3|J,[a_2,b_2]) - \hat{c}(t_{m-1},x_1,x_2,x_3|N,[a,b],J,[a_2,b_2])\\ &= \sum_{q=0}^{J-1} w_q f(\theta_q|x_2)\left(G(t_m^-,x_1,\theta_q,x_3) - \hat{G}(t_m^-,x_1,\theta_q,x_3)\right)\\ &\le \epsilon_{COS}(t_{m-1},x_3|N,[a,b])\sum_{q=0}^{J-1} w_q f_2(\theta_q|x_2)\\ &\approx \epsilon_{COS}(t_{m-1},x_3|N,[a,b])\int_{a_2}^{b_2} f_2(y_2|x_2)dy_2\\ &\le \epsilon_{COS}(t_{m-1},x_3|N,[a,b]). \end{aligned} \tag{8.48}$$

The local error of the Q-COS method can be bounded by

$$\begin{aligned}|\epsilon_{QCOS}(t_{m-1},x_1,x_2,x_3|N,[a,b])| &\le |\epsilon_{c1}(t_{m-1},x_1,x_2,x_3|[a_2,b_2])| + |\epsilon_{c2}(t_{m-1},x_1,x_2,x_3|J,[a_2,b_2])|\\ &+ |\epsilon_{COS}(t_{m-1},x_3|N,[a,b])|. \end{aligned} \tag{8.49}$$

The local error of the dike-Q-COS-method reads

$$\begin{aligned}\epsilon_{Loc}(t_{m-1},x_1,x_2,x_3) &:= v(t_{m-1},x_1,x_2,x_3) - \hat{v}(t_{m-1},x_1,x_2,x_3)\\ &= \exp(x_3)\epsilon_d(t_{m-1},t_m,x_1,x_2) + \epsilon_{QCOS}(t_{m-1},x_1,x_2,x_3). \end{aligned} \tag{8.50}$$

Following the arguments in Section 5.1 shows that for integration intervals $[a_Z, b_Z]$, $[a_2, b_2]$ and $[a, b]$ chosen sufficiently wide and N_t, J and N_Z sufficiently large, the series truncation error ϵ_2 of the COS method dominates the overall local error. The error convergence is exponentially in N dimension if $f_3(y_3|x_3) \in C^\infty([a, b])$, and quadratic in J dimension if $G(t_m^-, x_1, x, x_3) f_2(x|x_2) \in C^2([a_2, b_2])$.

Remark 8.4. *The dike-Q-COS method is inaccurate in the vicinity of boundary values a and b, like the dike-COS method. Besides, errors occur for x_2 close to the boundaries a_2 and b_2, because then the summation $\sum_{q=0}^{J-1} w_q f(\theta_q|x_2)$ is not accurate.*

8.5.2 Error propagation in the backward recursion

Again the coefficients $V_{kq}(t_m^-, x_1)$ are recovered recursively, backwards in time, as in the dike-COS method. The error ϵ may propagate through time. In this section we study the error in the Fourier coefficients,

$$\varepsilon_{kq}(t_m^-, x_1) := V_{kq}(t_m^-, x_1) - \hat{V}_{kq}(t_m^-, x_1) \tag{8.51}$$

and

$$|\varepsilon(t_m^-)|_\infty := \max_{k,q,x_1} |\varepsilon_{kq}(t_m^-, x_1)|. \tag{8.52}$$

Again the case of only two possible dike increase levels is considered, u^0 and u^1 and the results can easily be extended to the case of more dike increase levels. The *construction points* $y_m^*(x_1, \theta_q)$ denote the change from no dike increase to an optimal reinforcement by amount u^1. We assume that the construction points are exact, in other words the error resulting from applying the Bisection method is not significant. Errors may be introduced if incorrect points are found, then a similar analysis as in Section 5.3 applies. The theory in this section resembles the dike-COS method error analysis in Section 5.2.

Theorem 8.1. *With $[a, b] \subset \mathbb{R}$ sufficiently large the error $\varepsilon(t_m^-)$ converges as the local error ϵ_{Loc} for all $1 \le m \le M - 1$.*

Proof by induction:
Step 1: Base case
The terms B_k are exact, see equation (4.22), so at time t_{M-1}^- we have

$$\begin{aligned} \varepsilon_{kq}(t_{M-1}^-, x_1) &= C_{kq}(a, y_{M-1}^*(x_1, \theta_q), t_{M-1}, x_1) - \hat{C}_{kq}(a, y_{M-1}^*(x_1, \theta_q), t_{M-1}, x_1) \\ &+ C_{kq}(y_{M-1}^*(x_1, \theta_q), b, t_{M-1}, x_1 + u^1) - \hat{C}_{kq}(y_{M-1}^*(x_1, \theta_q), b, t_{M-1}, x_1 + u^1) \\ &:= \varepsilon_{kq}(a, y_{M-1}^*(x_1, \theta_q), t_{M-1}, x_1) + \varepsilon_{kq}(y_{M-1}^*(x_1, \theta_q), b, t_{M-1}, x_1 + u^1), \end{aligned} \tag{8.53}$$

where

$$\varepsilon_{kq}(z_1, z_2, t_{M-1}, y_1) = \frac{2}{b-a} \int_{z_1}^{z_2} (v(t_{M-1}, y_1, \theta_q, y) - \hat{v}(t_{M-1}, y_1, \theta_q, y)) \cos\left(k\pi \frac{y-a}{b-a}\right) dy. \tag{8.54}$$

The coefficients $V_{kq}(t_M^-, y_1)$ are exact, see equation (8.31), so the only error caused by the Q-COS formula is the local error ϵ_{Loc}. We obtain:

$$\varepsilon_{kq}(z_1, z_2, t_{M-1}, y_1) = \frac{2}{b-a} \int_{z_1}^{z_2} \epsilon_{Loc}(t_{M-1}, y_1, \theta_q, y|N, [a, b], J, [a_2, b_2], N_Z, [a_Z, b_Z], N_t) \cos\left(k\pi \frac{y-a}{b-a}\right) dy. \tag{8.55}$$

We can bound the error by:

$$\begin{aligned} |\varepsilon_{kq}(z_1, z_2, t_{M-1}, y_1)| &\le \frac{2}{b-a} \int_{z_1}^{z_2} |\epsilon_{Loc}(t_{M-1}, y_1, \theta_q, y|N, [a, b], J, [a_2, b_2], N_Z, [a_Z, b_Z], N_t)| dy \\ &\sim O(\epsilon_{Loc}). \end{aligned} \tag{8.56}$$

Adding up the two terms results in

$$|\varepsilon(t_{M-1}^-)|_\infty \sim O(\epsilon_{Loc}). \tag{8.57}$$

Step 2: Inductive step
If

$$|\varepsilon(t_{m+1}^-)|_\infty \sim O(\epsilon_{Loc}) \qquad \text{(Induction Hypothesis)} \tag{8.58}$$

then

$$|\varepsilon(t_m^-)|_\infty \sim O\left(\epsilon_{Loc}\right). \tag{8.59}$$

Proof: Take $m \in \{1, \ldots, M-2\}$ fixed. For the estimation of $v(t_m, x_1, x_2, x_3)$ the Q-COS formula with approximations $\hat{V}_{kq}(t_{m+1}^-, y_1)$ is used. This estimated real option value is denoted by $\overline{v}(t_m, x_1, x_2, x_3)$. The use of the approximations $\hat{V}_{kq}(t_{m+1}^-, y_1)$ introduces an extra error to $V_{kq}(t_m^-, x_1)$:

$$\begin{aligned}
\varepsilon_{kq}(t_m^-, x_1) &= C_{kq}(a, y_m^*(x_1, \theta_q), t_m, x_1) - \hat{C}_{kq}(a, y_m^*(x_1, \theta_q), t_m, x_1) \\
&+ C_{kq}(y_m^*(x_1, \theta_q), b, t_m, x_1 + u^1) - \hat{C}_{kq}(y_m^*(x_1, \theta_q), b, t_m, x_1 + u^1) \\
&:= \varepsilon_{kq}(a, y_m^*(x_1, \theta_q), t_m, x_1) + \varepsilon_{kq}(y_m^*(x_1, \theta_q), b, t_m, x_1 + u^1),
\end{aligned} \tag{8.60}$$

where

$$\begin{aligned}
\varepsilon_{kq}(z_1, z_2, t_m, y_1) &= \frac{2}{b-a}\int_{z_1}^{z_2} (v(t_m, y_1, \theta_q, y) - \overline{v}(t_m, y_1, \theta_q, y) \cos\left(k\pi \frac{y-a}{b-a}\right) dy \\
&= \frac{2}{b-a}\int_{z_1}^{z_2} (d(t_m, t_{m+1}, y_1, \theta_q) - \hat{d}(t_m, t_{m+1}, y_1, \theta_q)) e^y \cos\left(k\pi \frac{y-a}{b-a}\right) dy \\
&+ \frac{2}{b-a}\int_{z_1}^{z_2} (c(t_m, y_1, \theta_q, y) - \hat{c}(t_m, y_1, \theta_q, y) \cos\left(k\pi \frac{y-a}{b-a}\right) dy \\
&+ \frac{2}{b-a}\int_{z_1}^{z_2} (\hat{c}(t_m, y_1, \theta_q, y) - \overline{c}(t_m, y_1, \theta_q, y)) \cos\left(k\pi \frac{y-a}{b-a}\right) dy,
\end{aligned} \tag{8.61}$$

with $\overline{c}$ obtained by inserting $\hat{V}_{kq}(t_{m+1}^-, y_1)$ in the Q-COS formula:

$$\begin{aligned}
\overline{c}(t_m, y_1, \theta_q, y) &= e^{-\rho\Delta t} {\sum_{j=0}^{N-1}}' \sum_{p=0}^{J-1} \Re\left[w_p f(\theta_p|\theta_q) \varphi_{3levy}\left(\frac{j\pi}{b-a}\right) e^{ij\pi\frac{x_3-a}{b-a}} \right] \hat{V}_{jp}(t_m^-, x_1) \\
&= e^{-\rho\Delta t} {\sum_{j=0}^{N-1}}' \sum_{p=0}^{J-1} \Re\left[w_p f(\theta_p|\theta_q) \varphi_{3levy}\left(\frac{j\pi}{b-a}\right) e^{ij\pi\frac{x_3-a}{b-a}} \right] (V_{jp}(t_{m+1}^-, y_1) - \varepsilon_{jp}(t_{m+1}^-, y_1)) \\
&= \hat{c}(t_m, y_1, \theta_q, y) - e^{-\rho\Delta t} {\sum_{j=0}^{N-1}}' \sum_{p=0}^{J-1} \Re\left[w_p f(\theta_p|\theta_q) \varphi_{3levy}\left(\frac{j\pi}{b-a}\right) e^{ij\pi\frac{x_3-a}{b-a}} \right] \varepsilon_{jp}(t_{m+1}^-, y_1).
\end{aligned} \tag{8.62}$$

$\varepsilon_{kq}(z_1, z_2, t_m, y_1)$ consist of three parts, one related to error ϵ_d, one related to the local error of the Q-COS formula, and one related to the terms $\varepsilon_{jp}(t_{m+1}^-, y_1)$. The first part equals:

$$\frac{2}{b-a}(d(t_m, t_{m+1}, y_1, \theta_q) - \hat{d}(t_m, t_{m+1}, y_1, \theta_q))\chi(z_1, z_2) \sim O(\epsilon_d). \tag{8.63}$$

The second part can be bounded as before by:

$$\frac{2}{b-a}\int_{z_1}^{z_2} \epsilon_{QCOS}(y_1, \theta_q, y|N, [a,b], J, [a_2, b_2]) \cos\left(k\pi \frac{y-a}{b-a}\right) dy \sim O\left(\epsilon_{QCOS}\right). \tag{8.64}$$

The third part is equal to:

$$\varepsilon_{kq}(z_1, z_2, t_m, y_1) = \frac{2}{b-a}\int_{z_1}^{z_2} (\overline{\epsilon}(t_{m+1}^-, y_1, \theta_q, y)) \cos\left(k\pi \frac{y-a}{b-a}\right) dy, \tag{8.65}$$

where

$$\overline{\epsilon}(t_{m+1}^-, y_1, \theta_q, y) = e^{-\rho\Delta t} \sum_{j=0}^{N-1}{}' \sum_{p=0}^{J-1} \Re\left[w_p f(\theta_p|\theta_q) \varphi_{3levy}\left(\frac{j\pi}{b-a}\right) e^{ij\pi\frac{x_3-a}{b-a}} \right] \varepsilon_{jp}(t_{m+1}^-, y_1). \tag{8.66}$$

For this part we start with applying the Cauchy-Schwartz inequality to error $\overline{\epsilon}$:

$$\begin{aligned}(e^{\rho\Delta t}\overline{\epsilon}(t_{m+1}^-, y_1, \theta_q, y)))^2 &= \left(\sum_{p=0}^{J-1} w_p f(\theta_p|\theta_q) \left\{ \sum_{j=0}^{N-1}{}' \Re\left[\varphi_{3levy}\left(\frac{j\pi}{b-a}\right) e^{ij\pi\frac{x_3-a}{b-a}} \right] \varepsilon_{jp}(t_{m+1}^-, y_1) \right\} \right)^2 \\ &\leq \sum_{p=0}^{J-1} (w_p f(\theta_p|\theta_q))^2 \sum_{p=0}^{J-1} \left\{ \sum_{j=0}^{N-1}{}' \Re\left[\varphi_{3levy}\left(\frac{j\pi}{b-a}\right) e^{ij\pi\frac{x_3-a}{b-a}} \right] \varepsilon_{jp}(t_{m+1}^-, y_1) \right\}^2. \end{aligned} \tag{8.67}$$

Using the same arguments as in Section 5.2 we obtain

$$\begin{aligned}\left\{ \sum_{j=0}^{N-1}{}' \Re\left[\varphi_{3levy}\left(\frac{j\pi}{b-a}\right) e^{ij\pi\frac{x_3-a}{b-a}} \right] \varepsilon_{jp}(t_{m+1}^-, y_1) \right\}^2 &\leq \left(R(N) e^{-(N-1)\nu} (W(N)+N) \right)^2 \\ &\sim O\left(\epsilon_{Loc}^2\right), \end{aligned} \tag{8.68}$$

where the Induction Hypothesis is used for the inequality. $R(N)$ varies less than exponentially in N. Assume $\sum_{p=0}^{J-1}(w_p f(\theta_p|\theta_q))^2$ has an upper bound for all θ_q. Adding up the parts gives

$$\varepsilon_{kq}(t_m^-, x_1) \sim O(\epsilon_d) + O(\epsilon_{QCOS}) + O\left(\epsilon_{Loc}\right) = O\left(\epsilon_{Loc}\right). \tag{8.69}$$

This completes the proof. □

8.5.3 Numerical experiments COS convolution formula

In this section we go more deeply into the error of the COS convolution formula. Errors of the COS convolution formula are introduced in three steps: the truncation of the integration range, truncation of the series expansion and the substitution of the series coefficients of the convolution function by the characteristic functions approximation. Comparable to the errors in Section 5.1 we define

$$\epsilon_1^Z(t_{m-1}, x_1, x_2, \vartheta_p|[a_Z, b_Z]) := \lambda e^{(\vartheta_p - t_{m-1})(\mu_3 - \rho)} \int_{\mathbb{R}\setminus[a_Z,b_Z]} l_p(w(\vartheta_p) + z - x_1) f_{Z_{\vartheta_p}|X_{t_{m-1}}^{(2)}}(z|x_2) dz \tag{8.70}$$

and

$$\epsilon_4^Z(t_{m-1}, x_2, \vartheta_p) := \int_{\mathbb{R}\setminus[a_Z,b_Z]} f_{Z_{\vartheta_p}|X_{t_{m-1}}^{(2)}}(z|x_2) dz. \tag{8.71}$$

Also $\epsilon_3^Z(t_{m-1}, x_1, x_2, \vartheta_p|N_Z, [a_Z, b_Z])$ is defined in the same way as the errors in Section 5.1.

Integration range $[a_Z, b_Z]$
Similar to the truncation range $[a, b]$ in Section 6.3, we start with the suggestion

$$[a_Z, b_Z] = \left[c_1 - L_Z\sqrt{c_2 + \sqrt{c_4}},\ c_1 + L_Z\sqrt{c_2 + \sqrt{c_4}} \right], \qquad L_Z = 10, \tag{8.72}$$

with cumulants given by

$$\begin{aligned} c_1 &= E^{t_{m-1},x}[Z_{\vartheta_p}] &&= x_2 + k_2 + \gamma_{EM}/k_1, \\ c_2 &= \mathrm{Var}^{t_{m-1},x}(Z_{\vartheta_p}) &&= \sigma_w^2(\vartheta_p - t_{m-1}) + (\pi/k_1)^2/6, \\ c_4 &= \gamma_2(Z_{\vartheta_p})c_2^2 &&= \tfrac{12}{5}c_2^2, \end{aligned} \tag{8.73}$$

where γ_2 is the (excess) kurtosis. The kurtosis is a measure of the heaviness of the tails of a distribution. $\gamma_2(X_{\vartheta_p}^{(2)}) = 0$ and $\gamma_2(\mathcal{J}) = 12/5$. The kurtosis satisfies the following linearity property: If X and Y are two independent random variables, it holds that ([15])

$$\gamma_2(X+Y) = \gamma_2(X) + \gamma_2(Y). \tag{8.74}$$

This interval would result in a small error ϵ_4^Z. However, the error ϵ_1^Z might be large, even for larger values L_Z. This is illustrated by Figure 8.5.3, where we take

$$t_{m-1} = 0, x_1 = 425,\ x_2 = 0,\ \vartheta_p = 10 \text{ and } \sigma_w = 1. \tag{8.75}$$

Equation (8.72) gives $[a_Z, b_Z] = [-60.37, 451.41]$. The figure illustrates that the truncation range error ϵ_1^Z is larger, notwithstanding the fact that the total error will be reduced by ϵ_3^Z in the same way as we discussed in Section 6.3.2. We find the truncation range should not be based only on the density function, because then it does not include the properties of function l_p. We have found this by an numerical experiment below.

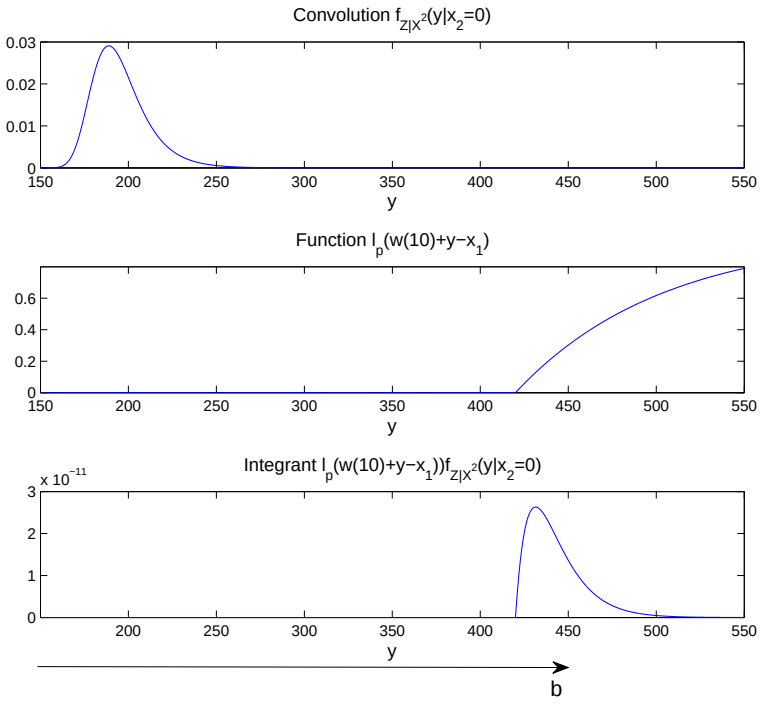

Figure 8.2: Functions $f_{Z_{\vartheta_p}|X_{t_{m-1}}^{(2)}}(z|x_2)$ and $l_p(w(\vartheta_p)+z-x_1)f_{Z_{\vartheta_p}|X_{t_{m-1}}^{(2)}}(z|x_2)$.

The characteristic function of the Gumbel distributed extreme water levels reads (see Appendix F):

$$\varphi_{\mathcal{J}}(u) = \Gamma\left(1 - i\frac{u}{k_1}\right) e^{ik_2 u}, \tag{8.76}$$

and the characteristic function of the normally distributed surplus water level is (see Appendix F)

$$\varphi_{X_s^{(2)} - X_{t_{m-1}}^{(2)}}(u) = e^{-\frac{1}{2}\sigma_w^2 (s - t_{m-1})u^2}. \tag{8.77}$$

We estimate the proportional damage function $d(t_{m-1}, t_m, x_1, x_2)$ for

$$t_{m-1} = 0,\ t_m = 150,\ x_1 = 425,\ x_2 = 0,\ \sigma_w = 0 \text{ and } N_t = 2000. \tag{8.78}$$

In other words, the average water level $Y_t^{(2)}$ is modelled as deterministic and equal to $w(t)$. The approximated proportional damage function converges in N_Z and L_Z (see Table 8.1) to

$$\hat{d}(0, 150, 425|N_t) \approx 0.141418867757724 \cdot 10^{-5}. \tag{8.79}$$

which is the proportional damage function with deterministic average water level $w(t)$ from Section 4. The roundoff plateaus are reached for $N_Z = 2^9$, so no further improvement is realised by using a higher value N_Z. The proportional damage function is increasing in L_Z, because this corresponds to a larger integration interval $[a_Z, b_Z]$. The results for $L_Z = 10$ are not very satisfactorily, although this corresponds to a very small error ϵ_4^Z. The expected flood losses are underestimated, primarily because of the integration range truncation error ϵ_1^Z. The same convergence results are obtained for $\sigma_w \neq 0$. The value $x_1 - w(\vartheta_p)$ denotes where function l_p becomes positive and varies from about 245 to 800 cm in our experiments in Section 8.6. In order to have a small error ϵ_1^Z we propose

$$[a_Z,\, b_Z] = [0,\, 900]. \tag{8.80}$$

This interval performs satisfactorily according to the results in Table 8.1. With this we showed that it is useful to take the characteristics of the function l_p into account too when choosing the integration interval $[a_Z, b_Z]$. We take $[a_Z, b_Z] = [0, 900]$ fixed in the sequel. Computation time is saved by this, since the interval is not computed for every separate set of variables anymore.

L_Z \ N_Z	2^7	2^8	2^9
10	$0.140806205630514 \cdot 10^{-5}$	$0.140925657279090 \cdot 10^{-5}$	$0.140925657289235 \cdot 10^{-5}$
12	$0.142558812124158 \cdot 10^{-5}$	$0.141414083553131 \cdot 10^{-5}$	$0.141414082290749 \cdot 10^{-5}$
14	$0.135325884579892 \cdot 10^{-5}$	$0.141418807923046 \cdot 10^{-5}$	$0.141418823563926 \cdot 10^{-5}$
$[a_Z, b_Z] = [0, 900]$	$0.100515090473518 \cdot 10^{-5}$	$0.141419199899692 \cdot 10^{-5}$	$0.141418868748732 \cdot 10^{-5}$

Table 8.1: Prop. damage $\hat{d}(0, 150, 425, 0|N_t = 2000)$ for $\sigma_w = 0$ ($\hat{d}(0, 150, 425|N_t = 2000) \approx 0.141 \cdot 10^{-5}$).

Next the influence of the surplus water level parameter σ_w is studied. Again we calculate the proportional damage function $\hat{d}(0, 150, 425, 0|N_t = 2000)$. The approximations are converging in N_Z and again the roundoff plateau was reached for $N_Z = 2^9$, so the results are the same as for a higher value N_Z. Not surprisingly, the results in Table 8.2 show a higher expected proportional loss for a higher water level volatility. This is due to the convexity of the function $\beta(h)$. The proportional damage function can also be approximated by application of two times a Composite Trapezoidal rule. We have validated that this method does result in similar values. We prefer to use the COS convolution formula to stay in line with the rest of the dike-Q-COS method.

σ_w	$\hat{d}(0, 150, 425, 0)$
0	$0.141418868 \cdot 10^{-5}$
0.0001	$0.141418869 \cdot 10^{-5}$
0.5	$0.157083287 \cdot 10^{-5}$
1	$0.215856522 \cdot 10^{-5}$
2	$0.794441701 \cdot 10^{-5}$
3	$6.758277069 \cdot 10^{-5}$

Table 8.2: Prop. damage function $\hat{d}(0, 150, 425, 0|N_t = 2000)$, effect σ_w ($[a_Z, b_Z] = [0, 900], N_Z = 2^9$).

8.6 Tests dike-Q-COS method for an island

In this section the dike-Q-COS method is tested with the model for an island. We use the same model parameters as is Section 7, except for $M = 60$ in order to save computation time. Besides, only two possible dike increase levels, $u^0 = 0$ and $u^1 = 40$ cm, are used. More possible dike increase levels may be used, but this takes more computation time. Further we take

$$L = 6,\ N_{bis} = 20,\ N_t = 200 \text{ and } X_0^{(2)} = 0 \text{ cm}. \tag{8.81}$$

The corresponding option values resulting from the dike-COS method in Section 4 are given in Table 8.3. For this method the average water level was modelled by a deterministic process. The real option values are somewhat higher than the results in Section 7.2, because we use lower values M and N_t and only one positive dike increase level is at one's disposal. The optimal dike reinforcements times are 145, 185, 230 and 290 years if the economic value follows its expected value.

dd	$\hat{v}(t_0, X_0^{(1)}, X_0^{(3)})$	CPU time (s)
7	0.055030149963327	3
8	0.055009861122490	4
9	0.055009861122647	7
10	0.055009861122485	12

Table 8.3: Real option values $\hat{v}(t_0, X_0^{(1)}, X_0^{(3)})$, dike-COS method (Algorithm 1).

We start in Section 8.6.1 with a low average water level volatility $\sigma_w = 0.0001$. This models a deterministic water level and enables us to validate the dike-Q-COS method. In Section 8.6.2 true water level volatility values $\sigma_w = 1$ and 2 are used. The standard deviation of the surplus water level at the terminal time is $\sigma_w\sqrt{T}$ cm. So, the probability that the terminal water level is between 162.7 and 197.3 cm is about 68% in the case of the model with $\sigma_w = 1$. Then with the same probability $Y_{100}^{(2)} \in [50,\ 70]$ cm.

We calculate the real option values and the optimal control for an economic value of endangered goods and surplus water level equal to their expected values, namely $e^{X_0^{(3)}} e^{\mu_3 t}$ and zero, respectively. Besides, the optimal impulse control strategies for surplus water levels equal to $-\sigma_w\sqrt{t}$ and $+\sigma_w\sqrt{t}$ are calculated.

Integration range $[a_2, b_2]$
In Section 8.6.2 we will discuss scenarios of various deterministic average water levels and we apply the dike-COS method to them. They show that both a lower and a higher average water level affect the costs of flood protection. Because of that we propose to take

$$[a_2, b_2] = \Big[-L_2\sqrt{c_2},\ L_2\sqrt{c_2}\Big], \tag{8.82}$$

where c_2 is the second cumulant of $X_T^{(2)}$, given $X_0^{(2)}$. For the zero mean Brownian process we have $c_2 = \sigma_w^2 T$.

8.6.1 Low water level volatility, $\sigma_w \approx 0$

For the first tests we take a very low value $\sigma_w = 0.0001$, representing an almost deterministic average water level equal to $w(t)$. The proportional damage function $\hat{d}(t_{m-1}, t_m, x_1)$ from Section 4, equation (4.5), is used since this resembles with $\hat{d}(t_{m-1}, t_m, x_1, x_2)$ for low value σ_w. The approximated option values are denoted by:

$$\tilde{v}(t_{m-1}, x_1, x_2, x_3) := \exp(x_3)\hat{d}(t_{m-1}, t_m, x_1 - x_2) + \hat{c}(t_{m-1}, x_1, x_2, x_3). \tag{8.83}$$

Different values L_2, corresponding to different interval $[a_2, b_2]$, are used. Besides, the number of integration points J and dd, with $N = 2^{dd}$, are varied. The results are shown in Table 8.4. The real option values converge in J and L_2 to the corresponding real option prices of the model without stochastic water level (Table 8.3), but they are a little bit higher since the volatility is not exactly equal to zero. Besides, the same dike construction times 145, 185, 230 and 290 years are found for an economic value and surplus water level that follow their expected value.

A larger value L_2 represents a larger integration interval $[a_2, b_2]$. A too low value L_2 excludes plausible surplus water level processes, which might underestimate the real option value. However, the convergence in J takes longer for higher values L_2, since a larger integration interval is subdivided in J sub-intervals. A compromise is obtained by $L_2 = 6$.

The computational complexity is almost linear in both $N \log_2 N$ and J, as follows from Table 8.5.

L_2	dd \ J	51	101	151	201
4	7	0.055037881292403	0.055030137064325	0.055030137326402	0.055030137422127
	8	0.055017592527721	0.055009848247368	0.055009848508300	0.055009848601505
	9	0.055017592527941	0.055009848247561	0.055009848508464	0.055009848601682
	10	0.055017592527903	0.055009848247445	0.055009848508396	0.055009848601586
5	7	0.055827112226863	0.055030149989055	0.055030149992631	0.055030149991798
	8	0.055806827547545	0.055009861146289	0.055009861147282	0.055009861148044
	9	0.055806827547646	0.055009861146469	0.055009861147398	0.055009861148211
	10	0.055806827547512	0.055009861146357	0.055009861147332	0.055009861148098
6	7	0.065741110812577	0.055030150382392	0.055030150029351	0.055030150029974
	8	0.065720751781606	0.055009861537914	0.055009861184444	0.055009861184390
	9	0.065720751781811	0.055009861538100	0.055009861184608	0.055009861184555
	10	0.065720751781684	0.055009861537961	0.055009861184493	0.055009861184484
7	7	0.124304206466018	0.055030301561679	0.055030150027933	0.055030150029507
	8	0.124285534058618	0.055010012718394	0.055009861184737	0.055009861184199
	9	0.124285534059254	0.055010012718554	0.055009861184953	0.055009861184332
	10	0.124285534059025	0.055010012718448	0.055009861184820	0.055009861184264
8	7	0.497631249069457	0.055037895545429	0.055030150029898	0.055030150029328
	8	0.497602903800888	0.055017606748362	0.055009861185167	0.055009861184529
	9	0.497602903802333	0.055017606748577	0.055009861185374	0.055009861184653
	10	0.497602903801567	0.055017606748379	0.055009861185309	0.055009861184532

Table 8.4: Real option values $\tilde{v}(t_0, X_0^{(1)}, X_0^{(2)}, X_0^{(3)})$ for $\sigma_w = 0.0001$.

dd \ J	51	101	151	201
7	56	114	175	238
8	78	162	249	342
9	123	256	398	552
10	215	452	707	992

Table 8.5: CPU times (s), $\sigma_w = 0.0001$, $L_2 = 6$.

COS-convolution formula
Now we study the convergence in N_Z using the true 'two-dimensional' proportional damage function from

Section 8.2. So, we calculate the option values

$$\hat{v}(t_{m-1}, x_1, x_2, x_3) = \exp(x_3)\hat{d}(t_{m-1}, t_m, x_1, x_2) + \hat{c}(t_{m-1}, x_1, x_2, x_3). \tag{8.84}$$

In order to save computation time we set $N_t = 10$. The convergence in dd, J and L_2 is the same as we saw before and we take $dd = 9$, $J = 151$ and $L_2 = 6$ fixed. We use interval $[a_Z, b_Z] = [0, 900]$, as we proposed in Section 8.5.3, and vary the number of coefficients N_Z in the series expansion of the COS convolution formula. The results in Table 8.6 demonstrate that the approximated option values are converging in value N_Z. The option value $\hat{v}$ equals $\tilde{v}$ closely for large N_Z, which justifies the use of the proportional damage function from Section 4 for low value σ_w.

$\tilde{v}(t_0, X_0^{(1)}, X_0^{(2)}, X_0^{(3)})$	CPU time (s)
0.055011014354350	465

		$\hat{v}(t_0, X_0^{(1)}, X_0^{(2)}, X_0^{(3)})$	CPU time (s)
N_Z	2^7	0.045328118714308	675
	2^8	0.055011129736715	869
	2^9	0.055011014657749	1168
	2^{10}	0.055011014657715	1810

Table 8.6: Real option values $\hat{v}(t_0, X_0^{(1)}, X_0^{(2)}, X_0^{(3)})$ for $\sigma_w = 0.0001$.

8.6.2 Stochastic average water level

Next we use a true stochastic average water level, with both $\sigma_w = 1$ and $\sigma_w = 2$. Again we save computation time by using the proportional damage function from Section 4 and consider the approximated option values $\tilde{v}(t_{m-1}, x_1, x_2, x_3)$.

The results for $\sigma_w = 1$, see Appendix G, show once more the convergence in the parameters L_2, J and dd and we obtain the real option value $\tilde{v}(t_0, X_0^{(1)}, X_0^{(2)}, X_0^{(3)}) \approx 0.061499$. Not surprisingly, the costs of flood protection increase if we use a stochastic water level. The computation times are comparable to the ones in Table 8.5. A volatility of value $\sigma_w = 2$ leads to similar convergence results and then an option value about 0.083085 is found.

The optimal heightening times are 145, 185, 230 and 290 years if the economic value and surplus water level follow their expected value. If instead the surplus water level follows the process $-\sigma_w\sqrt{t}$ or $+\sigma_w\sqrt{t}$, then construction times 160, 205 and 255 years, and 130, 165, 210 and 265 years are found, respectively. This indicates that dike reinforcements are advanced if the surplus water level is positive, which corresponds to a higher water level. The construction times for the three different water level volatilities are summarised in Table 8.7.

$X_t^{(2)}$ \ σ_w	0.0001	1	2
$-\sigma_w\sqrt{t}$	145 185 230 290	160 205 255	180 225 285
0	145 185 230 290	145 185 230 290	145 185 230 290
$+\sigma_w\sqrt{t}$	145 185 230 290	130 165 210 265	115 150 190 240 295

Table 8.7: Construction times for various surplus water level realisations.

COS-convolution formula
Again we study the convergence in the number of coefficients N_Z in the series expansion of the COS

convolution formula. In order to save computation time we set $N_t = 10$, $dd = 9$ and $J = 151$ and we use $L_2 = 6$. The results in Table 8.8 show that the approximated option values converge in N_Z. Besides, this demonstrates that the option value $\hat{v}$ is a little bit higher than $\tilde{v}$, because the proportional damage is higher for $\sigma_w = 1$ than for $\sigma_w = 0$ (see Table 8.2). Since it takes significantly longer to calculate $\tilde{v}$ compared to $\hat{v}$, we prefer the latter.

$\tilde{v}(t_0, X_0^{(1)}, X_0^{(2)}, X_0^{(3)})$	CPU time (s)
0.061500334602229	466

		$\hat{v}(t_0, X_0^{(1)}, X_0^{(2)}, X_0^{(3)})$	CPU time (s)
N_Z	2^7	0.055197115592179	712
	2^8	0.061801857554217	909
	2^9	0.061801837891613	1223
	2^{10}	0.061801837891611	1850

Table 8.8: Real option values $\hat{v}(t_0, X_0^{(1)}, X_0^{(2)}, X_0^{(3)})$ for $\sigma_w = 1$.

Deterministic water level scenarios

Many policymakers use scenarios to weigh up their decisions. For example, the Royal Netherlands Meteorological Institute (KNMI) uses four different scenarios to predict the future sea level rise. We wonder whether the use of a model with stochastic water level adds additional insight and relevance to the dike height analysis. Table 8.9 shows the real option values and construction times for different *deterministic* water level scenarios. In other words, we take the deterministic water level $w(t)$ in Section 4 equal to each of these scenarios and apply the dike-COS method, Algorithm 1. It is clear that a higher water level results in higher flood protection costs and advances the heightenings.

Average water level	Construction times	$\hat{v}(t_0, X_0^{(1)}, X_0^{(3)})$
$w(t) - 4\sqrt{t}$	200 265	0.0046716
$w(t) - 2\sqrt{t}$	120 220 280	0.0176809
$w(t) - 1\sqrt{t}$	155 200 250	0.0319046
$w(t)$	145 185 230 290	0.0550099
$w(t) + 1\sqrt{t}$	135 170 215 265	0.0911208
$w(t) + 2\sqrt{t}$	125 160 195 245 295	0.1458113
$w(t) + 4\sqrt{t}$	110 140 170 210 255 295	0.3427038

Table 8.9: Real option values for scenarios of deterministic water level (Algorithm 1).

We propose the following rule-of-thumb to estimate the real option value under a model with stochastic water level using various deterministic water level scenarios:

$$\breve{v}(t_0, x_1, x_3) := \begin{bmatrix} N(-2) & N(-1) & N(0) & N(1) & N(2) \end{bmatrix} \cdot \begin{bmatrix} \hat{v}(t_0, x_1, x_3)_{-2\sigma_w} \\ \hat{v}(t_0, x_1, x_3)_{-1\sigma_w} \\ \hat{v}(t_0, x_1, x_3)_{0\sigma_w} \\ \hat{v}(t_0, x_1, x_3)_{+1\sigma_w} \\ \hat{v}(t_0, x_1, x_3)_{+2\sigma_w} \end{bmatrix}, \tag{8.85}$$

where $N(.)$ is the standard normal distribution function and $\hat{v}(t_0, x_1, x_3)_{n\sigma_w}$ denotes the option value under the average water level scenario $w(t) + n\sigma_w\sqrt{t}$. The above equation represents a weighted average over five different water level scenarios. We obtain the following option values:

$$\breve{v}(t_0, X_0^{(1)}, X_0^{(3)}) = \begin{cases} 0.060577, & \text{for } \sigma_w = 1, \\ 0.080261, & \text{for } \sigma_w = 2. \end{cases} \tag{8.86}$$

They correspond closely to the option values we found using the dike-Q-COS method. We can argue whether it is better to use the scenarios and the dike-COS method with option value $\check{v}(t_0, x_1, x_3)$ or the dike-Q-COS method with stochastic average water level. The former is less time-consuming and the real options prices of both do not differ much. However, the latter ones can give a more complete picture of the effects of various water level realisations. Besides, we did not know beforehand whether the scenarios method would lead up to a similar real option value as the dike-Q-COS method. This is only established afterwards when both were implemented.

9 Summary and conclusion

This section presents a summary of the report and the main results that are obtained in this thesis. Also suggestions for further research are made.

9.1 Summary

Financial options are contracts which define rights on stocks in a financial market. *Real options* arise in for example economical, personal or societal context. The holder has a real option in the sense of a real 'choice'. Real options appear in for example the *dike height problem*, where one has to make optimal choices about when to increase the dike level and by which amount. Another example is the forest harvesting problem, where one can determine the harvesting time.

(Real) option prices can often be formulated as a *stochastic optimisation problem*. The impulse control problem represents a problem class which incorporates jumps on the state process, like an instantaneous jump in the dike level, with general form:

$$v(t,x) = \sup_{\{t_m,\xi_m\}} E^{t,x}\left[\int_t^T e^{-\rho(s-t)} f(s,X_s)ds + \sum_{t\leq t_m<T} c(X_{t_m^-},\xi_m)e^{-\rho(t_m-t)} + e^{-\rho(T-t)}g(X_T)\right]. \quad (9.1)$$

The dynamic programming principle can be derived from the above representation. The infinitesimal version results in the Hamilton-Jacobi-Bellman (HJB) equation. Two pricing methods for financial and real options have been discussed. The first method is called the *dynamic programming approach*. In this case we assume that risks cannot be hedged and the holder asks a risk adjusted discount rate for holding the option. In the second approach it is assumed that the asset markets are rich enough to be able to hedge risks and the market will not reward the holder for holding his risky option. This method is called the *contingent claims approach*.

We focused on the dike height problem based on [22] and [32]. The state dynamics of a basic model consisted of the dike height and the stochastic economic value of endangered goods, which is exposed to possible floods. The average water level was supposed to follow a deterministic function. Occurrences of extreme water level may cause flooding and they were added to the model. The controller can perform dike heightenings at certain construction costs. A recursive algorithm based on Fourier-cosine series expansions, called the *dike-COS method*, enabled us to solve the dike height problem. With this we obtained a control law, which describes when it is optimal to increase the dikes and by which amount, depending on the economic value of endangered goods and the current dike level in comparison with the water level. Parameter variation showed that the real option value, in other words the expected costs of flood protection under optimal heightenings, increases in the expected economic growth and the intensity rate of extreme water level and decreases in the risk adjusted discount rate.

An alternative model, incorporating a stochastic average water level, was also considered and we developed an extended two-dimensional algorithm. The results showed that the expected costs of flood protection increase if the volatility of the average water level is increased. A method which considers several scenarios of deterministic water level, instead of a stochastic level, may perform satisfactorily to estimate the real option value under uncertain water level rise.

9.2 Conclusion

A general conclusion is given in this section, based on the research questions defined in Section 1.1. Each question is answered below:

- Q(uestion): Can we adapt the COS pricing method for Bermudan or swing options to solve the

dike height impulse control problem?
A(nswer): Yes. The presented dike-COS method, for solving the dike height problem under the first basic model, is a combination of the COS method for pricing Bermudan and swing options. Similar to the Bermudan option we took a finite number of control times. The possibility to make an optimal decision between some choices is very similar to choices with pricing a swing option. The main difference between these two financial options and the dike height real option is the possible jump in the dike level at the control times in the dike height problem. Because of that we need to keep track of the dike level and an extra dimension was added to the COS method. Besides, our real option remains valid after a dike heightening and the dikes can be increased more than once, whereas a Bermudan option can be exercised only once. Also a kind of cashflow from flooding costs in the dike height problem was added, which is efficiently estimated using the analytical representation of the function $\beta(h)$.

- Q: How can we efficiently calculate the optimal dike increase level?
  A: The so-called construction domains are determined using the algorithm described in Section 4.2.1 and the Bisection method. Newton's method did not perform satisfactorily since it requires a 'good' initial value. Uniqueness of results to justify the algorithm for determination of the construction domains is assumed on the basis of the results in [32]. The determination of the construction domains takes a significant part of the computation time and an improvement in the future will be useful.

- Q: What can we tell about the error convergence of the numerical method and the errors close to the boundaries of the computational domain?
  A: The error of the dike-COS method converges exponentially in the number of terms N in the Fourier-cosine series expansions for density functions that belong to $C^\infty([a,b])$. However, the tests showed that the error convergence can be spoilt by roundoff errors. We performed extensive numerical tests to analyse the error by means of the COS formula for pricing European options. The error is large in the vicinity of the boundaries, which may give rise to incorrect construction domains. However, if the integration interval $[a,b]$ is sufficiently wide, then the incorrect construction domains at the boundaries will not significantly affect the option prices in the middle of the computational domain. Furthermore, a larger truncated integration interval resembles the original domain better. On the other hand, the roundoff errors are increasing for larger intervals $[a,b]$, which leads to a higher roundoff plateau, and convergence takes longer. We carefully tried to find a compromise between both inaccuracies. Besides, we found that it is not always accurate to define the interval $[a,b]$ only based on the density function or other characteristics of the stochastic process. It is advisable to take the characteristics of the payoff function into account too. The dike-COS method showed satisfactory convergence in the method parameters N, N_t and N_{bis} for an example of an island. The method is validated by the resulting control law (Figure 7.6), which matches to the results in [32]. The computational complexity is order $O(N \log_2 N)$. Possibly a method based on modified Fourier series expansion may improve the computation time.

- Q: Is it possible to extend the pricing method to using it with more than one stochastic process, such as both stochastic water level and economic value?
  A: Yes, we extended the dike-COS method to the dike-Q-COS method. The continuation value now also depended on a stochastic average water level. A quadrature rule was used to approximate the additional dimension. We used the *surplus water level* in order to reduce the size of the domain of the second stochastic process. For the expected flooding costs we developed the so-called COS convolution formula, which relies on the independence of two random variables. The method was validated using a very low water level volatility, which resembled the model of the island with the deterministic water level. A higher volatility gives rise to higher real option values. The computational complexity of the dike-Q-COS method is almost linear in the number of integration points, J, but the computation time is significantly increased by the second dimension.

In general, extensions such as stochastic water level, soil compression rate and recovery rate add an extra space-dimension to the value function. The calculation of the expected flood losses and the continuation value gets more involved by that. The expectations with respect to the additional ran-

dom variable can be estimated by using a quadrature rule. However, this will significantly increase the computational complexity. Maybe a PDE method to solving the associated Hamilton-Jacobi-Bellman equation will be easier to apply in some cases.

- Q: How do the real option prices differ when it is possible to hedge the risks of, for example, floods? A: The main drawback of the dynamic programming approach (DPPA) is the fact that it is difficult to determine the risk adjusted discount rate ρ. This rate, although it is not objective, is of interest for many policymakers. If the markets are rich enough to be able to hedge risks the holder will not be rewarded for holding his risky (real) option and we may apply the contingent claims approach (CCA). The partial differential equation resulting from the CCA can be converted back to a value function. Then a risk-free interest rate is used for discounting, which results in a higher option value. Besides, the expectation is taken under a risk-neutral measure, which may lead up to a lower option value. Unfortunately, there was no information available about possible hedge instruments for the example of an island. In [18] necessary and sufficient conditions were derived for the DPPA price equal to the CCA price in the harvesting problem. If hedge instruments exist to hedge the risks of floods or the economic uncertainty, then probably a same analysis applies for the dike height problem.

9.3 Outlook

In this final section we present some recommendations for future research.

Firstly, we would like to validate the dike-COS method using a more realistic model. The method may also be extended to the case of several dike rings of different heights and dunes, as done in [22] for a discrete model.

Secondly, we would further investigate the modified Fourier series expansions, which we introduced in Section 6.3.4. This field has received substantial interest and is explored by, for example, [19]. Faster converging series reduce the computation time. However, if the largest coefficients remain of the same order, and by that of the same accuracy, then we do not expect smaller errors.

The COS method for two-factor Lévy processes is extended by using a quadrature rule for the additional dimension. Fourier-cosine series are also available for more dimensional functions. However, the problem we face is how to calculate the corresponding coefficients. If the coefficients at the terminal time do not have an analytical solution this hampers the fast method. Interesting research to a 'true' two-dimension COS method can be performed.

Pricing Bermudan options is an example of an optimal stopping problem. In [11] the COS method was applied to this problem. The dike height problem is an example of a stochastic impulse control problem. On the other hand, in some stochastic control problem one has the possibility to control the drift or diffusion term of the state dynamics in many different ways. Adapting the COS method to such problems in general would introduce difficulties, because the characteristic function could depend on the control process. This is another challenge we may take.

Appendix

A Functions χ_k and ψ_k

The functions χ_k and ψ_k are given by:

$$\chi_k(z_1,z_2)=\int_{z_1}^{z_2} e^y \cos\left(k\pi\frac{y-a}{b-a}\right)dy \qquad \text{and} \qquad \psi_k(z_1,z_2)=\int_{z_1}^{z_2} \cos\left(k\pi\frac{y-a}{b-a}\right)dy. \tag{A.1}$$

Maple 9.5 provides the following analytically solutions:

$$\begin{aligned}\chi_k(z_1,z_2) &= \frac{1}{1+\left(\frac{k\pi}{b-a}\right)^2}\left[\cos\left(k\pi\frac{z_2-a}{b-a}\right)e^{z_2}-\cos\left(k\pi\frac{z_1-a}{b-a}\right)e^{z_1}\right.\\ &\left.+\frac{k\pi}{b-a}\sin\left(k\pi\frac{z_2-a}{b-a}\right)e^{z_2}-\frac{k\pi}{b-a}\sin\left(k\pi\frac{z_1-a}{b-a}\right)e^{z_1}\right].\end{aligned} \tag{A.2}$$

$$\psi_k(z_1,z_2)=\begin{cases}\left[\sin\left(k\pi\frac{z_2-a}{b-a}\right)-\sin\left(k\pi\frac{z_1-a}{b-a}\right)\right]\frac{b-a}{k\pi}, & \text{for } k\neq 0,\\ z_2-z_1, & \text{for } k=0.\end{cases} \tag{A.3}$$

B Functions χ_k^{SIN} and ψ_k^{SIN}

The functions χ_k^{SIN} and ψ_k^{SIN} are given by:

$$\chi_k(z_1,z_2)=\int_{z_1}^{z_2} e^y \sin\left(k\pi\frac{y-a}{b-a}\right)dy \qquad \text{and} \qquad \psi_k(z_1,z_2)=\int_{z_1}^{z_2} \sin\left(k\pi\frac{y-a}{b-a}\right)dy. \tag{B.1}$$

Maple 9.5 provides the following analytically solutions:

$$\begin{aligned}\chi_k^{SIN}(z_1,z_2) &= -\frac{1}{1+\left(\frac{k\pi}{b-a}\right)^2}\left[\frac{k\pi}{b-a}\cos\left(k\pi\frac{z_2-a}{b-a}\right)e^{z_2}-\frac{k\pi}{b-a}\cos\left(k\pi\frac{z_1-a}{b-a}\right)e^{z_1}\right.\\ &\left.-\sin\left(k\pi\frac{z_2-a}{b-a}\right)e^{z_2}+\sin\left(k\pi\frac{z_1-a}{b-a}\right)e^{z_1}\right].\end{aligned} \tag{B.2}$$

$$\psi_k^{SIN}(z_1,z_2)=\begin{cases}-\left[\cos\left(k\pi\frac{z_2-a}{b-a}\right)-\cos\left(k\pi\frac{z_1-a}{b-a}\right)\right]\frac{b-a}{k\pi}, & \text{for } k\neq 0,\\ 0, & \text{for } k=0.\end{cases} \tag{B.3}$$

C Functions χ_k^c, χ_k^s, ψ_k^c and ψ_k^s

The functions χ_k^c and ψ_k^c are given by:

$$\chi_k^c(z_1,z_2)=\int_{z_1}^{z_2} e^y \cos\left(k\pi\frac{2y-(b+a)}{b-a}\right)dy \qquad \text{and} \qquad \psi_k^c(z_1,z_2)=\int_{z_1}^{z_2} \cos\left(k\pi\frac{2y-(b+a)}{b-a}\right)dy. \tag{C.1}$$

Maple 9.5 provides the following analytically solutions:

$$\begin{aligned}\chi_k^c(z_1,z_2) &= \frac{1}{1+\left(\frac{2k\pi}{b-a}\right)^2}\left[\cos\left(k\pi\frac{2z_2-(b+a)}{b-a}\right)e^{z_2}-\cos\left(k\pi\frac{2z_1-(b+a)}{b-a}\right)e^{z_1}\right.\\ &\left.+\frac{2k\pi}{b-a}\sin\left(k\pi\frac{2z_2-(b+a)}{b-a}\right)e^{z_2}-\frac{2k\pi}{b-a}\sin\left(k\pi\frac{2z_1-(b+a)}{b-a}\right)e^{z_1}\right].\end{aligned} \tag{C.2}$$

$$\psi_k^c(z_1,z_2) = \begin{cases} \left[\sin\left(k\pi\frac{2z_2-(b+a)}{b-a}\right) - \sin\left(k\pi\frac{2z_1-(b+a)}{b-a}\right)\right]\frac{b-a}{2k\pi}, & \text{for } k\neq 0, \\ z_2 - z_1, & \text{for } k = 0. \end{cases} \tag{C.3}$$

The functions χ_k^s and ψ_k^s are given by:

$$\chi_k^s(z_1,z_2) = \int_{z_1}^{z_2} e^y \sin\left((k-\tfrac{1}{2})\pi\tfrac{2y-(b+a)}{b-a}\right) dy \qquad \text{and} \qquad \psi_k^s(z_1,z_2) = \int_{z_1}^{z_2} \sin\left((k-\tfrac{1}{2})\pi\tfrac{2y-(b+a)}{b-a}\right) dy \tag{C.4}$$

Maple 9.5 provides the following analytically solutions:

$$\begin{aligned} \chi_k^c(z_1,z_2) &= \frac{1}{1+\left(\frac{2(k-\frac{1}{2})\pi}{b-a}\right)^2}\left[\sin\left(k\pi\frac{2z_2-(b+a)}{b-a}\right)e^{z_2} - \sin\left(k\pi\frac{2z_1-(b+a)}{b-a}\right)e^{z_1}\right. \\ &\left. + \frac{2(k-\frac{1}{2})\pi}{b-a}\cos\left(k\pi\frac{2z_1-(b+a)}{b-a}\right)e^{z_1} - \frac{2(k-\frac{1}{2})\pi}{b-a}\cos\left(k\pi\frac{2z_2-(b+a)}{b-a}\right)e^{z_3}\right] \end{aligned} \tag{C.5}$$

$$\psi_k^c(z_1,z_2) = \left\{ \left[\cos\left((k-\tfrac{1}{2})\pi\tfrac{2z_1-(b+a)}{b-a}\right) - \cos\left((k-\tfrac{1}{2})\pi\tfrac{2z_2-(b+a)}{b-a}\right)\right]\frac{b-a}{2(k-\frac{1}{2})\pi}, \quad \text{for } k\geq 1, \right. \tag{C.6}$$

D Function $M_{k,j}$

The function $M_{k,j}$ is given by

$$M_{k,j}(z_1,z_2) := \frac{2}{b-a}\int_{z_1}^{z_2} e^{ij\pi\frac{y-a}{b-a}}\cos\left(k\pi\frac{y-a}{b-a}\right)dy. \tag{D.1}$$

Using the relation

$$e^{iu} = \cos(u) + i\sin(u) \tag{D.2}$$

gives

$$M_{k,j}(z_1,z_2) = -\frac{i}{\pi}\left(M_{k,j}^c(z_2,z_2) + M_{k,j}^s(z_1,z_2)\right),$$

where

$$M_{k,j}^c(z_2,z_2) = \begin{cases} \frac{(z_2-z_1)\pi i}{b-a}, & \text{for } k=j=0, \\ \frac{\exp\left(i(j+k)\frac{(z_2-a)\pi}{b-a}\right)-\exp\left(i(j+k)\frac{(z_1-a)\pi}{b-a}\right)}{j+k}, & \text{otherwise}, \end{cases} \tag{D.3}$$

and

$$M_{k,j}^s(z_2,z_2) = \begin{cases} \frac{(z_2-z_1)\pi i}{b-a}, & \text{for } k=j, \\ \frac{\exp\left(i(j-k)\frac{(z_2-a)\pi}{b-a}\right)-\exp\left(i(j-k)\frac{(z_1-a)\pi}{b-a}\right)}{j-k}, & \text{for } k\neq j. \end{cases} \tag{D.4}$$

E Black-Scholes price and errors

The value of a European call option, under geometric Brownian motion asset price, reads

$$v(t,x) = E^{t,x}[g(X_T)], \tag{E.1}$$

with $(\Delta t = T - t_0)$

$$X_T|X_0 \sim \mathcal{N}\left(X_0 + (r-\frac{1}{2}\sigma^2)\Delta t, \sigma^2\Delta t\right). \tag{E.2}$$

We find

$$\begin{aligned} v_{BScall}(t_0,x) &= e^{-r\Delta t}\int_{\mathbb{R}} K(e^y-1)^+ f(y|x)dy \\ &= \frac{e^{-r\Delta t}}{\sqrt{2\pi}\sigma\sqrt{\Delta t}} K\int_0^\infty (e^y-1)e^{-\frac{1}{2}\left(\frac{y-x-(r-\frac{1}{2}\sigma^2)\Delta t}{\sigma\sqrt{\Delta t}}\right)^2} dy \\ &= \frac{e^{-r\Delta t}}{\sqrt{2\pi}} K\int_{c_1}^\infty (e^{z\sigma\sqrt{\Delta t}+x+(r-\frac{1}{2}\sigma^2)\Delta t}-1)e^{-\frac{1}{2}z^2}dz \\ &= \frac{e^x}{\sqrt{2\pi}} K\int_{c_1}^\infty e^{-\frac{1}{2}(z-\sigma\sqrt{\Delta t})^2}dz - Ke^{-r\Delta t}(1-N(c_1)) \\ &= e^x K(1-N(c_2)) - Ke^{-r\Delta t}(1-N(c_1)) \end{aligned} \tag{E.3}$$

where

$$c_1 = \frac{-x-(r-\frac{1}{2}\sigma^2)\Delta t}{\sigma\sqrt{\Delta t}} \quad \text{and} \quad c_2 = c_1 - \sigma\sqrt{\Delta t}. \tag{E.4}$$

Using similar arguments we find the integration range truncation error ($a \le 0 \le b$):

$$\begin{aligned} \epsilon_1(x|[a,b]) &= e^{-r\Delta t}\int_{\mathbb{R}\setminus[a,b]} K(e^y-1)^+ f(y-x)dy \\ &= e^{-r\Delta t}\int_b^\infty K(e^y-1)f(y-x)dy \\ &= e^x K(1-N(b_2)) - Ke^{-r\Delta t}(1-N(b_1)), \end{aligned} \tag{E.5}$$

where

$$b_1 = \frac{b-x-(r-\frac{1}{2}\sigma^2)\Delta t}{\sigma\sqrt{\Delta t}} \quad \text{and} \quad b_2 = b_1 - \sigma\sqrt{\Delta t}. \tag{E.6}$$

The put-call parity ([14]) yields

$$v_{BSput}(t_0,x) = Ke^{-r\Delta t} - Ke^x + v_{BScall}(t_0,x), \tag{E.7}$$

For a put option we find ($a \le 0 \le b$):

$$\begin{aligned} \epsilon_1(x|[a,b]) &= e^{-r\Delta t}\int_{\mathbb{R}\setminus[a,b]} K(1-e^y)^+ f(y|x)dy \\ &= e^{-r\Delta t}K\int_{-\infty}^a (1-e^y)f(y-x)dy \\ &= -e^x KN(a_2) + Ke^{-r\Delta t}N(a_1), \end{aligned} \tag{E.8}$$

where

$$a_1 = \frac{a-x-(r-\frac{1}{2}\sigma^2)\Delta t}{\sigma\sqrt{\Delta t}} \quad \text{and} \quad a_2 = a_1 - \sigma\sqrt{\Delta t}. \tag{E.9}$$

The error ϵ_4 for both options reads

$$\begin{aligned} \epsilon_4(x|[a,b]) &= \int_{\mathbb{R}\setminus[a,b]} f(y|x)dy \\ &= \frac{1}{\sqrt{2\pi}\sigma\sqrt{\Delta t}}\int_{\mathbb{R}\setminus[a,b]} e^{-\frac{1}{2}\left(\frac{y-x-(r-\frac{1}{2}\sigma^2)\Delta t}{\sigma\sqrt{\Delta t}}\right)^2} dy \\ &= N(a_1) + (1-N(b_1)). \end{aligned} \tag{E.10}$$

F Characteristic functions

Definition F.1. *(Characteristic function)*
The characteristic function of a random variable X is defined by ([13])

$$\varphi(u) = E[e^{iuX}]. \tag{F.1}$$

Gumbel distribution
The characteristic function of a Gumbel distributed random variable $\mathcal{J}$, with scale parameter $1/k_1 > 0$ and location parameter $k_2 \in \mathbb{R}$, reads

$$\begin{aligned}
\varphi_{\mathcal{J}}(u) &= \int_{\mathbb{R}} e^{iuy} f_{\mathcal{J}}(y) dy \\
&= k_1 \int_{\mathbb{R}} e^{iuy} e^{k_1(k_2-y) - e^{k_1(k_2-y)}} dy \\
&= k_1 e^{iuk_2} \int_{\mathbb{R}} e^{iux} e^{-k_1 x - e^{-k_1 x}} dx \\
&= k_1 e^{iuk_2} \int_{\mathbb{R}} (e^{-k_1 x})^{-i\frac{u}{k_1}+1} e^{-(e^{-k_1 x})} dx \\
&= -e^{iuk_2} \int_{\infty}^{0} z^{i\frac{u}{k_1}+1} e^{-z} \frac{dz}{z} \\
&= e^{iuk_2} \int_{0}^{\infty} z^{i\frac{u}{k_1}+1-1} e^{-z} dz \\
&= \Gamma\left(1 + i\frac{u}{k_1}\right) e^{iuk_2},
\end{aligned} \tag{F.2}$$

with Γ the gamma function $\Gamma(s) = \int_0^\infty z^{s-1} e^{-z}\, dz$.

Normal distribution
The characteristic function of a normally distributed random variable $\mathcal{N}$, with mean μ and standard deviation σ, reads

$$\begin{aligned}
\varphi_{\mathcal{N}}(u) &= \int_{\mathbb{R}} e^{iuy} f_{\mathcal{N}}(y) dy \\
&= \frac{1}{\sqrt{2\pi}\sigma} \int_{\mathbb{R}} e^{iuy} e^{-\frac{1}{2}\left(\frac{y-\mu}{\sigma}\right)^2} dy \\
&= e^{iu\mu} \frac{1}{\sqrt{2\pi}} \int_{\mathbb{R}} e^{iu\sigma z} e^{-\frac{1}{2}z^2} dz \\
&= e^{iu\mu - \frac{1}{2}\sigma^2 u^2} \frac{1}{\sqrt{2\pi}} \int_{\mathbb{R}} e^{-\frac{1}{2}(z - iu\sigma)^2} dz \\
&= e^{iu\mu - \frac{1}{2}\sigma^2 u^2}.
\end{aligned} \tag{F.3}$$

G Results for average water level volatility $\sigma_w = 1$

L_2	dd \ J	51	101	151	201
4	7	0.061528296819761	0.061520746952236	0.061520787226090	0.061520780009096
	8	0.061506626843016	0.061499059910717	0.061499060125004	0.061499060201963
	9	0.061506626843262	0.061499059911018	0.061499060125160	0.061499060202116
	10	0.061506626843205	0.061499059910837	0.061499060125093	0.061499060202022
5	7	0.062331197833475	0.061520516504900	0.061520475802555	0.061520681339659
	8	0.062309563770279	0.061499070851573	0.061499070852184	0.061499070852947
	9	0.062309563770589	0.061499070851752	0.061499070852377	0.061499070853188
	10	0.062309563770514	0.061499070851625	0.061499070852239	0.061499070853089
6	7	0.072611304220836	0.061520964137796	0.061520766949960	0.061520905427958
	8	0.072589386809512	0.061499071200220	0.061499070884378	0.061499070884533
	9	0.072589386809631	0.061499071200406	0.061499070884673	0.061499070884785
	10	0.072589386809593	0.061499071200247	0.061499070884465	0.061499070884687
7	7	0.133315995968833	0.061520953969986	0.061520942235856	0.061520840147851
	8	0.133293349995292	0.061499213849266	0.061499070884488	0.061499070884377
	9	0.133293349995844	0.061499213849528	0.061499070884684	0.061499070884603
	10	0.133293349995467	0.061499213849410	0.061499070884535	0.061499070884411
8	7	0.514188273979021	0.061528308901562	0.061520720467859	0.061520766931375
	8	0.514132465218316	0.061506638874520	0.061499070884759	0.061499070884489
	9	0.514132465220316	0.061506638874829	0.061499070885044	0.061499070884735
	10	0.514132465219732	0.061506638874664	0.061499070884868	0.061499070884547

Table G.1: Real option values $\tilde{v}(t_0, X_0^{(1)}, X_0^{(2)}, X_0^{(3)})$ for $\sigma_w = 1$.

References

[1] R.A. Adams, *Calculus, A complete course*, Addison Wesley Longman, Toronto, 2002.

[2] M. Bardi, I.C. Dolcetta, *Optimal control and viscosity solutions of Hamilton-Jacobi-Bellman equations*, Springer, 1997.

[3] R.E. Bellman, *Dynamic programming*, Courier Dover Publications, 2003.

[4] C.M. Bender, S.A. Orszag, *Advanced mathematical methods for scientists and engineers*, McGraw-Hill, New York, 1978

[5] J.P. Boyd, *Chebyshev and Fourier spectral methods*, Courier Dover Publications, 2001.

[6] M.G. Crandall, H. Ishii, P.L. Lions, A user's guide to viscosity solutions, *Bulletin of the A.A.M.S.,N.S.* Vol. 27, 1-67, 1992.

[7] D. van Dantzig, Economic decision problems for flood prevention, *Econometrica*, Vol. 24(3), 276-287, 1956.

[8] A.K. Dixit, R.S. Pindyck, *Investment under uncertainty*, Princeton University Press, Princeton, 1994.

[9] C.J.J. Eijgenraam, CPB Discussion Paper - Optimal safety standards for dike-ring areas, Technical Report 62, Centraal Planbureau, 2006.

[10] F.Fang, C.W. Oosterlee, A novel pricing method for European options based on Fourier-cosine series expansions, *SIAM Journal on Scientific Comp*, Vol 31(2), 826-848, 2008.

[11] F. Fang, C.W. Oosterlee, Pricing early-exercise and discrete barrier options by Fourier-cosine series expansions, *Numerische Mathematik*, Vol 114(1), 27-62, 2009.

[12] F. Fang, C.W. Oosterlee, Under Heston's model: A fast and accurate pricing method for Bermudan and discrete barrier options, Internal report, 2010.

[13] F.B. Hanson *Applied stochastic processes and control for jump-diffusions: modeling, analysis, and computation*, Society for Industrial and Applied Mathematics, 2007.

[14] D.J. Higham, *An introduction to financial option valuation: mathematics, stochastics and computation*, Cambridge University Press, 2004.

[15] A. Hyvarinen, J. Karhunen, E. Oja, *Independent component analysis*, John Wiley and Sons, 2001.

[16] M. Insley, K. Rollins, On solving the multirotational timber harvesting problem with stochastic prices: A linear complementarity formulation, *American Journal of Agricultural Economics*, Vol. 87(3), 735-755, 2005.

[17] M. Insley, M. Lei, Hedging and trees: Incorporating fire risk into optimal decisions in forestry using a no-arbitrage approach, *Journal of Agricultural and Resource Economics*, Vol. 32(03), 492-514, 2007.

[18] M.C. Insley, T.S. Wirjanto, Contrasting two approaches in real options valuation: Contingent claims versus dynamic programming, *Journal of Forest Economics*, Vol. 16(2), 157-176, 2010.

[19] A. Iserles, S. Nørsett, From high oscillation to rapid approximation I: modified Fourier expansions, *IMA Journal of Numerical Analysis*, Vol. 28(4), 862-887, 2008.

[20] C.J. Jepma, M. Munasinghe, *Climate change policy: facts, issues and analyses*, Cambridge University Press, 1998.

[21] R. Korn, Some applications of impulse control in mathematical finance, *Mathematical Methods of Operations Research*, Vol. 50(3), 493-518, 1999.

[22] P. Kempker, *Optimal control for dike levels*. Master thesis, Vrije Universiteit Amsterdam, the Netherlands, 2008.

[23] KNMI, KNMI Klimaatscenarios - Zeespiegel, `www.knmi.nl/klimaatscenarios/knmi06/gegevens/zeespiegel`.

[24] P.L. Lions, Optimal control of diffusion processes and Hamilton-Jacobi-Bellman equations part 2 : viscosity solutions and uniqueness, *Communications in partial differential equations*, Vol. 8(11), 1229-1276, 1983. Vol. 136(1), 47-77, 2003.

[25] R. Lord, F. Fang, F. Bervoets, C.W. Oosterlee, A fast and accurate FFT-based method for pricing early-exercise options under Lévy processes, *SIAM Journal on Scientific Computing*, Vol. 30(4), 1678-1705, 2008.

[26] Mathworld, Extreme Value Distribution, visited at 23 July 2010, `http://mathworld.wolfram.com/ExtremeValueDistribution.html`.

[27] R.C. Merton, Lifetime portfolio selection under uncertainty: The continuous-time case, *Review of Economics & Statistics*, Vol. 51(3), 247-257, 1969.

[28] B.K. Øksendal, A. Sulem, *Applied stochastic calculus and jump diffusion*, Springer, 2005.

[29] B.K. Øksendal, A. Sulem, Optimal stochastic impulse control with delayed reaction, *Applied Mathematics and Optimization*, Vol. 58(2), 243-255, 2008.

[30] H. Pham, On some recent aspects of stochastic control and their applications, *Probab. Surveys*, Vol. 2, 506-549, 2005.

[31] H. Pham, *Continuous-time stochastic control and optimization with financial applications*, Springer, 2009.

[32] S.P. van der Pijl, C.W. Oosterlee, An ENO-based numerical method for the control of dike levels in continuous time, Internal report, 2009.

[33] M.J. Ruijter, *Het prijzen en hedgen van opties met Lévy processen*, Bachelorproject, Technische Universiteit Delft, the Netherlands, 2008.

[34] M.J. Ruijter, *Stochastic control problems*, Literature report Master thesis, Technische Universiteit Delft, the Netherlands, 2010.

[35] Seydel, Existence and uniqueness of viscosity solutions for QVI associated with impulse control of jump-diffusions, *Stochastic Processes and their Applications*, Vol. 119, 3719-3748, 2009.

[36] S.E. Shreve, *Stochastic calculus for finance II, Continuous-Time models*, Springer, Berlin, 2008.

[37] J.M. Steele, *Stochastic calculus and financial applications*, Springer, Berlin, 2001.

[38] L. Trigeorgis, *Real Options: managerial flexibility and strategy in resource allocation*, MIT Press, Cambridge, 2002.

[39] A. Vollert, *A stochastic control framework for real options in strategic valuation*, Springer, 2003.

[40] C. Vuik, P. van Beek, F. Vermolen, J. van Kan, *Numerical methods in scientific computing*, VSSD, Delft, 2005.

[41] B. Zhang, C.W.Oosterlee, An efficient pricing algorithm for swing options based on Fourier cosine expansions, Internal report, 2010.